2008

Retro Models of the Cisplatin-DNA Cross-link with Carrier Ligands Having sp2 N-donor Triazine Rings

Vidhi Maheshwari
Louisiana State University and Agricultural and Mechanical College, vmahes1@lsu.edu

RETRO MODELS OF THE CISPLATIN-DNA CROSS-LINK WITH CARRIER LIGANDS HAVING sp^2 N-DONOR TRIAZINE RINGS

A Dissertation

Submitted to the Graduate Faculty of the
Louisiana State University and
Agricultural and Mechanical College
in partial fulfillment of the
requirements for the degree of
Doctor of Philosophy

in

The Department of Chemistry

by
Vidhi Maheshwari
B.Sc., Delhi University, 2000
M.S., University of Louisiana at Lafayette, 2003
August 2008

Dedicated to

my parents

and

to my loving husband

ACKNOWLEDGEMENTS

I would like to acknowledge many people for helping me during my doctoral work. I would especially like to thank my advisor, Dr. Luigi G. Marzilli, for his generous time and commitment. Throughout my doctoral work he encouraged me to develop independent thinking and research skills. He continually stimulated my analytical thinking and greatly helped me with scientific writing.

I am also very grateful to Dr. Patricia Marzilli for useful discussions and for endlessly correcting my manuscripts. I wish to thank my doctoral committee, Dr. Andrew Maverick, Dr. Brian Hales, Dr. Jayne Garno and Dr. Norimoto Murai for their continual support and encouragement. I am also very grateful to Dr. Frank Fronczek for helpful discussions and X-ray crystal structure determination; Dr. Dale Treleaven and Dr. Thomas Weldeghiorghis for their technical help and initially teaching me how to use the NMR spectrometers; Dr. Kresimir Rupnik and Dr Brian Hales for letting me use the CD instrument in their lab.

I extend many thanks to my colleagues and friends, Dr. Debadeep Bhattacharyya, Dr. Anna Christoforou, Dr. Kristie Adams, Janet Manono and Theshini Perera for their help and for all the things we shared together in the lab. Our former post-docs Dr. Maria Carlone and Dr. Patrizia Siega, and visiting researcher Dr. Rosita Ranaldo for their friendship. I owe a special note of gratitude to Ms. Sherry Wilkes for helping me with all the official paper work during my graduate studies.

Finally, I'd like to thank my family. My parents were a constant source of support and inspiration. I'm grateful to my sister and brother for their love, encouragement and enthusiasm. My deepest appreciation goes to my husband and best friend, Sumeer, for his

patience and for helping me keep my life in proper perspective and balance. His knowledge of computers was also extremely helpful and I'm thankful to him for inspiring me and being on my side throughout this journey.

TABLE OF CONTENTS

LIST OF TABLES

LIST OF FIGURES

LIST OF ABBREVIATIONS

Abbreviations	Definition
NMR	Nuclear Magnetic Resonance
ROESY	Rotating Frame Nuclear Overhauser Effect SpectroscopY
NOESY	Nuclear Overhauser Effect SpectroscopY
COSY	COrrelated SpectroscopY
EXSY	EXchange SpectroscopY
CD	Circular Dichroism
UV-vis	ultraviolet-visible
HPLC	high performance liquid chromatography
FPLC	fast performance liquid chromatography
DNA	deoxyribonucleic acid
RNA	ribonucleic acid
HMG	high-mobility group
A_2	two amines or a diamine carrier ligand
X	anionic leaving group
L	bidentate ligand
G	guanine base derivative
G*	guanine bases linked by a sugar-phosphodiester backbone
Guo	guanosine
5′-GMP	guanosine-5′-monophosphate
3′-GMP	guanosine-3′-monophosphate
d(GpG)	2′-deoxyguanylyl(3′→5′)-2′-deoxyguanosine

HH	head-to-head
HT	head-to-tail
h	hour
min	minute
Hz	hertz
MHz	megahertz
ppm	parts per milion
ms	millisecond
mM	millimolar
μM	micromolar
nm	nanometer
μL	microliter
ε	extinction coefficient
Δε	molar circular dichroism ($M^{-1}cm^{-1}$)
conc	concentration
equiv	equivalent
fwhm	full width at half maximum
SSC	"second-sphere" communication
Me_2bipy	dimethyl-2,2′-bipyridine
4,4′-Me_2bipy	4,4′-dimethyl-2,2′-bipyridine
5,5′-Me_2bipy	5,5′-dimethyl-2,2′-bipyridine
6,6′-Me_2bipy	6,6′-dimethyl-2,2′-bipyridine
pyt	3-(pyridin-2′-yl)-1,2,4-triazine

$MepyMe_2t$	3-(4′-methylpyridin-2′-yl)-5,6-dimethyl-1,2,4-triazine
$MepyMe_2t$	3-(4′-methylpyridin-2′-yl)-5,6-dimethyl-1,2,4-triazine
$pyMe_2t$	3-(pyridin-2′-yl)-5,6-dimethyl-1,2,4-triazine
$pyPh_2t$	3-(pyridin-2′-yl)-5,6-diphenyl-1,2,4-triazine
pyPht	3-(pyridin-2′-yl)-5-phenyl-1,2,4-triazine
R_4dt	bis-3,3′-(5,6-dialkyl-1,2,4-triazine)
Me_4dt	bis-3,3′-(5,6-dimethyl-1,2,4-triazine)
Et_4dt	bis-3,3′-(5,6-diethyl-1,2,4-triazine)
Bip	bipiperidine
Me_2ppz	*N,N′*- dimethylpiperazine
Me_2DAB	*N,N′*-dimethyl-2,3-diaminobutane
Phen	1,10-phenanthroline
θ_P	in-plane bending
θ_B	bowing angle
θ_T	twist angle
θ_{di}	dihedral angle between the best planes through the two pyridyl rings in a bipyridine ligand
θ_S	dihedral angle between the Pt coordination plane and the plane of the aromatic portion of the bipyridine ligand
d_s	S-shaped distortion
DMSO	dimethyl sulfoxide

ABSTRACT

Rapid rotation of guanine base derivatives about Pt–N7 bonds results in fluxional behavior of models of the key DNA intrastrand G–G cross-link leading to anticancer activity of Pt(II) drugs (G = deoxyguanosine). This behavior impedes the characterization of **L**Pt**G**$_2$ models (**L** = one bidentate or two *cis*-unidentate carrier ligands; **G** = guanine derivative). The objective of this study is to understand the types of conformers formed as **L** is systematically varied. This work, relevant to Pt(II) anticancer drugs, has evolved from published studies with sp^3 N-ligands (e.g., 2,2′-bipiperidine), to C_2 symmetrical or unsymmetrical sp^2 N-ligands having pyridine and/or triazine rings.

NMR spectroscopy provided conclusive evidence that **L**Pt**G**$_2$ (**L** = 5,5′-dimethyl-2,2′-bipyridine (**5,5′-Me$_2$bipy**), 3-(4′-methylpyridin-2′-yl)-5,6-dimethyl-1,2,4-triazine) (**MepyMe$_2$t**), and bis-3,3′-(5,6-dialkyl-1,2,4-triazine) (**R$_4$dt**)) complexes exist as interconverting mixtures of head-to-tail (HT) and head-to-head (HH) conformers. The triazine rings have a N plus lone pair in the same position as the C6H of pyridine rings, and NMR spectral studies indicate that the **L**Pt**G**$_2$ adducts are more dynamic when **L** has a triazine ring. For the first time, the two possible HH conformers (HHa and HHb) were identified for (**MepyMe$_2$t**)Pt(5′-GMP)$_2$, an adduct having an unsymmetrical **L**. Although O6–O6 clashes involving the two cis **G** bases favor the HT over the HH arrangement, the HH conformer of (**R$_4$dt**)Pt(5′-GMP)$_2$ adducts has a high abundance (~50%), a finding attributed to a reduction in O6–O6 steric clashes permitted by the overall low steric effects of **R$_4$dt** ligands.

The (**R$_4$dt**)Pt(d(G*pG*)) adduct (G* = N7 platinated G residue linked with a sugar-phosphodiester backbone), is the first adduct having a high abundance of a fourth

form. The characteristics of this form suggest it is the elusive ΛHT conformer; in addition, this adduct had the normally observed HH1, HH2 and ΔHT conformers. Studies with the (**R$_4$dt**)Pt(d(G*pG*)) adducts provided the first clear evidence that the sugar-phosphodiester backbone between two adjacent **G**'s slows the rate of exchange between the conformers. For (**R$_4$dt**)Pt(d(G*pG*)), a 3′-flanking T has no significant influence on the structure of the d(G*pG*) cross-link or the distribution of conformers, whereas the 5′-T residue led to the exclusive presence of the HH1 conformer.

CHAPTER 1. INTRODUCTION

Rosenberg's serendipitous discovery of the anticancer activity of cisplatin, *cis*-$Pt(NH_3)_2Cl_2$[1], has stimulated extensive interest in the interaction of platinum complexes with nucleic acids. Despite the success of cisplatin in treating several forms of cancer, including ovarian, testicular, cervical, head and neck, and non-small-cell lung cancer,[2-5] the exact features that render this simple molecule an effective anticancer agent are still controversial. Also, the treatment is limited by side effects including nephrotoxicity, emetogenesis and neurotoxicity.[6-8] Thousands of platinum analogues have been synthesized and screened for anticancer activity in an attempt to overcome these limitations and to broaden the range of treatable tumors.[2,9-14]

1.1 Cisplatin

1.1.1 Cellular Pathway

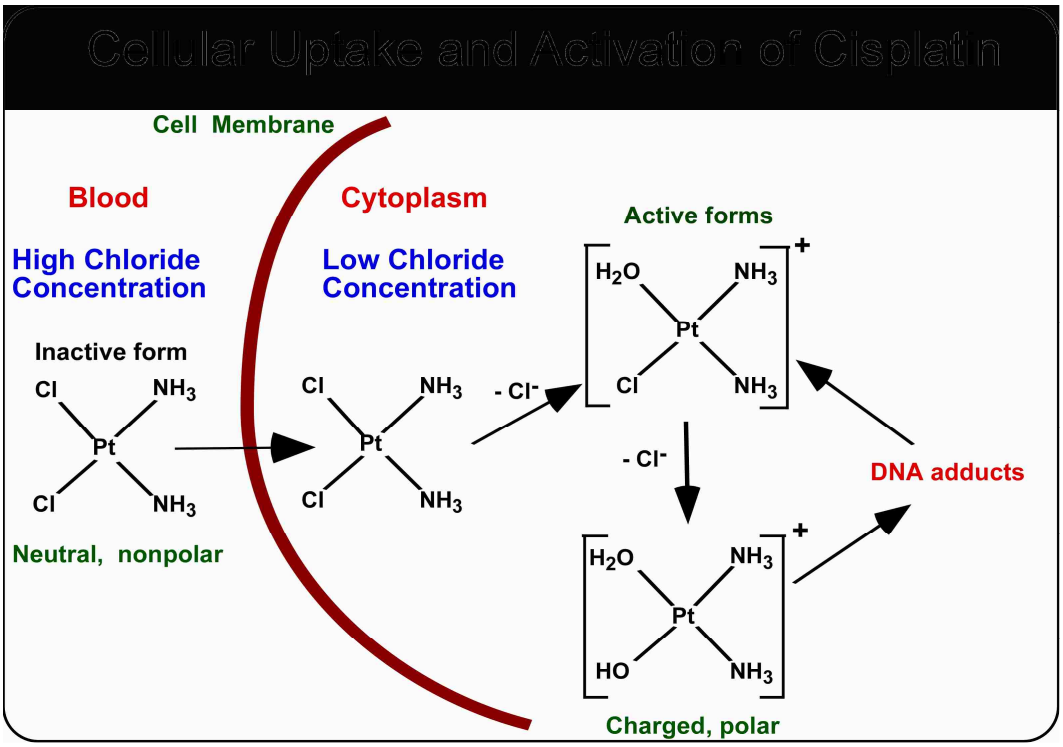

Figure 1.1 Schematic representation of cellular uptake and activation of cisplatin (*cis*-$Pt(NH_3)_2Cl_2$) prior to DNA binding.

Cisplatin circulates in the bloodstream, primarily as the chloride form. Upon entering the cell, where the chloride ion concentration is significantly lower (~4 mM) than in the blood plasma (100 mM), the chloride ligands are displaced by water to form aqua and hydroxo species (Figure 1.1).[5,15-20] These hydrolyzed cisplatin complexes are thought to be the active form of the drug.[5,15,16] Within the cell, cisplatin can form covalent adducts with a number of macromolecules including peptides, proteins, and nucleic acids.[16,21] However, DNA is widely accepted as the critical target responsible for the anticancer activity of cisplatin.[2,5,15,16,21]

1.1.2 DNA Binding

Platinum compounds can bind to DNA by either covalent or non-covalent interactions. X-ray structures and NMR data have established that at biologically relevant pH values platinum complexes bind almost exclusively at the N7 atom in purine bases, with a preference for guanine over adenine (Figure 1.2).[2,5,10,15,22-29] Several types of DNA adducts occur with platinum compounds, including monofunctional, intrastrand cross-links, and interstrand cross-links (Figure 1.3).[30-32] Cisplatin forms predominantly 1,2-intrastrand d(G*pG*) and d(A*pG*) cross-links (G* = N7-platinated G), and to a lesser extent, 1,3-intrastrand and interstrand cross-links.[33-36] Consequently, attention has focused on these adducts as the active lesions responsible for the anticancer activity of cisplatin.[2,4,29,37-39] Additional support for this conclusion arises from the inability of the inactive trans isomer (transplatin) to form this 1,2-intrastrand adduct because of geometrical constraints.[40,41] These discoveries suggested that the cytotoxicity of cisplatin originated from the 1,2-intrastrand cross-links, which the geometry of transplatin does not allow.[25] The extent of this cross-link formation is correlated with treatment outcomes.[42,43] The distortions induced in the DNA structure upon formation of the 1,2-intrastrand cisplatin-DNA

lesion have been shown to inhibit the processes of replication and transcription, resulting in cell death.[41,44]

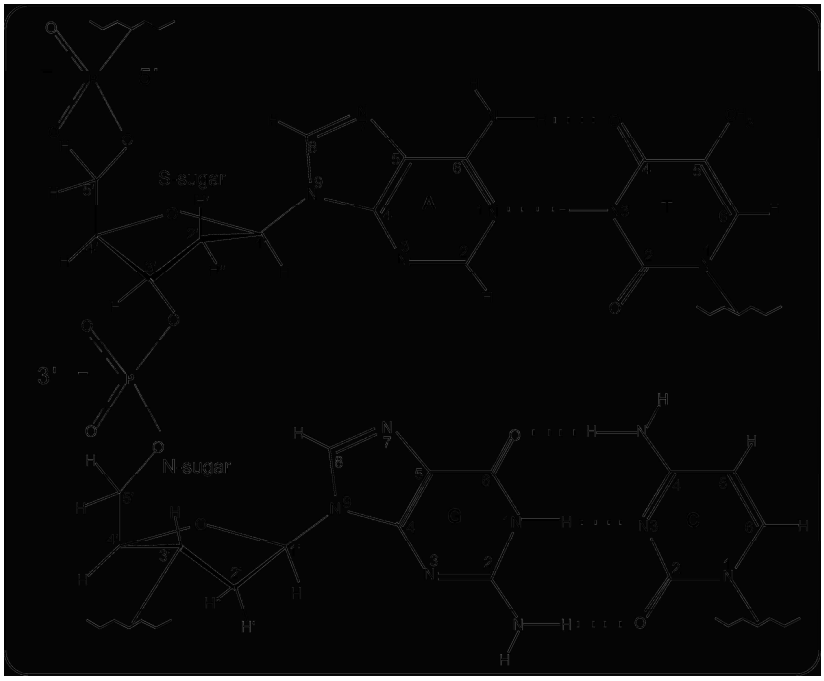

Figure 1.2 Structure and numbering scheme for DNA nucleobases. Dashed lines represent base-pair hydrogen bonds. Base and sugar are in the anti conformation. N- and S-pucker conformations are given for sugar moieties.

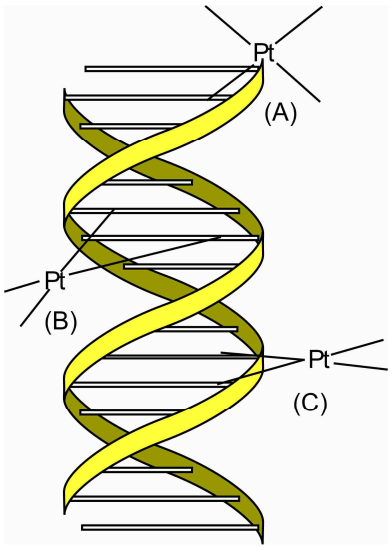

Figure 1.3 Chart showing common Pt-DNA binding modes resulting in monofunctional adducts (A), interstrand (B) and 1,2-intrastrand bifunctional cross-links (C).

Alterations of the B-DNA structure caused by cisplatin binding have been detected by several methods such as melting temperature and CD spectroscopy.[45-50] There is a degree of uncertainty in defining the structure of duplexes bearing Pt drug lesions, and controversy exists as to the details of the structure.[26,29] For this reason and because one might gain better insight into the causes of the distortions and interactions in duplexes by examining small models, many investigators have been drawn to the study of small non-duplex models by both crystallography and spectroscopy. Three classes of models are often employed to study the structural consequences of platinum binding and formation of the 1,2-d(G*pG*) intrastrand adduct in DNA: (i) DNA oligonucleotide duplexes with intrastrand and interstrand G-Pt-G cross-links,[29,37,40,51-58] (ii) adducts with single-stranded DNA have been studied as models of the intrastrand cross-link,[22,29,39,59-65] and (iii) complexes formed with unlinked guanine derivatives (**G**) are the simplest models.[29,66-68] These model types also allow the practical application of NMR spectroscopy, an invaluable technique for structural characterization in the biologically relevant solution state.[29,47]

1.2 Conformations of $LPtG_2$ Adducts

Although the Pt-duplex DNA adducts are the most reliable model types, their size often complicates analysis designed to uncover the specific conformational changes inducted by cisplatin bonding. For the other two simpler model types, namely *cis*-$Pt(NH_3)_2\mathbf{G}_2$ and *cis*-$Pt(NH_3)_2$(d(G*pG*)), bases can adopt a head-to-head (HH) or head-to-tail (HT) conformation (Figure 1.4). In the HH conformer, the H8 atoms of both G bases are on the same side of the platinum coordination plane, whereas in the HT conformer, the two H8 atoms are on the opposite sides of the platinum coordination plane. Two chiralities are possible for the HT form: Δ or Λ. These conformers can interconvert via rotation of the bases about the Pt–N7 bond (Figure

1.4).[29,66] The untethered **G**'s normally preferentially adopt an HT orientation,[69,70] whereas the bases in d(GpG) cross-links having a sugar phosphate backbone preferably adopt the HH orientation, especially when there is a 5′ residue.[39,59,61,63-65,69,71-73]

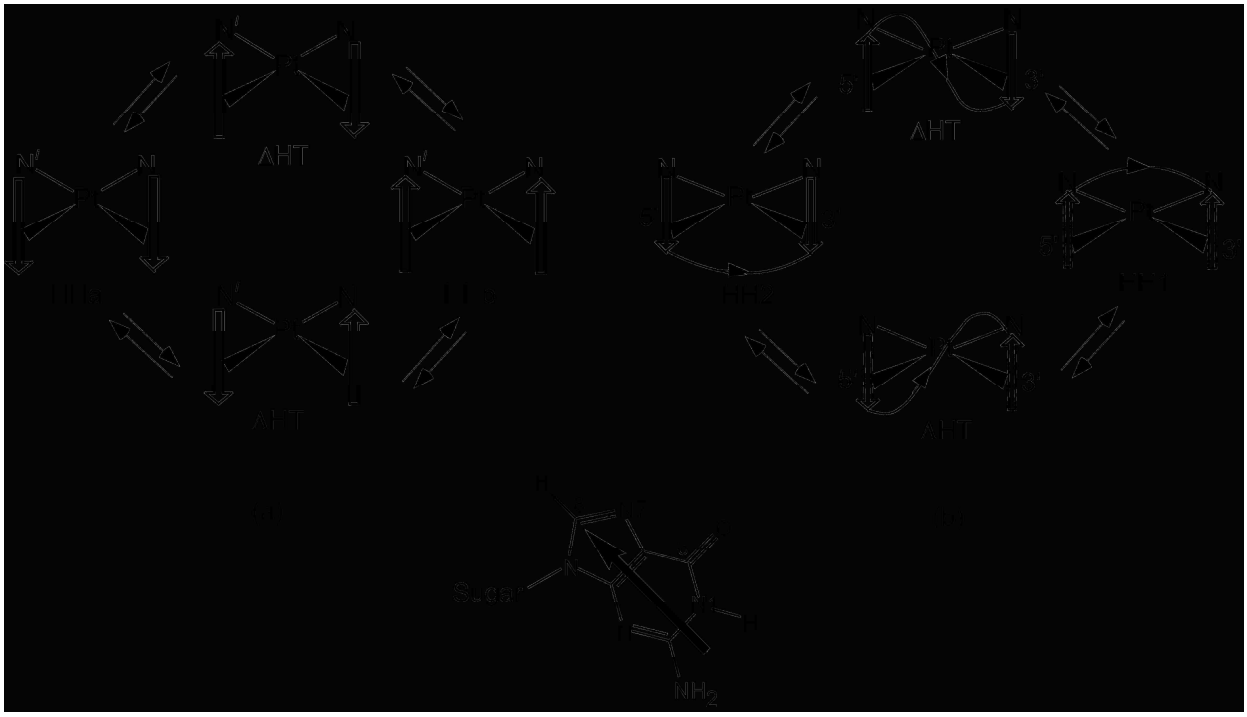

Figure 1.4 Schematic representation of possible HH and HT conformers in (a) **L**Pt**G**$_2$ and (b) **L**Pt(d(G*pG*)) type model complexes. The large arrows represent the guanine base, with the arrowhead representing the H8 (shown below the scheme), and the small arrows in (b) indicate the direction of propagation of the phosphodiester backbone. The platinum carrier ligand is to the rear; for **L**Pt**G**$_2$ adducts when **L** is unsymmetrical (N′ ≠ N), there are two HH conformers, but when symmetrical (N′ = N), only one HH conformer is possible. Rotation of one base about the Pt–N7 bond leads to another conformer, but in each case the base orientation changes from HT to HH and vice-versa.

1.3 Dynamic Motion Problem

Both *cis*-Pt(NH$_3$)$_2$**G**$_2$ and *cis*-Pt(NH$_3$)$_2$(d(G*pG*)) model adducts exhibit only one set of ^{1}H NMR resonances for each type of **G** or G* residue.[61,63,66,68] However, two different interpretations have been proposed for this same observation. Detection of one set of ^{1}H NMR signals for *cis*-Pt(NH$_3$)$_2$**G**$_2$ complexes has been attributed to a dynamic interchange between multiple conformers.[66,68] However, in the absence of an X-ray structure, the observation of only

one set of ^{1}H NMR signals for *cis*-Pt(NH_3)$_2$(d(G*pG*))[61,63] has been interpreted to imply that the presence of the phosphodiester backbone in this cross-link model favors only one conformer (*anti, anti* HH1), which undergoes slow Pt–N7 bond rotation.[41,59,61,63-65] Because of these conflicting interpretations, the *cis*-Pt(NH_3)$_2$(d(G*pG*)) model of the cisplatin-DNA intrastrand adduct is said to suffer from the "dynamic motion problem".[69,74-77]

1.4 Retro-modeling

To resolve the "dynamic motion problem", the "retro modeling" approach has been employed. In this approach analogues of cisplatin are synthesized with bulky ligands designed to reduce dynamic motion by destabilizing the transition state for Pt–N7 rotation.[29,69-71,74,78,79] These carrier ligands are more complex than the freely rotating ammonia groups of the parent compound, cisplatin. An important feature of the design is to minimize steric effects of the ground state equilibrium species to allow conformers likely to be present in dynamic *cis*-Pt(NH_3)$_2$**G**$_2$ adduct to exist in the new adducts also. The carrier-ligand bulk plays a role in influencing both the biological activity and the properties of adducts.

NMR spectroscopy provides evidence of coexistence of multiple conformers for **L**Pt**G**$_2$ models (**L** = one bidentate or two *cis*-mondentate N-donor carrier ligands) suggesting slow rotation about the Pt–N7 bond. The number of observable NMR signals for **L**Pt**G**$_2$ complexes is determined by the local symmetry of the ligand and the asymmetry of the **G** ribose residue. For the most simple case, in which the **L** is C_2 symmetrical and **G** does not have a ribose group (e.g., 9-ethylguanine), the two HT rotamers (Δ and Λ) are enantiomers and the two HH forms are equivalent because they are related by C_2 symmetry; each base arrangement (HH or HT) gives rise to only one ^{1}H NMR resonance for each proton type because the two **G** bases, in either the HH or HT arrangement, are equivalent. When the **G** contains a sugar moiety, the chirality of the

ribose group breaks the enantiomeric relationship of the two HT conformers, but the two HH forms are still equivalent; the two **G** bases are still related by C_2 symmetry in the HT conformers, but are no longer equivalent in the HH arrangement. Thus, for a **L**Pt**G**$_2$ complexes with a C_2-symmetrical **L** and a **G** containing a sugar moiety, observation of up to four ^{1}H NMR signals for each proton type is possible (one for each HT form (Δ and Λ) and two signals of equal intensity for the HH form). When **L** is an unsymmetrical carrier ligand, the two HH (HHa and HHb) and the HT (Δ and Λ) conformers are not equivalent and maximum of eight H8 signals are possible.

1.4.1 sp^3 N-donor Ligands

Unlike the *cis*-Pt(NH$_3$)$_2$**G**$_2$ complexes, for which conformer distributions are not known, observation of individual forms for retro-model complexes allows assessment of conformers. The downfield **G** H8 signals, in a less crowded, more disperse region of the spectra, are particularly useful for assessing the nature and distribution of conformer. Early retro-modeling studies employing Pt complexes of *N,N´*-dimethyl-2,3-diaminobutane (**Me$_2$DAB**)[71,72,78] and 2,2′-bipiperidine (**Bip**)[69,70] carrier ligands produced some interesting results. The Pt coordinated chelate ligands have two energetically favored C_2-symmetrical geometries, with *S, R, R, S* or *R, S, S, R* configurations at the asymmetric N, C, C, and N chelate ring atoms (Figure 1.5). These retro models provided the opportunity to define the solution structure of conformers by NMR methods, allowing the identification of the HH form of an **L**Pt**G**$_2$ adduct for the first time[80] and to define the absolute conformation in solution.[38]

In addition to the commonly found HH1 conformer, a novel HH form (HH2) was discovered for (*R, S, S, R*)-**Bip**Pt(d(G*pG*)).[74] This new form, comparable in stability to the HH1 conformer, differs from HH1 with respect to the direction of propagation of the

phosphodiester backbone. HH1 and an HT form (ΔHT1) were observed for the (*S, R, R, S*)-**Bip**Pt(d(G*pG*)) adduct.[79] Secondly, the stereochemistry of these ligands was found to dictate the favored HT chirality; subsequently, they were termed chirality-controlling chelate (**CCC**) ligands.[78] Thirdly, for all **Me$_2$DAB**Pt**G**$_2$ adducts, the favored HT form was always one having the **G** O6 atoms and the cis **Me$_2$DAB** NH groups on opposite sides of the platinum coordination plane; such results suggested that carrier ligand NH-**G** O6 H-bonds are not a great stabilizing force in such conformers.[78] Fourthly, it was found that the **G** N1H is a key feature stabilizing the favored HT conformer by participating in hydrogen bonding to the phosphate group of the cis **G**; such interligand phosphate-cis **G** N1H interactions were called "second-sphere communication" (SSC).[26,76,81,82] The fifth and the final key point that emerged from these studies was the establishment of a strong correlation between the observed CD signal and the dominant HT rotamer (Δ or Λ).[78]

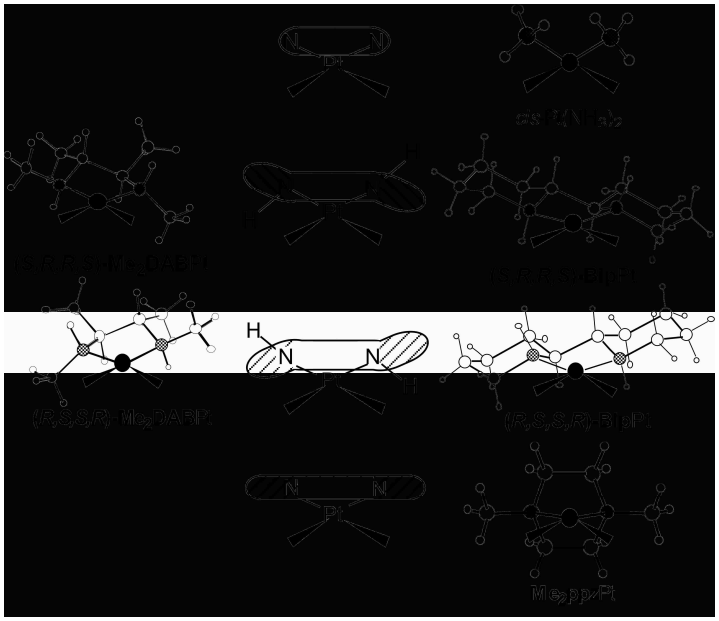

Figure 1.5 Ball-and-stick representation of Pt**G**$_2$ adducts of sp^3 N-donor ligands (**Me$_2$DAB** and **Bip**). Balloon-type structures (middle) depict the ligand bulk relative to the Pt coordination plane. Stereochemistry is indicated for the N, C, C, and N ring atoms of the **Bip** and **Me$_2$DAB** ligands.

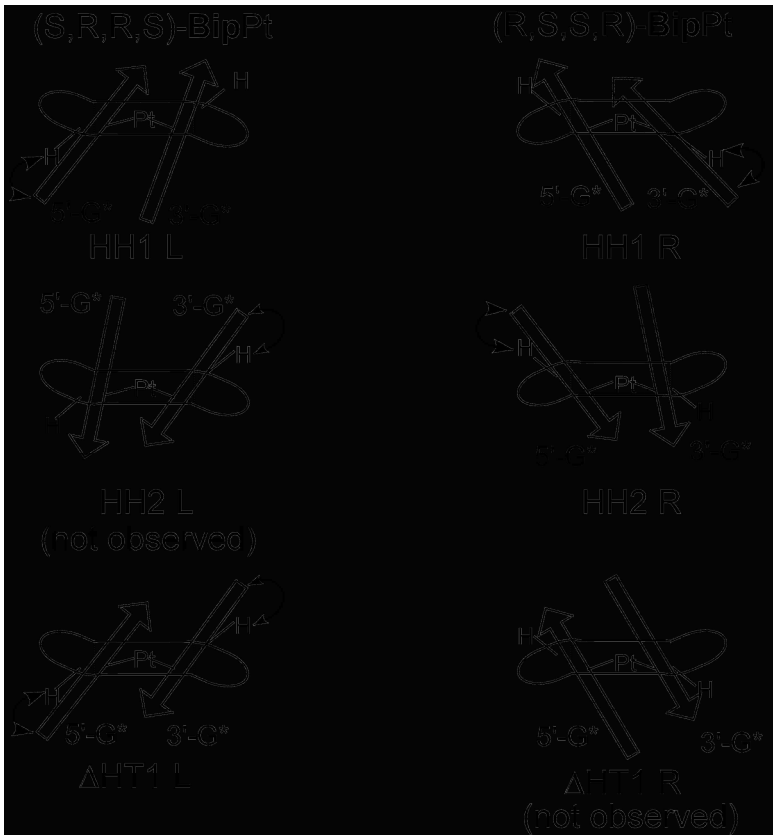

Figure 1.6 Schematic representation of canting orientations for the BipPt(d(G*pG*)) HH1, HH2 and ΔHT conformers. Shaded balloon-like shapes depict the bulk of the **Bip** ligand distributed slightly above and/or below the Pt coordination plane. Each arrow represents the guanine base. The phosphodiester backbone is omitted for clarity. Double-headed arrows show the possible **Bip** NH–G*O6 hydrogen bonds.

Studies on cross-linked adducts employing the **Bip** carrier ligand proved to be very revealing. As for the **Bip**Pt**G**$_2$ systems, the chirality of the **Bip** ligand was found to play a role in conformer distribution in cross-linked adducts. Carrier-ligand chirality also influenced structural properties of observed conformers; namely, G* base canting orientations. Canting can be either right (R)- or left (L)-handed (Figure 1.6). (*S, R, R, S*)-**Bip**Pt(d(G*pG*)) forms had L-canting, whereas conformers of (*R, S, S, R*)-**Bip**Pt(d(G*pG*)) favored R-canting (Figure 1.6). For all conformers, the favored canting orientation was consistent with the presence of at least one **Bip** NH-G O6 H-bond. Consequently, carrier ligand-NH group-G O6 H-bonds were postulated to influence conformer stabilities and base canting for the forms of **Bip**Pt(d(G*pG*)) adducts.[74,75,79]

This proposed role regarding carrier-ligand NH-**G** O6 H-bonds thus seems to contrast with conclusions drawn from unlinked model (i.e., $\mathbf{G}_2$) studies.

Another sp^3 N-donor carrier ligand studied earlier is *N,N′*- dimethylpiperazine (**Me$_2$ppz**, Figure 1.5). The ligand possess in-plane bulk to slow the dynamic motion, but lack the chirality and NH groups typically designed into cisplatin derivatives.[66,83-85] The reduced dynamic nature of **Me$_2$ppz**Pt$\mathbf{G}_2$ complexes allowed assessment and potential identification of factors relevant to the relative stabilities of different conformers.[76,86] The absence of NH groups in the **Me$_2$ppz** ligand eliminates the possibility of any carrier ligand NH-G O6/phosphate group H-bond. The three typical conformers (ΔHT, ΛHT, and HH) were observed for **Me$_2$ppz**Pt$\mathbf{G}_2$ adducts. Furthermore, in a rare example of cross-link models, three conformers (HH1, HH2, and ΔHT1) were observed and characterized for **Me$_2$ppz**Pt(d(G*pG*)).[87] This marked the first report of three conformers in one Pt cross-link adduct. Comparison of the results for **Bip**Pt(d(G*pG*)) and **Me$_2$ppz**Pt(d(G*pG*)) adducts suggested that carrier ligand NH-**G** O6 H-bond has no influence on base canting orientations and is not a significant stabilizing factor for conformers.[87]

1.4.2 sp^2 N-donor Ligands

Retro models with sp^3 N-donor ligands have been studied more often[69,86,88,89] than those with sp^2 N-donor heterocyclic chelating ligands. Studies of (**Me$_2$phen**)Pt$(Guo)_2$ complex[90] (**Me$_2$phen** = 2,9-dimethyl-1,10-phenanthroline; Guo = guanosine) and (**5,5′-Me$_2$bipy**)Pt(d(G*pG*)),[77] (**5,5′-Me$_2$bipy =** 5,5′-dimethyl-2,2′-bipyridine) have demonstrated the coexistence of different rotamers exchanging slowly relative to the NMR time scale. A Pt(II) complex having aromatic ligands can not only bind to nucleobases but can also intercalate into DNA.[8,91-97] Aromatic ring stacking between nucleobases and the intercalating molecule is considered to be one of the driving forces leading to binding; the extent of binding is expected to

depend on the planarity of the complex.[94,98] Because of the planar nature of bipyridine ligands, intercalation of Pt bipyridine complexes has been a focus of considerable interest.[92,94,99,100]

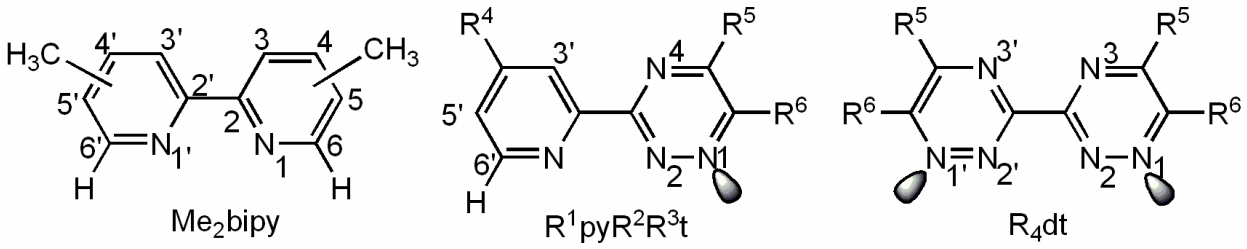

Figure 1.7 Line drawing and numbering scheme for the sp^2 N-donor ligands; **Me_2bipy** = dimethyl-2,2′-bipyridine, **$R^1pyR^2R^3t$** = 3-(Pyridin-2′-yl)-5,6-disubstituted-1,2,4-triazine and **R_4dt** = bis-3,3′-(5,6-alkyl-1,2,4-triazine).

The studies presented here utilize sp^2 N-donor heterocyclic aromatic bidentate ligands, namely dimethyl-2,2′-bipyridine (**Me_2bipy**), 3-(Pyridin-2′-yl)-5,6-disubstituted-1,2,4-triazine (**$R^1pyR^2R^3t$**) and bis-3,3′-(5,6-disubstituted-1,2,4-triazine **(R_4dt**) ligands (Figure 1.7). These ligands like **Me_2ppz** lack the NH group and the ligand bulk lie in the Pt coordination plane. Platinum complexes of these ligands were synthesized and crystallized. Structural analysis of these complexes allowed evaluation of the effect of substituents and their positions on distortions from planarity of these complexes. In **L**Pt**G_2** adducts, the effect of the presence of H6/6′ protons in **Me_2bipy** that project toward the **G** bases compared to the equivalently placed lone pairs on the N atoms in **R_4dt** ligands on the conformer distribution and canting of the bases is analyzed. The unsymmetrical **$R^1pyR^2R^3t$** ligand forms a connecting link between the two symmetrical ligands above, in having both the pyridyl and the triazine ring.

Studies involving the above sp^2 N-donor ligands, using linked (d(GpG) and oligos) and unlinked (guanosine, 5′- and 3′-GMP's) model types were undertaken in order to have a better understanding of the factors that contribute to the conformer stability and their structural properties. Specifically, the importance of electrostatic interaction between the carrier ligand and

the bases will be addressed. In addition to the characteristic H8 and sugar proton shifts of the **G** bases, the chemical shifts of the H6 or H6′ proton signals will also be used to explain the structural features of the adducts. The concept that the ability of the carrier ligand to favor specific conformers may be related to the activity (or inactivity) of cisplatin derivatives has been discussed.[75] The populations of conformers other than the HH1 conformer favored by the cisplatin-DNA intrastrand cross-linked adduct may reduce anticancer activity because such lesions may be better recognized and more easily corrected by DNA repair mechanisms. For example, proteins bearing the HMG domain are assumed to play an essential role in cisplatin's anticancer activity;[44,101,102] such proteins recognize the cisplatin-DNA lesion and are believed to protect the site from repair mechanisms. This protein may not recognize other conformers. Thus, identification of carrier-ligand features which favor the biologically relevant lesion may ultimately prove beneficial in designing better and hence more active platinum anticancer drugs.

1.5 References

1. Rosenberg, B.; VanCamp, L.; Krigas, T. *Nature (London)* **1965**, *205*, 698-699.

2. Jamieson, E. R.; Lippard, S. J. *Chem. Rev.* **1999**, *99*, 2467-2498.

3. Rosenberg, B. In *Cisplatin: Chemistry and Biochemistry of a Leading Anticancer Drug*; Lippert, B., Ed.; Wiley-VCH: Weinheim, 1999, pp 3-30.

4. O'Dwyer, P. J.; Stevenson, J. P.; Johnson, S. W. In *Cisplatin: Chemistry and Biochemistry of a Leading Anticancer Drug*; Lippert, B., Ed.; Wiley-VCH: Weinheim, 1999, pp 31-72.

5. Bloemink, M. J.; Engelking, H.; Karentzopoulos, S.; Krebs, B.; Reedijk, J. *Inorg. Chem.* **1996**, *35*, 619-627.

6. Reedijk, J. *Chem. Commun.* **1996**, 801-806.

7. Lippert, B., Ed. *Cisplatin: Chemistry and Biochemistry of a Leading Anticancer Drug*; Wiley-VCH: Weinheim, 1999.

8. Lippard, S. J.; Bond, P. J.; Wu, K. C.; Bauer, W. R. *Science (Washington, D. C.)* **1976**, *194*, 726-728.

9. Lebwohl, D.; Canetta, R. *Eur. J. Cancer* **1998**, *34*, 1522-1534.

10. Hambley, T. W. *Coordination Chem. Rev.* **1997**, *166*, 181-223.

11. Balcarová, Z.; Kašpárková, J.; Žákovská, A.; Novakává, O.; Sivo, M. F.; Natile, G.; Brabec, V. *Molecular Pharmacology* **1998**, *53*, 846-855.

12. Margiotta, N.; Bergamo, A.; Sava, G.; Padovano, G.; De Clercq, E.; Natile, G. *J. Inorg. Biochem.* **2004**, *98*, 1385-1390.

13. Kelland, L. *Nature (London)* **2007**, *7*, 573-584.

14. Kidani, Y.; Inagaki, K.; Ligo, M.; Hoshi, A.; Kuretani, K. *J. Med. Chem.* **1978**, *21*, 1315-1318.

15. Martin, R. B. In *Cisplatin. Chemistry and Biochemistry of a Leading Anticancer Drug*; Lippert, B., Ed.; Wiley-VCH: Weinheim, 1999, pp 183-205.

16. Legendre, F.; Chottard, J.-C. In *Cisplatin. Chemistry and Biochemistry of a Leading Anticancer Drug*; Lippert, B., Ed.; Wiley-VCH: Weinheim, 1999, pp 223-245.

17. Hindmarsh, K.; House, D. A.; Turnbull, M. M. *Inorg. Chim. Acta* **1997**, *257*, 11-18.

18. Lee, K. W.; Martin, D. S., Jr. *Inorg. Chim. Acta* **1976**, *17*, 105-110.

19. Reishus, J. W.; Martin, D. S., Jr. *J. Am. Chem. Soc.* **1961**, *83*, 2457-2467.

20. Davies, M. S.; Berners-Price, S. J.; Hambley, T. W. *Inorg. Chem.* **2000**, *39*, 5603-5613.

21. Reedijk, J.; Teuben, J. M. In *Cisplatin. Chemistry and Biochemistry of a Leading Anticancer Drug*; Lippert, B., Ed.; Wiley-VCH: Weinheim, 1999, pp 338-362.

22. Sherman, S. E.; Gibson, D.; Wang, A.; Lippard, S. J. *J. Am. Chem. Soc.* **1988**, *110*, 7368-7381.

23. Sherman, S. E.; Gibson, D.; Wang, A. H.-J.; Lippard, S. J. *Science* **1985**, *230*, 412-417.

24. Sherman, S. E.; Lippard, S. J. *Chem. Rev.* **1987**, *87*, 1153-1181.

25. Cohen, S. M.; Lippard, S. J. *Prog. Nucleic Acid Res. Mol. Biol.* **2001**, *67*, 93-130.

26. Natile, G.; Marzilli, L. G. *Coord. Chem. Rev.* **2006**, *250*, 1315-1331.

27. Reedijk, J. *Chem. Commun.* **1996**, 801-806.

28. Marzilli, L. G.; Saad, J. S.; Kuklenyik, Z.; Keating, K. A.; Xu, Y. *J. Am. Chem. Soc.* **2001**, *123*, 2764-2770.

29. Ano, S. O.; Kuklenyik, Z.; Marzilli, L. G. In *Cisplatin. Chemistry and Biochemistry of a Leading Anticancer Drug*; Lippert, B., Ed.; Wiley-VCH: Weinheim, 1999, pp 247-291.

30. Eastman, A. In *Cisplatin. Chemistry and Biiochemstry of a Leading Anticancer Drug.*; Lippert, B., Ed.; Wiley-VCH: Weinheim, 1999, pp 111-134.

31. Spingler, B.; Whittington, D. A.; Lippard, S. J. *Inorg. Chem.* **2001**, *40*, 5596-5602.

32. Takahara, P. M.; Christin, F. A.; Lippard, S. J. *J. Am. Chem. Soc.* **1996**, *86*, 12309-12321.

33. Eastman, A. *Biochemistry* **1983**, *22*, 3927-3933.

34. Eastman, A. *Biochemistry* **1986**, *25*, 3912-3915.

35. Johnson, N. P.; Mazard, A. M.; Escalier, J.; Macquet, J. P. *J. Am. Chem. Soc.* **1985**, *107*, 6376-6380.

36. Fichtinger-Schepman, A. M. J.; Lohman, P. H. M.; Reedijk, J. *Biochemistry* **1985**, *24*, 707-713.

37. Kline, T. P.; Marzilli, L. G.; Live, D.; Zon, G. *J. Am. Chem. Soc.* **1989**, *111*, 7057-7068.

38. Iwamoto, M.; Mukundan, S., Jr.; Marzilli, L. G. *J. Am. Chem. Soc.* **1994**, *116*, 6238-6244.

39. Fouts, C.; Marzilli, L. G.; Byrd, R.; Summers, M. F.; Zon, G.; Shinozuka, K. *Inorg. Chem.* **1988**, *27*, 366-376.

40. Malinge, J.-M.; Leng, M. In *Cisplatin. Chemistry and Biochemistry of a Leading Anticancer Drug*; Lippert, B., Ed.; Wiley-VCH: Weinheim, 1999.

41. Bloemink, M. J.; Reedijk, J. In *Met. Ions Biol. Syst.*; Sigel, A., Sigel, H., Eds.; Marcel Dekker, Inc.: New York, NY, 1996; Vol. 32, pp 641-685.

42. Reed, E.; Ozols, R. F.; Tarone, R.; Yuspa, S. H.; Poirier, M. C. *Proc. Natl. Acad. Sci. U.S.A.* **1987**, *84*, 5024-5028.

43. Van de Vaart, P. J. M.; Belderbos, J.; Jong, D. D.; Sneeuw, K. C. A.; Majoor, D.; Bartelink, H.; Begg, A. C. *Int. J. Cancer* **2000**, *89*, 160-166.

44. Zlatanova, J.; Yaneva, J.; Leuba, S. H. *FASEB J.* **1998**, *12*, 791-799.

45. Brabec, V.; Vrana, O.; Kleinwachter, V.; Kiss, F. *Studia Biophysica* **1984**, *101*, 135-139.

46. Brabec, V.; Kleinwachter, V.; Butour, J. L.; Johnson, N. P. *Biophys. Chem.* **1990**, *35*, 129-141.

47. Butour, J. L.; Macquet, J. P. *Eur. J. Biochem.* **1977**, *78*, 455-463.

48. Kleinwachter, V.; Rau, H. *Studia Biophysica* **1984**, *103*, 5-12.

49. Horacek, P.; Drobnik, J. *Biochim. Biophys. Acta* **1971**, *254*, 341-347.

50. Vrana, O.; Brabec, V.; Kleinwachter, V. *Anticancer Drug Desgin* **1986**, *1*, 95-109.

51. Coste, F.; Malinge, J.-M.; Serre, L.; Shepard, W.; Roth, M.; Leng, M.; Zelwer, C. *Nucleic Acids Res.* **1999**, *27*, 1837-1846.

52. Marzilli, L. G.; Saad, J. S.; Kuklenyik, Z.; Keating, K. A.; Xu, Y. *J. Am. Chem. Soc.* **2001**, *123*, 2764-2770.

53. Ohndorf, U.-M.; Rould, M. A.; He, Q.; Pabo, C. O.; Lippard, S. J. *Nature* **1999**, *399*, 708-712.

54. Yang, D.; van Boom, S.; Reedijk, J.; van Boom, J.; Wang, A. *Biochemistry* **1995**, *34*, 12912-12920.

55. Gelasco, A.; Lippard, S. J. In *Topics in Biological Inorganic Chemistry*; Clarke, M., Sadler, P. J., Eds.; Springer-Verlag: Heidelberg, 1999; Vol. 1, pp 1-43.

56. Takahara, P. M.; Rosenzweig, A. C.; Frederick, C. A.; Lippard, S. J. *Nature (London)* **1995**, *377*, 649-652.

57. Huang, H.; Zhu, L.; Drobny, G. P.; Hopkins, P. B.; Reid, B. R. *Science* **1995**, *270*, 1842-1845.

58. Paquet, F.; Perez, C.; Leng, M.; Lancelot, G.; Malinge, J.-M. *J. Biomol. Struct. Dyn.* **1996**, *14*, 67-77.

59. Berners-Price, S. J.; Ranford, J. D.; Sadler, P. J. *Inorg. Chem.* **1994**, *33*, 5842-5846.

60. Chottard, J. C.; Girault, J.-P.; Chottard, G.; Lallemand, J.-Y.; Mansuy, D. *J. Am. Chem. Soc.* **1980**, *102*, 5565-5572.

61. den Hartog, J. H. J.; Altona, C.; Chottard, J.-C.; Girault, J.-P.; Lallemand, J.-Y.; de Leeuw, F. A.; Marcelis, A. T. M.; Reedijk, J. *Nucleic Acids Res.* **1982**, *10*, 4715-4730.

62. den Hartog, J. H. J.; Altona, C.; van der Marel, G. A.; Reedijk, J. *Eur. J. Biochem.* **1985**, *147*, 371-379.

63. Girault, J.-P.; Chottard, G.; Lallemand, J.-Y.; Chottard, J.-C. *Biochemistry* **1982**, *21*, 1352-1356.

64. Kozelka, J.; Fouchet, M. H.; Chottard, J.-C. *Eur. J. Biochem.* **1992**, *205*, 895-906.

65. Neumann, J.-M.; Tran-Dinh, S.; Girault, J.-P.; Chottard, J.-C.; Huynh-Dinh, T.; Igolen, J. *Eur. J. Biochem.* **1984**, *141*, 465-472.

66. Cramer, R. E.; Dahlstrom, P. L. *J. Am. Chem. Soc.* **1979**, *101*, 3679-3681.

67. Cramer, R. E.; Dahlstrom, P. L.; Seu, M. J. T.; Norton, T.; Kashiwagi, M. *Inorg. Chem.* **1980**, *19*, 148-154.

68. Dijt, F. J.; Canters, G. W.; den Hartog, J. H.; Marcelis, A. T. M.; Reedijk, J. *J. Am. Chem. Soc.* **1984**, *106*, 3644-3647.

69. Ano, S. O.; Intini, F. P.; Natile, G.; Marzilli, L. G. *Inorg. Chem.* **1999**, *38*, 2989-2999.

70. Ano, S. O.; Intini, F. P.; Natile, G.; Marzilli, L. G. *J. Am. Chem. Soc.* **1997**, *119*, 8570-8571.

71. Kiser, D.; Intini, F. P.; Xu, Y.; Natile, G.; Marzilli, L. G. *Inorg. Chem.* **1994**, *33*, 4149-4158.

72. Xu, Y.; Natile, G.; Intini, F. P.; Marzilli, L. G. *J. Am. Chem. Soc.* **1990**, *112*, 8177-8179.

73. Alessio, E.; Zangrando, E.; Roppa, R.; Marzilli, L. G. *Inorg. Chem.* **1998**, *37*, 2458-2463.

74. Ano, S. O.; Intini, F. P.; Natile, G.; Marzilli, L. G. *J. Am. Chem. Soc.* **1998**, *120*, 12017-12022.

75. Williams, K. M.; Cerasino, L.; Natile, G.; Marzilli, L. G. *J. Am. Chem. Soc.* **2000**, *122*, 8021-8030.

76. Sullivan, S. T.; Ciccarese, A.; Fanizzi, F. P.; Marzilli, L. G. *Inorg. Chem.* **2001**, *40*, 455-462.

77. Vzorov, A. N.; Bhattacharyya, D.; Marzilli, L. G.; Compans, R. W. *Antiviral Research* **2005**, *65*, 57-67.

78. Marzilli, L. G.; Intini, F. P.; Kiser, D.; Wong, H. C.; Ano, S. O.; Marzilli, P. A.; Natile, G. *Inorg. Chem.* **1998**, *37*, 6898-6905.

79. Marzilli, L. G.; Ano, S. O.; Intini, F. P.; Natile, G. *J. Am. Chem. Soc.* **1999**, *121*, 9133-9142.

80. Ciccarese, A.; Clemente, D. A.; Fanizzi, F. P.; Marzotto, A.; Valle, G. *Inorg. Chim. Acta* **1998**, *275-276*, 410-418.

81. Wong, H. C.; Shinozuka, K.; Natile, G.; Marzilli, L. G. *Inorg. Chim. Acta* **2000**, *297*, 36-46.

82. Benedetti, M.; Tamasi, G.; Cini, R.; Marzilli, L. G.; Natile, G. *Chem. Eur. J.* **2007**, *13*, 3131-3142.

83. Marcelis, A. T. M.; van der Veer, J. L.; Zwetsloot, J. C. M.; Reedijk, J. *Inorg. Chim. Acta* **1983**, *78*, 195-203.

84. Carlone, M.; Fanizzi, F. P.; Intini, F. P.; Margiotta, N.; Marzilli, L. G.; Natile, G. *Inorg. Chem.* **2000**, *39*, 634-641.

85. Elizondo-Riojas, M.-A.; Kozelka, J. *Inorg. Chim. Acta* **2000**, *297*, 417-420.

86. Sullivan, S. T.; Ciccarese, A.; Fanizzi, F. P.; Marzilli, L. G. *Inorg. Chem.* **2000**, *39*, 836-842.

87. Sullivan, S. T.; Ciccarese, A.; Fanizzi, F. P.; Marzilli, L. G. *J. Am. Chem. Soc.* **2001**, *123*, 9345-9355.

88. Saad, J. S.; Scarcia, T.; Shinozuka, K.; Natile, G.; Marzilli, L. G. *Inorg. Chem.* **2002**, *41*, 546-557.

89. Williams, K. M.; Cerasino, L.; Intini, F. P.; Natile, G.; Marzilli, L. G. *Inorg. Chem.* **1998**, *37*, 5260-5268.

90. Margiotta, N.; Papadia, P.; Fanizzi, F. P.; Natile, G. *European Journal of Inorganic Chemistry* **2003**, 1136-1144.

91. Sundquist, W.; Lippard, S. J. *Coord. Chem. Rev.* **1990**, *100*, 293-322.

92. Cusumano, M.; Di Pietro, M. L.; Giannetto, A. *Inorg. Chem.* **1999**, *38*, 1754-1758.

93. Wang, A. H. J.; Nathans, J.; Van der Marel, G.; Van Boom, J. H.; Rich, A. *Nature (London)* **1978**, *276*, 471-474.

94. Cusumano, M.; Giannetto, A. *J. Inorg. Biochem.* **1997**, *65*, 137-144.
95. Brodie, C. R.; Collins, J. G.; Aldrich-Wright, J. R. *Dalton Transactions* **2004**, *8*, 1145-1152.

96. Collins, J. G.; Rixon, R. M.; Wright, J. R. A. *Inorg. Chem.* **2000**, *39*, 4377-4379.

97. Jaramillo, D.; Buck, D. P.; Collins, J. G.; Fenton, R. R.; Stootman, F. H.; Wheate, N. J.; Aldrich-Wright, J. R. *European Journal of Inorganic Chemistry* **2006**, 839-849.

98. Wilson, W. D.; Jones, R. L. In *Intercalation Chemistry*; Wittingham, N. S., Jacobson, A. J., Eds.; Academic Press: New York, 1982, pp 445-501.

99. Cusumano, M.; Di Pietro, M. L.; Giannetto, A.; Vainiglia, P. A. *J. Inorg. Biochem.* **2005**, *99*, 560-565.

100. Heng-Qian, L.; Shei-Ming, P.; Chi Ming, C. *J. Chem. Soc. Chem. Commun.* **1995**, *5*, 509-510.

101. Zamble, D. B.; Lippard, S. J. In *Cisplatin: Chemistry and Biochemistry of a Leading Anticancer Drug*; Lippert, B., Ed.; Wiley-VCH: Weinheim, 1999, pp 73-110.

102. Pil, P.; Lippard, S. J. *Science* **1992**, *256*, 234-237.

CHAPTER 2. CHEMISTRY OF HIV-1 VIRUCIDAL Pt COMPLEXES HAVING NEGLECTED BIDENTATE sp^2 N-DONOR CARRIER LIGANDS WITH LINKED TRIAZINE AND PYRIDINE RINGS: SYNTHESIS, NMR SPECTRAL FEATURES, STRUCTURE, AND REACTION WITH GUANOSINE*

2.1 Introduction

In comparison to agents of purely organic molecules, considerably less effort has been devoted to studying metal-containing drugs. Platinum complexes, which have been found to be the most promising,[1-7] have the advantages of inertness, low coordination number, and preferential binding to the more limited soft centers in proteins and nucleic acids. The non-leaving carrier ligand on Pt can modify binding sites and thus activity. Cisplatin (*cis*-$Pt(NH_3)_2Cl_2$) and its analogues, *cis*-PtA_2X_2 (A_2 = two amines or a diamine), interact with DNA by forming a 1,2-intrastrand N7–Pt–N7 crosslink between two adjacent guanines.[8] Pt(II) compounds also have an extensive history of exhibiting antiviral activity against numerous viruses, including topical antiviral activity.[9-15] In addition, we have clear evidence that the carrier ligand influences the antiviral activity.[13] Structural modifications of the carrier ligand in cisplatin may broaden the range of antitumor and antiviral activity and may provide valuable insight into the mechanism of action of the drug.[3,16]

Development of multi-purpose drugs with wider application is desirable. Numerous platinum coordination compounds have been synthesized and shown to have both antiviral and antitumor activities.[14] Hybrid drugs of the type, *cis*-$[Pt(NH_3)_2(B)Cl]^+$, containing a cisplatin-like moiety and an antiviral guanosine-type ligand (B = acyclovir or penciclovir),[14,15] are known.

---

* Reproduced with permission from American Chemical Society: Maheshwari, V.; Bhattacharyya, D.; Fronczek, F. R.; Marzilli, P. A.; Marzilli, L. G., "Chemistry of HIV-1 Virucidal Pt Complexes Having Neglected Bidentate sp^2 N-donor Carrier Ligands with Linked Triazine and Pyridine Rings. Synthesis, NMR Spectral Features, Structure, and Reaction with Guanosine," *Inorganic Chemistry*, **2006**, 45, 7182-7190. Copyright 2006 American Chemical Society.

Collaborative studies from this laboratory have shown that platinum compounds containing one or two N-donor aromatic 3-(pyridin-2′-yl)-1,2,4-triazine ligands (**ptt**) possess great potential as anti-HIV microbicides.[13]

The $[(\mathbf{ferene})PtCl_2]^{2-}$ and $[(\mathbf{ferene})_2Pt]^{2-}$ (**ferene** = 3-(pyridin-2′-yl)-5,6-bis(5-sulfo-2-furyl)-1,2,4-triazine; in Figure 2.1, $R^2 = R^3$ = 5-sulfo-2-furyl) complexes are among the most virucidal **ptt** compounds.[13] However, these agents with sulfonated ring substituents were not isolated as crystals, have very complicated ^1H NMR spectra, and thus were not well defined chemically. For example, the triazine ring binding mode (N2 or N4, Figure 2.1) or a mixture of such binding modes, could not be resolved for the **ferene** agents.

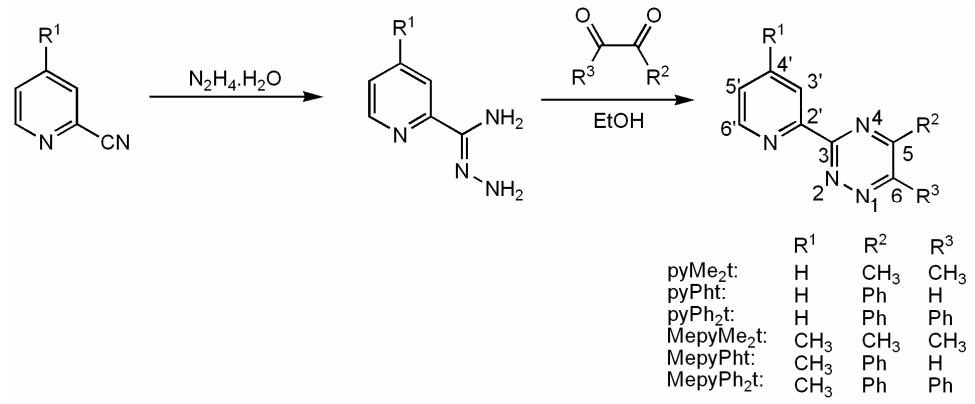

	R^1	R^2	R^3
$pyMe_2t$:	H	CH_3	CH_3
pyPht:	H	Ph	H
$pyPh_2t$:	H	Ph	Ph
$MepyMe_2t$:	CH_3	CH_3	CH_3
MepyPht:	CH_3	Ph	H
$MepyPh_2t$:	CH_3	Ph	Ph

Figure 2.1 Synthesis of 3-(Pyridin-2′-yl)-5,6-disubstituted-1,2,4-triazine (**L**)

In this study, we utilize six ligands, **L**, bearing a 3-(pyridin-2′-yl)-1,2,4-triazine moiety (Figure 2.1). Three ligands contain the pyridin-2′-yl group: 3-(pyridin-2′-yl)-5,6-dimethyl-1,2,4-triazine (**$pyMe_2t$**), 3-(pyridin-2′-yl)-5-phenyl-1,2,4-triazine (**pyPht**), and 3-(pyridin-2′-yl)-5,6-diphenyl-1,2,4-triazine (**$pyPh_2t$**)), and the other three ligands contain the 4′-methylpyridin-2′-yl group: 3-(4′-methylpyridin-2′-yl)-5,6-dimethyl-1,2,4-triazine (**$MepyMe_2t$**), 3-(4′-methylpyridin-2′-yl)-5-phenyl-1,2,4-triazine (**MepyPht**), and 3-(4′-methylpyridin-2′-yl)-5,6-diphenyl-1,2,4-triazine (**$MepyPh_2t$**)). We describe here the synthesis of $\mathbf{L}PtCl_2$ and $[\mathbf{L}_2Pt]X_2$ complexes (Figure

2.2), along with their characterization by ^{1}H NMR spectroscopy and, for selected examples, by single-crystal X-ray diffraction methods. The pyridyl triazines are relatively neglected ligands; no crystal structures involving 3-(pyridin-2′-yl)-1,2,4-triazines with Pt have been reported. However, crystal structures of **pyPh$_2$t** complexes of Cu,[17] Sn,[18] and Ru[19] have been reported. Also known is a crystal structure of $[Ce(\mathbf{Mebtp})_3]^{3+}$ (**Mebtp** = 2,6-bis(5,6-dimethyl-1,2,4-triazin-3-yl)-pyridine) complex with the **Mebtp** tridentate ligand containing the **pyMe$_2$t** moiety.[20]

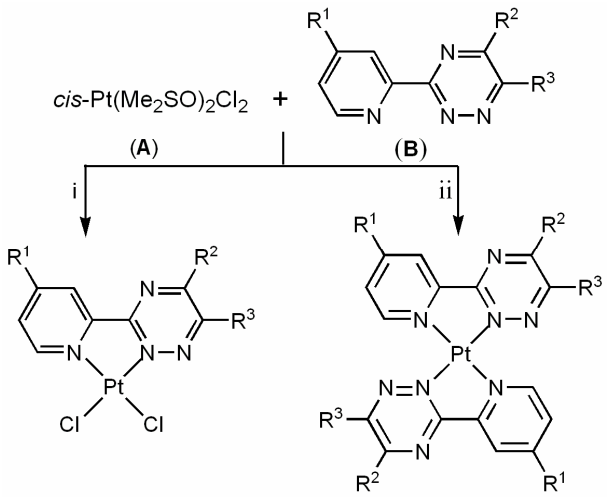

Figure 2.2 Synthesis of **L**$PtCl_2$ and $[\mathbf{L}_2Pt]^{2+}$ Complexes. Reagents and conditions: (i) A:B = 1:1, CH_3OH, 60 °C, 12 h; (ii) A:B = 1:2, CH_3OH, 60 °C, 24 h.

Pt(II) compounds have high affinity for reacting with S-containing biomolecules such as methionine and also with N7 of purine bases in nucleic acids, but the target for virucidal activity is not known. Carrier-ligand bulk plays a role in influencing both biological activity and the properties of adducts. Because platinum complexes of 3-(pyridin-2′-yl)-1,2,4-triazines may form 1,2-intrastrand GG crosslinks with RNA in HIV-1 and because the observation of rotamers formed by restricted rotation about the N7 bonds in $Pt(Guo)_2$ adducts provides information on ligand steric bulk, we assessed whether rotamers can be detected for $[(\mathbf{MepyMe_2t})Pt(Guo)_2]^{2+}$. The carrier ligands in cisplatin and other Pt(II) anticancer drugs usually are not bulky enough to impede rotation of N7-bound guanine about the Pt–N7 bond, but planar sp^2 N-donor ligands such

as 5,5′-dimethyl-2,2′-bipyridine (**5,5′-Me$_2$bipy**)[21] and 1,10-phenanthroline (**phen**)[22] allow detection of rotamers on the NMR time scale. The aromatic portion of the 3-(pyridin-2′-yl)-1,2,4-triazine carrier ligands in **ptt** compounds can also possibly intercalate into nucleic acids.[23] Thus, all these reasons prompted us to conduct this study of the synthesis and characterization of **ptt** compounds related to **ptt** compounds with **ferene** that are known to be HIV-1 virucidal.[13]

2.2 Experimental Section

2.2.1 Starting Materials

The starting material, pyridine-2-carboxamide hydrazone (2-pyridylamidrazone), was synthesized by a known method[24] (Figure 2.1) in yields above 90%. 4′-Methyl-substituted pyridine-2-carboxamide hydrazone (4′-methyl-2-pyridylamidrazone) was synthesized as described by Case.[25] Guanosine (Guo) (Sigma) and **pyPh$_2$t** (Fluka) were obtained from commercial sources. *cis*-Pt(Me$_2$SO)$_2$Cl$_2$ was prepared as described in the literature.[26] Elemental analyses (C,H,N) were performed by Atlantic Microlabs, Atlanta, GA.

2.2.2 NMR Measurements

^{1}H NMR spectra were recorded on Bruker spectrometers operating at 400 or 500 MHz. We used the values of 0.00 and 4.78 ppm to reference signals to TMS in DMSO-d_6 solutions and to the residual HOD signal in D$_2$O/DMSO-d_6 solutions, respectively. DNO$_3$ and NaOD solutions (0.1 M in D$_2$O) were used to adjust the pH of D$_2$O/DMSO-d_6 solutions. 2D ROESY experiments[27] were performed at 25 °C by using a 500 ms mixing time (128 scans per t_1 increment). NMR data were processed with XWINNMR or Mestre-C software.

2.2.3 Synthesis of L = 3-(Pyridin-2′-yl)-5,6-disubstituted-1,2,4-triazine and 3-(4′-Methylpyridin-2′-yl)-5,6-disubstituted-1,2,4-triazine

The **pyMe$_2$t, pyPht, pyPh$_2$t** ligands and their 3-(4-methylpyridin-2′-yl) analogues, **MepyMe$_2$t, MepyPht,** and **MepyPh$_2$t,** were prepared as described in the literature[25,28,29] (Figure

2.1), with minor modifications. An ethanol solution (30 mL) containing 2-pyridylamidrazone, or its 4′-methyl analogue (2.5 mmol), and an α-diketone (2.5 mmol) was heated at reflux for 3 h. The volume of the solution was reduced to one-fourth by rotary evaporation. Addition of an excess of hexane afforded the desired pure crystalline 3-(pyridin-2′-yl)-1,2,4-triazine in 90% yield.

2.2.4 Synthesis of $LPtCl_2$ Complexes

Two methods, A and B, were employed to obtain **L**$PtCl_2$ complexes (Figure 2.2). Method A involved heating a methanol solution (30 mL) of *cis*-$Pt(Me_2SO)_2Cl_2$ (0.101 g, 0.24 mmol) and **L** (0.24 mmol) at 60 °C for 12 h. The yellow solid that precipitated was collected, washed with diethyl ether followed by chloroform, and dried in vacuo. Method A resulted in high yields of powdered **L**$PtCl_2$ product that required no further purification. Method B, employed to obtain X-ray quality crystals, involved mixing an acetonitrile solution of *cis*-$Pt(Me_2SO)_2Cl_2$ (4.22 mg,10 mM in 1 mL) with **L** (10 mM in 1 mL) and allowing this mixture to stand at 23 °C. Thin needles of **L**$PtCl_2$, varying in color from greenish-yellow to orange, were obtained in ~15% yield after 24 hours.

2.2.4.1 ($pyMe_2t$)$PtCl_2$ (1). Method A gave a yellow precipitate; yield, 0.077 g (71%). Method B afforded orange needle-shaped crystals. ^{1}H NMR (ppm) in DMSO-d_6 : 9.57 (d, H6′), 8.60 (d, H3′), 8.48 (t, H4′), 8.03 (t, H5′), 2.75 (s, CH_3), 2.59 (s, CH_3). Anal. Calcd for $C_{10}H_{10}Cl_2N_4Pt$: C, 26.56; H, 2.23; N, 12.39. Found: C, 26.77; H, 2.29; N, 12.37.

2.2.4.2 (pyPht)$PtCl_2$ (2). Method A gave a yellow powder; yield, 0.084g (75%). Method B produced yellow-green needles. ^{1}H NMR (ppm) in DMSO-d_6: 10.18 (s, H6), 9.62 (d, H6′), 8.78 (d, H3′), 8.54 (t, H4′), 8.11 (t, H5′), 8.64 (d, *o*-PhH), 7.85 (t, *p*-PhH), 7.71 (t, *m*-PhH). Anal. Calcd for $C_{14}H_{10}Cl_2N_4Pt$: C, 33.61; H, 2.01; N, 11.20. Found: C, 33.48; H, 1.95; N, 11.10.

2.2.4.3 (pyPh$_2$t)PtCl$_2$ (3). Method A gave a yellow solid; yield, 0.099 g (83%). Orange needles were obtained by method B. ^{1}H NMR (ppm) in DMSO-d_6: 9.63 (d, H6′), 8.62 (d, H3′), 8.53 (t, H4′), 8.09 (t, H5′), 7.38-7.51 (PhH). Anal. Calcd for $C_{20}H_{14}Cl_2N_4Pt$: C, 41.68; H, 2.45; N, 9.72. Found: C, 41.45; H, 2.37; N, 9.80.

2.2.4.4 (MepyMe$_2$t)PtCl$_2$ (4). Method A resulted in a yellow powder; yield, 0.096 g (77%). X-ray quality crystals in the form of yellow needles were obtained by method B. ^{1}H NMR (ppm) DMSO-d_6: 9.35 (d, H6′), 8.26 (s, H3′), 7.85 (d, H5′), 2.74 (s, CH_3), 2.57 (s, CH_3), 2.53 (s, CH_3). Anal. Calcd for $C_{11}H_{12}Cl_2N_4Pt$: C, 28.34; H, 2.59; N, 12.02. Found: C, 28.32; H, 2.58; N, 11.82.

2.2.4.5 (MepyPht)PtCl$_2$ (5). The complex was obtained as a yellow powder by method A; yield, 0.095 g (68%). ^{1}H NMR (ppm) in DMSO-d_6: 10.15 (s, H6), 9.41 (d, H6′), 8.61 (s, H3′), 7.91 (d, H5′), 8.65 (d, *o*-PhH), 7.84 (t, *p*-PhH), 7.70 (t, *m*-PhH), 2.59 (s, CH_3). Anal. Calcd for $C_{15}H_{12}Cl_2N_4Pt$: C, 35.03; H, 2.35; N, 10.89. Found: C, 34.81; H, 2.31; N, 10.65.

2.2.4.6 (MepyPh$_2$t)PtCl$_2$ (6). Method A resulted in a reddish-yellow precipitate; yield, 0.112 g (79%). Method B produced yellow needles. ^{1}H NMR (ppm) in DMSO-d_6: 9.44 (d, H6′), 8.49 (s, H3′), 7.93 (d, H5′), 7.75 (d, *o*-PhH), 7.45-7.63 (*m*, *p*-PhH), 2.58 (s, CH_3). Anal. Calcd for $C_{21}H_{16}Cl_2N_4Pt$: C, 42.72; H, 2.73; N, 9.49. Found: C, 42.75, H, 2.58; N, 9.43.

2.2.5 Synthesis of [L$_2$Pt]X$_2$ Salts

cis-Pt(Me$_2$SO)$_2$Cl$_2$ (0.042 g, 0.1 mmol) was added to a methanol solution of **L** (0.4 mmol, 10 mL) and the resulting suspension became a solution when stirred at 60 °C for 24 h (Figure 2.2). The mixture was allowed to cool to room temperature. Any precipitate that formed was removed by filtration, and the clear filtrate was treated with a methanol solution of an excess of $NaBF_4$ or $NaPF_6$ to precipitate the [**L**$_2$Pt]X$_2$ salt. The solid was collected, washed twice with

methanol followed by anhydrous diethyl ether and allowed to dry in air. Yields of the [$\mathbf{L}_2$Pt]X_2 salts were 35-45%. The ^{1}H NMR spectra and shifts for representative [$\mathbf{L}_2$Pt]X_2 complexes appear in Supporting Information.

2.2.5.1 [(pyPht)$_2$Pt](PF$_6$)$_2$ (7). The method described above afforded a yellow solid upon addition of an excess of $NaPF_6$; yield, 0.30 g (36%). The ^{1}H NMR spectra of the BF_4 and PF_6 salts were identical. Anal. Calcd for $C_{28}H_{20}N_8P_2F_{12}Pt$: C, 35.27; H, 2.11; N, 11.75. Found: C, 35.54; H, 1.89; N, 11.85.

2.2.5.2 [(pyPh$_2$t)$_2$Pt](BF$_4$)$_2$ (8). Crystals were obtained by the general method described above, but by very careful dropwise addition of a methanol solution of $NaBF_4$ (5 mmol) to the filtrate, until the solution first became cloudy. Thin, yellow, needle-shaped crystals were obtained by allowing the solution to stand undisturbed for 2 days.

2.2.5.3 [(MepyPh$_2$t)$_2$Pt](PF$_6$)$_2$ (9). This product was obtained as a yellow solid in the same way as for (**7**); yield, 0.041 g (40%). The ^{1}H NMR spectra of the BF_4 and PF_6 salts were identical. Anal. Calcd for $C_{42}H_{32}N_8P_2F_{12}Pt$: C, 44.49; H, 2.84; N, 9.88. Found: C, 44.58; H, 2.68; N, 9.94.

2.2.6 Reaction of ptt's with Guo

A 14 mM (1.63 mg) solution of (**MepyMe$_2$t**)$PtCl_2$ (**4**) in DMSO-d_6 (250 μL) was treated with a Guo solution (1.98 mg, 15.5 mM in 450 μL of D_2O) to give a 1:2 ratio (5 mM: 10 mM) of Pt:Guo, and the solution (pH ~4.6) was kept at 25 °C. The mixture of D_2O and DMSO-d_6 solutions was used to improve the solubility of **4**. The pH of the solution decreased with time and had to be adjusted to ~4.6. The solution was monitored for six days until the ^{1}H NMR signals of free Guo disappeared. However, the reaction was repeated several times, and to decrease the time for the reaction to reach completion, an excess of Guo was often employed. A DMSO-d_6

solution (250 μL) of [(**MepyMe$_2$t**)$_2$Pt](BF$_4$)$_2$ (2.69 mg, 14 mM) was treated with Guo (1.98 mg, 15.5 mM) solution in D_2O (450 μL) to give a 1:2 ratio of Pt:Guo, and the solution maintained at pH ~4.6 at 25 °C. The solution was monitored by ^{1}H NMR spectroscopy, and no evidence of any reaction was found even after 36 h.

2.2.7 X-ray Data Collection and Structure Determination

Single crystals were placed in a cooled nitrogen gas stream at ~100 K on a Nonius Kappa CCD diffractometer fitted with an Oxford Cryostream cooler with graphite-monochromated Mo Kα (0.71073 Å) radiation. Data reduction included absorption corrections by the multi-scan method, with HKL SCALEPACK.[30]

All X-ray structures were determined by direct methods and difference Fourier techniques and refined by full-matrix least squares, using SHELXL97.[31] All non-hydrogen atoms were refined anisotropically. All H atoms were visible in difference maps, but were placed in idealized positions. A torsional parameter was refined for each methyl group. For all structures, maximum residual densities were located near the Pt positions.

2.3 Results and Discussion

2.3.1 X-ray Crystallography

Structures of pseudo square-planar complexes reported here include **L**PtCl$_2$ (**L = pyMe$_2$t**, **pyPht**, **pyPh$_2$t**), and [(**pyPh$_2$t**)$_2$Pt](BF$_4$)$_2$ (Tables 2.1 and 2.2; Figures 2.3 and 2.4). The atom numbering systems in these ORTEP figures are used to discuss the solid-state structures. A superscript i denotes the atoms of the other ligand in [**L**$_2$Pt]X$_2$ salts. When referring to the X-ray numbering system, the number will appear in parentheses, whereas for other purposes (e.g., NMR discussion) we shall use the general numbering system in Figure 2.1, and the number will not be enclosed in parentheses. Likewise, in some cases we shall designate the Pt-bound N's as

N(t) and N(py), in the triazine and pyridine rings, respectively. The numbering scheme for bipyridines is given below in Figure 2.5.

Table 2.1 Crystal Data and Structure Refinement for **L**$PtCl_2$ (**L = pyMe$_2$t** (**1**)**, pyPht** (**2**)**, pyPh$_2$t** (**3**)) and [(**pyPh$_2$t**)$_2$Pt]$(BF_4)_2$ (**8**)

	(**pyMe$_2$t**)$PtCl_2$	(**pyPht**)$PtCl_2$	(**pyPh$_2$t**)$PtCl_2$	[(**pyPh$_2$t**)$_2$Pt] $(BF_4)_2$
Empirical formula	$C_{10}H_{10}Cl_2N_4Pt$	$C_{14}H_{10}Cl_2N_4Pt$	$C_{20}H_{14}Cl_2N_4Pt{\cdot}CH_3CN$	$C_{40}H_{28}B_2F_8N_8Pt{\cdot}0.59H_2O$
Fw	452.21	500.25	617.40	1000.00
space group	P*bca*	$P2_1/c$	$P2_1/c$	$C2/c$
Unit cell dimensions				
a (Å)	7.3055 (10)	9.236 (5)	10.202 (2)	35.253 (5)
b (Å)	17.923 (4)	7.496 (4)	7.4820 (10)	7.8417 (15)
c (Å)	17.977 (4)	19.789 (13)	27.278 (7)	13.811 (3)
β (°)	90	94.312 (18)	93.513 (7)	99.270 (7)
V (Å^3)	2353.8 (8)	1366.2 (14)	2078.3 (7)	3768.1 (12)
T (K)	102	100	100	110
Z	8	4	4	4
ρ_{calc} (mg/m^3)	2.552	2.432	1.973	1.763
abs coeff (mm^{-1})	12.356	10.658	7.029	3.809
$2\theta_{max}$ (°)	65.2	55.0	63.0	56.6
R indices[a]	0.029	0.062	0.034	0.033
wR2 = [$I > 2\sigma(I)$][b]	0.060	0.155	0.059	0.065
data/param	4267/157	3085/190	6483/272	4639/275

[a] $R = (\sum||F_o| - |F_c||)/\sum|F_o|$; [b] $wR2 = [\sum[w(F_o^2 - F_c^2)^2]/\sum[w(F_o^2)^2]]^{1/2}$, in which $w = 1/[\sigma^2(F_o^2) + (0.0787P)^2]$ and $P = (F_o^2 + 2F_c^2)/3$

Table 2.2 Selected Bond Distances (Å) and Angles (deg) for **L**$PtCl_2$ (**L = pyMe$_2$t** (**1**)**, pyPht** (**2**)**, pyPh$_2$t** (**3**)) and [(**pyPh$_2$t**)$_2$Pt]$(BF_4)_2$ (**8**)

	(**pyMe$_2$t**)$PtCl_2$	(**pyPht**)$PtCl_2$	(**pyPh$_2$t**)$PtCl_2$	[(**pyPh$_2$t**)$_2$Pt]$(BF_4)_2$
		bond distances		
Pt–N(1)	2.001(3)	1.996(11)	1.996(3)	2.019(3)
Pt–N(4)	2.020(3)	2.011(11)	2.027(3)	2.050(3)
Pt–Cl(1)	2.2969(11)	2.304(4)	2.2920(10)	Pt–N(4)^i 2.050(3)
Pt–Cl(2)	2.2899(10)	2.292(4)	2.2972(10)	Pt–N(1)^i 2.019(3)
		bond angles		
N(4)–Pt–N(1)	80.33(12)	79.8(4)	80.38(11)	78.68(13)
N(1)–Pt–Cl(1)	174.83(9)	173.3(3)	174.90(8)	N(1)–Pt–N(1)^i 180.0
N(1)–Pt–Cl(2)	96.05(9)	96.2(3)	95.86(8)	N(1)–Pt–N(4)^i 101.32(13)
N(4)–Pt–Cl(1)	94.50(10)	93.8(3)	94.60(8)	N(4)–Pt–N(1)^i 101.32(13)
N(4)–Pt–Cl(2)	176.30(9)	176.0(3)	176.24(8)	N(4)–Pt–N(4)^i 180.0
Cl(2)–Pt–Cl(1)	89.13(3)	90.12(13)	89.16(3)	N(4)^i–Pt–N(1)^i 78.68(13)
C(5)–C(4)–C(3)	123.0(3)	124.7(13)	122.9(3)	123.1(4)
N(4)–C(4)–C(3)	114.1(3)	113.6(12)	114.5(3)	114.4(3)
N(3)–C(3)–C(4)	120.1(3)	119.4(12)	121.0(3)	120.6(3)
N(1)–C(3)–C(4)	114.8(3)	114.2(11)	115.0(3)	114.6(3)

In order to discuss structural features of the pyridyl triazine ligands, we shall use some of the terminology employed for the common symmetrical sp^2 N-donor **L**'s, e.g. 2,2′-bipyridine (**bipy**) or **phen** ligands. The M–N distance for which there would be no in-plane distortion (Figure 2.5) has been estimated to be 2.72 Å.[32] Hazell concluded that the stress in coordinated 2,2′-bipyridines caused by the close proximity of the hydrogen atoms on the carbons *ortho* to the bridging atoms is reduced by the twisting of the pyridine rings about the bond bridging the two pyridine rings and by an in-plane bending (Figure 2.5).[33] Likewise, in compounds such as

[(**bipy**)$_2$Pt]$^{2+}$ the M–N distance for which there would be no distortion of the overall coordination environment from planarity has been estimated to be 2.8 Å.[34] Therefore, we begin our discussion of the structures with bond lengths and angles involving Pt.

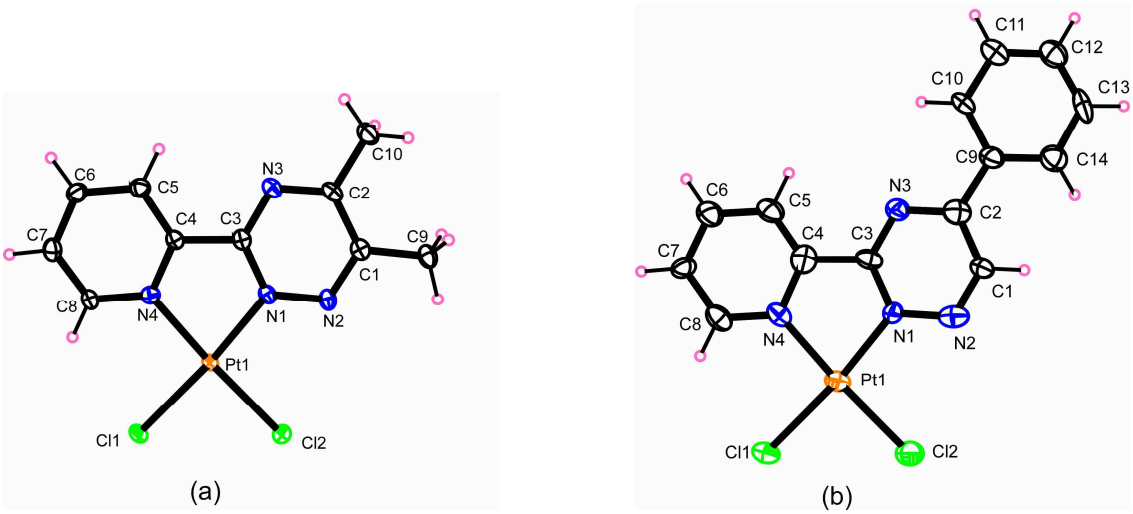

Figure 2.3 ORTEP plots of (a) (**pyMe$_2$t**)PtCl$_2$ (**1**) and (b) (**pyPht**)PtCl$_2$ (**2**). Thermal ellipsoids are drawn with 50% probability.

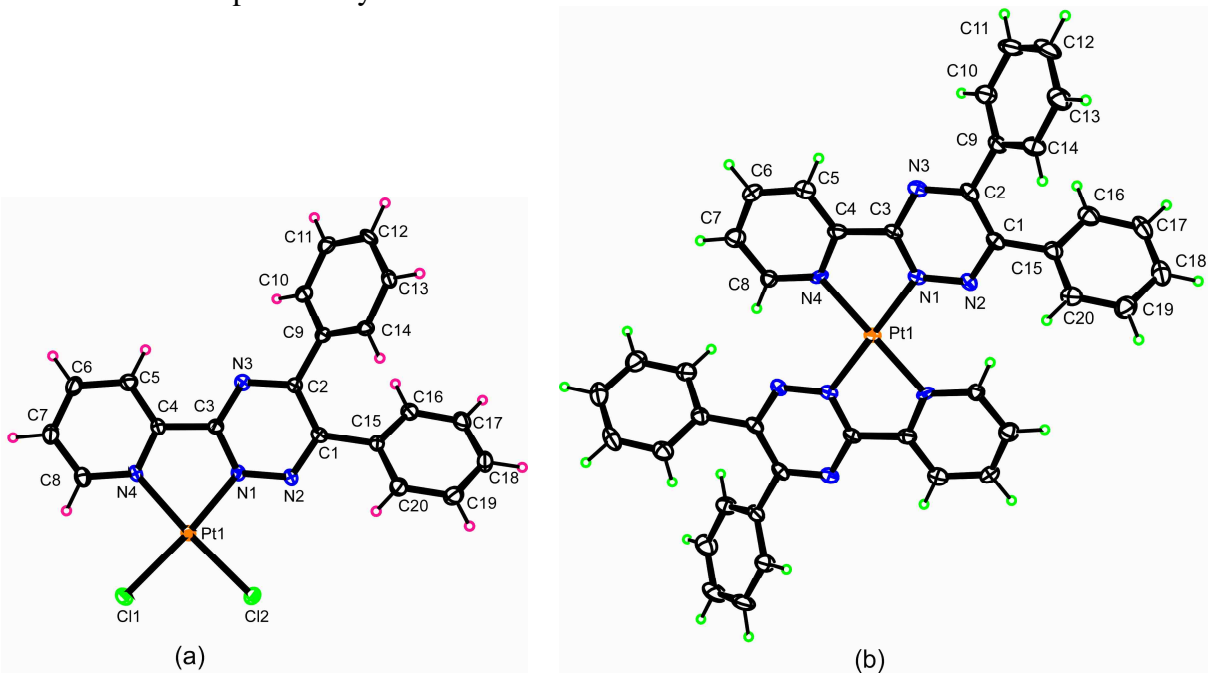

Figure 2.4 ORTEP plots of (a) (**pyPh$_2$t**)PtCl$_2$ (**3**) and (b) [(**pyPh$_2$t**)$_2$Pt](BF$_4$)$_2$ (**8**). Thermal ellipsoids are drawn with 50% probability.

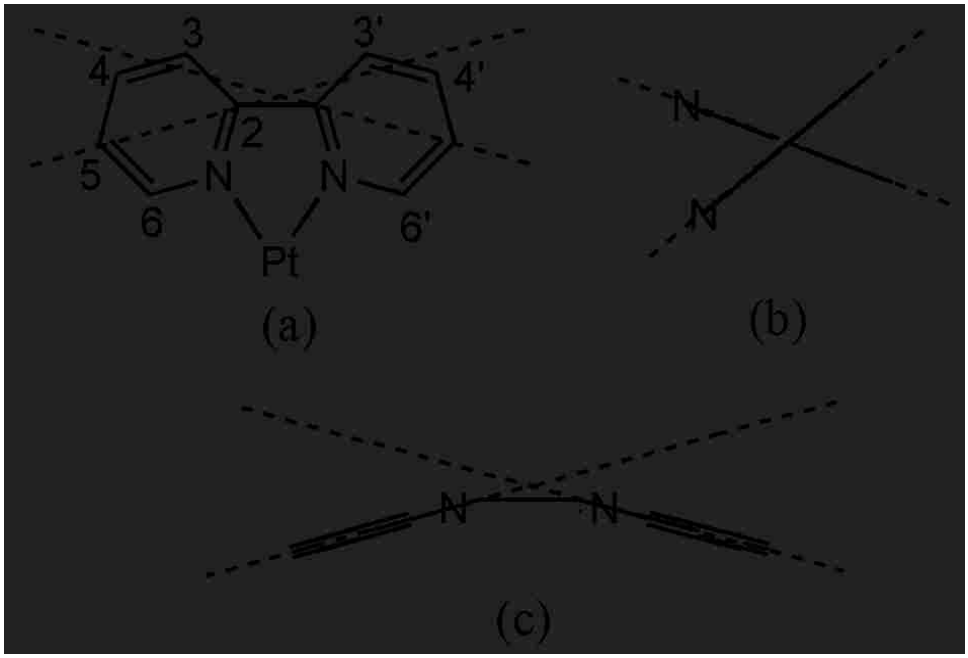

Figure 2.5 Distortions in bipyridyl ligands: (a) in-plane, (b) twist, and (c) bowing.

2.3.1.1 Structures of $LPtCl_2$

- **Coordination Parameters**. The size of the group on the C(1) and C(2) positions has little effect on the coordinated bond distances and angles (Table 2.2). The Pt–Cl or Pt–N(py) bond distances found for **1**, **2**, and **3** are not significantly different from those in the structure of (**4,4′-Me$_2$bipy**)$PtCl_2$ (work in progress). All three **L**$PtCl_2$ complexes and (**4,4′-Me$_2$bipy**)$PtCl_2$ have comparable N–Pt–N bite angles. For **1** and **3**, in which the Pt–N distances are more precisely determined, the Pt–N(py) bond (Pt–N(4)) is slightly longer than the Pt–N(t) bond (Pt–N(1)) (Table 2.2). We attribute this apparently slightly smaller Pt–N(t) bond to an attractive interaction of the positive Pt center with the lone pair on N(2), the triazine N bound to N(1). In contrast, the hydrogen on the C(8) atom of the pyridine ring (in the position corresponding to N(2)) will have a repulsive interaction with the positive Pt center.

In **1**, **2**, and **3**, the cis N(t)–Pt–Cl(2) angle is significantly larger than the cis N(py)–Pt–Cl(1) angle. There is a slight attractive interaction between Cl's cis to a pyridyl ring and the

nearby pyridine ring H atom (labeled A, Figure 2.6). The repulsion (labeled R, Figure 2.6) between the lone pair on N(2) and the cis Cl creates a larger than normal N–Pt–Cl angle. The apparent net effects of the non-bonding interactions involving the lone pair are a shorter Pt–N(t) bond and a wider cis N(t)–Pt–Cl angle.

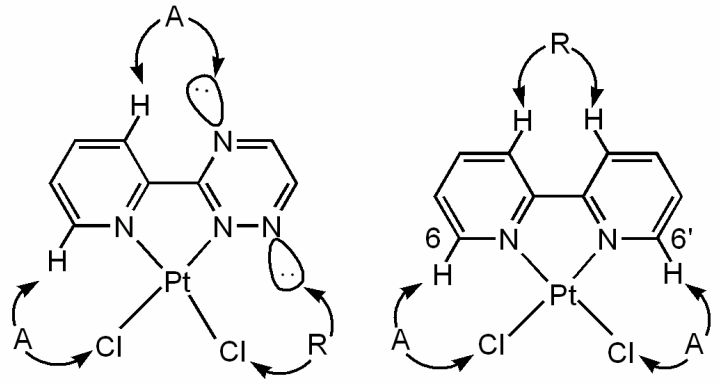

Figure 2.6 Attractive and repulsive interactions in **L**$PtCl_2$ and (**bipy**)$PtCl_2$.

- **Bidentate Ligand Parameters**. Distortions in the ligand (Figure 2.5) will occur if the M–N distance is typical (~2.0 to 2.2 Å).[33] Because the distances of the C3H and C3′H atoms of bipyridines (Figure 2.5) to the C3′ and H3′ atoms and the C3 and H3 atoms on the other ring, respectively, are less than the sum of the van der Waals radii,[35] it has been suggested that the resulting repulsive interactions (labeled R, Figure 2.6) cause distortions.[32,33] The difference in two exocyclic angles (C(5)–C(4)–C(3) and N(4)–C(4)–C(3), see Figure 2.4) of the pyridine ring can be used as a simple means for estimating the in-plane bending (Figure 2.5).[33] The differences in these two angles for (**4,4′-Me$_2$bipy**)$PtCl_2$ are comparable to the differences for **L**$PtCl_2$ complexes (Table 2.2), although for **L**$PtCl_2$ complexes the hydrogen on the pyridyl C *ortho* to the bridging carbons and the lone-pair-bearing triazine N(3) (in **3**, Figure 2.4, the H(5) to N(3) distance = 2.630 Å, and the C(5) to N(3) distance = 2.900 Å) should create a slight favorable attractive interaction (labeled A, Figure 2.6). Therefore, any stress due to H3-H3′ repulsion in

(**4,4′-Me$_2$bipy**)PtCl$_2$ does not lead to an apparent substantial effect on the in-plane bending. However, this repulsion could account for the slight twisting or bowing in (**4,4′-Me$_2$bipy**)PtCl$_2$ compared to the minimal distortions found for the three **L**PtCl$_2$ complexes (Figure 2.7).

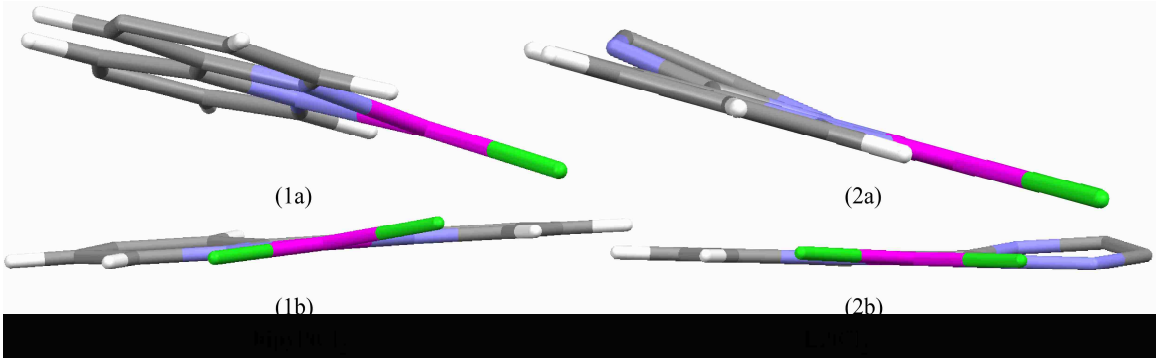

Figure 2.7 In-plane views of the two rings in **bipy**PtCl$_2$ (left) and **L**PtCl$_2$ (right).

2.3.1.2 Structure of [(pyPh$_2$t)$_2$Pt](BF$_4$)$_2$ (8)

- **Coordination Parameters**. The ORTEP drawing for **8** appears in Figure 2.4. The Pt–N(py) bond length (2.050(3) Å) in **8** is similar to the Pt–N(py) bond length (2.032(3) Å) in [(**4,4′-Me$_2$bipy**)$_2$Pt](BF$_4$)$_2$ (work in progress), but it is significantly longer than the Pt–N(t) bond distance (2.019(3) Å) in **8** (Table 2.2). The reason for the shorter Pt–N(t) bond distance was suggested above. The N–Pt–N bite angle in **8** is similar to that in [(**4,4′-Me$_2$bipy**)$_2$Pt](BF$_4$)$_2$. These N–Pt–N bite angles are slightly smaller than those for **L**PtCl$_2$ (Table 2.2). The Pt–N bond distances in **8** are larger than the corresponding bond distances in **3**.

- **Relative Bidentate Ligand Relationships**. The ligand distortion due to in-plane bending for [(**pyPh$_2$t**)$_2$Pt](BF$_4$)$_2$ (**8**) was less than that for [(**4,4′-Me$_2$bipy**)$_2$Pt](BF$_4$)$_2$ but comparable with those of **L**PtCl$_2$ (Table 2.2). For bipyridine complexes with ~2 Å M–N distances, the strain induced by the close approach of the hydrogen atoms of opposing ligands can be reduced by two different types of distortions. First, a tetrahedral deformation at the metal can occur, resulting in the ligands being canted relative to each other (Figure 2.8). Second, the ligand rings can be

bowed away from the ring directly across (Figure 2.8).[32,33,36] The opposing ligands in [(**4,4′-Me$_2$bipy**)$_2$Pt](BF$_4$)$_2$ are bowlike distorted (Figure 2.9), while canting of the two ligands occurs in [(**2,2′-bipy**)$_2$Pt](NO$_3$)$_2$.[33] In contrast, for [(**pyPh$_2$t**)$_2$Pt](BF$_4$)$_2$ (**8**) the platinum lies on an inversion center, and the coordination geometry is totally planar and symmetrical (Figure 2.9). In [(**4,4′-Me$_2$bipy**)$_2$Pt](BF$_4$)$_2$ the distances found between the H6 (H on the C *ortho* to the N, Figure 2.5) and the opposing C6 of the other ligand are 2.557 and 2.597 Å. For [(**pyPh$_2$t**)$_2$Pt](BF$_4$)$_2$ (**8**), in contrast, the distance between the related pyridyl proton (H(8), Figure 2.4) and the opposing triazine non-bonded N(2) of the other ligand is 2.160 Å. The unusually small distance suggests a possibility of two weak favorable H···N interactions between the two opposing **pyPh$_2$t** ligands of **8**. Thus, the metal center exhibits no distortion.

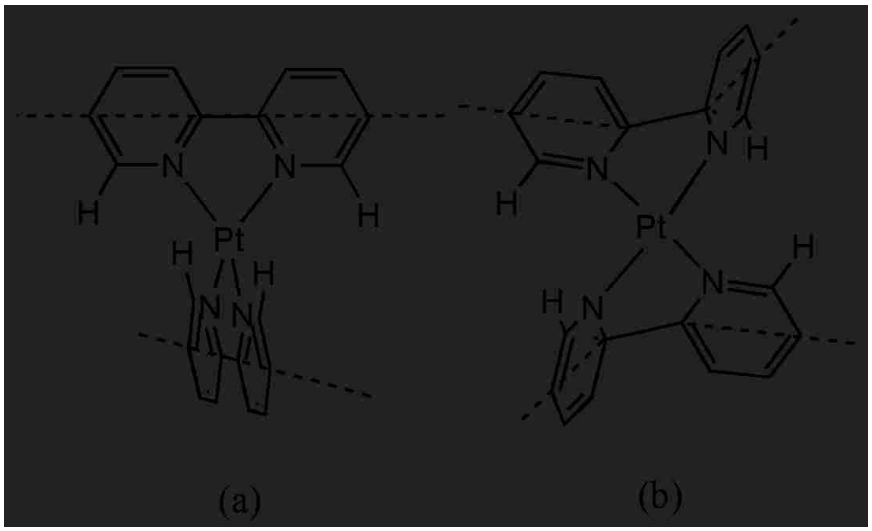

Figure 2.8 Canting (a) and bowing (b) of the two bipyridyl ligands with respect to each other in [(**bipy**)$_2$Pt]X$_2$.

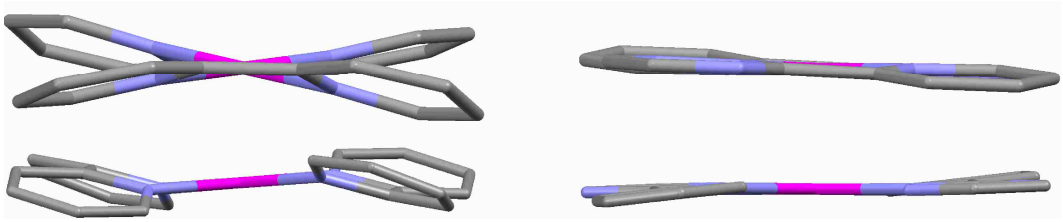

Figure 2.9 Side view of [(**bipy**)$_2$Pt]X$_2$ (left) and [(**pyt**)$_2$Pt]X$_2$ (right).

2.3.2 NMR Spectroscopy

As mentioned, both the reaction of **ferene** with *cis*-$Pt(Me_2SO)_2Cl_2$ and the resulting products are difficult to assess by ^1H NMR spectroscopy because of many overlapping signals. Also, simpler 3-(pyridin-2′-yl)-1,2,4-triazines (**L**) analogues which form $\mathbf{L}PtCl_2$ and $[\mathbf{L}_2Pt]^{2+}$ complexes with less complicated spectra have not been studied. Hence, we have investigated by ^1H NMR spectroscopy the formation and properties, such as degree of solvolysis, of these simpler **ptt** compounds. We use the standard numbering system for these **L** (Figure 2.1).

Reactions of **L** (20 mM) with *cis*-$Pt(Me_2SO)_2Cl_2$ (5 mM) in DMSO-d_6 were monitored with time until no further changes were observed. The H6′ doublet was usually observed between ~9.3 to 9.6 ppm within ~1 h of mixing. After ~1 day, a weaker doublet appeared farther downfield (~10.0 to 10.2 ppm). (These findings are consistent with the **ferene** results: H6′ doublet at ~9.6 ppm for $[(\mathbf{ferene})PtCl_2]^{2-}$ and at ~10.7 ppm for $[(\mathbf{ferene})_2Pt]^{2-}$).[13] Addition of $[NEt_4]Cl$ caused an increase in the intensity of the doublet between 9.3 and 9.6 ppm, and the disappearance of the more downfield doublet (~10 to 10.2 ppm), indicating that these are signals of $\mathbf{L}PtCl_2$ and $[\mathbf{L}_2Pt]^{2+}$, respectively.

For all **L**, $[\mathbf{L}_2Pt]^{2+}$ did not form completely and was less abundant than $\mathbf{L}PtCl_2$ in DMSO-d_6, even with a threefold excess of **L**. In order to form bis product exclusively, D_2O (10% by volume) was added to a separate solution of **L** and *cis*-$Pt(Me_2SO)_2Cl_2$ (in a 4:1 ratio). After ~1 h the $[\mathbf{L}_2Pt]^{2+}$ signals were the only bound **L** signals present. The greater solvation of the chloride ions in D_2O compared to that in DMSO-d_6 facilitates the formation of bis complexes. The reaction of **pyMe$_2$t** with *cis*-$Pt(Me_2SO)_2Cl_2$ described in the Supporting Information provides a detailed set of results that are representative of studies with other **L**.

2.3.2.1 [(MepyMe$_2$t)Pt(Guo)$_2$]$^{2+}$ Characterization. Within 30 min of mixing (**MepyMe$_2$t**)PtCl$_2$ and Guo in a 1:2 molar ratio in a D$_2$O/DMSO-d_6 solution at pH = 4.60 at 25 °C, the [(**MepyMe$_2$t**)Pt(Guo)$_2$]$^{2+}$ adduct was formed. The adduct has H8 signals at ~8.7 to 8.9 ppm, downfield from the free Guo H8 signal at 8.11 ppm, indicating that Guo is bound to Pt via N7. Two guanine base arrangements HH (Head-to-Head) and HT (Head-to-Tail) are possible for [**L**Pt(Guo)$_2$]$^{2+}$ type adducts. Three rotamers (HH, ΔHT, ΛHT) may be observed when **L** = a symmetrical bidentate ligand, whereas four rotamers (HHa, HHb, ΔHT, ΛHT) are possible when **L** = an unsymmetrical bidentate ligand (Figure 2.10).

Figure 2.10 Possible base orientations of two cis guanine bases coordinated to Pt. Each arrow represents a guanine base (bottom). The platinum carrier ligand is to the rear; when it is unsymmetrical (N1 ≠ N2), there are two HH conformers. Rotation of one base about the Pt–N7 bond leads to another conformer, but in each case the base orientation changes from HT to HH and vice-versa. When the carrier ligand has unsymmetrical bulk, it is possible that on the NMR time scale the base next to the bulky side of the carrier ligand does not rotate quickly, whereas the other base rotates rapidly. For example, the ΔHT conformer would interchange rapidly with the HHa conformer if the base next to N1 rotated slowly while the base next to N2 rotated readily. In contrast, the ΔHT conformer would form the HHb conformer only slowly.

The symmetry of the carrier ligand influences not only the number of conformers but also the number of sets of Guo signals detectable for each $[\mathbf{L}Pt(Guo)_2]^{2+}$ rotamer. For a non-bulky **L**, rotation about the Pt–N7 Guo bond is very fast on the NMR time scale; the rapid equilibration of rotamers in this case leads to one set or two sets of Guo NMR signals for $[\mathbf{L}Pt(Guo)_2]^{2+}$ adducts with symmetrical and unsymmetrical **L**, respectively. Bulky carrier ligands restrict the rotation of Guo about the Pt–N7 bond sufficiently to allow detection of different rotamers by NMR spectroscopy.[21,37-43] Because the Guo H8 signals are downfield, they can be particularly informative for assessing the nature and distribution of rotamers. For an $[\mathbf{L}Pt(Guo)_2]^{2+}$ adduct with an unsymmetrical **L**, the four rotamers should give two and eight H8 signals for rapidly and slowly exchanging conformers, respectively.

For $[(\mathbf{MepyMe_2t})Pt(Guo)_2]^{2+}$, three bound Guo H8 signals were present (Figure 2.11): two H8 signals of comparable intensity at 8.90 and 8.87 ppm (integrating to a total of one proton) and another larger H8 signal upfield at 8.75 ppm (integrating to a single proton). The observation of three H8 signals (not two for fast or eight for slow isomerization) suggests the occurrence of a complicated equilibration process between rotamers and/or an intermediate exchange rate.

The most likely process accounting for the three signals is rapid rotation of a Guo in one of the coordination positions and slow rotation of the other Guo. This situation would give two pairs of HT and HH conformers that interchange within the pair but not between pairs. In this case, the presence of three H8 signals with one large (the upfield H8) signal requires an overlap of two of the four expected H8 signals. The upfield Guo H8 signal could not be resolved, even at -4.0 °C. However, when the pH was raised to 7.75, four distinct H8 peaks of comparable intensity were observed at 8.88, 8.86, 8.71 and 8.68 ppm (Figure 2.11). At this pH the N1H of coordinated Guo is deprotonated, resulting in greater dispersion of H8 signals, but less dispersion

for the H1' signals, which all overlap. However, at pH 4.60 there are two H1' signals. One H1' signal (at 6.06 ppm, for one Guo) is one-third as large as the other, overlapped H1' signal (at 6.04 ppm, for three Guo). Thus, results for both H8 and H1' signals at both pH's support the presence of four different Guo's in two sets of similarly abundant HT/HH pairs.

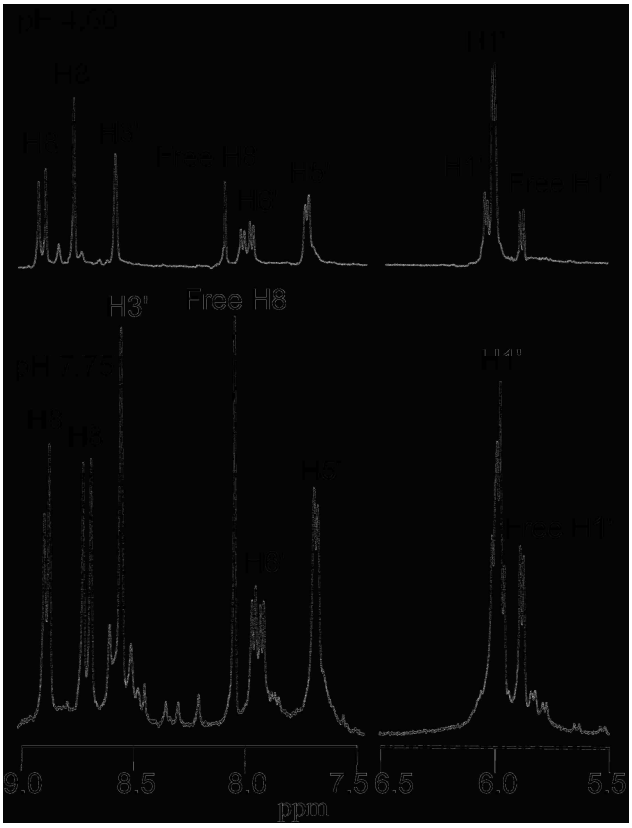

Figure 2.11 Aromatic and H1′ signals of the ^{1}H NMR spectrum of the [(**MepyMe$_2$t**)Pt(Guo)$_2$]$^{2+}$ adduct in D_2O/DMSO-d6 solution at pH 4.60 (top) and pH 7.75 (bottom) at 25 °C. Numbers are taken from the numbering system in Figure 2.1 for **L** and are shown in Figure 2.10 for Guo.

Extensive studies in which both the symmetrical carrier ligand and the guanine derivative (**G**) were varied systematically indicate that, for a given adduct, the HT rotamers (in total) are favored over the HH rotamer(s) (in total).[44] Although the reasons for this observation are not fully understood, the most compelling explanations are that base dipole-dipole alignment favors the HT over the HH arrangement of guanines and that clashes between the exocyclic O6 on each guanine in the HH arrangement disfavor the HH rotamer. When **G** is a GMP, additional

complications arise, increasing the abundance of the HH form in some cases, but in general Guo adducts have a particularly low amount of the HH rotamer.[21,41,43] In a previous study of [**L**Pt**G**$_2$]$^{2+}$ adducts with an unsymmetrical **L**, 2-aminomethylpiperidine (**pipen**), four H8 signals were observed for each adduct,[45,46] as found here. The results were interpreted as indicating that each pair of H8 signals arose from a rapidly interchanging pair of conformers, ΔHT/HHa and ΛHT/HHb (Figure 2.10), with the HT form dominating. In the **pipen** case, the amino group allows rapid rotation of the cis **G**, whereas the piperidine ring hinders rotation of the cis **G**.[45,46]

The properties of the [(**MepyMe$_2$t**)Pt(Guo)$_2$]$^{2+}$ adduct at pH 7.75 were explored further by using 2D NMR spectroscopy. An additional equivalent of Guo was added to ensure that all the Pt compound was consumed prior to a ROESY experiment, which allows us to probe the exchange processes and the through-space interactions between Guo and the **MepyMe$_2$t** ligand. Neither NOE nor EXSY cross-peaks were observed between the H8 signals. An HH conformer would give an H8-H8 NOE cross-peak, and even for a rapid HT/HH equilibrium, a cross-peak would be found if either HT/HH pair had a significant amount of the HH conformer. The four [(**MepyMe$_2$t**)Pt(Guo)$_2$]$^{2+}$ H8 signals thus reflect mainly the two HT conformers, ΔHT and ΛHT, present in a nearly 1:1 ratio. The H8 NMR signals of the HH conformer were not detectable, indicating a more rapid rate of rotation about the Pt–N7 bond for one Guo in [(**MepyMe$_2$t**)Pt(Guo)$_2$]$^{2+}$, a result more similar to that found for (**pipen**)Pt**G**$_2$ adducts[45,46] than for (**5,5′-Me$_2$bipy**)Pt**G**$_2$ adducts[21] and (**Me$_2$ppz**)Pt**G**$_2$ adducts[41] (**Me$_2$ppz** = *N,N′*-dimethylpiperazine).

NOE cross-peaks in the [(**MepyMe$_2$t**)Pt(Guo)$_2$]$^{2+}$ ROESY spectrum between the Guo H8 at 8.86 ppm and the pyridyl H6′ doublet at 7.96 ppm and between the Guo H8 singlet at 8.88 ppm and the pyridyl H6′ doublet at 7.94 ppm indicate that the two most downfield H8 signals

belong to the Guo bound cis to the pyridyl ring. The more upfield H8 signals, at 8.71 and 8.68 ppm, belong to the Guo bound cis to the triazine ring.

Compared to the signals of [(**MepyMe$_2$t**)Pt(Me$_2$SO-d_6)Cl]$^+$ in D$_2$O/DMSO-d_6 at pH 4.60, the H5′ (7.76 ppm) and H3′ (8.60 ppm) signals of the [(**MepyMe$_2$t**)Pt(Guo)$_2$]$^{2+}$ adduct at pH 4.60 shifted only slightly upfield and downfield, respectively. In contrast, the H6′ doublets at 8.04 and at 8.00 ppm (integrating to a total of one proton) for this adduct were shifted upfield by ~1.26 ppm from the H6′ signal at 9.28 ppm of [(**MepyMe$_2$t**)Pt(Me$_2$SO-d_6)Cl]$^+$. The anisotropy of the cis-coordinated guanine base is responsible for these large upfield shifts. These shifts and the H8-H6′ NOE cross-peaks leave no doubt that the guanine in the adduct is positioned very close to H6′. Two considerations [a) the pyridyl H6′ proton is known to hinder the rate of rotation about the Pt–N7 Guo bond,[21] and b) two upfield-shifted H6′ signals are resolved for the [(**MepyMe$_2$t**)Pt(Guo)$_2$]$^{2+}$ adduct] leave no doubt that the slowly rotating Guo is cis to the pyridyl ring and that the Guo cis to the triazine ring is in fast rotation. Otherwise, the H6′ doublets would probably be time averaged.

2.4 Conclusions

Regardless of the presence of various exocylic groups, 3-(2′-pyridyl)-1,2,4-triazine ligands are excellent bidentate sp^2 N-donors and form both **L**PtCl$_2$ and [**L**$_2$Pt]$^{2+}$ complexes. The juxtaposition of the pyridyl H6′ proton and the triazine lone pair of electrons in [**L**$_2$Pt]X$_2$ allows formation of a planar structure. Also, this juxtaposition favors the trans arrangement of the bidentate ligands in [**L**$_2$Pt]X$_2$. The ligands prefer to bind via only the N2 of the triazine ring. No evidence was found for isomers having N4 coordinated to Pt. Very likely this result arises from the effect of the group ortho to the bound N. For a given bidentate ligand, the interactions between the juxtaposed groups on the two rings ortho to the bridging carbons and on the

periphery of the bidentate ligand are favorable for 3-(2′-pyridyl)-1,2,4-triazine ligands but unfavorable for 2,2′-bipyridines. This favorable factor would be present if the triazine ring binds to metals via either N2 or N4. For N2 binding, the N1 lone pair is readily accommodated sterically, but the substituent on C5 would create steric clashes if metal binding were to occur via N4. Thus, the observation that only N2 binding was detected can be understood. When combined with the X-ray structural results, the H6′ NMR spectral shifts of the complexes containing the **L**'s examined here establish that the structures of virucidal **ptt** compounds containing **ferene** proposed earlier were correct.[13]

The dynamic properties of the[(**MepyMe$_2$t**)Pt(Guo)$_2$]$^{2+}$ adduct indicate that the lone pair on the non-bonded nitrogen, N1, of the triazine ring is not sterically demanding. This lone pair does not strongly impede the rotation of Guo about the Pt–N7 bond, whereas the equivalently placed CH group of the pyridyl ring does impede rotation. This behavior and the structural data all point to a lower overall steric effect of the N2-metal-bound triazine ring compared to the metal-bound pyridine ring. Dynamic behavior similar to that of the [(**MepyMe$_2$t**)Pt(Guo)$_2$]$^{2+}$ adduct has been well documented previously only in the case of **pipen** complexes.[45,46]

Our result that Guo did not add to [(**MepyMe$_2$t**)$_2$Pt]$^{2+}$ suggests the possibility that the virucidal activity of the **L**PtCl$_2$ and the [**L**$_2$Pt]$^{2+}$ **ptt** agents arises, respectively, from covalent and non-covalent (possibly intercalative nucleic acid interactions favored by [**L**$_2$Pt]$^{2+}$ planarity) binding to biomolecular targets. These results suggest that the relatively neglected 3-(2′-pyridyl)-1,2,4-triazine ligands should be examined more widely in coordination chemistry.

2.4 References

1. Wang, D.; Lippard, S. J. *Nature Reviews Drug Discovery* **2005**, *4*, 307-320.

2. Lippert, B., Ed. *Cisplatin: Chemistry and Biochemistry of a Leading Anticancer Drug*; Wiley-VCH: Weinheim, 1999.

3. Beljanski, V.; Villanueva, J. M.; Doetsch, P. W.; Natile, G.; Marzilli, L. G. *J. Am. Chem. Soc.* **2005**, *127*, 15833-15842.

4. Harris, A. L.; Ryan, J. J.; Farrell, N. *Mol. Pharmacol.* **2006**, *69*, 666–672.

5. van Zutphen, S.; Reedijk, J. *Coord. Chem. Rev.* **2005**, *249*, 2845-2853.

6. Coluccia, M.; Boccarelli, A.; Mariggió, M.; Cardellicchio, N.; Caputo, P.; Intini, F. P.; Natile, G. *Chem. Biol. Interact.* **1995**, *98*, 251-266.

7. Quiroga, A. G.; Perez, J. M.; Alonso, C.; Navarro-Ranninger, C.; Farrell, N. *J. Med. Chem.* **2006**, *49*, 224-231.

8. Blommaert, F. A.; Van Dijk-Knijnenburg, H. C. M.; Dijt, F. J.; Den Engelse, L.; Baan, R. A.; Berends, F.; Fichtinger-Schepman, A. M. J. *Biochemistry* **1995**, *34*, 8474-8480.

9. Farrell, N.; Bierbach, U.; PCT Int. Appl.: USA, 1999, p 20.

10. Sartori, D. A.; Miller, B.; Bierbach, U.; Farrell, N. *J. Biol. Inorg. Chem.* **2000**, *5*, 575-583.

11. Snyder, M. B.; Saravolatz, L. D.; Markowitz, N.; Pohlod, D.; Taylor, R. C.; Ward, S. G. *J. Antimicrob. Chemother.* **1987**, *19*, 815-822.

12. Taylor, R. C.; Ward, S. G.; Schmidt, P. P.; U.S. Pat. Appl.: USA, 1986, p 4.

13. Vzorov, A. N.; Bhattacharyya, D.; Marzilli, L. G.; Compans, R. W. *Antiviral Res.* **2005**, *65*, 57-67.

14. Balcarová, Z.; Kašpárková, J.; Žákovská, A.; Novakává, O.; Sivo, M. F.; Natile, G.; Brabec, V. *Mol. Pharmacol.* **1998**, *53*, 846-855.

15. Margiotta, N.; Bergamo, A.; Sava, G.; Padovano, G.; De Clercq, E.; Natile, G. *J. Inorg. Biochem.* **2004**, *98*, 1385-1390.

16. Fuertes, M. A.; Alonso, C.; Perez, J. M. *Chem. Rev.* **2003**, *103*, 645-662.

17. Uma, R.; Palaniandavar, M.; Butcher, R. J. *J. Chem. Soc., Dalton Trans.* **1996**, *10*, 2061-2066.

18. Prasad, L.; Page, L. E.; Smith, F. E. *Inorg. Chim. Acta* **1983**, *68*, 45-49.

19. Pal, P. K.; Chowdhury, S.; Drew, M. G. B.; Datta, D. *New J. Chem.* **2000**, *24*, 931-933.

20. Iveson, P. B.; Riviere, C.; Guillaneux, D.; Nierlich, M.; Thuery, P.; Ephritikhine, M.; Madic, C. *J. Chem. Soc., Chem. Commun.* **2001**, 1512-1513.

21. Bhattacharyya, D.; Marzilli, P. A.; Marzilli, L. G. *Inorg. Chem.* **2005**, *44*, 7644-7651.

22. Margiotta, N.; Papadia, P.; Fanizzi, F. P.; Natile, G. *Eur. J. Inorg. Chem.* **2003**, 1136-1144.

23. Collins, J. G.; Rixon, R. M.; Wright, J. R. A. *Inorg. Chem.* **2000**, *39*, 4377-4379.

24. Hage, R.; Van Diemen, J. H.; Ehrlich, G.; Haasnoot, J. G.; Stufkens, D. J.; Snoeck, T. L.; Vos, J. G.; Reedijk, J. *Inorg. Chem.* **1990**, *29*, 988-993.

25. Case, F. H. *J. Org. Chem.* **1965**, *30*, 931-933.

26. Price, J. H.; Williamson, A. N.; Schramm, R. F.; Wayland, B. B. *Inorg. Chem.* **1972**, *11*, 1280-1284.

27. Sullivan, S. T.; Ciccarese, A.; Fanizzi, F. P.; Marzilli, L. G. *J. Am. Chem. Soc.* **2001**, *123*, 9345-9355.

28. Hage, R.; Haasnoot, J. G.; Reedijk, J. *Inorg. Chim. Acta* **1990**, *172*, 19-23.

29. Islam, M. A.; Stephen, W. I. *Talanta* **1992**, *39*, 1429-1435.

30. Otwinowski, Z.; Minor, W. *Macromolecular Crystallography, part A*; New York Academic Press: New York, 1997; Vol. 276.

31. Sheldrick, G. M. In *Program for Crystal Structure Solution and Refinement*; University of Gottingen: Gottingen, Germany, 1997.

32. Hazell, A. *Polyhedron* **2004**, *23*, 2081-2083.

33. Hazell, A.; Simenson, O.; Wernberg, O. *Acta Crystallogr.* **1986**, *C42*, 1707-1711.

34. Rund, J. V. *Inorg. Chem.* **1967**, *7*, 24-27.

35. Bondi, A. *J. Phys. Chem.* **1964**, *68*, 441-451.

36. Chassot, L.; Muller, E.; Zelewsky, A. V. *Inorg. Chem.* **1984**, *23*, 4249-4253.

37. Cramer, R. E.; Dahlstrom, P. L. *Inorg. Chem.* **1985**, *24*, 3420-3424.

38. Cramer, R. E.; Dahlstrom, P. L. *J. Am. Chem. Soc.* **1979**, *101*, 3679-3681.

39. Xu, Y.; Natile, G.; Intini, F. P.; Marzilli, L. G. *J. Am. Chem. Soc.* **1990**, *112*, 8177-8179.

40. Ano, S. O.; Intini, F. P.; Natile, G.; Marzilli, L. G. *Inorg. Chem.* **1999**, *38*, 2989-2999.

41. Sullivan, S. T.; Ciccarese, A.; Fanizzi, F. P.; Marzilli, L. G. *Inorg. Chem.* **2001**, *40*, 455-462.

42. Kiser, D.; Intini, F. P.; Xu, Y.; Natile, G.; Marzilli, L. G. *Inorg. Chem.* **1994**, *33*, 4149-4158.

43. Saad, J. S.; Scarcia, T.; Shinozuka, K.; Natile, G.; Marzilli, L. G. *Inorg. Chem.* **2002**, *41*, 546-557.

44. Natile, G.; Marzilli, L. G. *Coord. Chem. Rev.* **2006**, *250*, 1315-1331.

45. Wong, H. C.; Coogan, R.; Intini, F. P.; Natile, G.; Marzilli, L. G. *Inorg. Chem.* **1999**, *38*, 777-787.

46. Wong, H. C.; Intini, F. P.; Natile, G.; Marzilli, L. G. *Inorg. Chem.* **1999**, *38*, 1006-1014.

CHAPTER 3. NEGLECTED BIDENTATE sp^2 N-DONOR CARRIER LIGANDS WITH TRIAZINE NITROGEN LONE PAIRS. PLATINUM COMPLEXES RETROMODELING CISPLATIN GUANINE NUCLEOBASE-ADDUCTS*

3.1 Introduction

Cisplatin (*cis*-$Pt(NH_3)_2Cl_2$) is one of the most widely used anticancer drugs.[1,2] Cisplatin and its analogues, **L**PtX_2 models (**L** = one bidentate or two *cis*-unidentate N-donor carrier ligands), interact with DNA by forming a 1,2-intrastrand N7–Pt–N7 crosslink between two adjacent guanines of d(GpG) sequences in DNA.[1-6] The cross-links formed by cisplatin (and its analogues) have been investigated and identified from X-ray structures,[1,3] NMR spectroscopy,[1,3] and enzyme digestion studies.[2,3,5]

Within the cross-link adduct, hydrogen bonding between the NH_3 ligands of the *cis*-$Pt(NH_3)_2$ moiety and residues in or near the cross-link has been an important component of hypotheses concerning both the mode of stabilization of distorted DNA induced by drug binding.[7-12] However, examination of an X-ray structure of an HMG-bound 16-oligomer[13] and an X-ray/NMR-derived model of a duplex 9-oligomer,[14] both of which contain an intrastrand cisplatin lesion, suggests that hydrogen-bonding interactions involving the NH_3 ligands are weak or even nonexistent. If the NH_3 ligands are replaced by **L** carrier ligands having sp^3 N atoms bearing two or more alkyl groups, modeling with the 9-mer structure suggests that clashes will occur.[14] These results on duplex models have led to the hypothesis that the small size of the NH group, not its hydrogen-bonding ability, facilitates the anticancer activity of Pt compounds bearing multiple NH groups.[15]

A degree of uncertainty exists in defining the structure of duplexes bearing Pt drug lesions.[15,16] Relatively few X-ray structures are available,[13,15,17] and NMR characterization is

---

* Contents of this chapter are under review by American Chemical Society.

because the carrier ligands in cisplatin are not bulky enough to impede the rotation of N7-bound guanine about the Pt–N7 bond.[16,18] Thus, cisplatin adducts with nucleic acids and their constituents exist as a fluxional mixture of conformers, making elucidation of the structures in the solution state difficult; this complication is termed the dynamic motion problem.[14,16,18,19]

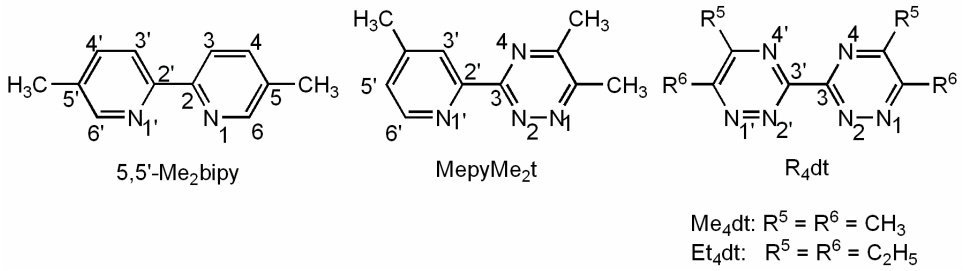

Figure 3.1. Line drawing and numbering scheme for 5,5′-dimethyl-2,2′-bipyridine (**5,5′-Me$_2$bipy**) (top), 3-(4′-methylpyridin-2′-yl)-5,6-dimethyl-1,2,4-triazine) (**MepyMe$_2$t**) (bottom left), and bis-3,3′-(5,6-dialkyl-1,2,4-triazine) (**R$_4$dt**) (bottom right) ligands.

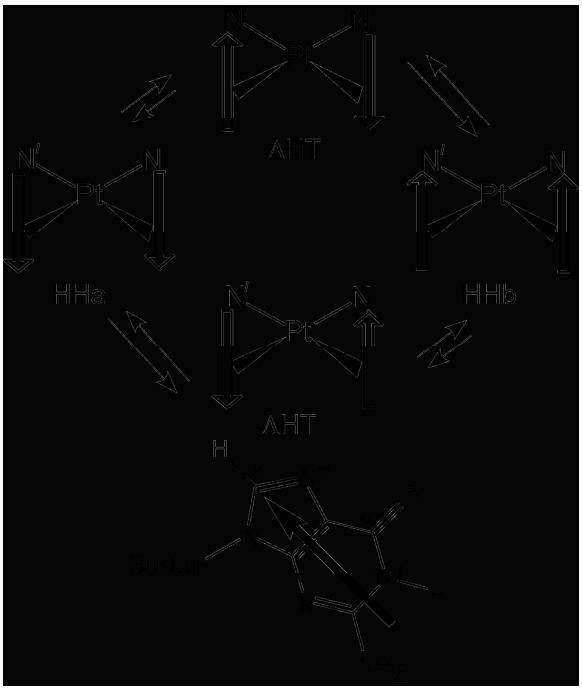

Figure 3.2. Possible base orientations of two cis guanine bases coordinated to Pt. Each arrow represents the base with the H8 atom at its head. In all cases, two HT conformers are possible. Two HH conformers are possible when **L** (to the rear) is unsymmetrical (N′ ≠ N, e.g., as in **MepyMe$_2$t**, N′ = pyridyl N and N = triazine N, see below), but only one HH conformer is possible when **L** is symmetrical (N′ = N). Each rotation of one base about the Pt–N7 bond leads to changes in the relative base orientation from HT to HH, or vice-versa.

To overcome the dynamic motion problem, a retro-modeling approach can be used by introducing features in the carrier ligand to make the spectral properties more informative.[14,19-22] Retro models are essentially analogues of cisplatin with carrier ligands designed to reduce the dynamic motion by destabilizing the transition state for Pt–N7 rotation, but having bulk in or near the coordination plane, thereby allowing the coexistence of multiple conformers. In this study, we compare the **L**Pt(GMP)$_2$ adducts containing the **L** depicted in Figure 3.1. For an **L**Pt**G**$_2$ adduct (**G** = guanine derivative not linked by a phosphodiester group), the **G** bases can have head-to-tail (HT) or head-to-head (HH) orientations (Figure 3.2). The untethered **G**'s normally adopt preferentially an HT orientation,[16,23] whereas the bases in d(GpG) cross-links having a sugar phosphate backbone are found most often in the HH orientation, especially when a 5′ residue is present.[6,19,24-31]

In order to gain a better understanding of a number of fundamental factors influencing properties of **L**Pt**G$_2$** adducts, we must know the effect of the carrier-ligand interactions with the nucleic acid constituents (bases, sugars, etc.). These interactions, present in very small adducts, also occur in larger models, including duplexes. However, they can be more difficult to assess in the larger adducts, particularly because larger adducts manifest additional interactions involving both flanking residues in the cross-link strand and residues in the complementary strand. Retro models with sp^3 N-donor ligands have been investigated more often[16,19-21,32] than those with sp^2 N-donor heterocyclic chelating ligands.

Studies of **L**Pt(Guo)$_2$ complexes (**L** = **2,9-dimethyl-1,10-phenanthroline**,[33] **MepyMe$_2$t**;[34] Guo = guanosine) and (**5,5′-Me$_2$bipy**)Pt(d(GpG))[22] have demonstrated the coexistence of different rotamers exchanging slowly relative to the NMR time scale. In cisplatin intrastrand cross-linked DNA adducts, the dominant conformer appears to have the guanines in a

HH orientation.[21] For most **L**Pt**G**$_2$ adducts, the HH conformers are minor conformers, when compared to the HT conformers, and are favored more in the 5′-GMP adduct than in the corresponding 3′-GMP adduct.[19,20,30,31,35] When the **L** carrier ligand is unsymmetrical, two HH conformers are possible (Figure 3.2). However, in all previous work, even with the 5′-GMP adducts, it was not possible to assign the HHa and HHb conformers (Figure 3.2). The (**MepyMe$_2$t**)Pt(5′-GMP)$_2$ adduct studied here allowed, for the first time, the determination of the conformation of two such HH conformers.

3.2 Experimental Section

3.2.1 Starting Materials

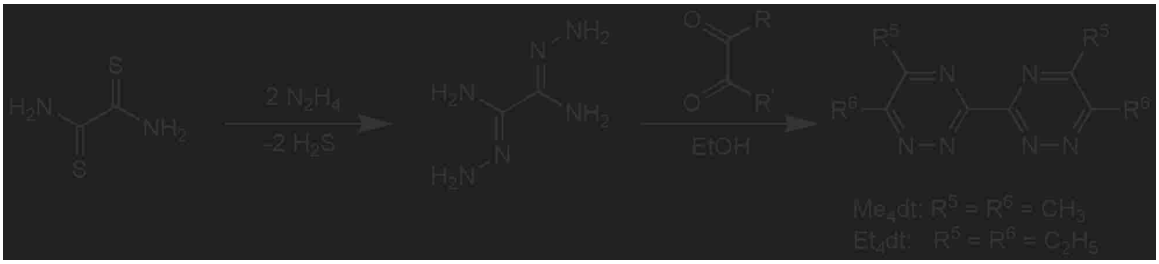

Figure 3.3 Synthesis of bis-3,3′-(5,6-dialkyl-1,2,4-triazine) (**R$_4$dt**) ligands.

5′-GMP, 3′-GMP (Sigma), and **5,5′-Me$_2$bipy** (Aldrich) were used as received. *cis*-Pt(Me$_2$SO)$_2$Cl$_2$ was prepared as described in the literature.[36] The syntheses of (**5,5′-Me$_2$bipy**)PtCl$_2$ and (**MepyMe$_2$t**)PtCl$_2$ are described elsewhere.[22,34,37] Bis-3,3′-(5,6-dialkyl-1,2,4-triazine) (**R$_4$dt**, R = Me or Et) ligands were prepared by a known method[38] (Figure 3.3). Elemental analyses (C,H,N) were performed by Atlantic Microlabs, Atlanta, GA.

3.2.2 NMR Measurements

^{1}H NMR spectra were recorded on a Bruker spectrometer operating at 400 MHz. We used the values of 0.00, 4.78, and 4.98 ppm to reference signals to TMS in DMSO-d_6 solutions at 25 °C and to the residual HOD signal at 25 °C and 5 °C in D$_2$O/DMSO-d_6 solutions, respectively. A

presaturation pulse to suppress the water peak was used when necessary. 2D ROESY experiments[39] were performed at 5 °C by using a 500 ms mixing time (128 scans per t_1 increment). ROESY and 1D NMR data, processed with *XWINNMR* or *Mestre-C* software, were used to assign signals and (along with CD data) to assess the conformation of the adducts under various pH conditions. DNO_3 and NaOD solutions (0.1 M in D_2O) were used to adjust the pH of D_2O/DMSO-d_6 solutions, especially during the reactions in which the pH decreased with time.

3.2.3 Circular Dichroism (CD) Spectroscopy

All samples used for CD experiments were prepared from the respective NMR samples by diluting to ~0.025 mM Pt with deionized water. Spectra were recorded from 400 to 200 nm at a scan speed of 50 nm/min on a JASCO J-600 CD spectropolarimeter. Six scans were recorded and averaged for each sample.

3.2.4 Synthesis of (R_4dt)$PtCl_2$ Complexes

The (**R_4dt**)$PtCl_2$ complexes were obtained as yellow precipitates upon heating a methanol solution (10 mL) of *cis*-$Pt(Me_2SO)_2Cl_2$ (42.2 mg, 0.1 mmol) and the desired **R_4dt** ligand (0.1 mmol) at 60 °C for 6 h. The precipitates were collected, washed with diethyl ether, followed by chloroform, and then dried in vacuo.

3.2.4.1 (Me_4dt)$PtCl_2$. The method described above afforded a yellow precipitate; yield, 26.5 mg (55%). ^{1}H NMR (ppm) in DMSO-d_6 : 2.62 (s, 5-CH_3), 2.81 (s, 6-CH_3). Anal. Calcd for $C_{10}H_{12}Cl_2N_6Pt \cdot 1/3(H_2O)$: C, 24.58; H, 2.59; N, 17.21. Found: C, 24.66; H, 2.69; N, 16.91.

3.2.4.2 (Et_4dt)$PtCl_2$. The product was obtained as a yellow powder; yield, 36.1 mg (67%). ^{1}H NMR (ppm) in DMSO-d_6: 3.20 (quartet, 6-CH_2), 2.96 (quartet, 5-CH_2), 1.30-1.41 (m, 5,6-CH_3). X-ray quality crystals were obtained by mixing equal volumes of 10 mM solutions of *cis*-$Pt(Me_2SO)_2Cl_2$ (8.44 mg, 10 mM) and the **Et_4dt** ligand (5.44 mg) in 2 mL of acetonitrile and

allowing this solution to stand at 25 °C. Thin yellow needles of (**Et$_4$dt**)PtCl$_2$ were obtained in ~25% yield after 24 h. The structure was determined by X-ray diffraction.

3.2.5. Formation of LPt(GMP)$_2$ (L = 5,5′-Me$_2$bipy, MepyMe$_2$t, Me$_4$dt, Et$_4$dt and GMP = 5′- and 3′-GMP)

A typical preparation of **L**Pt(GMP)$_2$ involved mixing a solution containing ~2 equiv of GMP dissolved in 350 μL of D_2O at pH ~4 and a solution containing 1 equiv (~5 mM) of **L**PtCl$_2$ complex in 250 μL of DMSO-d_6 to give a 1:2 ratio of Pt:GMP, and the mixture (pH ~4) was kept at 25 °C. The mixture of D_2O and DMSO-d_6 solutions was employed to improve the solubility of the **L**PtCl$_2$ complex. The solution was monitored by ^{1}H NMR spectroscopy until no change in the bound vs. free H8 signal intensity was observed. The **L**PtCl$_2$ complex in a D_2O/DMSO-d_6 mixture forms a solvated complex that always remained in small amounts, along with some free GMP.

3.3 Results and Discussion

3.3.1 Conformational Assignments and Conformer Properties

The asymmetry of the **G** ribose residue and the local symmetry of the **L**Pt moiety influence the number of NMR signals that can be observed for each **L**Pt**G**$_2$ conformer. ^{1}H NMR spectra in the ribose region are very crowded and complex, especially for adducts with unsymmetrical carrier ligands. The downfield **G** H8 signals, in a less crowded, more disperse region of the spectra, are particularly useful for assessing the nature and distribution of conformers (Figure 3.2). Because the **G** bears a chiral ribose moiety, **L**Pt**G**$_2$ adducts with C_2-symmetrical carrier ligands (e.g., **Me$_4$dt**, **Et$_4$dt**) have one HH and two HT (ΔHT and ΛHT) NMR-distinguishable conformers (maximum total of four H8 signals), and models with unsymmetrical carrier ligands (e.g., **MepyMe$_2$t**) have two HH (HHa and HHb) and two HT (ΔHT and ΛHT) conformers (maximum total of eight H8 signals). The conformation and signal

assignments of the HH atropisomers are based on the presence of NOE cross-peaks between the two H8 signals.

At pH 6-7 for **L**Pt(GMP)$_2$ adducts, the phosphate group is deprotonated and N1 is protonated,[40,41] creating the possibility of H-bonding between the phosphate group and the imino hydrogen (N1H) of the cis GMP. This interligand interaction is called "second-to-second sphere communication" (SSC) because the interacting groups are at the periphery of the cis nucleotides.[21,42,43] Such SSC interactions have been identified as important factors stabilizing the ΛHT and ΔHT conformers of the Pt adducts of 5′-GMP and 3′-GMP, respectively.[35] The CD signal shape provides a definitive means for assigning the chirality of the major HT form of **L**Pt**G**$_2$ complexes when that form clearly dominates. A CD signal shape having a positive feature at ~290 nm and a negative feature at ~256 nm is characteristic of the ΛHT **L**Pt**G**$_2$ conformer,[21,31,32,42,44] whereas a CD signal shape having a negative feature at ~290 nm and a positive feature at ~256 nm is characteristic of the ΔHT conformer of **L**Pt**G**$_2$ adducts.[31,32,42,45] The CD signal of HH conformers is generally weak, a feature attributable to the inherent symmetry of the base chromophore, with the two bases having a pseudo mirror relationship in HH conformers.

3.3.2 H8 Shifts and Base Canting

In addition to the HH or HT **G** base orientation, **G** base canting is another significant structural parameter of **L**Pt**G**$_2$ conformers. A given base is generally not oriented with its plane exactly perpendicular to the coordination plane, but is canted. The canting can be either left-handed (L) or right-handed (R) (Figure 3.4). Useful indications for assessing the degree of **G** base canting are provided by the **G** H8 signal shifts.[14] The H8 shift is influenced by the positioning of the H8 atom with respect to the shielding cone of the cis **G** base. In an HT

arrangement, the canting may move the six-membered rings either closer to the midpoint between the N7 atoms ('6-in' form) or farther from this midpoint ('6-out' form). The canting of the bases in the direction ('6-out' form) that moves each H8 toward the cis **G** will lead to greater H8 shielding and, hence, an upfield H8 signal relative to the average H8 signal. The minor HT conformer typically is '6-out'. In contrast, the canting of the base that moves its H8 away from the cis **G** will lead to less H8 shielding or perhaps deshielding in the HT form[26] and thus a more downfield H8 signal. The major HT conformer typically is '6-in'.

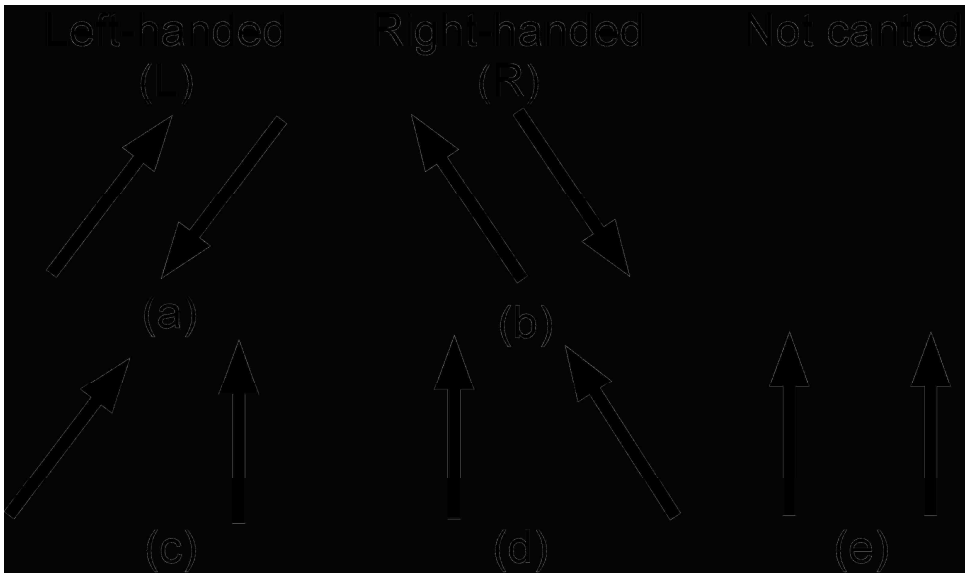

Figure 3.4 Shorthand representation for left-handed (L) (a, c) and right-handed (R) (b, d) canting for **L**Pt**G**$_2$ adducts. In the ΔHT conformer shown (a, b), L and R canting have the six-membered ring far from the C_2 axis for L canting ('6-out') and close to the axis for R canting ('6-in'). For the ΛHT conformer (not shown), the arrows are all rotated by 180°. The HH conformer can be left-handed (c), right-handed (d) or not canted (e).

For the HH orientation, one base is typically more canted, with its H8 toward the other cis base, which is less canted.[19,30,31] The H8 atom of the more canted **G** is closest to the shielding region of the cis **G** and has a relatively upfield H8 signal (HH_u). The H8 signal of the less canted base is relatively downfield (HH_d) because this H8 is farthest from the cis **G** base shielding region and may be in the deshielding region of this base.[31,43] Typically the HH_u and HH_d H8

signals are separated by ~1 ppm and straddle the HT H8 signals. In less common cases, the HH bases are not canted and the two signals are relatively downfield.

3.3.3. (5,5′-Me$_2$bipy)Pt(5′-GMP)$_2$

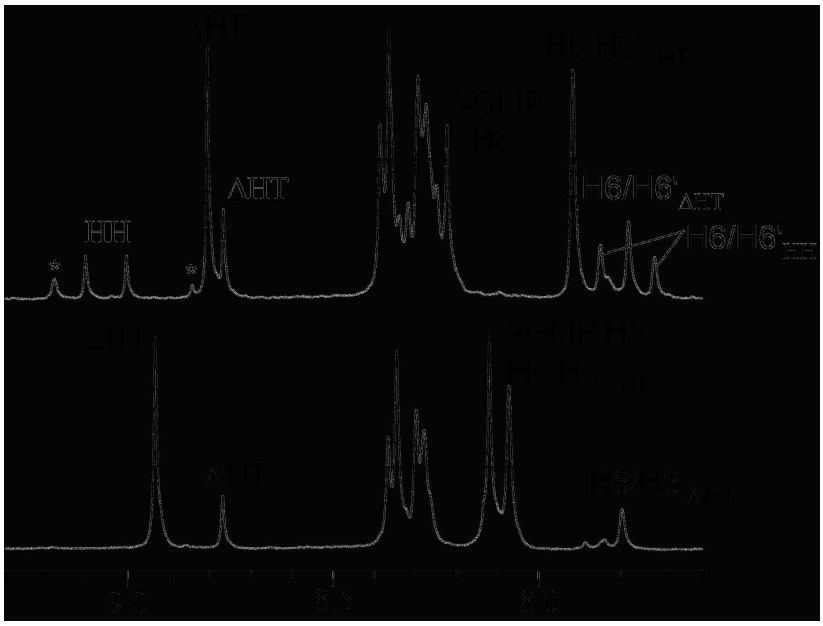

Figure 3.5 Aromatic region of ^{1}H NMR spectra of (**5,5′-Me$_2$bipy**)Pt(5′-GMP)$_2$ (top) and (**5,5′-Me$_2$bipy**)Pt(3′-GMP)$_2$ (bottom) at pH ~ 4.0 and 25 °C. The H8 signals for the conformers are designated by the conformation. (Pyridyl H6′ signals attributed to the solvated Pt complex are indicated by asterisks.)

Four new H8 signals of the (**5,5′-Me$_2$bipy**)Pt(5′-GMP)$_2$ adduct downfield from the free 5′-GMP H8 signal at 8.22 ppm were observed at 25 °C (Figure 3.5). When the pH was raised from 4.0 to 7.5, the H8 signal at 8.81 ppm shifted slightly upfield by 0.02 ppm and became the most dominant signal. The CD signal shape observed for this adduct at pH 7.5 is characteristic of the ΛHT conformer (Figure 3.6). For the 5′-GMP adducts, the ΛHT conformer is more favored by SSC upon phosphate deprotonation;[16] therefore, the dominant H8 signal of the (**5,5′-Me$_2$bipy**)Pt(5′-GMP)$_2$ adduct was assigned to the ΛHT conformer. The intensity of the H8 signals at 9.11 and 9.01 ppm (pH 4.0) remained comparable throughout the pH titration. These H8 signals shifted downfield by ~0.11-0.14 ppm when the pH was increased to 7.5. The two H8

signals were connected through an NOE cross-peak in a ROESY spectrum collected at 5 °C and were thus assigned to the HH conformer. The signal at 8.77 ppm was assigned to the ΔHT conformer, the only remaining possible conformer. The H8 chemical shifts at pH 4.0 and 7.5 are listed in Table 3.1. From pH 4.0 to 7.5, the distribution of the ΛHT, ΔHT and HH conformers changed from 42%, 29%, and 29% to 58%, 23%, and 18%, respectively.

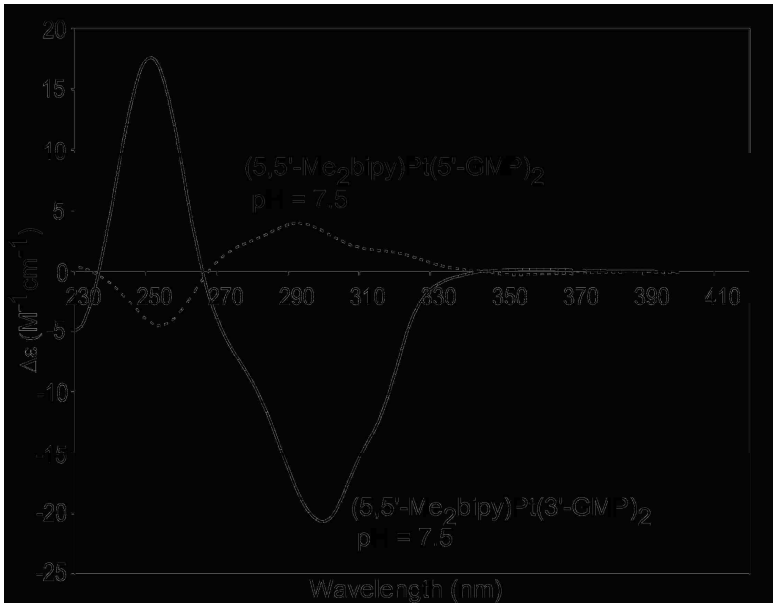

Figure 3.6 CD spectra of (**5,5′-Me$_2$bipy**)Pt(5′-GMP)$_2$ and (**5,5′-Me$_2$bipy**)Pt(3′-GMP)$_2$ at 25 °C.

The H8 signals of the HH conformer of the (**5,5′-Me$_2$bipy**)Pt(5′-GMP)$_2$ adduct have low dispersion (0.10 ppm) and both are relatively downfield when compared to the HT H8 signals. A similar unusual H8 shift pattern was reported for the HH conformer of the (**Me$_2$ppz**)Pt(5′-GMP)$_2$ adduct (**Me$_2$ppz** = *N,N′*-dimethylpiperazine) and was attributed to a low degree of base canting.[21] The H8 signals of the (**5,5′-Me$_2$bipy**)Pt(5′-GMP)$_2$ HH conformer have a downfield shift because the two bases have relatively little canting, and as a result H8 experiences less shielding by the cis **G** and possibly greater deshielding by the anisotropic Pt atom.[35,46-48] For the (**5,5′-Me$_2$bipy**)Pt(5′-GMP)$_2$ adduct, the H8 signal of the major ΛHT conformer is downfield to that of

the minor ΔHT conformer. In typical cases for the HT conformers, the '6-in' form is favored.[20,49] The H8 signal of the '6-in' form is downfield because the H8 atoms are positioned away from the cis base, while the H8 signal of the '6-out' form is upfield because the H8 signals of the two bases are shielded by the cis base. For the (**5,5′-Me$_2$bipy**)Pt(5′-GMP)$_2$ adduct, the major ΛHT conformer is the '6-in' form, thus L canted, and the minor ΔHT conformer is the '6-out' form with L canting (Figure 3.4).

Table 3.1 Chemical Shifts of the H8 Signals of **L**Pt(GMP)$_2$ Adducts (**L = 5,5′-Me$_2$bipy**, **Et$_4$dt**, **Me$_4$dt**) at 5 °C [a]

complex	pH	ΔHT	ΛHT	HH_d	HH_u
(**5,5′-Me$_2$bipy**)Pt(5′-GMP)$_2$ [b]	4.0	8.77	8.81	9.11	9.01
	7.5	8.72	8.79	9.25	9.12
(**5,5′-Me$_2$bipy**)Pt(3′-GMP)$_2$ [b]	4.0	8.88	8.76	*c*	*c*
	7.5	8.87	8.75	*c*	*c*
(**Et$_4$dt**)Pt(5′-GMP)$_2$	4.0	9.06	8.96	9.18	8.83
	7.5	9.04	8.99	9.37	8.96
(**Et$_4$dt**)Pt(3′-GMP)$_2$	4.0	9.01	8.87	*c*	*c*
	7.5	9.01	8.88	*c*	*c*
(**Me$_4$dt**)Pt(5′-GMP)$_2$	4.0	9.08	8.96	9.10	8.66
	7.0	9.06	8.95	9.27	8.74
(**Me$_4$dt**)Pt(3′-GMP)$_2$	4.0	8.85	8.83	*c*	*c*
	7.0	8.89	8.92	*c*	*c*

[a] Subscripted letters d and u are used to distinguish the downfield and the upfield H8 signals, respectively. Signal assignments are based on the 2D NMR and pH titration studies. [b] NMR spectrum recorded at 25 °C. [c] Signal not detected.

The absence of H8–H8 EXSY cross-peaks in the ROESY spectrum of (**5,5′-Me$_2$bipy**)Pt(5′-GMP)$_2$ indicates that interconversion between the rotamers is slow. Rotation is probably impeded by the steric effect of the pyridyl H6/H6′ atoms of **5,5′-Me$_2$bipy**, which are the pyridyl ring atoms closest to the cis 5′-GMP's, as evident from models and from the observation of H8–H6/H6′ NOE cross-peaks. During rotation, the **G** O6 clashes with the pyridyl ring C6H. A further indication of this proximity is the finding that the pyridyl H6/H6′ signals of the (**5,5′-Me$_2$bipy**)Pt(5′-GMP)$_2$ adduct are shifted upfield by 1.0-1.4 ppm, when compared to the H6/H6′ signals (9.19 and 8.81 ppm) of the solvated Pt precursor. The anisotropy of the cis-coordinated **G** base is responsible for these large upfield shifts. A similar upfield shift was observed for the H6/H6′ signal of the [(**MepyMe$_2$t**)Pt(Guo)$_2$]$^{2+}$ adduct[34] and for the signals of the similarly positioned phenanthroline (**phen**) protons in the [(**phen**)Pt(Guo)$_2$]$^{2+}$ adduct.[33]

3.3.4. (5,5′-Me$_2$bipy)Pt(3′-GMP)$_2$

Two H8 signals downfield to the free 3′-GMP H8 signal at 8.11 ppm were observed at 25 °C and were assigned to the HT conformers of the (**5,5′-Me$_2$bipy**)Pt(3′-GMP)$_2$ adduct (Table 3.1 and Figure 3.5). From pH 4.0 to 7.5, the intensity of the H8 signal at 8.88 ppm increased, while that for the H8 signal at 8.76 ppm decreased. The CD signal shape at pH 7.5 was characteristic of the ΔHT conformer (Figure 3.6). For the 3′-GMP adducts, the ΔHT conformer is known to be stabilized by SSC upon phosphate deprotonation (pH ~7.0).[19,32,35,45] Therefore, this major H8 signal was assigned to the ΔHT conformer. The H8 signal at 8.76 ppm was assigned to the ΛHT conformer. From pH 4.0 to 7.5, the conformation distribution of the ΔHT and ΛHT conformers changed from 73% and 27% to 80% and 20%, respectively. The H8 signal of the major ΔHT conformer is 0.17 ppm downfield from that of the minor ΛHT conformer. From this relationship,

the '6-in' major form is ΔHT R, and the '6-out' minor form is ΛHT R (cf. Figure 3.4). Neither NOE nor EXSY cross-peaks were observed between the H8 signals of the (**5,5′-Me$_2$bipy**)Pt(3′-GMP)$_2$ adduct. Strong H8–H6/H6′ NOE cross-peaks at 8.06, 8.88 ppm for the ΔHT conformer and at 7.79, 8.76 ppm were observed for the ΛHT conformer. Of particular note, the HH conformer was not detected for this adduct, even at 5 °C, thus reinforcing the general finding that the 5′-phosphate group stabilizes the HH conformer more than the 3′-phosphate group does.[35,43] When conformer interchange is slow, the HH conformer is usually found for **L**Pt(3′-GMP)$_2$ adducts. For example, at pH 3.3 for the (**Me$_2$ppz**)Pt(GMP)$_2$ adducts, the amount of HH conformer observed for the 3′-GMP adduct was small (~8%), in comparison to ~24% HH conformer for the 5′-GMP adduct.[21] The (**5,5′-Me$_2$bipy**)Pt(3′-GMP)$_2$ adduct, in fact, presents the first case in which no HH conformer is found for a 3′-GMP adduct with slowly interchanging rotamers.

3.3.5. (MepyMe$_2$t)Pt(5′-GMP)$_2$

Within two hours of mixing (**MepyMe$_2$t**)PtCl$_2$ with 5′-GMP in a 1:2 molar ratio at pH ~4.0 at 25 °C, four pairs of new H8 signals downfield from the free 5′-GMP H8 signal were present. As the pH was varied from 2.5 to 7.5, the H8 signals at 8.96 and 8.78 ppm became the most dominant signals (Figure 3.7). A CD signal shape characteristic of the ΛHT conformer was observed for (**MepyMe$_2$t**)Pt(5′-GMP)$_2$ at pH 7.5 and below (Figure 3.8). The CD signal intensity was stronger at pH 7.5 than at pH 2.5, consistent with the higher stability of the ΛHT conformer caused on phosphate deprotonation resulting from SSC.[21,42,43] Thus, the larger H8 signals (at 8.96 and 8.78 ppm at pH 2.5) were assigned to the ΛHT conformer.

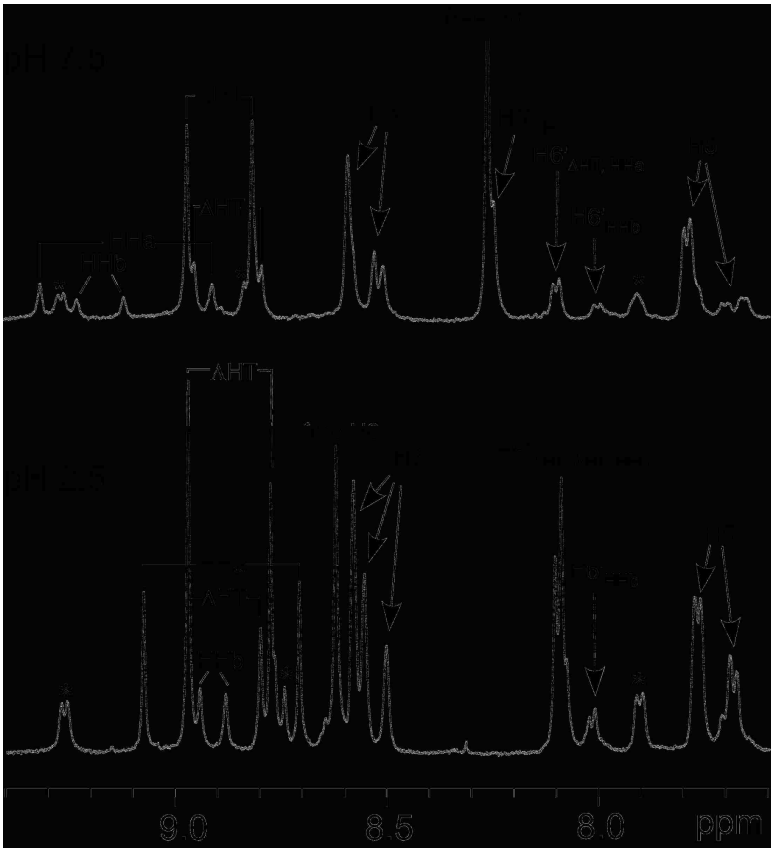

Figure 3.7 Aromatic region of ^{1}H NMR spectra of (**MepyMe$_2$t**)Pt(5′-GMP)$_2$ at pH 2.5 (bottom) and pH 7.5 (top) at 25 °C. The H8 signals for the conformers are designated by the conformation. (Pyridyl signals attributed to the solvated Pt complex are indicated by asterisks.)

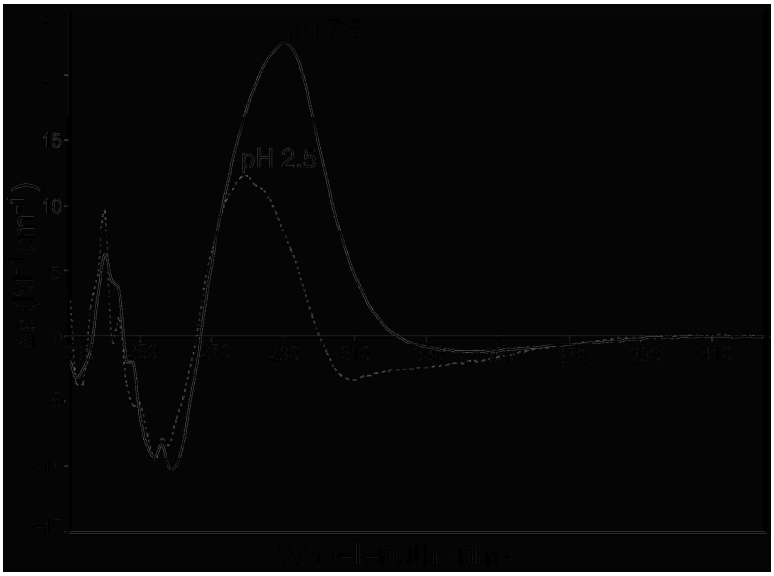

Figure 3.8 CD spectra of (**MepyMe$_2$t**)Pt(5′-GMP)$_2$ at pH 2.5 and pH 7.5 at 25 °C.

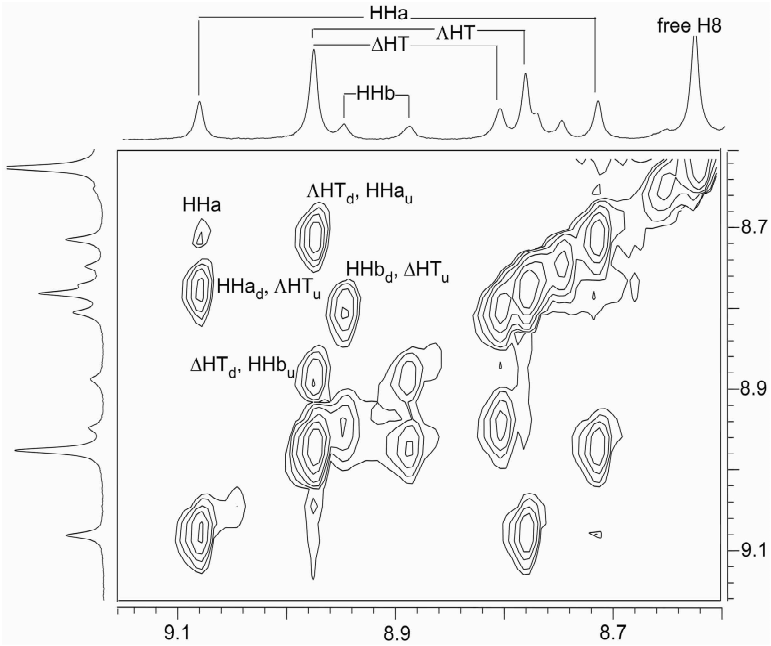

Figure 3.9 ROESY spectrum of the (**MepyMe$_2$t**)Pt(5′-GMP)$_2$ adduct in the aromatic region at pH 2.5 and 25 °C. The cross-peak labeled as HHa is an NOE between the two H8 signals of the HHa conformer. The other labeled cross-peaks are EXSY peaks between the H8 signals of two different conformers.

Table 3.2 Chemical Shifts of the H8 Signals of (**MepyMe$_2$t**)Pt(GMP)$_2$ Adducts at 25 °C [a]

complex	pH	ΔHT		ΛHT		HHa		HHb	
		ΔHT$_d$ (py)	ΔHT$_u$ (t)	ΛHT$_d$ (py)	ΛHT$_u$ (t)	HHa$_d$ (t)	HHa$_u$ (py)	HHb$_d$ (t)	HHb$_u$ (py)
(**MepyMe$_2$t**)Pt(5′-GMP)$_2$	2.5	8.96	8.83	8.96	8.78	9.08	8.71	8.94	8.88
	7.5	8.96_2	8.81_4	8.95_8	8.80_7	9.31	8.91	9.23	9.10
(**MepyMe$_2$t**)Pt(3′-GMP)$_2$	4.5	8.95	8.84	8.89	8.74	*b*		*b*	
	7.5	8.89	8.81	8.89	8.74	*b*		*b*	

[a] The py and t notations designate **G**'s cis to the pyridyl and triazine rings, respectively. Subscripted letters d and u are used for downfield and upfield H8 signals, respectively. Third decimal place subscripted numbers are used to distinguish signals with very similar chemical shifts. Signal assignments are based on the 2D NMR and pH titration studies. [b] Signal not detected.

In a ROESY spectrum of the (**MepyMe$_2$t**)Pt(5′-GMP)$_2$ adduct at pH 2.5 (where the H8 signals of this adduct were most widely dispersed), a weak NOE cross-peak present between the

two comparably sized H8 signals at 9.08 and 8.71 ppm establishes the HH conformation (Figure 3.9 and Table 3.2). This HH conformer (assigned as HHa, see below) is the second most abundant conformer of the (**MepyMe$_2$t**)Pt(5′-GMP)$_2$ adduct. These two HH H8 signals are well dispersed and straddle the signals of the HT conformers, the usual H8 chemical shift pattern.[19,30,31] The remaining two pairs of H8 signals must belong to the ΔHT and HHb conformers. However, because of the unusual properties of these conformers and the unsymmetrical nature of the carrier ligand, we turned to a pH study to make the assignment of conformation.

From pH 2.5 to pH 7.5 the H8 signals for the (**MepyMe$_2$t**)Pt(5′-GMP)$_2$ HHa rotamer shifted significantly downfield by 0.23 and 0.20 ppm (Figure 3.7). Typically, a ca. 0.2 ppm downfield shift was observed for HH rotamers[20,21] upon phosphate deprotonation; this effect may be explained by the "wrong-way shift" attributed to the higher deshielding effect of the deprotonated phosphate group as it is positioned in the HH conformer.[20,50] However, the H8 signals of the HT conformers do not shift significantly in the pH ~2-7 range.[21,35,43] Consistent with this pattern, the H8 signals of the (**MepyMe$_2$t**)Pt(5′-GMP)$_2$ ΛHT conformer shifted very little (Table 3.2, Figure 3.7), whereas a ca. 0.2 ppm downfield shift occurred for the H8 signal of the HH conformer of the (**R$_4$dt**)Pt(5′-GMP)$_2$ adducts discussed below.

One of the two pairs of H8 signals of the (**MepyMe$_2$t**)Pt(5′-GMP)$_2$ adduct (at 8.94 and 8.88 ppm) not assigned above shifted downfield by more than 0.2 ppm from pH 2.5 to 7.5 (Table 3.2, Figure 3.7); this pair is assigned to HHb. However, because of the low abundance of the HHb conformer, no H8 to H8 NOE cross-peak was observed in the ROESY spectrum for the (**MepyMe$_2$t**)Pt(5′-GMP)$_2$ adduct. The remaining pair of H8 signals shifted only slightly upfield (Table 3.2, Figure 3.7), consistent with an assignment to the only other possible conformer, ΔHT.

For the (**MepyMe$_2$t**)Pt(5′-GMP)$_2$ adduct, the H8 to pyridyl H6′ NOE cross-peaks can be used to determine which H8 signal belongs to the 5′-GMP cis to the pyridyl ring and by default which H8 signal belongs to the 5′-GMP cis to the triazine ring. Because the ΔHT and ΛHT conformers are assigned, the orientation of the **G** bases relative to these ligand rings is established for the HT conformers. The pyridyl H6′ signals of the (**MepyMe$_2$t**)Pt(5′-GMP)$_2$ adduct (overlapping at 8.0-8.1 ppm) have NOE cross-peaks to the downfield H8 signals of the ΛHT and ΔHT conformers (overlapping at 8.96 ppm) and to the upfield H8 signals of the HHa conformer (at 8.71 ppm) and the HHb conformer (at 8.88 ppm). These H8 signals are assigned to the 5′-GMP cis to the pyridyl ring.

As can be seen from Figure 3.2, where N′ represents the pyridyl ring, the base next to this ring has an orientation with respect to the coordination plane that is the same in the ΛHT and HHa pair. Likewise, the orientation of this base is the same in the ΔHT and HHb pair. The rotation of the 5′-GMP cis to the pyridyl ring is expected to be slow; thus, conformer interchange involving such rotation will be too slow to generate detectable EXSY cross-peaks. (Slow interconversion between rotamers is depicted by short arrows in this figure.) Each HT conformer can exchange rapidly (depicted by long arrows) with only one HH conformer because only the base cis to the triazine ring can rotate rapidly. For example, the H8 signal of the **G** in the ΔHT rotamer cis to the triazine ring at 8.83 ppm has an EXSY cross-peak with the downfield H8 signal of the HHb rotamer at 8.94 ppm; this H8 signal of the HHb rotamer belongs to the 5′-GMP cis to the triazine ring. Such EXSY cross-peaks between the H8 signals of the 5′-GMP cis to the triazine ring of the HH and HT rotamers were used for the unambiguous assignment of the HH conformers as HHa and HHb because the ΔHT and the ΛHT H8 signals of the 5′-GMP cis to the pyridyl ring overlap at 8.96 ppm.

We apply the foregoing reasoning to all four H8-H8 EXSY cross-peaks in the ROESY spectrum of the (**MepyMe$_2$t**)Pt(5′-GMP)$_2$ adduct at 25 □C (Figure 3.9). The EXSY cross-peaks observed are between the H8 signals of the HHa and the ΛHT rotamers (9.08 and 8.78 ppm (cis to the triazine ring) and 8.71 and 8.96 ppm (cis to the pyridyl ring)) and between the H8 signals of the HHb and the ΔHT rotamers (8.94 and 8.83 ppm (cis to the triazine ring) and 8.88 and 8.96 ppm (cis to the pyridyl ring)).

For the (**MepyMe$_2$t**)Pt(5′-GMP)$_2$ adduct, as the pH was increased from 2.5 to 7.5, the population of the ΛHT, HHa, ΔHT, and HHb conformers changed from 40%, 30%, 20%, and 10% to 65%, 10%, 20%, and 5%, respectively (Figure 3.7). For this adduct, the combined abundance of the HT conformers is greater than the combined abundance of the HH conformers, a typical situation.[49] It is also typical for the percentage of the HH conformers to decrease with increasing pH.[20]

At pH 7.5 and below, the HHa conformer of (**MepyMe$_2$t**)Pt(5′-GMP)$_2$ is more abundant and has more H8 to H8 signal dispersion (0.37 ppm) than the HHb conformer (0.06 ppm). For HHa, the 5′-GMP cis to the pyridyl ring has the upfield shift so the base is canted with its H8 atom projecting toward the shielding region of the 5′-GMP cis to the triazine ring. This 5′-GMP is either not canted or only slightly canted. Canting in the HHa conformer (Figure 3.2, where N′ represents the pyridyl ring) is right-handed (R). However, the small H8 signal dispersion for the HHb conformer of the (**MepyMe$_2$t**)Pt(5′-GMP)$_2$ adduct is associated with a low degree of canting,[21,22] similar to that observed for the (**5,5′-Me$_2$bipy**)Pt(5′-GMP)$_2$ adduct. The orientation of the two 5′-GMP bases in HHb may be nearly perpendicular to the Pt coordination plane or may be slightly canted. Alternatively, the two bases may be "wagging", rapidly changing the

canting direction between the R- and L-canted orientations, leading to shift averaging and thereby accounting for the small HH H8 signal dispersion.

3.3.6. (MepyMe$_2$t)Pt(3′-GMP)$_2$

Qualitatively, for **G** derivatives the rate of rotation about the Pt–N7 bond increases in the order, 5′-GMP < 3′-GMP < Guo < 9-Et**G** (9-Et**G** = 9-ethylguanine).[19,31,32,46,51] Previously we observed only four H8 signals for (**MepyMe$_2$t**)Pt(Guo)$_2$.[34] We attributed this finding to fast interchange within each of the pairs (ΛHT, HHa and ΔHT, HHb), a process involving **G** base rotation for the Guo cis to the triazine ring (Figure 3.2). Also, rotation of the Guo cis to the pyridyl group was postulated to be a slow process, as now confirmed for the (**MepyMe$_2$t**)Pt(5′-GMP)$_2$ adduct, which exhibited no interchange (no EXSY peaks) between the two pairs.

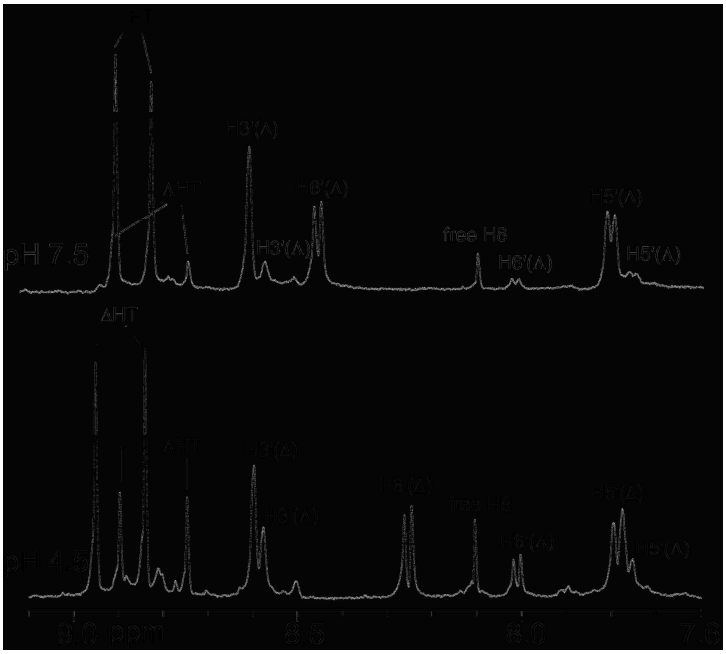

Figure 3.10 Aromatic region of ^{1}H NMR spectra of (**MepyMe$_2$t**)Pt(3′-GMP)$_2$ at pH 4.5 (bottom) and pH 7.5 (top) at 25 °C. The H8 signals for the conformers are designated by the conformation.

Two pairs of H8 signals in a 2:1 ratio were observed for the (**MepyMe$_2$t**)Pt(3′-GMP)$_2$ adduct at pH 4.5 and 25 °C (Figure 3.10). Neither NOE nor EXSY cross-peaks were observed

between these H8 signals; an NOE cross-peak is expected for an HH conformer. Therefore, even for a rapid HT/HH equilibrium, an NOE cross-peak would be found if either HT/HH pair had a significant amount of the HH conformer. The H8 NMR signals of the HH conformer were not detectable even at low temperature (0 °C), a result similar to that found for the (**pipen**)Pt(3′-GMP)$_2$[45] (**pipen** = 2-aminomethylpiperidine) and [(**MepyMe$_2$t**)Pt(Guo)$_2$]$^{2+}$ adducts. Thus, the H8 signals of the (**MepyMe$_2$t**)Pt(3′-GMP)$_2$ adduct arising from two sets of rapidly interchanging pairs of conformers, ΔHT/HHa and ΛHT/HHb, reflect primarily a dominant HT conformer, as discussed previously.[34] The two pairs of HT and HH conformers interchange within the pair but not between pairs. The four H8 signals for the (**MepyMe$_2$t**)Pt(3′-GMP)$_2$ adduct thus reflect mainly the two HT conformers, ΔHT and ΛHT. From the order of rotation rates for the various **G** derivatives it was uncertain what pattern of behavior to expect, but now it is clear that (**MepyMe$_2$t**)Pt(3′-GMP)$_2$ has dynamic properties more similar to those of (**MepyMe$_2$t**)Pt(Guo)$_2$ than to those of (**MepyMe$_2$t**)Pt(5′-GMP)$_2$.

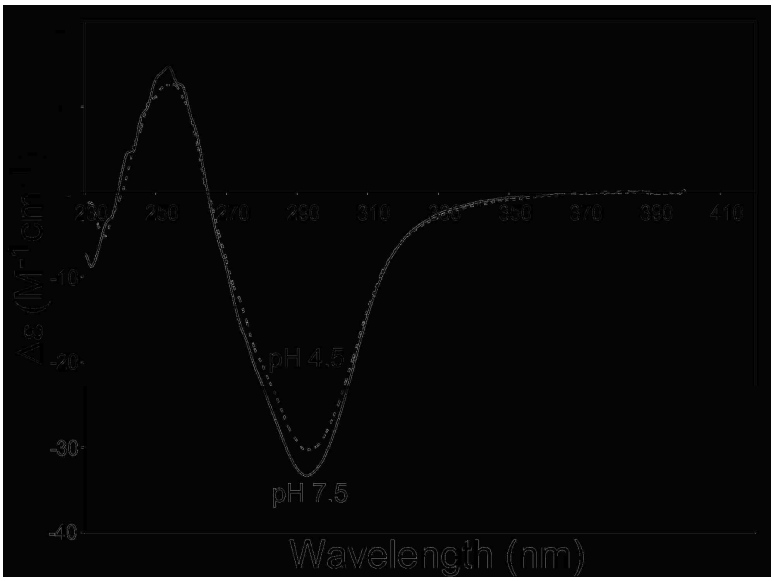

Figure 3.11 CD spectra of (**MepyMe$_2$t**)Pt(3′-GMP)$_2$ at pH 4.5 and 7.5 at 25 °C.

From 4.5 to 7.5, the more downfield of the two H8 signals of the major HT rotamer of (**MepyMe$_2$t**)Pt(3′-GMP)$_2$ (at 8.95 ppm) shifted slightly upfield, overlapping with the downfield H8 signal of the minor HT rotamer at 8.89 ppm (Table 2). The other H8 signals showed no significant shift until pH 7.5. As the pH was increased from 4.5 to 7.5, the major HT rotamer became the almost exclusively observed atropisomer (Figure 3.10). The CD spectra collected at pH 4.5 and 7.5 are characteristic of the ΔHT conformer (Figure 3.11). Therefore, at pH 4.5, the H8 signals at 8.95 and 8.84 ppm belonging to the major HT conformer are assigned to the ΔHT conformer stabilized by SSC, while the H8 signals at 8.89 and 8.74 ppm are assigned to the ΛHT conformer (minor). This previously reported downfield relationship of the H8 signal of the major HT conformer to the respective H8 signal of the minor HT conformer[19,23,30,31,43] is consistent with the major ΔHT conformer being '6-in' (R canting) and the minor ΛHT conformer being '6-out' (L canting).

The properties of the (**MepyMe$_2$t**)Pt(3′-GMP)$_2$ adduct at pH 4.5 were explored further in ROESY studies. From the NOE cross-peaks, the H8 signals belonging to the 3′-GMP cis to the pyridyl ring of the HT conformers of the (**MepyMe$_2$t**)Pt(5′-GMP)$_2$ adduct were also downfield compared to those of the 3′-GMP cis to the triazine ring. For the (**MepyMe$_2$t**)Pt(3′-GMP)$_2$ adduct, the H6′ doublets of the ΔHT and ΛHT conformers (Supporting Information) were shifted upfield by 1.01 and 1.24 ppm from the H6′ signal of the solvated Pt complex at 9.26 ppm (Figure 3.10); similar behavior was observed for the H6′ signal of (**5,5′-Me$_2$bipy**)Pt(3′-GMP)$_2$ adduct. These large H6′ upfield shifts can be attributed to the anisotropic effect of the cis coordinated base but cannot easily be correlated with the degree of canting.

3.3.7 (Et$_4$dt)Pt(5′-GMP)$_2$

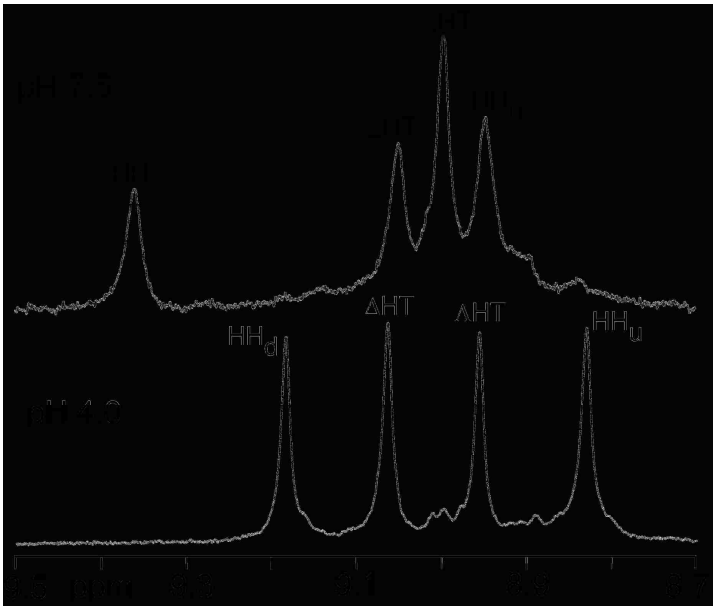

Figure 3.12 H8 region of the ^{1}H NMR spectra of (**Et$_4$dt**)Pt(5′-GMP)$_2$ at 5 °C.

Four new H8 signals of comparable intensities were observed within 24 h of mixing 1 equiv of (**Et$_4$dt**)PtCl$_2$ with 2 equiv of 5′-GMP at 25 °C (Figure 3.12). Sharp ^{1}H NMR signals were observed at 25 °C for the (**Et$_4$dt**)Pt(5′-GMP)$_2$ adduct at pH ~4; however, in order to compare the data with the (**Me$_4$dt**)Pt(5′-GMP)$_2$ adduct (Supporting Information), 1D ^{1}H NMR spectra and a ROESY spectrum were collected at 5 °C. At 25 °C, the full width at half maximum (fwhm) of the H8 signals for (**Et$_4$dt**)Pt(5′-GMP)$_2$ was 6 Hz for all three rotamers, as compared to the fwhm of the H8 signals of (**Me$_4$dt**)Pt(5′-GMP)$_2$ of 11 (ΔHT), 10 (ΛHT), 12 (HH$_d$) and 11 (HH$_u$) Hz. These H8 signals of the (**Et$_4$dt**)Pt(5′-GMP)$_2$ adduct at 25 °C were even sharper than those of the (**Me$_4$dt**)Pt(5′-GMP)$_2$ adduct at 5 °C, where all fwhm values were ~7 Hz. These comparisons clearly indicate that the rotation rate about the Pt–N7 bond is considerably slower for (**Et$_4$dt**)Pt(5′-GMP)$_2$ than for (**Me$_4$dt**)Pt(5′-GMP)$_2$, probably because of

steric clashes between the 5′-GMP O6 and the methyl group of the 6,6′ ethyl groups of the **Et$_4$dt** ligand in the (**Et$_4$dt**)Pt(5′-GMP)$_2$ adduct as the **G** base rotates (Figure 3.13).

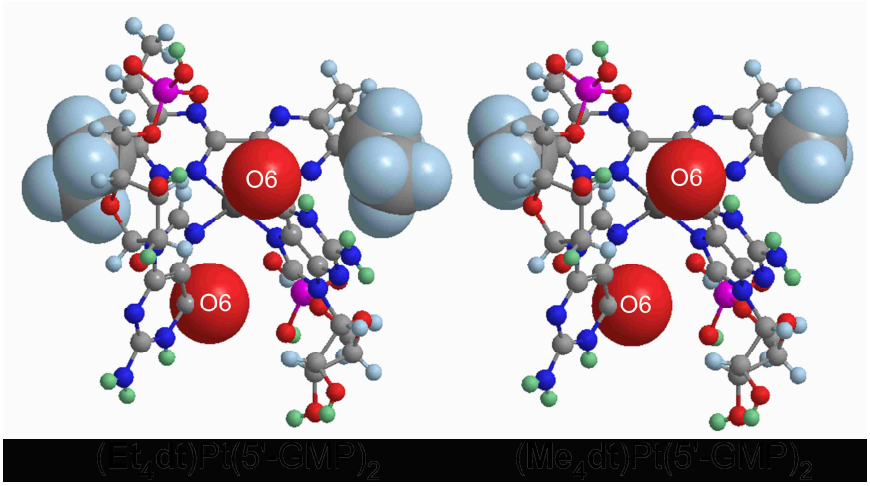

Figure 3.13 Greater steric clashes between substitutents at the 6,6′ position of the **R$_4$dt** carrier ligand and the **G** O6 for the **Et$_4$dt** adduct compared to the **Me$_4$dt** adduct.

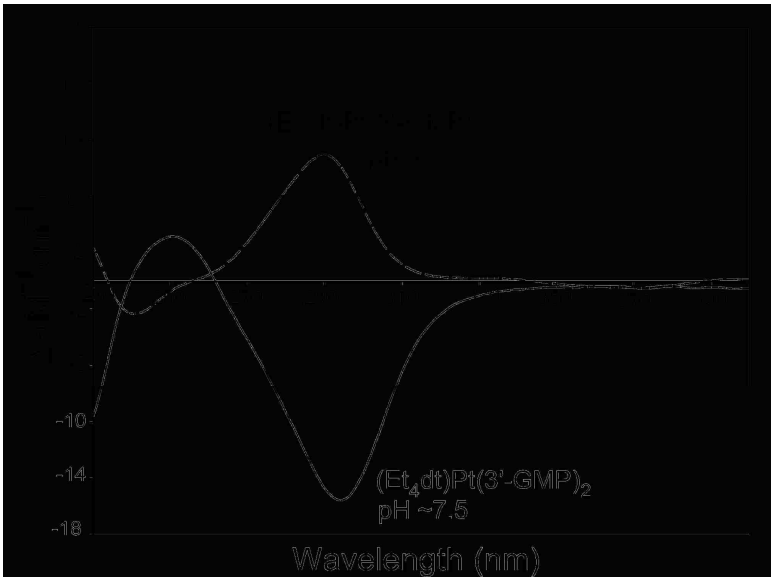

Figure 3.14 CD spectra of (**Et$_4$dt**)Pt(5′-GMP)$_2$ and (**Et$_4$dt**)Pt(3′-GMP)$_2$ at 25 °C.

When the pH of solutions containing (**Et$_4$dt**)Pt(GMP)$_2$ adducts was raised from ~4 to 7.5 (above pH 7.5 the adduct decomposed, as evidenced by an increase in the intensity of the free GMP H8 signal), the H8 signal at 8.96 ppm shifted slightly downfield to 8.99 ppm and became

the most dominant signal (Figure 3.12); this peak was assigned to the ΛHT conformer because the CD signal shape observed for this solution is characteristic of the ΛHT conformation (Figure 3.14).[31,32,35,44,45] SSC interactions stabilize the ΛHT conformer of **L**Pt(5′-GMP)$_2$ adducts at or near neutral pH.[35,42,43] At pH 4.0, an NOE cross-peak was observed between the two dispersed, comparably sized H8 signals at 9.18 and 8.83 ppm (Figure 3.15). These characteristics allow unambiguous assignment of these H8 signals to the HH rotamer. The H8 signals of the HH rotamer for the (**Et$_4$dt**)Pt(5′-GMP)$_2$ adduct at both high and low pH values were ~0.08-0.22 ppm more downfield than those for the (**Me$_4$dt**)Pt(5′-GMP)$_2$ adduct (Table 3.1). The remaining H8 signal of the (**Et$_4$dt**)Pt(5′-GMP)$_2$ adduct at 9.06 ppm (pH 4.0) was assigned to the ΔHT rotamer. From pH 4.0-7.5, no significant shift was observed for the H8 signals of the HT rotamers; however, the HH$_d$ and the HH$_u$ signals shifted downfield by 0.19 and 0.13 ppm, respectively.

In contrast to the typical H8 chemical shift pattern of the major and the minor HT conformers,[19,23,30,31,43] the H8 signal of the major HT conformer (ΛHT) of the (**Et$_4$dt**)Pt(5′-GMP)$_2$ adduct (at pH 7.5) is upfield to that of the minor HT conformer (ΔHT). Because the H8 signals of the HT conformers are relatively more downfield and the difference in the chemical shifts is small (0.10 ppm), it is not clear if this unusual HT H8 signal shift pattern is because of a relatively more upfield ΛHT H8 signal or a more downfield ΔHT H8 signal. The H8 signals of the HT conformers of the (**Et$_4$dt**)Pt(5′-GMP)$_2$ adduct are positioned between the two H8 signals of the HH conformer. Thus, the H8 shifts of the HT conformers are not particularly unusual. Because of the symmetrical nature of the carrier ligand in (**Et$_4$dt**)Pt(5′-GMP)$_2$, the bases in HT conformers may 'wag' between R and L canting, causing the H8 signals of the conformers to have similar shifts. The H8 chemical shift pattern (separation of 0.35 ppm) for the HH conformer of (**Et$_4$dt**)Pt(5′-GMP)$_2$ is similar to that of the HH conformer of (**MepyMe$_2$t**)Pt(5′-GMP)$_2$. The

moderately large H8 signal dispersion (0.35 ppm) for the (**Et$_4$dt**)Pt(5′-GMP)$_2$ HH conformer is attributable to different canting of the two bases.

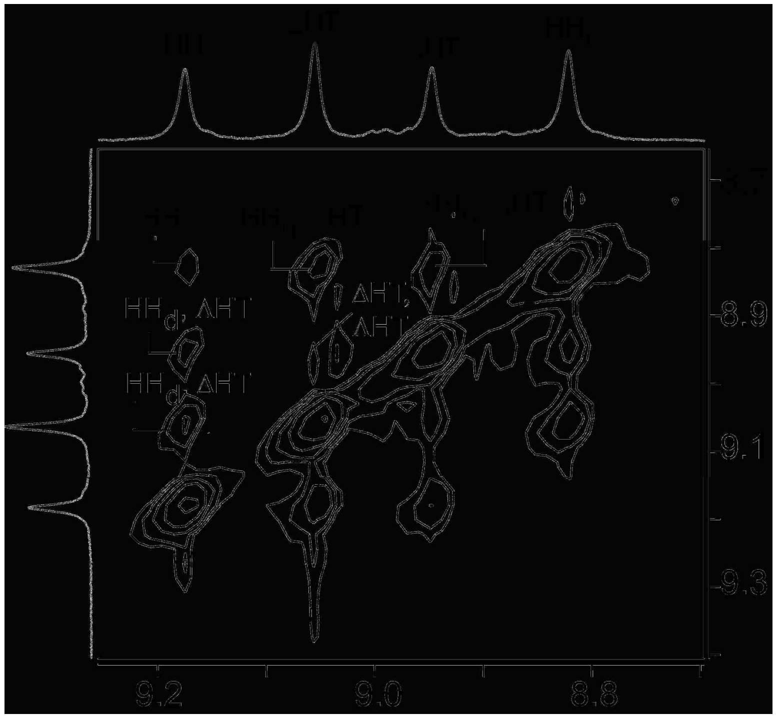

Figure 3.15 H8 region of the ROESY spectrum of (**Et$_4$dt**)Pt(5′-GMP)$_2$ at pH 4.0 and 5 °C. The cross-peak labeled as HH is an NOE between the H8 signals of an HH conformer. The other labeled cross-peaks are EXSY peaks between the H8 signals of different rotamers.

Five EXSY cross-peaks were observed in a ROESY spectrum of (**Et$_4$dt**)Pt(5′-GMP)$_2$, collected at 5 °C (Figure 3.15). The two H8 signals of the HH rotamer have cross-peaks with the H8 signals of both the ΛHT and ΔHT rotamers. Also, a weak EXSY cross-peak was observed between the H8 signals of the ΛHT and the ΔHT rotamers. Because both 5′-GMP's are cis to the sterically less impeding triazine rings, Pt–N7 rotation is fast enough for the H8 signals of the rotamers to have EXSY cross-peaks. In contrast, interchange between rotamers is slower in ligands containing a pyridyl moiety, as evidenced by the absence of any H8-H8 EXSY cross-peaks for (**5,5′-Me$_2$bipy**)Pt(5′-GMP)$_2$. In addition H8-H8 cross-peaks between the ΛHT and the ΔHT conformers were absent for the (**MepyMe$_2$t**)Pt(5′-GMP)$_2$ adduct. The broad NMR signals

observed at 25 °C for the (**Me$_4$dt**)Pt(5′-GMP)$_2$ adduct can be attributed to exchange between conformers and provide further evidence for facile interchange between rotamers in the (**R$_4$dt**)Pt(5′-GMP)$_2$ adducts.

For the (**Et$_4$dt**)Pt(5′-GMP)$_2$ adduct, increasing the pH from 4.0 to 7.5 changed the distribution of the HH, ΛHT and ΔHT rotamers from 50%, 25% and 25% to 40%, 37% and 23%, respectively (Figure 3.12). For both (**Et$_4$dt**)Pt(5′-GMP)$_2$ (Figure 3.12) and (**Me$_4$dt**)Pt(5′-GMP)$_2$ (Supporting Information) at pH 4.0, the two HT conformers are almost equally abundant, and the HH conformer has a relatively high abundance; these features are unusual when compared to the other **L**Pt(5′-GMP)$_2$ adducts, including the (**5,5′-Me$_2$bipy**)Pt(5′-GMP)$_2$ and (**MepyMe$_2$t**)Pt(5′-GMP)$_2$ adducts studied here. This larger abundance of the HH conformer of the (**R$_4$dt**)Pt(5′-GMP)$_2$ adducts is attributable to the overall low steric effects of the **R$_4$dt** (**R = Me** and **Et**) ligand.

The chemical shift of the H8 signals and the HH rotamer abundance in (**Et$_4$dt**)Pt(5′-GMP)$_2$, when compared to values for (**Me$_4$dt**)Pt(5′-GMP)$_2$ (Supporting Information), suggest some interaction between the ethyl groups of **Et$_4$dt** and the bound 5′-GMP's. As mentioned above, the 6,6′ ethyl groups impede **G** base rotation. However, at pH 4 the 50% abundance of the HH rotamer for the (**Et$_4$dt**)Pt(5′-GMP)$_2$ adduct was slightly higher than the 40% abundance observed for the (**Me$_4$dt**)Pt(5′-GMP)$_2$ HH rotamer. Thus, the greater bulk of **Et** vs. **Me** is reflected primarily in the **G** base rotation rate.

3.3.8 (Et$_4$dt)Pt(3′-GMP)$_2$

The two H8 signals observed in a 2:1 ratio for the (**Et$_4$dt**)Pt(3′-GMP)$_2$ adduct (Figure 3.16) did not shift when the pH was raised from 4.0 to 7.5. However, the signal at 9.01 ppm

became the dominant H8 signal. The CD signal shape at pH 7.5 (Figure 3.14) is characteristic of the ΔHT conformation.[31,32,42,45] Thus, the 9.01 ppm signal was assigned to the ΔHT conformer, the conformer stabilized by SSC on phosphate deprotonation for 3′-GMP adducts.[35,42,43] The other H8 signal (at 8.87 ppm) is assigned to the ΛHT conformer. The conformer distributions (respective amounts of ΔHT and ΛHT = 67% and 33% at pH 4.0 and 75% and 25% at pH 7) are comparable with those for (**Me$_4$dt**)Pt(3′-GMP)$_2$ (Supporting Information).

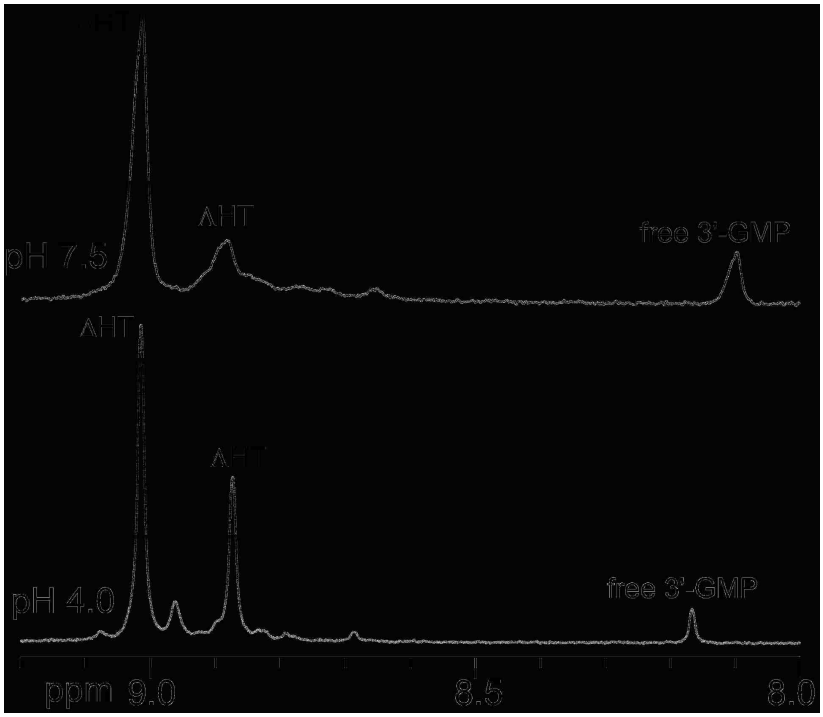

Figure 3.16. H8 region of the ^{1}H NMR spectra of (**Et$_4$dt**)Pt(3′-GMP)$_2$ at 5 °C.

The HH conformer was not detected for either (**R$_4$dt**)Pt(3′-GMP)$_2$ adduct. The dispersion of the two H8 signals of the (**Et$_4$dt**)Pt(3′-GMP)$_2$ adduct (Table 3.1) was sufficient for us to resolve an EXSY cross-peak between these H8 signals. The cross-peak confirms that the two observable HT signals are mainly from rapidly interchanging ΔHT and ΛHT conformers; interchange undoubtedly proceeds via the HH conformer (Figure 3.2). The same exchange

process obviously occurs for the (**Me$_4$dt**)Pt(3′-GMP)$_2$ adduct, but the H8 signals are not separated well enough for us to detect the EXSY cross-peak (Supporting Information).

3.4 Conclusions

The bulk of the bidentate sp^2 N-donor ligands is sufficient to impede the rotation of the GMP's about the Pt–N7 bonds of the **L**Pt(GMP)$_2$ adducts; thus, H8 signals for conformers could be resolved and assigned. From NMR data (including EXSY results), the qualitative rates of conformer interconversion follow the order, **Me$_4$dt > Et$_4$dt > MepyMe$_2$t > 5,5′-Me$_2$bipy.** Thus, we conclude that the pyridyl H6′ atom strongly impedes the rotation of the cis **G** base about the Pt–N7 bond by clashing with **G** O6, whereas the equivalently placed lone pair of the relevant non-bonded N of the triazine does not so strongly impede **G** rotation. Thus, the triazine ring has a lower overall steric effect than the pyridyl ring. The intermediate properties of **MepyMe$_2$t**, with one triazine and one pyridyl ring led to EXSY data for the (**MepyMe$_2$t**)Pt(5′-GMP)$_2$ adduct that allowed us to unambiguously determine and assign the conformation of the two HH conformers, HHa and HHb.

The nature of both the GMP and the carrier ligand in **L**Pt**G**$_2$ adducts influences the distribution of conformers and their characteristics. The **L**Pt**G**$_2$ adducts studied here have a higher abundance of the HH conformer when **G** = 5′-GMP's than when **G** = 3′-GMP's, supporting the general finding that the 5′-phosphate group stabilizes the HH conformer.[35,43] Typically, one HT conformer dominates over the other HT and the HH conformer at low pH (~4), especially at neutral pH. We have discovered that carrier ligands of the type, **R$_4$dt**, lead to the HH having almost comparable abundance to the total of the two HT conformers for the (**R$_4$dt**)Pt(5′-GMP)$_2$ adduct at equilibrium at pH 4. We conclude that the sterically less demanding nature of the **R$_4$dt** ligand allows ample space for the HH conformer to exist with less significant

clashes between the O6 atoms of the 5′-GMP's. Normally, second-sphere communication raises the abundance of one HT conformer as the pH is raised to near neutrality. This trend was found for the (**R$_4$dt**)Pt(5′-GMP)$_2$ adducts. However, the abundance of the HH isomer remains high. Given the finding that carrier ligands favoring the HH conformer in the cross-link are associated with anticancer activity,[16] Pt complexes of **R$_4$dt** ligand should be tested for activity.

In previous studies of **L**Pt(5′-GMP)$_2$ complexes, the CD and NMR spectroscopic data indicate that the ΛHT atropisomer predominates in solution at neutral pH.[19,21,35,42,44,45] The distribution of conformers for the (**5,5′-Me$_2$bipy**)Pt(5′-GMP)$_2$ and (**MepyMe$_2$t**)Pt(5′-GMP)$_2$ adducts agrees with the results for other **L**Pt(5′-GMP)$_2$ adducts. However, the two HT conformers of the (**R$_4$dt**)Pt(5′-GMP)$_2$ (**R** = **Me** or **Et**) adducts are unusual in having an approximately equal abundance at low pH and in having an H8 signal for the minor HT form (ΔHT) downfield to that of the major HT form (ΛHT) near physiological pH. At this time the reason for these differences is not apparent, and additional studies are in progress in order to understand the unique features of (**R$_4$dt**)Pt**G**$_2$ complexes. However, because **R$_4$dt** ligands are sterically less demanding when compared to other sp^2 N-donor ligands, it is possible that steric factors may limit the abundance of the minor HT conformer for **L**Pt(GMP)$_2$ adducts for other **L**. Nevertheless, we have made the surprising observation that placing greater bulk at the 6,6′ positions by changing **R** in **R$_4$dt** from Me to Et has a clear effect on the **G** base rotation rate about Pt–N7 bond. We attribute this effect to clashes between the **G** O6 and the methyl group of the 6,6′ ethyl groups (Figure 3.13).

Finally, our results indicate that adduct formation between **L**PtCl$_2$ (**L** = **5,5′-Me$_2$bipy** and **MepyMe$_2$t**) and 5′- and 3′-GMP does not go to completion, and residual solvated Pt complexes exist at equilibrium. Because the solutions contain DMSO, this solvent both complicates the

identification of the solvato species and probably is responsible for incomplete adduct formation. However, this situation presents a rare opportunity to compare the relative binding affinity of 3′-GMP vs. 5′-GMP toward Pt(II) in cis bis adducts. The ratio of **L**Pt(3′-GMP)$_2$: solvated Pt complex was 46:1 for **L = 5,5′-Me$_2$bipy** and 38:1 for **L = MepyMe$_2$t**, but the ratio of **L**Pt(5′-GMP)$_2$: solvated Pt complex was only 5:1 for **L = 5,5′-Me$_2$bipy** and only 4:1 for **L = MepyMe$_2$t**. This greater stability of **L**Pt(3′-GMP)$_2$ compared to **L**Pt(5′-GMP)$_2$ parallels the results observed for the *fac*-[Re(CO)$_3$(H$_2$O)(3′-GMP)$_2$]$^-$ and *fac*-[Re(CO)$_3$(H$_2$O)(5′-GMP)$_2$]$^-$ adducts.[52] This difference in the binding propensity of 3′-GMP vs. 5′-GMP is very unlikely to be due to electronic effects because N7 should have very similar donor ability for both 3′-GMP and 5′-GMP. Rather, the difference more likely arises from SSC effects involving the positioning of the phosphate groups. Perhaps the 3′-phosphate group is better positioned to form stabilizing H-bonds with N1H of the cis 3′-GMP than is the 5′-phosphate group. Such stabilization of an HT conformer could also explain the generally observed low abundance of the HH conformer of **L**Pt(3′-GMP)$_2$ adducts. The (**5,5′-Me$_2$bipy**)Pt(3′-GMP)$_2$ adduct studied presents an unusual case, in which no HH conformer was detected by using high-field NMR spectroscopy for a 3′-GMP adduct that has rotamers interchanging relatively slowly on the NMR time scale.

3.5 References

1. Bloemink, M. J.; Reedijk, J. In *Metal Ions in Biological Systems*; Sigel, A., Sigel, H., Eds.; Marcel Dekker: New York, 1996; Vol. 32, pp 641-685.

2. Reedijk, J. *J. Chem. Soc. Chem. Commun.* **1996**, 801-806.

3. Sherman, S. E.; Lippard, S. J. *Chem. Rev.* **1987**, *87*, 1153-1181.

4. Iwamoto, M.; Mukundan, S., Jr.; Marzilli, L. G. *J. Am. Chem. Soc.* **1994**, *116*, 6238-6244.

5. Kline, T. P.; Marzilli, L. G.; Live, D.; Zon, G. *J. Am. Chem. Soc.* **1989**, *111*, 7057-7068.

6. Fouts, C.; Marzilli, L. G.; Byrd, R.; Summers, M. F.; Zon, G.; Shinozuka, K. *Inorg. Chem.* **1988**, *27*, 366-376.

7. Jamieson, E. R.; Lippard, S. J. *Chem. Rev.* **1999**, *99*, 2467-2498.

8. van Garderen, C. J.; Bloemink, M. J.; Richardson, E.; Reedijk, J. *J. Inorg. Biochem.* **1991**, *42*, 199-205.

9. Laoui, A.; Kozelka, J.; Chottard, J.-C. *Inorg. Chem.* **1988**, *27*, 2751-2753.

10. Sherman, S. E.; Gibson, D.; Wang, A.; Lippard, S. J. *J. Am. Chem. Soc.* **1988**, *110*, 7368-7381.

11. Farrell, N. In *Metal Ions in Biological Systems*; Sigel, A., Sigel, H., Eds.; Marcel Dekker: New York, 1996; Vol. 32, pp 603-639.

12. Bloemink, M. J.; Heetebrij, R. J.; Inagaki, K.; Kidani, Y.; Reedijk, J. *Inorg. Chem.* **1992**, *31*, 4656-4661.

13. Ohndorf, U.-M.; Rould, M. A.; He, Q.; Pabo, C. O.; Lippard, S. J. *Nature (London)* **1999**, *399*, 708-712.

14. Marzilli, L. G.; Ano, S. O.; Intini, F. P.; Natile, G. *J. Am. Chem. Soc.* **1999**, *121*, 9133-9142.

15. Marzilli, L. G.; Saad, J. S.; Kuklenyik, Z.; Keating, K. A.; Xu, Y. *J. Am. Chem. Soc.* **2001**, *123*, 2764-2770.

16. Ano, S. O.; Kuklenyik, Z.; Marzilli, L. G. In *Cisplatin. Chemistry and Biochemistry of a Leading Anticancer Drug*; Lippert, B., Ed.; Wiley-VCH: Weinheim, 1999, pp 247-291.

17. Spingler, B.; Whittington, D. A.; Lippard, S. J. *Inorg. Chem.* **2001**, *40*, 5596-5602.

18. Williams, K. M.; Cerasino, L.; Natile, G.; Marzilli, L. G. *J. Am. Chem. Soc.* **2000**, *122*, 8021-8030.

19. Ano, S. O.; Intini, F. P.; Natile, G.; Marzilli, L. G. *Inorg. Chem.* **1999**, *38*, 2989-2999.

20. Saad, J. S.; Scarcia, T.; Natile, G.; Marzilli, L. G. *Inorg. Chem.* **2002**, *41*, 4923-4935.

21. Sullivan, S. T.; Ciccarese, A.; Fanizzi, F. P.; Marzilli, L. G. *Inorg. Chem.* **2000**, *39*, 836-842.

22. Bhattacharyya, D.; Marzilli, P. A.; Marzilli, L. G. *Inorg. Chem.* **2005**, *44*, 7644-7651.

23. Ano, S. O.; Intini, F. P.; Natile, G.; Marzilli, L. G. *J. Am. Chem. Soc.* **1997**, *119*, 8570-8571.

24. den Hartog, J. H. J.; Altona, C.; Chottard, J.-C.; Girault, J.-P.; Lallemand, J.-Y.; de Leeuw, F. A. A. M.; Marcelis, A. T. M.; Reedijk, J. *Nucleic Acids Res.* **1982**, *10*, 4715-4730.

25. Girault, J.-P.; Chottard, G.; Lallemand, J.-Y.; Chottard, J.-C. *Biochemistry* **1982**, *21*, 1352-1356.

26. Kozelka, J.; Fouchet, M. H.; Chottard, J.-C. *Eur. J. Biochem.* **1992**, *205*, 895-906.

27. Berners-Price, S. J.; Ranford, J. D.; Sadler, P. J. *Inorg. Chem.* **1994**, *33*, 584-5846.

28. Neumann, J.-M.; Tran-Dinh, S.; Girault, J.-P.; Chottard, J.-C.; Huynh-Dinh, T. *Eur. J. Biochem.* **1984**, *141*, 465-472.

29. Kiser, D.; Intini, F. P.; Xu, Y.; Natile, G.; Marzilli, L. G. *Inorg. Chem.* **1994**, *33*, 4149-4158.

30. Xu, Y.; Natile, G.; Intini, F. P.; Marzilli, L. G. *J. Am. Chem. Soc.* **1990**, *112*, 8177-8179.

31. Marzilli, L. G.; Intini, F. P.; Kiser, D.; Wong, H. C.; Ano, S. O.; Marzilli, P. A.; Natile, G. *Inorg. Chem.* **1998**, *37*, 6898-6905.

32. Williams, K. M.; Cerasino, L.; Intini, F. P.; Natile, G.; Marzilli, L. G. *Inorg. Chem.* **1998**, *37*, 5260-5268.

33. Margiotta, N.; Papadia, P.; Fanizzi, F. P.; Natile, G. *Eur. J. Inorg. Chem.* **2003**, 1136-1144.

34. Maheshwari, V.; Bhattacharyya, D.; Fronczek, F. R.; Marzilli, P. A.; Marzilli, L. G. *Inorg. Chem.* **2006**, *45*, 7182-7190.

35. Sullivan, S. T.; Ciccarese, A.; Fanizzi, F. P.; Marzilli, L. G. *Inorg. Chem.* **2001**, *40*, 455-462.

36. Price, J. H.; Williamson, A. N.; Schramm, R. F.; Wayland, B. B. *Inorg. Chem.* **1972**, *11*, 1280-1284.

37. Maheshwari, V.; Carlone, M.; Fronczek, F. R.; Marzilli, L. G. *Acta Crystallogr., Sect. B: Struct. Sci.* **2007**, *B63*, 603-611.

38. Jensen, R. E.; Pflaum, R. T. *Anal. Chim. Acta* **1965**, *32*, 235-244.

39. Sullivan, S. T.; Ciccarese, A.; Fanizzi, F. P.; Marzilli, L. G. *J. Am. Chem. Soc.* **2001**, *123*, 9345-9355.

40. Sigel, H.; Lippert, B. *Pure Appl. Chem.* **1998**, *70*, 845.

41. Sigel, H.; Massoud, S. S.; Corfu, N. A. *J. Am. Chem. Soc.* **1994**, *116*, 2958-2971.

42. Wong, H. C.; Shinozuka, K.; Natile, G.; Marzilli, L. G. *Inorg. Chim. Acta* **2000**, *297*, 36-46.

43. Saad, J. S.; Scarcia, T.; Shinozuka, K.; Natile, G.; Marzilli, L. G. *Inorg. Chem.* **2002**, *41*, 546-557.

44. Wong, H. C.; Coogan, R.; Intini, F. P.; Natile, G.; Marzilli, L. G. *Inorg. Chem.* **1999**, *38*, 777-787.

45. Wong, H. C.; Intini, F. P.; Natile, G.; Marzilli, L. G. *Inorg. Chem.* **1999**, *38*, 1006-1014.

46. Carlone, M.; Fanizzi, F. P.; Intini, F. P.; Margiotta, N.; Marzilli, L. G.; Natile, G. *Inorg. Chem.* **2000**, *39*, 634-641.

47. Elizondo-Riojas, M.-A.; Kozelka, J. *Inorg. Chim. Acta* **2000**, *297*, 417-420.

48. Sundquist, W. I.; Lippard, S. J. *Coord. Chem. Rev.* **1990**, *100*, 293-322.

49. Natile, G.; Marzilli, L. G. *Coord. Chem. Rev.* **2006**, *250*, 1315-1331.

50. Martin, R. B. *Acc. Chem. Res.* **1985**, *18*, 32-38.

51. Colonna, G.; Di Masi, N. G.; Marzilli, L. G.; Natile, G. *Inorg. Chem.* **2003**, *42*, 997-1005.

52. Adams, K. A.; Marzilli, L. G. *Inorg. Chem.* **2007**, *46*, 4926-4936.

CHAPTER 4. USE OF NEGLECTED BIS(TRIAZINE)-TYPE LIGANDS TO ASSESS COMPARATIVE CARRIER-LIGAND EFFECTS RELATIVE TO THE LIGANDS IN CLINICALLY USED Pt ANTICANCER DRUGS: d(GpG) AND OLIGONUCLEOTIDES CONTAINING THE N7–Pt–N7 CROSS-LINK

4.1 Introduction

Cisplatin (*cis*-$Pt(NH_3)_2Cl_2$) and related analogues continue to enjoy expanding clinical use in the fight against cancer, even though the original discovery was made many years ago.[1-8] Although analogues of the type **L**PtX_2 (**L** = one bidentate or two *cis*-unidentate N-donor ligands, X_2 = anionic leaving ligands) are generally less active,[2,5,9-12] there is evidence that the carrier ligand can modulate the anticancer and mutagenic properties. Oxaliplatin [(1R,2R-diaminocyclohexane)oxalatoplatinum(II)] is a third generation Pt based anticancer agent that forms the same kind of intra- and interstrand DNA cross-links as cisplatin[13-16] and has activity against some cisplatin-resistant tumor cells.[13,17] An intrastrand DNA cross-link with Pt linking N7's of adjacent guanines of DNA, Pt(d(G*pG*)) (G* = N7-platinated G linked by a phosphodiester backbone), is thought to be the critical lesion accounting for activity.[5,15,18-23] The guanine base G* residues in such cross-links are generally accepted to have a head-to-head (HH) orientation, with the two G* residues maintaining the anti conformation characteristic of B-DNA;[24-32] this HH conformation is designated as HH1 (Figure 4.1). Virtually all reports on both single-stranded and duplex adducts indicate that the HH1 conformer predominates.[27,30,33-35]

An implicit assumption in drug design is that the HH conformers are relevant to activity.[36] It is hypothesized that the cisplatin anticancer activity involves specific recognition of kinked DNA adducts by proteins with an HMG domain.[12,37-42] Tight binding to the HMG-containing protein may be required for such recognition, which by inhibiting repair, leads to cell death. The most favorable protein-DNA contacts may require this HH1 conformation, and, indeed, even variations in the flanking sequence influence protein binding.[41] However, carrier

ligands that favor a non-HH1 conformation for the cross-link could form DNA adducts with this different conformation (Figure 4.1). Such cross-link adducts might bind the HMG proteins less strongly, and thus may be readily repaired (repair diminishes activity).[36,43] On the basis of this HMG protection mechanism, we hypothesize that understanding those factors that favor HH1 over other conformers is important for designing new anticancer drugs. In turn, if we can force unusual conformations onto the cross-link, such conformers may be useful 'tools' for probing the mechanism of action, which has still not been fully elucidated.

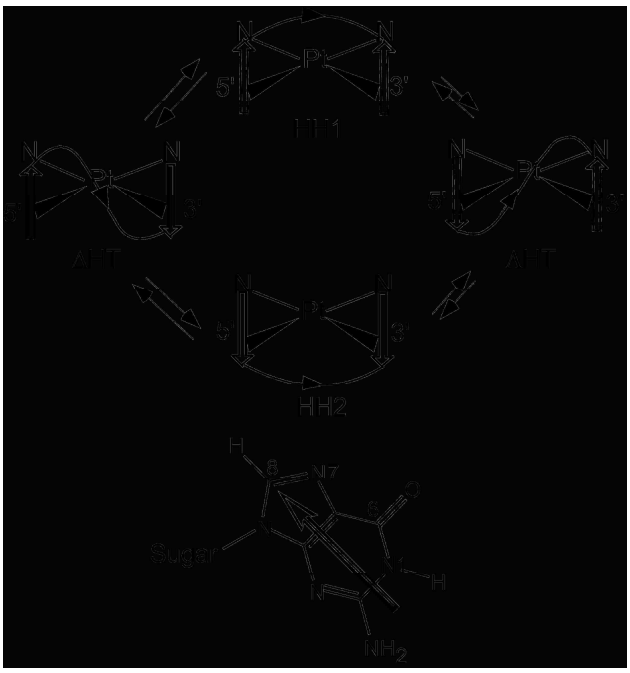

Figure 4.1. The possible base orientations (head-to-head, HH and head-to-tail, HT) of two G* bases coordinated to cis positions on Pt. The large arrows represent the G* base, with the arrowhead denoting the G* H8 (shown below the scheme). The small curved arrows connecting the G* base arrows indicate the direction of propagation of the sugar-phosphodiester backbone. G* coordination sites are forward, and the carrier ligand (not shown except for N-donor atoms) is to the rear. The four recognized conformers are shown. Interconversion between these conformers requires base rotation about the Pt–N7(G*) bond. Slow isomerization from the two HH conformers to the ΛHT conformer is depicted by short counter-parallel arrows.

In simple **L**Pt**G**$_2$ adducts (boldface **G** indicates a guanine derivative not linked to another nucleoside by a phosphodiester group), the bases favor the head-to-tail (HT) arrangement,[44,45] whereas the adducts with single-stranded d(G*pG*) cross-links are thought to favor the HH1

conformation.[32,33,46-48] In the absence of an X-ray structure, the observation of only one set of ^{1}H NMR signals[33,46] for the simplest cross-link adduct, *cis*-Pt(NH_3)$_2$(d(G*pG*)) has been taken to imply that the presence of the backbone favors the HH base arrangement over the otherwise favored HT arrangement.[33,43,46,47,49-52] We believe that the observation of only one set of ^{1}H NMR signals for the *cis*-Pt(NH_3)$_2$(d(G*pG*)) adduct is best attributed to dynamic interchange between multiple conformers. Because of these conflicting interpretations, the *cis*-Pt(NH_3)$_2$(d(G*pG*)) model of the cisplatin-DNA intrastrand adduct is said to suffer from the 'dynamic motion problem'.[23,43,44,50,53,54]

To overcome this dynamic motion problem, a retro-modeling approach has been employed. In this approach, the carrier ligands are designed to reduce the dynamic motion by a billion-fold compared to *cis*-Pt(NH_3)$_2$ adducts, thereby permitting the coexistence of multiple conformers and leading to more informative spectral properties.[23,36,55-57] The study of the reaction of chiral enantiomers of [**Bip**Pt(H_2O)$_2$]$^{2+}$ (**Bip** = 2,2′-bipiperidine) with d(GpG) provided the first definitive evidence for the existence of **L**Pt(d(G*pG*)) non-HH1 conformers.[43,50] For (*S,R,R,S*)-**Bip**Pt(d(G*pG*)), conformers of comparable stability, HH1 and HH2, were found (the 2 indicates that the direction of propagation of the sugar-phosphodiester backbone is opposite to that in B-DNA, Figure 4.1);[50] these conformers are designated as HH1 R and HH2 R to indicate that the canting is right-handed for both HH conformers. For (*R,S,S,R*)-**Bip**Pt(d(G*pG*)), the HH1 L conformer and the ΔHT conformer (with an anti-5′-G* and a syn-3′-G*, Figure 4.1) were abundant.[43] After the initial discovery of these conformers, retro-models with the *N,N*′-dimethylpiperazine (**Me$_2$ppz**)[58] and 5,5′-dimethyl bipyridine (**5,5′-Me$_2$bipy**)[23] ligands allowed the simultaneous detection of both the HH2 and the ΔHT conformers, in addition to the well-known HH1 conformer.

The antiparallel alignment of the base dipole and the minimal O6 clash of the two **G** bases favor the HT over the HH arrangement. To observe the conformers in solution, the carrier ligand must be made bulky. In early work, no HH conformer was found when the carrier ligand had two sp^3 N's and no NH groups.[59,60] Later, less bulky ligands of the type used in the retromodeling approach, but with one hydrogen on each of the two sp^3 N's, revealed that the HH form could be observed.[45,55,56,61-63] With such models, it was found that the nature of the **G** derivative influenced the distribution. The percentage of HH conformer generally increases along the series, Guo < 3'-GMP < 5'-GMP. The reason for this order is not totally clear, but it was found that the phosphate groups of one **G** interacted with the base of the other **G** in the cis position. This interaction favors a particular HT chirality and may be stronger in 3'-GMP than in 5'-GMP. If such is the case, the higher abundance of the HH conformer in 5'-GMP adducts is explained.[58,62,64]

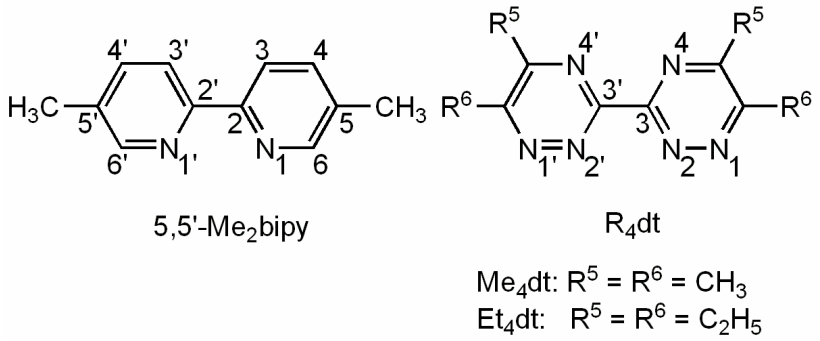

Figure 4.2. Numbering scheme for 5,5′-dimethyl bipyridine (**5,5′-Me$_2$bipy**) and bis-3,3′-(5,6-disubstituted-1,2,4-triazine) (**R$_4$dt**) ligands.

The abundance for the HT conformers was similar for some **L**Pt**G**$_2$ adducts having in-plane ligand bulk (**L** = **5,5′-Me$_2$bipy** and 3-(4′-methylpyridin-2′-yl)-5,6-dimethyl-1,2,4-triazine)).[65] However, we have discovered that carrier ligands of the type, bis-3,3′-(5,6-dialkyl-1,2,4-triazine) (**R$_4$dt**, Figure 4.2), led to almost comparable abundance of HH and HT conformers for the (**R$_4$dt**)Pt(5′-GMP)$_2$ adduct.[65] The overall low steric effects of the **R$_4$dt** ligand,

with two N + N lone pair groupings, allow enough space for the HH conformer to exist without significant clashes between the O6 atoms of the 5′-GMP's.[65] The **R_4dt** ligand is unique in that it has the in-plane bulk needed to reduce the Pt–N7(**G**) rotation, but at the same time it is sterically less demanding, enough to allow a high abundance of the HH conformer. Given the finding that carrier ligands favoring the HH conformer in the cross-link are associated with anticancer activity,[44] we evaluate here the (**R_4dt**)Pt(d(G*pG*)) adduct for the distribution and the characteristics of its conformers.

Earlier studies with the **L**Pt(d(G*pG*)) adduct having L = the sp^2 N-donor **5,5′-Me_2bipy** achiral carrier ligand was particularly informative. The **5,5′-Me_2bipy** H6/H6′ protons (Figure 4.2), which project toward the cis G*, were used as probes to elucidate conformer structures.[23] We have now investigated (**R_4dt**)Pt(d(G*pG*)) (**R_4dt** = **Me_4dt**, **Et_4dt**) (Figure 4.2) adducts containing another sp^2 N-donor achiral carrier ligand. This ligand has in-plane bulk that is expected to destabilize the transition state for rotation about both Pt–N7(G*) bonds and thus eliminate the dynamic motion problem. Nevertheless, the presence of the sterically less demanding lone pairs on the N1/N1′ atoms in **R_4dt** (positioned in the same location as the H6/H6′ protons of **5,5′-Me_2bipy**, Figure 4.2) pointing toward the 5′-G* and the 3′-G* alters the steric properties.

We begin with our results on (**R_4dt**)Pt(d(G*pG*)) adducts, followed by the (**R_4dt**)Pt(oligo) adducts (oligo = GGT, TGG, TGGT), in which 5′- and 3′-flanking residues are introduced. The flanking residues can be viewed as substituents on the Pt(d(G*pG*)) chelate ring. The oligos examined have T residues because GGT and TGG are a part of the repetitive sequence found in telomeres, a potential cisplatin single-strand (ss) DNA target,[66,67] and also because T residues were used in the (**Me_2ppz**)Pt(oligo) studies.[68] Comparison of results obtained

for (**R$_4$dt**)Pt(oligo) with (**Me$_2$ppz**)Pt(oligo)[68] will allow us to understand the effect of carrier ligands on conformer distribution and their characteristics. A comparative study for **L**Pt(d(G*pG*)) and **L**Pt(oligo) is presented here for the first time for **L** = sp^2 N-donor carrier ligand to assess the effect of a flanking residue on the conformer distribution in DNA cross-link adducts.

4.2 Experimental Section

4.2.1 Starting Materials

2′-Deoxyguanyl(3′→5′)-2′-deoxyguanosine (d(GpG)) from Sigma was used as received. Bis-3,3′-(5,6-dialkyl-1,2,4-triazine) (**R$_4$dt**) ligands (Figure 4.2) were synthesized by a known method.[69] (**Me$_4$dt**)PtCl$_2$ (**Me$_4$dt** = bis-3,3′-(5,6-dimethyl-1,2,4-triazine)) and (**Et$_4$dt**)PtCl$_2$ (**Et$_4$dt** = bis-3,3′-(5,6-diethyl-1,2,4-triazine)) were prepared as described elsewhere.[65] d(TGG), d(GGT), and d(TGGT) oligonucleotides, obtained from the Microchemical Facility at Emory University, were purified by ÄKTA FPLC (Amersham Biosciences). Failure sequences were removed by using ion exchange chromatography on an Amersham Biosciences Mono Q HR 10/10 anion exchange FPLC column (A = 2 M NaCl, B = H_2O, 0-50% A over ~50 min). Collected fractions were desalted on an Amersham Biosciences HiTrap desalting FPLC column (A = H_2O, 3.5 mL/min for 20 min), taken to dryness by rotary evaporation, and then dissolved in ~0.5-1.0 mL of D_2O.

4.2.2 Reaction of (R$_4$dt)PtCl$_2$ with d(GpG)

A 5 mM and a 7 mM solution containing an equimolar ratio of Pt:d(GpG) were prepared by mixing a DMSO-d_6 solution of (**Me$_4$dt**)PtCl$_2$ (1.32 mg, 200 μL) and (**Et$_4$dt**)PtCl$_2$ (2.07 mg, 400 μL), respectively, with a D_2O solution of d(GpG) (1.70 mg, 350 μL and 2.38 mg, 150 μL, respectively). Because of low solubility of (**R$_4$dt**)PtCl$_2$ in D_2O, the reaction was carried out in a

mixture of D_2O and DMSO-d_6 (64:36 by volume when R = Me and 27:73 by volume when R = Et). The solutions were maintained at pH 4.0 and 5° C and carefully monitored for two days by ^{1}H NMR spectroscopy until no free d(GpG) signals were observed. For comparison, 275 μL of the (**Et$_4$dt**)Pt(d(G*pG*)) solution was diluted with 275 μL of D_2O, to obtain a 64:36 ratio of D_2O and DMSO-d_6, the same ratio as that used for (**Me$_4$dt**)Pt(d(GpG)). The final concentration of Pt in the (**Et$_4$dt**)Pt(d(GpG)) solution was 3.5 mM. The (**R$_4$dt**)Pt(d(GpG)) solutions were monitored by ^{1}H NMR spectroscopy every 24 h for the initial 6 days and then weekly up to 4 months until no change in the H8 signal intensity was observed.

4.2.3 Reaction of (R$_4$dt)PtCl$_2$ (R$_4$dt = Me$_4$dt, Et$_4$dt) with Oligonucleotides

The concentration of the FPLC purified oligos (dissolved in 500 μL of D_2O) was determined by using UV spectroscopy. (Oligo ε_{260} values were calculated[70] to be 30.0, 29.1 and 37.6 $cm^{-1}mM^{-1}$ for d(GGT), d(TGG) and d(TGGT), respectively.) A 1:1 molar Pt:oligo solution was prepared (~1.5 mM) in 550 μL of a 64:36 mixture of D_2O:DMSO-d_6. A solution of the desired (**R$_4$dt**)$PtCl_2$ complex was dissolved in 200 μL of DMSO-d_6 and mixed with the appropriate volume of the oligo in D_2O. The volume of the solution was brought to 550 μL by adding the required amount of D_2O. The pH of the solution was maintained at 4.0 and the solution was kept at 5 °C. The solution was carefully monitored by ^{1}H NMR spectroscopy until no free oligo signals were observed and then weekly up to 2 months to monitor any change in the H8 signal intensity.

4.2.4 NMR Measurements

^{1}H NMR spectra were recorded on a Bruker spectrometer operating at 400 MHz or a Varian spectrometer at 700 MHz. We used a value of 4.78 ppm to reference signals to the residual HOD signal in D_2O/DMSO-d_6 solutions. A presaturation pulse to suppress the water

peak was used when necessary. ^{31}P NMR spectra were referenced to external trimethyl phosphate (0 ppm) in a 64:36 mixture of D_2O:DMSO-d_6. DNO_3 and NaOD solutions (0.1 M in D_2O) were used to adjust the pH of D_2O/DMSO-d_6 solutions. NMR data were processed with XWINNMR or Mestre-C software.

^{1}H-^{1}H COSY and ROESY spectra were recorded in order to assign the signals of the products. Matrixes (512 x 2048) were collected for COSY and (500 ms delay) ROESY experiments, both conducted at 25 °C with a spectral window of ~6000 Hz, and a presaturation pulse of ~1 s to reduce the HOD signal. Typically, 32 scans were collected per block. An exponential apodization function with a line broadening of 0.2 Hz and a phase-shifted 90° sine bell function were used to process the ROESY t_2 and t_1 data, respectively.

4.2.5 Circular Dichroism (CD) Spectroscopy

All samples used for CD experiments were prepared from the respective NMR samples by diluting to ~0.025 mM Pt with deionized water. The concentration of the CD samples was determined by measuring the absorption at 260 nm on a UV-vis spectrometer (d(GpG) $\varepsilon_{260} = 21.6$ $cm^{-1}mM^{-1}$). Spectra were recorded from 400 to 200 nm at a scan speed of 50 nm/min on a JASCO J-600 CD spectropolarimeter. Six scans were recorded and averaged for each sample.

4.2.6 High Performance Liquid Chromatography (HPLC)

Chromatograms were obtained on a Varian ProStar HPLC instrument with a PDA detector operating at 254 nm. Separations employed a Microsorb 100-5 C8 150 x 4.6 mm reverse-phase column. Eluants A and B both contained 0.02 M ammonium acetate buffer, pH 5.5. Solvent A was water and solvent B was a 2:1 methanol:water mixture. A flow rate of 0.70 mL/min was maintained over the course of a 40 min linear gradient (0 min = 95% A and 5% B, 40 min = 48% A and 52% B) for the (**R$_4$dt**)Pt(d(G*pG*)) adducts. The NMR sample was diluted to obtain a 1.7 mM solution. Each eluted fraction was collected, concentrated to a small volume

(200 μL), and stored at 25 °C to see if equilibration occurred. An aliquot of each fraction was re-injected after 2 h and then after intervals of 24 h for 7 days, and finally at weekly intervals for two months. The percentage of each product separated by HPLC was measured by integration of the corresponding peak area.

4.3 Results

4.3.1 Conformer Assignment and Conformational Features

For the (**R$_4$dt**)Pt(d(G*pG*)) adducts ^{1}H-^{1}H ROESY and COSY data were used to assign H8 and sugar proton signals. Structural features were assessed by standard methods. The S- and N-sugar pucker conformations were identified from the characteristic H1′ coupling patterns and the existence of H8-H3′ NOE cross-peaks for N-sugars.[71,72] For all conformers of **L**Ptd(G*pG*) adducts, the sugar residue of the 5′-G* typically adopts an N-pucker conformation, while the 3′-G* sugar has the S-pucker.[43,44,50,54] The anti or syn G* nucleotide conformations can be assessed by strong intraresidue H8-H2′/H2″ NOE cross-peaks and weak (or unobservable) H8-H1′ cross-peaks for the anti conformation and stronger H8-H1′ NOE cross-peaks for the syn conformation .[72-74] Because the G* H8 atoms are closer to each other in the HH conformers than in the HT conformers, the observation of an H8-H8 cross-peak is characteristic of an HH conformer, whereas the absence of such a cross-peak is indicative of an HT conformer.[43,75] HH and ΔHT conformers of **L**Pt(d(G*pG*)) complexes often give rise to characteristic NMR shift changes compared to free d(GpG); more downfield H8 and ^{31}P signals indicate HH conformers,[27,29,33,46,48,76] whereas more upfield H8 and ^{31}P NMR signals indicate a ΔHT conformer.[43,53] Such observations are used below to assign conformations of (**R$_4$dt**)Pt(d(G*pG*)) and (**R$_4$dt**)Pt(oligo) adducts.

4.3.2 (Me$_4$dt)Pt(d(G*pG*))

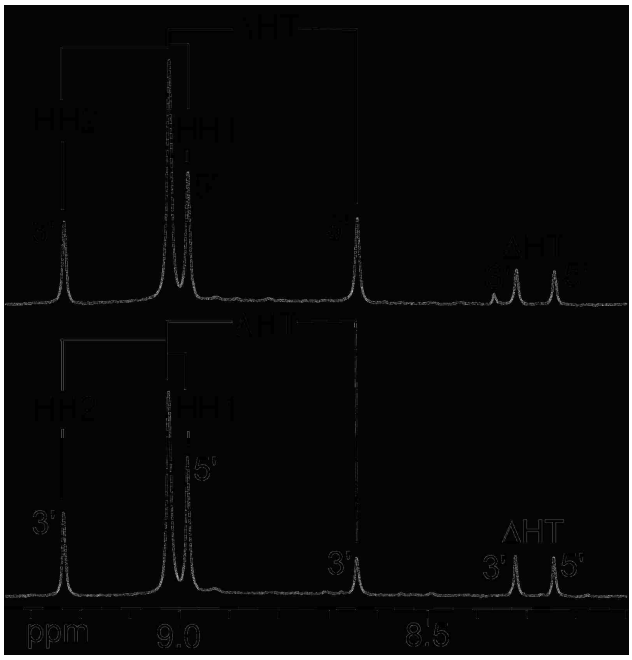

Figure 4.3. ^{1}H NMR spectra (400 MHz) in the H8 region for (**Me$_4$dt**)Pt(d(G*pG*)) collected at room temperature after 1 week (bottom) and after 8 weeks (top) (pH 4.0, in D$_2$O/DMSO-d_6). The H8 signals for the various conformers are labeled.

Within ~30 min of mixing (**Me$_4$dt**)PtCl$_2$ and d(GpG) in a 1:1 molar ratio in 64:36 D$_2$O:DMSO-d_6 solution at pH ~4.0 at 5 °C, the (**Me$_4$dt**)Pt(d(G*pG*)) adduct was fully formed. This reaction was repeated several times with similar results; however, small variations in conditions, such as the ratio of D$_2$O:DMSO-d_6 in the reaction solvent mixture due to adventitious water and the temperature in the various NMR probes used, eight H8 signals for the (**Me$_4$dt**)Pt(d(G*pG*)) adduct were resolved in some cases (Supporting Information, Figure C2) while some H8 signals overlapped in other cases (Figure 4.3). In the spectrum in Figure 4.3, six new peaks downfield from the free d(GpG) H8 signals at 8.06 and 7.83 ppm, indicating that the adduct consisted of several species with both bases of d(GpG) bound to Pt via N7. The intensity of these peaks and the spectrum in Supporting Information (Figure C2) indicate that some peaks contain overlapping signals. Indeed the G* H8 peak at 9.03 ppm in ^{1}H 400 MHz NMR spectra

can clearly be interpreted as three overlapped signals (Figure 4.3). However, for the same sample at 700 MHz this peak was slightly better resolved to give two distinct G* H8 peaks at 9.03 and 9.02 ppm, with ROESY and COSY data indicating that two G* H8 signals still overlapped to give the peak at 9.03 ppm.

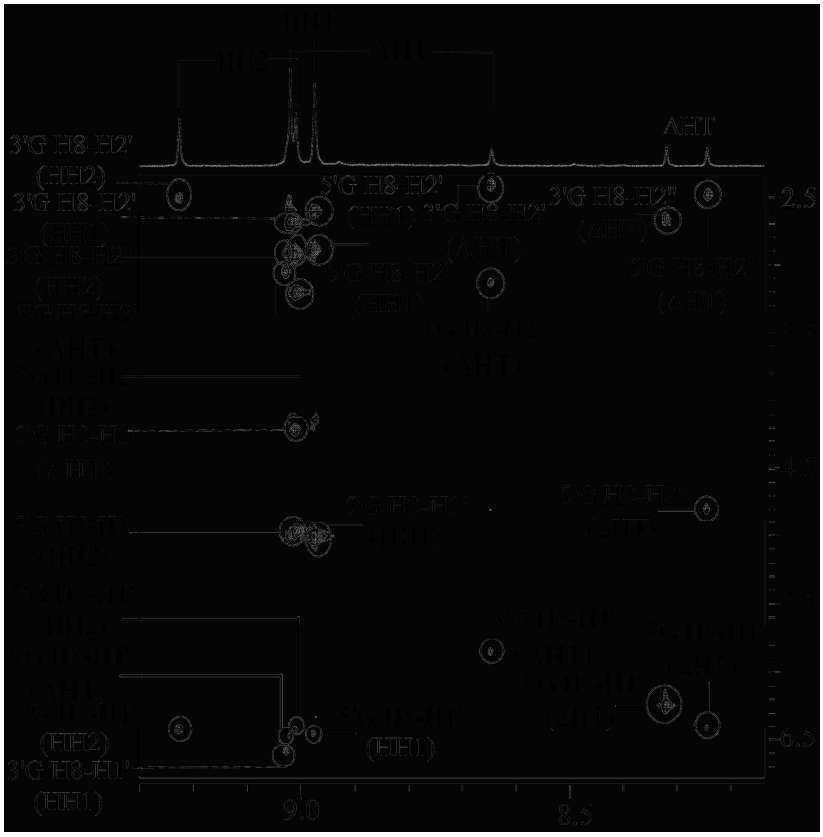

Figure 4.4. ^{1}H-^{1}H ROESY spectrum (700 MHz, 600 ms mixing time) of a 1-week-old (**Me$_4$dt**)Pt(d(G*pG*)) sample at pH 4.0 and 25 °C, showing G* H8 to sugar NOE cross-peaks.

The NOE cross-peaks (not shown) in the ROESY spectrum between H8 signals at 9.02 and 8.98 ppm and at 9.23 and 9.03 ppm (most abundant and next most abundant conformers, respectively) indicate that both are HH conformers (Table 4.1 and 4.2). For the more abundant HH conformer, the G* H8-H2′/H2″ cross-peaks were stronger than the H8-H1′ cross-peaks (Figure 4.4), indicating a predominantly anti conformation for both the 5′-G* and 3′-G* residues. Because the 5′-G* and 3′-G* H1′ resonances overlap, the coupling patterns could not be

determined. However, the presence of an NOE cross-peak between the H8 signal at 8.98 ppm and that of H3′ confirms the N-sugar pucker (Figure 4.4). This signal is therefore assigned to the 5′-G* residue, which typically has an N-pucker in such cross-links.[21,27,43,50,54,76] The H8 signal at 9.02 ppm, which must be the 3′-G* H8 signal, has no H8-H3′ cross-peak, thus indicating an S-sugar pucker. Therefore, the dominant (**Me$_4$dt**)Pt(d(G*pG*)) conformer is one of the anti,anti-HH conformers (either HH1 or HH2).

Table 4.1. ^{1}H and ^{31}P NMR Signal Assignments (ppm) for the (**R$_4$dt**)Pt(d(G*pG*)) Adducts at pH ~4 and 25 °C [a]

adduct	conformer	G*/T	H8	H1′	H2′	H2″	H3′	H4′	base sugar[a]	^{31}P
(**Me$_4$dt**)Pt(d(G*pG*))	HH1	5′	8.98	6.44	2.60	2.89	5.00	4.16	anti	-3.43
		3′	9.02	6.46	2.69	2.60	4.70	4.25	anti	
(**Et$_4$dt**)Pt(d(G*pG*))	HH1	5′	9.04	6.39	2.55	2.80	4.92	4.08	anti	-3.41
		3′	8.97	6.43	2.61	2.53	4.64	4.22	anti	
(**Me$_4$dt**)Pt(d(G*pG*))	HH2	5′	9.03	6.42	3.19	2.91	4.96	4.14	anti	-2.76
		3′	9.23	6.40	2.51	2.82	4.74	4.50	anti	
(**Et$_4$dt**)Pt(d(G*pG*))	HH2	5′	9.10	6.37	3.15	2.88	5.01	4.08	anti	-2.51
		3′	9.23	6.32	2.32	2.72	4.65	4.41	anti	
(**Me$_4$dt**)Pt(d(G*pG*))	ΔHT	5′	8.24	6.40	3.22	2.49	4.74	4.19	anti	-5.01
		3′	8.31	6.24	3.48	2.66	4.81	4.12	syn	
(**Et$_4$dt**)Pt(d(G*pG*))	ΔHT	5′	8.32	6.35	3.52	2.65	4.76	4.02	anti	-4.72
		3′	8.29	6.19	3.35	2.61	4.88	4.10	syn	
(**Me$_4$dt**)Pt(d(G*pG*))	ΛHT	5′	9.03	6.57	3.04	2.90	4.13	4.99	anti	-4.09
		3′	8.65	5.84	2.40	2.84	4.83	4.69	anti	
(**Et$_4$dt**)Pt(d(G*pG*))	ΛHT	5′	8.99	6.50	2.82	2.78	4.59	*b*	anti	-4.01
		3′	8.66	5.98	2.39	2.72	*b*	*b*	anti	
(**Me$_4$dt**)Pt(d(TG*G*T))	HH1	5′	8.98	6.49	2.84	2.66	4.87	4.32	anti	

(table 4.1 continued)

		3′	9.40	6.42	2.77	2.91	4.06	4.45	anti	
		5′-T	7.52	6.09	2.15	2.51	3.67	4.08		
		3′-T	7.84	6.40	2.42	2.35	4.64	4.19		
(**Me$_4$dt**)Pt(d(TG*G*))	HH1	5′	8.97	6.51	2.50	2.78	4.72	4.28	anti	
		3′	9.41	6.44	2.98	2.58	4.60	4.25	anti	
		5′-T	7.48	6.05	2.15	2.55	4.75	3.50		
(**Me$_4$dt**)Pt(d(G*G*T))	HH1	5′	8.98	6.45	2.57	2.89			anti	-3.49
		3′	9.03	6.41	2.73	2.62			anti	
	HH2	5′	9.02	6.39	3.18	2.93	4.96		anti	-2.64
		3′	9.25	6.41	2.41	2.96			anti	
	ΔHT	5′	8.21	6.41	3.12	2.44			anti	
		3′	8.31	6.24	3.47	2.83			syn	
	ΛHT	5′	8.86	6.60	3.12	2.86			anti	
		3′	8.59	6.10	2.44	2.81			anti	

[a] Conformational assignment (anti/syn) based on the relative strength of NOE cross-peaks between H8 resonances and H1′ or H2′/H2″ signals in the ROESY spectrum. [b] Signals not detected.

For the other HH conformer of the (**Me$_4$dt**)Pt(d(G*pG*)) adduct, the G* H8 signal at 9.03 ppm has a strong H8-H3′ cross-peak, indicating a 5′-G* N-sugar pucker, and the H8 signal at 9.23 ppm has no H8-H3′ NOE cross-peak, indicating a 3′-G* S-sugar pucker (Figure 4.4). The observation of stronger 5′-G* H8-H2′/H2″ cross-peaks than the H8-H1′ cross-peak is consistent with an anti conformation.[19,23,43,49,54] For the 3′-G*, weak H8-H2′ and H8-H1′ NOE cross-peaks were observed (Figure 4.4). Thus, the minor HH conformer adopts an anti,anti conformation. The distances between the H8 atom and sugar protons determined by molecular mechanics/dynamics computations on the HH conformers of (**Me$_2$ppz**)Pt(d(G*pG*)) indicated that observable H8-

sugar NOEs are unlikely for the 3′-G* residue of the HH2 conformer.[54] The observation of weak 3′-G* H8-to-sugar cross-peaks for the minor HH conformer and strong 3′-G* H8-to-sugar cross-peaks for the major HH conformer led us to assign the minor and the major HH conformers to the HH2 and HH1 conformers, respectively. Our results for the minor and the major HH conformers are consistent with the HH2 and HH1 conformers of (*R,S,S,R*)-**Bip**Pt(d(G*pG*))[50] and (**Me$_2$ppz**)Pt(d(G*pG*)).[54]

Table 4.2. H8 Chemical Shifts of the (**R$_4$dt**)Pt(d(G*pG*)) and (**R$_4$dt**)Pt(oligo) Adducts at pH ~4 at 25 °C

adduct	G*	H8 shifts (ppm)			
		HH1	HH2	ΔHT	ΛHT
(**Me$_4$dt**)Pt(d(G*pG*))	5′	8.98	9.03	8.24	9.03
	3′	9.02	9.23	8.31	8.65
(**Me$_4$dt**)Pt(d(G*G*T))	5′	8.98	9.02	8.21	8.86
	3′	9.03	9.25	8.31	8.59
(**Me$_4$dt**)Pt(d(TG*G*))	5′	8.97			
	3′	9.41			
(**Me$_4$dt**)Pt(d(TG*G*T))	5′	8.98			
	3′	9.40			
(**Et$_4$dt**)Pt(d(G*pG*))	5′	9.04	9.10	8.32	8.99
	3′	8.97	9.23	8.29	8.66
(**Et$_4$dt**)Pt(d(G*G*T))	5′	9.07	9.17	8.36	
	3′	9.11	9.33	8.35	
(**Et$_4$dt**)Pt(d(TG*G*))	5′	9.04			
	3′	9.59			

For the (**Me$_4$dt**)Pt(d(G*pG*)) adduct, there are two other pairs of H8 signals at 8.31 and 8.24 ppm and at 8.65 ppm and within the 9.03 ppm peak; except for the overlapped signal, these

signals are upfield to the G* H8 signals of the HH1 and HH2 conformers. These two pairs of signals, which indicate the presence of two conformers, showed no H8-H8 NOE cross-peaks, in the ROESY spectra collected for the 1-week-old as well as for the 3-months-old (**Me$_4$dt**)Pt(d(G*pG*)) sample indicating that the bases of these conformers adopt the HT arrangement.[23,43,50,53]

On the basis of the relative intensity of the H8 signals and the ^{31}P NMR signals, the H8 signals at 8.31 and 8.24 ppm and the ^{31}P NMR signal at -5.01 ppm were assigned to one HT conformer. Such an upfield ^{31}P NMR shift is characteristic of the ΔHT conformer and is consistent with the shift values of the ΔHT conformer of both (**5,5′-Me$_2$bipy**)Pt(d(G*pG*)) (-4.74 ppm) and (**Me$_2$ppz**)Pt(d(G*pG*)) (-5.12 ppm). For the (**Me$_4$dt**)Pt(d(G*pG*)) ΔHT conformer, the G* H8 signal at 8.24 ppm exhibits an intraresidue H8-H3′ NOE cross-peak (Figure 4.4) consistent with a 5′-G* N-sugar pucker. A strong 5′-G* H8-H2″ cross-peak and a weak H8-H1′ cross-peak indicate an anti 5′-G* conformation (Figure 4.4). For the H8 signal at 8.31 ppm, the absence of an H8-H3′ NOE and the observation of a doublet of doublets coupling pattern for the H1′ signal (6.24 ppm) are indicative of a 3′-G* S-sugar pucker. Strong 3′-G* H8-H1′ NOE and weak H8-H2″ cross-peaks indicate a syn 3′-G* conformation. Thus, the ΔHT conformer adopts an anti,syn conformation, as has been found previously.[23,43,53,54]

The intensity of the H8 signals for the other HT conformer (a fourth conformer at 8.65 and 9.03 ppm remained relatively unchanged for ~3 weeks after initiation of the reaction. However, these signals increased slowly over a period of ~3 months, finally becoming the most dominant. Thus, this HT conformer, which is thermodynamically favorable, could possibly be the elusive ΛHT conformer. The distribution of the HH1, HH2, ΔHT, and the putative ΛHT conformers changed from 42%, 37%, 11% and 10% (after 1 week) to 36%, 18%, 6% and 40%

(after ~3 months), respectively (Supporting Information Figure C2). The CD signal shape provides a definitive means for assigning the chirality of the major HT conformer when that conformer clearly dominates.[54] For the (**Me$_4$dt**)Pt(d(G*pG*)) sample, 8 weeks after initiation of the reaction, the distribution of the HH1, HH2, ΔHT, and the putative ΛHT conformers was 40%, 25%, 10% and 25%. A positive feature at ~290 nm (Figure 4.5) in the CD spectrum for this sample is characteristic of the ΛHT conformer of **L**Pt**G**$_2$ adducts.[36,53,57,58,61,77] This feature is consistent with the suggestion that the slowly forming HT conformer is the elusive ΛHT conformer.

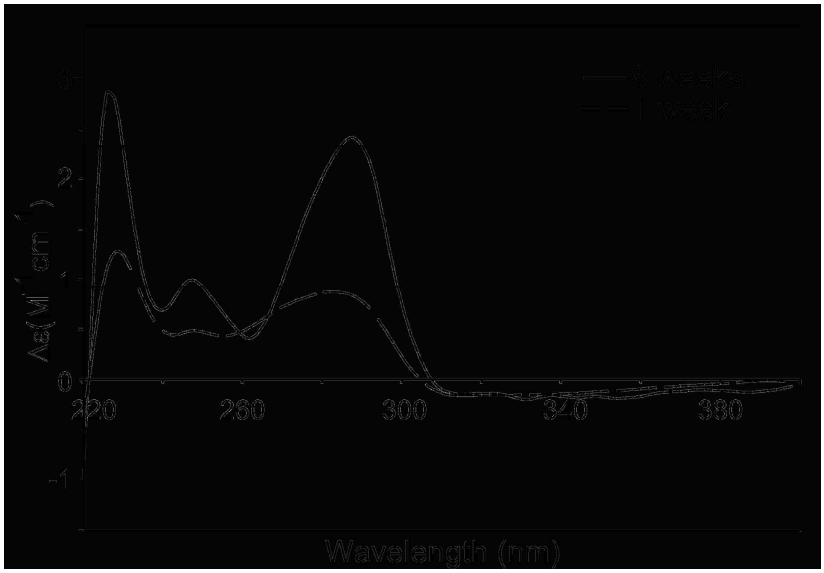

Figure 4.5. CD spectra of an (**Me$_4$dt**)Pt(d(G*pG*)) sample recorded in water at pH ~ 4 and 25 °C. The positive feature at ~290 nm is indicative of a ΛHT conformation.

For the putative ΛHT conformer of the (**Me$_4$dt**)Pt(d(G*pG*)) adduct, the G* H8 signals at 8.65 and 9.03 ppm have H8-H2′/H2″ cross-peaks stronger than the H8-H1′ cross-peak (Figure 4.4), indicating an anti conformation for both G* resdiues. The H8-H3′ NOE cross-peak (9.03-4.13 ppm) and an H1′ doublet for this residue are consistent with a 5′-G* N-sugar pucker. The absence of an observable H8-H3′ cross-peak (8.65-4.83 ppm) and the doublet of doublets

coupling pattern for the H1′ signal indicate a 3′-G* S-sugar pucker for the putative ΛHT conformer.

EXSY cross-peaks were absent in the ROESY spectrum of the (**Me$_4$dt**)Pt(d(G*pG*)) adduct, indicating that interconversion between the rotamers is very slow. These slowly interconverting rotamers were separated and analyzed by HPLC (see below).

Figure 4.6. ^{31}P NMR spectrum (400 MHz) of (**Me$_4$dt**)Pt(d(G*pG*)) after 6 days (bottom) and after 8 weeks (top) in D_2O/DMSO-d_6 at pH 4.0 and 25 °C.

4.3.2.1 ^{31}P NMR Spectroscopy. Compared to the -4.2 ppm value of the unstrained d(GpG) phosphodiester group, the ^{31}P NMR signal of HH conformers is downfield and that for the ΔHT conformer is upfield. From their relative intensities, ^{31}P NMR signals at -2.76, -3.43 and -5.01 ppm for the (**Me$_4$dt**)Pt(d(G*pG*)) adduct were assigned to the HH2, HH1, and the ΔHT conformers, respectively (Figure 4.6). In addition, a fourth peak at -4.09 ppm slowly increased with time, indicating that this signal belongs to the putative ΛHT conformer of the (**Me$_4$dt**)Pt(d(G*pG*)) adduct (Figure 4.6). The ^{31}P NMR chemical shifts for the ΔHT and the two HH conformers are more upfield than those reported for (**5,5′-Me$_2$bipy**)Pt(d(G*pG*))[23] (-

2.23 (HH2), -2.64 (HH1) and -4.74 (ΔHT) ppm) and more comparable to those of (**Me$_2$ppz**)Pt(d(G*pG*)).[54]

4.3.2.2 HPLC Analysis. The rate of interconversion between the (**R$_4$dt**)Pt(d(G*pG*)) rotamers is considerably slower than that for the adducts lacking the sugar-phosphodiester backbone (e.g., (**R$_4$dt**)Pt(GMP)$_2$[65]), thus permitting the separation of the (**R$_4$dt**)Pt(d(G*pG*)) conformers by HPLC.

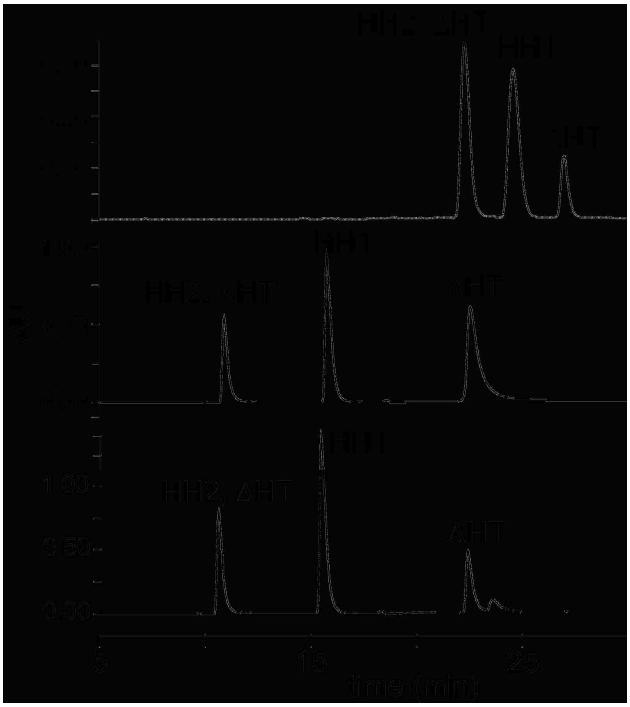

Figure 4.7. HPLC chromatograms of a week-old (**Me$_4$dt**)Pt(d(G*pG*)) sample (bottom), an 8-week-old (**Me$_4$dt**)Pt(d(G*pG*)) sample (middle), and a week-old (**Et$_4$dt**)Pt(d(G*pG*)) sample (top).

For the (**Me$_4$dt**)Pt(d(G*pG*)) adduct at 25 °C, three fractions were collected with retention times (RT) of 10.8, 15.7 and 20.3 min and present in 28%, 52% and 20% abundance, respectively (Figure 4.7). The percent population of each product was determined by calculating the area under each peak. An aliquot of each fraction when re-injected gave a chromatogram with four peaks (RT = 11.3, 12.2, 16.0 and 20.9 min). The small difference in the retention times of

the products at equilibrium and those found upon re-injecting the fractions can be attributed to the presence of ammonium acetate in the fractions after initial collection. Because of very similar retention times, the two products eluting at 11.3 min and 12.2 min came together at 10.8 min when the (**Me$_4$dt**)Pt(d(G*pG*)) adduct was first injected into the column. Because the product in each fraction equilibrated with time to give all four product peaks, each peak must belong to one of the four (**Me$_4$dt**)Pt(d(G*pG*)) conformers. The intensity of the peak at RT = 20.3 min increased with time, suggesting that this fraction contains the ΛHT conformer (Figure 4.7).

For the (**Me$_4$dt**)Pt(d(G*pG*)) adduct, the fraction eluted at 15.7 min, after 1 day, gave a chromatogram with peaks at 11.3 (16%), 12.2 (12%), and 16.0 (72%) min. After four days, upon re-injecting an aliquot of the same fraction, the conformers redistributed [11.3 min (14%), 12.2 min (32%), and 16.0 min (51%)]. Also, a small peak (~3%, RT = 20.9 min) was detected. The fraction that eluted at 10.8 min after one day gave a chromatogram with three peaks at 11.3, 12.2 and 16.0 min. After four days the distribution of these products changed from 42%, 40% and 18% to 21%, 30% and 48%. A very small peak at RT = 20.9 min (1%) was also observed after four days. The fraction collected at 20.3 min redistributed very slowly into the other conformers. The peaks at smaller retention times were not detected when this fraction was injected even after 2 days. Re-injection of this fraction after four days revealed four product peaks at 11.3 min (5%), 12.2 min (27%), 16.0 min (9%) and 20.9 min (59%). Clearly, the conformers eluting at 11.3, 12.2 and 16.0 min interconvert more rapidly than the one eluting at 20.9 min. A correlation of the intensities of the H8 signals in the NMR spectrum with the product peaks in the HPLC chromatograms suggests that the fraction eluting at 16.0 min contains the most abundant HH1 conformer, and the fraction at 20.9 min contains the fourth form of the (**Me$_4$dt**)Pt(d(G*pG*)) adduct. The HPLC data suggest that the fourth form seen by ^{1}H NMR spectroscopy could be the elusive ΛHT conformer. The rotation of one base about the Pt–N7 bond leads to changes in the

relative base orientation from HH to HT, or vice-versa. The HH1 conformer with RT = 16.0 min converts to the ΔHT conformer (RT = 11.3 min), which rapidly interconverts to the HH2 conformer (RT = 12.2 min). The postulated ΛHT conformer eluting at 20.9 min converts first to the HH2 conformer, which then equilibrates to give the ΔHT and HH1 conformers. The rate of interconversion for the HH1, HH2 and ΔHT conformers is faster than that of the ΛHT conformer.

4.3.3 (Et$_4$dt)Pt(d(G*pG*))

Four new pairs of G* H8 signals, downfield of the H8 signals of free d(GpG), were observed within minutes after mixing (**Et$_4$dt**)PtCl$_2$ and d(GpG) solutions. After 1 day no free d(GpG) signals were observed, indicating complete reaction. A 275-μL aliquot of this solution was diluted with D_2O to obtain a ratio of 64:36 for D_2O:DMSO-d_6 (as used for the (**Me$_4$dt**)Pt(d(G*pG*)) reaction). Signal assignments and conformational features were determined by established methods using ROESY and COSY data.[23,43] The H8 peaks at 9.23 and 9.10 ppm and 8.97 and 9.04 ppm were connected by H8-H8 NOE cross-peaks, indicating two HH conformers. The 2D NMR data indicate that the two HH conformers have an anti,anti HH conformation, with a 3′-G* S-sugar and a 5′-G* N-sugar (Table 4.1 and Supporting Information). NOE cross-peaks between the H8 signals at 8.66 and 8.99 ppm and at 8.29 and 8.32 ppm were absent, indicating HT conformers (Tables 4.1 and 4.2). The ^{31}P NMR signals for the (**Et$_4$dt**)Pt(d(G*pG*)) adduct were observed at -3.41, -2.51, -4.72 and -4.01 ppm. On the basis of the characteristic shifts of the ^{31}P NMR signals and the relative intensities of the (**Et$_4$dt**)Pt(d(G*pG*)) H8 signals and their similarity to the shifts of the (**Me$_4$dt**)Pt(d(G*pG*)) H8 signals, the more downfield H8 signals belonging to the minor HH conformer were assigned to the HH2 conformer and those at 8.97 and 9.04 ppm were assigned to the major HH1 conformer (Table 4.1). For HT conformers, the most upfield H8 signals were assigned to the ΔHT

conformer, and the H8 signals at 8.66 and 8.99 ppm were assigned to the ΛHT conformer (Table 4.1). The ΔHT conformer has an anti,syn HT conformation and the ΛHT conformer has an anti,anti HT conformation with a 3′-G* S-sugar and a 5′-G* N-sugar (Supporting Information).

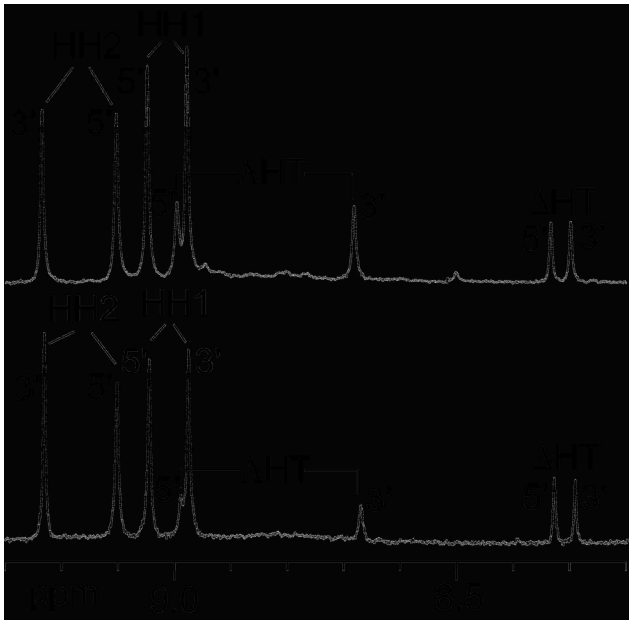

Figure 4.8. H8 region of the ^{1}H NMR spectrum (400 MHz) of (**Et$_4$dt**)Pt(d(G*pG*)) after 1 week (bottom) and after 8 weeks (top) in D_2O/DMSO-d_6 at pH 4.0 and 25 °C.

For (**Et$_4$dt**)Pt(d(G*pG*)), the distribution of the HH1, HH2, ΔHT and ΛHT conformers changed from 42%, 37%, 11%, and 10%, respectively, at one week after initiation of the reaction to 41%, 33%, 9% and 17%, respectively, after another seven weeks (Figure 4.8). The abundance of the ΛHT conformer increased slowly with time, as found for the (**Me$_4$dt**)Pt(d(G*pG*)) adduct. However, at equilibrium the 17% relative abundance of the ΛHT conformer of the (**Et$_4$dt**)Pt(d(G*pG*)) adduct was considerably less than the 40% observed for the (**Me$_4$dt**)Pt(d(G*pG*)) adduct. Evidently, the ΛHT conformer for (**Et$_4$dt**)Pt(d(G*pG*)) adduct is less favored than for (**Me$_4$dt**)Pt(d(G*pG*)) adduct because of the bulk of the Et group, a result suggesting that in-plane bulk does not disfavor the ΛHT conformer.

In a ROESY spectrum of (**Et$_4$dt**)Pt(d(G*pG*)), NOE cross-peaks were observed between the G* H8 signals and the **Et$_4$dt** methyl signals, which overlap in the 0.90 to 1.10 ppm region. NOE cross-peaks were observed between these methyl signals and the H8 signals of the 3′-G* of the HH2 conformer, the 3′- and the 5′-G* of the HH1 conformer and the 3′-G* of the ΛHT conformer. Also, NOE cross-peaks between the methyl signals and the H1′ sugar signals were observed. No such NOE cross-peaks were observed in the ROESY spectrum of the (**Me$_4$dt**)Pt(d(G*pG*)) adduct. The NOE cross-peaks between the G* residue and the carrier ligand clearly indicate that the substituents at the 6/6′ position in a bis-3,3′-(1,2,4-triazine) can interact with the Pt-bound guanine derivatives, and thus affect the rate of rotation of G* bases about the Pt–N7 bond.

4.3.3.1 HPLC Analysis. For the (**Et$_4$dt**)Pt(d(G*pG*)) adduct, the three fractions collected, with retention times of 27.2 (42%), 29.5 (44%), and 31.9 (14%) min (Figure 4.7), followed a pattern similar to that for (**Me$_4$dt**)Pt(d(G*pG*)). The HH1 conformer eluted at 29.5 min, the HH2 and ΔHT conformers eluted together at 27.2 min, and the ΛHT conformer eluted at 31.9 min. Because of the more hydrophobic ethyl group, the retention times for the (**Et$_4$dt**)Pt(d(G*pG*)) peaks were longer than those for (**Me$_4$dt**)Pt(d(G*pG*)) peaks.

Each product upon re-injecting into the HPLC column as observed for (**Me$_4$dt**)Pt(d(G*pG*)), redistributed to give four product peaks (RT = 27.7, 28.4, 30.0 and 32.5 min). Because of very similar retention times, the two products eluting at 27.7 min and 28.4 min came together at 27.2 min when the (**Et$_4$dt**)Pt(d(G*pG*)) adduct at equilibrium was first injected into the column. Again, as we found for the **R = Me** analogue, the results indicate that each peak belongs to one of the four (**Et$_4$dt**)Pt(d(G*pG*)) conformers. For reasons given above, these HPLC observations provide compelling evidence that the four forms detected by NMR spectra

must be conformers that re-equilibrate. However, each fraction, upon re-injecting, redistributed significantly only after two days, indicating that the rate of interconversion between the conformers was slower than that observed for the (**Me$_4$dt**)Pt(d(G*pG*)) conformers, which interconvert after ~1 day.

For (**Et$_4$dt**)Pt(d(G*pG*)), each isolated fraction when injected after 1 day, gave a chromatogram with ~99% of the peak of the fraction injected, the peaks for other conformers were observed only after two days indicating slow redistribution in comparison to (**Me$_4$dt**)Pt(d(G*pG*)). After four days, substantial conformer redistribution was observed for each isolated fraction. The fraction that eluted at 27.2 min redistributed to give four peaks [27.7 min (18 %), 28.4 (50%), 30.0 (21%) and 32.5 (11%)]. Likewise, four conformer peaks were observed for the fractions for the HH1 conformer eluting at 29.5 min (27.7 min (10 %), 28.4 (19%), 30.0 (63%), and 32.5 (8%) and for the ΛHT conformer eluting at 31.9 min (27.7 min (7%), 28.4 (38%), 30.0 (26%), and 32.5 (29%)). In contrast to the slowly redistributing ΛHT conformer of (**Me$_4$dt**)Pt(d(G*pG*)), the ΛHT conformer of (**Et$_4$dt**)Pt(d(G*pG*)) redistributed somewhat faster than the other conformers. This provides further support to the NMR finding that the ΛHT conformer is less favored for the more bulky **Et$_4$dt** ligand than for the **Me$_4$dt** ligand in the (**R$_4$dt**)Pt(d(G*pG*)) adducts.

The sequence of conformer interconversion for (**Et$_4$dt**)Pt(d(G*pG*)) was similar to that observed for (**Me$_4$dt**)Pt(d(G*pG*)). The HH1 conformer with RT = 30.0 min converts to the ΔHT conformer (RT = 27.7 min), which rapidly interconverts to the HH2 conformer (RT = 28.4 min). The postulated ΛHT (RT = 32.5 min) converts first to the HH2 conformer, which then equilibrates to give the ΔHT and HH1 conformers.

4.3.4 (Me$_4$dt)Pt(d(TG*G*T))

Within 1 h after mixing a 2.2 mM solution of d(TGGT) in D_2O (350 μL) with a 3.9 mM solution of (**Me$_4$dt**)$PtCl_2$ in DMSO-d_6 (200 μL) solution, four new pairs of G* H8 signals were observed downfield to the H8 signals of the free d(TGGT). The reaction was complete after ~1 day, as indicated by the disappearance of the free d(TGGT) signals. After 1 day only one pair of G* H8 signals remained, and thus the short-lived H8 signals were from intermediates or unstable conformers.

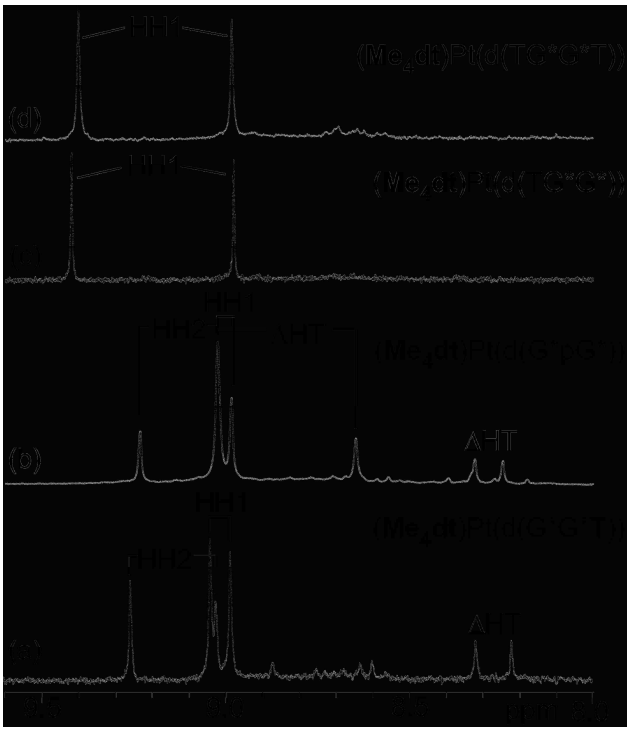

Figure 4.9. H8 region of the ^{1}H NMR spectra (400 MHz) of (a) (**Me$_4$dt**)Pt(d(G*G*T)), (b) (**Me$_4$dt**)Pt(d(G*pG*)), (c) (**Me$_4$dt**)Pt(d(TG*G*)), and (d) (**Me$_4$dt**)Pt(d(TG*G*T)) after 7 days in D_2O/DMSO-d_6 at pH ~4 and 25 °C.

For the (**Me$_4$dt**)Pt(d(TG*G*T)) adduct, the two G* H8 signals at 9.40 and 8.98 ppm (Figure 4.9) were connected by an NOE cross-peak, which is consistent with an HH arrangement. A weak H8-H1′ and a strong H8-H2′/H2″ NOE cross-peak indicated that both G* residues of the HH conformer are anti. The 3′- and 5′-T H6 signals were observed at 7.52 and 7.84 ppm,

respectively. NOE data were used to assign the sugar signals for the G* and T residues (Table 4.1). The H1′ coupling patterns indicated an S- and N-sugar for the 3′- and 5′-G* residues, respectively, and an S-sugar for both the 3′- and 5′-T residues. The (**Me$_4$dt**)Pt(d(TG*G*T)) adduct at equilibrium existed as ~100% HH1 conformer. The ^{31}P NMR signals for the HH1 conformer of the (**Me$_4$dt**)Pt(d(TG*G*T)) adduct were observed at -4.24, -4.30 and -4.52 ppm. The signal for the phosphate group between the adjacent G* residues is ~1 ppm upfield to that of the HH1 conformer of the (**Me$_4$dt**)Pt(d(G*pG*)) adduct.

4.3.5. (Me$_4$dt)Pt(d(TG*G*))

Within two hours after mixing a 1.9 mM solution of d(TGG) in D_2O (350 μL) with a 3.3 mM solution of (**Me$_4$dt**)$PtCl_2$ in DMSO-d_6 (200 μL), a new set of signals was observed (Figure 4.9) in addition to those of free d(TGG) signals (8.09 (3′-G H8), 7.92 (5′-G H8) and 7.41 (5′-TH6) ppm). These free d(TGG) signals disappeared after a day, indicating that the reaction was complete. The two G* H8 signals (at 9.41 and 8.97 ppm) of the adduct were connected by an NOE cross-peak, indicating an HH conformation. The ROESY data indicate that this dominant conformer has a normal anti,anti-HH conformation. The 5′-G* has an H8-H3′ NOE (a finding typical for an N-sugar), while the absence of an H8-H3′ NOE indicated an S-sugar for the 3′-G*. The H1′ coupling pattern of the signals at 6.44 and 6.51 ppm for the 3′-G* and the 5′-G*, respectively, was also consistent with this sugar pucker assignment. The H6 signal of the 5′-T was observed at 7.48 ppm. The doublet of doublets coupling pattern of the 5′T H1′ signal (6.05 ppm) indicated an S-sugar. The (**Me$_4$dt**)Pt(d(TG*G*)) adduct at equilibrium existed as ~100% HH1 conformer. The ^{31}P NMR signals for the HH1 conformer at -4.51 and -4.66 ppm are ~1 ppm upfield from the ^{31}P NMR signal (at -3.43 ppm) for the HH1 (**Me$_4$dt**)Pt(d(G*pG*)) conformer.

4.3.6 (**Et$_4$dt**)Pt(d(TG*G*))

For (**Et$_4$dt**)Pt(d(TG*G*)), one new set of signals downfield to the free d(TGG) signals was observed when a 1.4 mM solution of d(TGG) in D_2O (350 μL) was treated with a 2.5 mM solution of (**Et$_4$dt**)$PtCl_2$ in DMSO-d_6 (200 μL). The three singlets at 9.59, 9.04 and 7.41 ppm belonged to the 3′-G* and 5′-G* H8 signals and the 5′-T H6 signal, respectively. The H1′ signals at 6.51, 6.53, and 5.98 ppm belonged to 3′-G*, 5′-G* and 5′-T, respectively. From the H1′ coupling pattern, the 5′-G* has an N-sugar, and the 3′-G* and the 5′-T have an S-sugar. The presence of exclusively one conformer for the (**Et$_4$dt**)Pt(d(TG*G*)) adduct (Figure 4.10), as found for the (**Me$_4$dt**)Pt(d(TG*G*)) adduct, led us to assign these signals to the HH1 conformer. The ^{31}P NMR signals for the HH1 conformer of the (**Et$_4$dt**)Pt(d(TG*G*)) adduct were observed at -4.58 and -4.86 ppm.

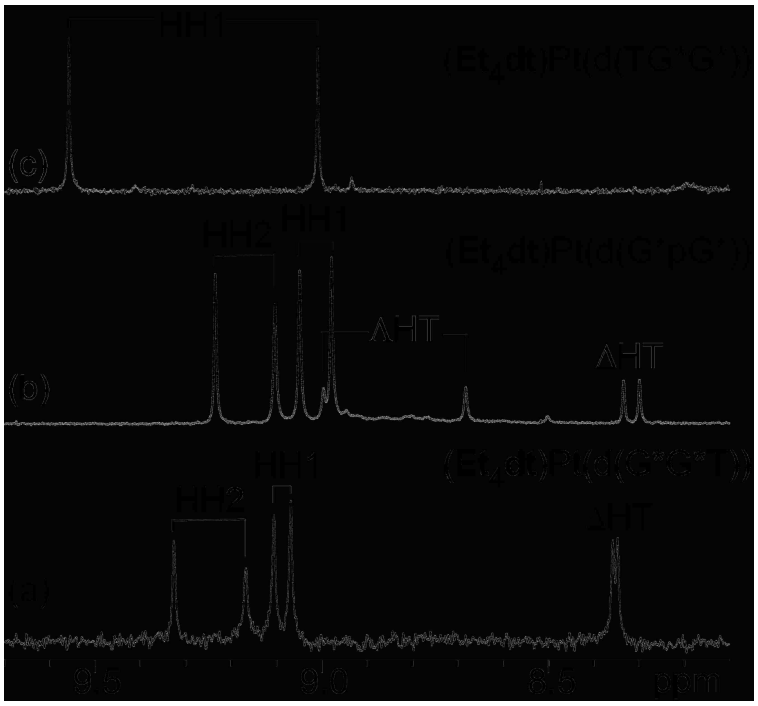

Figure 4.10. H8 region of ^{1}H NMR spectra (400 MHz) of (a) (**Et$_4$dt**)Pt(d(G*G*T)), (b) (**Et$_4$dt**)Pt(d(G*pG*)), and (c) (**Et$_4$dt**)Pt(d(TG*G*)) after 7 days in D_2O/DMSO-d_6 at pH ~4 and 25 °C.

4.3.7 (Me$_4$dt)Pt(d(G*G*T))

Three new pairs of G* H8 signals, downfield to the H8 signals of the free d(GGT) (8.15 (3′-G H8), 7.98 (5′-G H8) and 7.74 (5′-TH6) ppm), were observed within ~15 min of treating a 1.7 mM solution of d(GGT) in D_2O (350 μL) with a 3.0 mM solution of (**Me$_4$dt**)$PtCl_2$ in DMSO-d_6 (200 μL). After ~2 days, no free d(GGT) signals were observed, indicating complete reaction. For (**Me$_4$dt**)Pt(d(G*G*T)), the relative intensities and shifts of the G* H8 signals were very similar to the values observed for the (**Me$_4$dt**)Pt(d(G*pG*)) adduct (Table 4.1 and Figure 4.9). The H8 signals at 9.03 and 8.98 ppm and at 9.25 and 9.02 ppm were respectively connected with NOE cross-peaks, indicating an HH conformation. The two G* residues of both the HH conformers are anti, with an N-sugar for the 5′-G* and an S-sugar for the 3′-G*. The G* H8 signals mentioned above were assigned to the HH1 and HH2 conformers, respectively. The signal assignment was based on the similarity in the H8 chemical shifts of (**Me$_4$dt**)Pt(d(G*G*T)) with those of the (**Me$_4$dt**)Pt(d(G*pG*)) adduct. The ^{31}P NMR signal shifts at -3.49 and -2.64 ppm for (**Me$_4$dt**)Pt(d(G*G*T)) were similar to those of the HH1 and HH2 conformers of the (**Me$_4$dt**)Pt(d(G*pG*)) adduct, respectively. The T H6 signals at 7.83 and 7.90 ppm were respectively assigned to the HH1 and HH2 conformers.

The absence of an NOE cross-peak between the H8 signals at 8.31 and 8.21 ppm indicated an HT conformer for the (**Me$_4$dt**)Pt(d(G*G*T)) adduct. The NMR data indicated an anti,syn conformation, with an N- and S-sugar for the 5′- and 3′-G* bases, respectively. The similarity of these H8 shifts to those of the ΔHT conformer of the (**Me$_4$dt**)Pt(d(G*pG*)) adduct allowed us to assign these signals to the ΔHT conformer of the (**Me$_4$dt**)Pt(d(G*G*T)) adduct. The T H6 signal at 7.93 ppm was assigned to the ΔHT conformer; the G*pG* ^{31}P NMR signal in the ΔHT conformer could not be identified because of the overlapping G*pT signals in the -4 to -

4.6 ppm region of all the conformers. A very small fourth pair of G* H8 signals (at 8.59 and 8.86 ppm) was observed 4 days after initiation of the reaction but was not evaluated further because of the low abundance (3%).The chemical shift pattern was similar to the ΛHT conformer (8.65 and 9.03 ppm) of the (**Me$_4$dt**)Pt(d(G*pG*)) adduct. The final distribution of conformers for the (**Me$_4$dt**)Pt(d(G*G*T)) adduct was 48% HH2, 32% HH1, 17% ΔHT, and 3% ΛHT conformer (Figure 4.9).

4.3.8 (Et$_4$dt)Pt(d(G*G*T))

Three new pairs of G* H8 signals, downfield to the H8 signals of the free d(GGT), were observed within ~20 min of mixing a 1.3 mM solution of d(GGT) in D_2O (350 μL) with a 2.2 mM solution of (**Et$_4$dt**)$PtCl_2$ in DMSO-d_6 (200 μL). After ~7 days, no free d(GGT) signals were observed, indicating complete reaction. Assignments were based on the relative intensities and the characteristic shifts of the G* H8 signals, as determined above for the (**Et$_4$dt**)Pt(d(G*pG*)) and the (**Me$_4$dt**)Pt(d(G*G*T)) adducts. The H8 signals of the (**Et$_4$dt**)Pt(d(G*G*T)) adduct at 9.33 and 9.17 ppm and at 9.11 and 9.07 ppm were assigned to the HH1 and HH2 conformers, respectively. The two most upfield G* H8 signals at 8.36 and 8.35 ppm were assigned to the ΔHT conformer of the (**Et$_4$dt**)Pt(d(G*G*T)) adduct. The downfield ^{31}P NMR signals at -3.25 and -2.46 ppm are characteristic of the HH1 and HH2 conformers, respectively; these shifts are consistent with the shifts of the respective HH conformers of the (**Et$_4$dt**)Pt(d(G*pG*)) adduct. However, the ^{31}P NMR signal for the ΔHT conformer could not be identified because the G*pT phosphate group signals overlapped in the -3.8 to -4.5 ppm region. The T H6 signals at 7.85, 7.91, and 7.78 ppm were assigned to the HH1, the HH2 and the ΔHT conformers, respectively. Although observed for (**Et$_4$dt**)Pt(d(G*pG*)), the signals for the ΛHT conformer of

(**Et$_4$dt**)Pt(d(G*G*T)) were not detected, even two weeks after initiation of the reaction (final distribution of the conformers was 43% HH2, 35% HH1, and 22% ΔHT, Figure 4.10).

4.4 Discussion

To understand the effect of the carrier ligand, we compare the properties of the (**R$_4$dt**)Pt(d(G*pG*)) adducts with the results reported for other **L**Pt(d(G*pG*)) (**L** = **5,5′-Me$_2$bipy**,[23] **Me$_2$ppz**,[54] and **Bip**[43,53]) adducts. Both **Me$_2$ppz** and **Bip** are sp^3 N-donor ligands with the bulk of the ligand lying out of the Pt coordination plane. However, **R$_4$dt** and **5,5′-Me$_2$bipy** are planar, aromatic sp^2 N-donor ligands with significant bulk located in the coordination plane. For the (**5,5′-Me$_2$bipy**)Pt(d(G*pG*)) adduct, the H6/H6′ atoms of the carrier ligand point toward the cis G* residues, restricting the rate of rotation about the Pt–N7 bond.[23] In contrast, it was our hypothesis that the sterically less demanding N lone pair on each triazine ring in the (**R$_4$dt**)Pt(d(G*pG*)) adducts is expected to provide space for the cis G* residue to seek a more favorable position and to undergo rotation. We tested this hypothesis by assessing conformer distribution for (**R$_4$dt**)Pt(d(G*pG*)) and (**R$_4$dt**)Pt(oligo) adducts. Fortunately, the observation of the previously elusive ΛHT conformer provided both a novel observation as well as evidence suggesting that the hypothesis was correct.

4.4.1 Distribution of (R$_4$dt)Pt(d(G*pG*)) (R$_4$dt = Me$_4$dt, Et$_4$dt) Conformers

In addition to the HH1, HH2, and ΔHT conformers commonly observed in **L**Pt(d(G*pG*)) adducts, for the first time, a fourth form of an **L**Pt(d(G*pG*)) adduct was observed at low pH. This unusually abundant and slowly forming species appears to be the elusive ΛHT conformer.

By monitoring HPLC traces and NMR signals, the now well-established HH, HH2, and ΔHT conformers were identified and found to be present in the HPLC peak with the shortest

retention time (contains ΔHT and HH2) and the peak with an intermediate retention time (HH1). The fourth form, which became abundant only very slowly, was present in the peak with the longest retention time (Figure 4.7). The isolation of the peaks, followed by re-injection after various time periods, led to better separation (probably related to the residual HPLC buffer from the initial separation). The HPLC analysis of the re-injected peaks gave evidence that the ΔHT, HH2, and HH1 conformers interchanged relatively quickly. Considering the dilute conditions and the fact that the adducts were formed prior to separation, the interconversion of these conformers, which involves rotation of the G* bases and in some cases backbone rearrangement, is expected.

Of particular importance, the peaks with the common conformers on re-injection gave evidence for formation of the peak with the long retention time. In turn, re-injection of this peak, isolated by HPLC from the reaction solution in which the adduct was formed, led to the formation of the well-known conformers. These findings are compelling evidence that this fourth form is the elusive ΛHT conformer, the only conformer previously not present in an abundant amount under conditions where the d(G*pG*) moiety is in the normal protonation state with N1 of both guanines protonated.

We can suggest with reasonable confidence that the ΛHT conformer, despite the normally favorable HT base arrangement, which avoids base-base clashes and which benefits from antiparallel base dipole - base dipole interactions, may be a sterically large conformer unable to fit easily into the cavity provided by the typical **L** carrier ligand. Other results, in addition to the previous failure to detect any such abundant species, support this viewpoint. In particular, the amount of the ΛHT conformer was considerably less (17%) for **R = Et** than the 40% observed for **R = Me** in (**R$_4$dt**)Pt(d(G*pG*)) adducts. This increase means that low bulk favors the ΛHT

conformer. In addition, whereas the 3′-T flanking a crosslink normally has no effect, the ΛHT conformer becomes much less abundant in adducts with a 3′-residue.

Although our study was not designed to assess mechanism, the results provide a particularly good indication of the likely processes involved in conformer interchange. As mentioned, the interchange from one conformer to another involves at the very least rotation of a G* base. Rotation of the 5′-G* base could in theory convert HH1 to ΛHT, and vice versa. We cannot rule out this process completely, but we see no evidence for this isomerization. Because the backbone propagation direction differs for these two conformers, (1) for HH1 and (2) for ΛHT, both base rotation and backbone rearrangement are required. This combination of processes may be extremely slow.

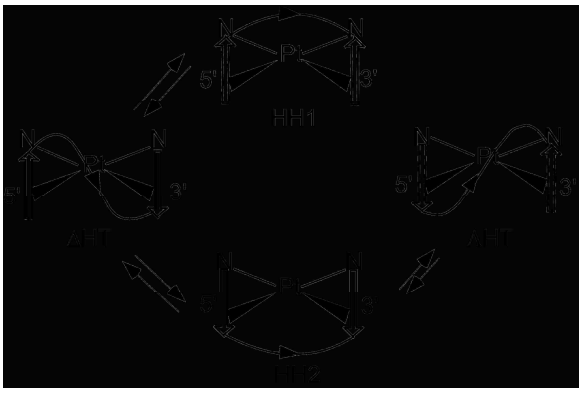

Figure 4.11. Scheme relating the conformers of an (**R$_4$dt**)Pt(d(G*pG*)) adduct modified from Figure 1 to show fast interconversion (depicted by long counter-parallel arrows) between the two HH conformers and the ΔHT conformer and slow interconversion (depicted by short counter-parallel arrows) between the HH2 conformer and the ΛHT conformer. The interconversion between the HH1 and ΛHT conformer requires both backbone rearrangement and base rotation (a process expected to be extremely slow) while the interconversion between the HH2 and ΛHT conformer requires only a simple rotation of the 3′-G* base (a process expected to be relatively fast)

On the other hand, HH2 could convert to ΛHT without backbone rearrangement by simple rotation of the 3′-G* base. However, our data suggest that whatever process leads to ΛHT, the interconversion between the now more commonly identified conformers is relatively

much faster (although not fast in the normal sense of the word). Thus, it could be rather difficult to decide which of the conformers produced ΛHT by using results obtained starting with these conformers.

Fortunately, under the solution conditions dictated by the isolation of the HPLC peaks, the data using the peak for the uncommon fourth conformer are rather informative. The rates of interconversion are such that ΛHT preferentially forms the HH2 conformer. Thus we can modify the general scheme relating the conformers as shown in figure 4.11.

For the (**5,5-Me$_2$bipy**)Pt(d(G*pG*)) adduct, a fourth set of signals was detected but was not evaluated further because of the low abundance (~4%).[23] The first evidence for a ΛHT conformer (called ΛHT2) was reported for the (*R,S,S,R*)-**Bip**Pt(G*pG*) adduct at pH ~10.[53] However, this conformer was not detected for the (**Me$_2$ppz**)Pt(d(G*pG*)) adduct. Apparently, the ΛHT conformer forms more slowly than the other conformers in **L**Pt(d(G*pG*)) adducts. At equilibrium, the distribution of the HH1, HH2, ΔHT, and ΛHT conformers was 36%, 18%, 6%, and 40%, respectively, for the (**Me$_4$dt**)Pt(d(G*pG*)) adduct and 41%, 33%, 9%, and 17%, respectively, for the (**Et$_4$dt**)Pt(d(G*pG*)) adduct. Evidently at equilibrium, the HH2 conformer is more favored and the ΛHT conformer is less favored for (**Et$_4$dt**)Pt(d(G*pG*)) than for (**Me$_4$dt**)Pt(d(G*pG*)).

At equilibrium, a relatively large percentage of the HH2 conformer was obtained for the (**Et$_4$dt**)Pt(d(G*pG*)) adduct when compared to the (**5,5′-Me$_2$bipy**)Pt(d(G*pG*))[23] and (**Me$_2$ppz**)Pt(d(G*pG*))[54] adducts (Table 4.3). During the early stages of the formation reaction for (**Me$_4$dt**)Pt(d(G*pG*)), a large abundance (37%) of the HH2 conformer was observed, which redistributed with other conformers to give a final distribution of 18%. The large abundance of the HH conformers can be attributed to the overall low steric effects of the **R$_4$dt** ligand, allowing

ample space for the HH conformers to exist without significant clashes between the O6 groups of the d(G*pG*) moiety. (A triazine ring N atom + N lone pair grouping is sterically less impeding than the C6 atom + H atom grouping in the sp^2 N-donor **5,5′-Me$_2$bipy** ligand studied earlier.)

Table 4.3. Conformer Distribution (%) for **L**Pt(d(G*pG*)) and **L**Pt(oligo) Adducts at equilibrium.

adduct	HH1	HH2	ΔHT	ΛHT
(**Me$_4$dt**)Pt(d(G*pG*))	36	18	6	40
(**Me$_4$dt**)Pt(d(G*G*T))	48	32	17	3
(**Me$_4$dt**)Pt(d(TG*G*))	99			
(**Me$_4$dt**)Pt(d(TG*G*T))	99			
(**Et$_4$dt**)Pt(d(G*pG*))	41	33	9	17
(**Et$_4$dt**)Pt(d(G*G*T))	43	35	22	
(**Et$_4$dt**)Pt(d(TG*G*))	99			
(**5,5-Me$_4$bipy**)Pt(d(G*pG*))[23]	52	10	34	
(**Me$_2$ppz**)Pt(d(G*pG*))[54]	50	20	30	

In Table 4.3, the conformer distributions of (**R$_4$dt**)Pt(oligo) adducts are compared to those for the respective (**R$_4$dt**)Pt(d(G*pG*)) adducts. For the (**R$_4$dt**)Pt(d(G*G*T)) adducts, the three HH1, HH2 and ΔHT conformers were abundant, but the distribution of these conformers was different from that for the (**R$_4$dt**)Pt(d(G*pG*)) adducts (Table 4.3). A low abundance of the ΛHT conformer (3%) was observed four days after initiation of the reaction for the (**Me$_4$dt**)Pt(d(G*G*T)) adduct. However, for (**Et$_4$dt**)Pt(d(G*G*T)) the H8 signals of this conformer were not detected even 4 weeks after initiation of the reaction. This finding is consistent with the slow isomerization to the ΛHT conformer for the (**Et$_4$dt**)Pt(d(G*pG*)) adducts. The ΛHT conformer is less favored for the (**R$_4$dt**)Pt(d(G*G*T)) adducts when R = Et than when R = Me. The number of conformers and the H8 signal shifts for the

(**R_4dt**)Pt(d(G*G*T)) and (**R_4dt**)Pt(d(G*pG*)) adducts were very similar. Thus, it can be inferred that the 3′-T residue does not influence the structure of the d(G*pG*) cross-link.

In contrast, for the (**Me_4dt**)Pt(d(TG*G*)), (**Et_4dt**)Pt(d(TG*G*)) and (**Me_4dt**)Pt(d(TG*G*T)) adducts, the HH1 L conformer was ~100% favored at equilibrium (Figures 4.8 and 4.9). The remaining three possible conformers were not detected for these adducts. A preference for the HH1 conformer was also observed for (**Me_2ppz**)Pt(d(TG*G*)) and (**Me_2ppz**)Pt(d(TG*G*T)).[54] Thus, the presence of a 5′-flanking T residue highly favors the HH1 conformer, and this propensity is not affected by the addition of a 3′-T residue. The 5′-substituent remains the key factor in influencing the distribution and H8 shifts of the cross-link moiety.

4.4.2 Sugar-phosphodiester Backbone of (R_4dt)Pt(d(G*pG*)) and (R_4dt)Pt(oligo) Conformers

The observation of a 5′-G* H8-H3′ NOE cross-peak indicated that the 5′-G* residue of all the conformers of (**R_4dt**)Pt(d(G*pG*)) (**R_4 = Me_4** and **Et_4**) adopts the N-sugar pucker universally found for the 5′-G* sugar in **L**Pt(d(G*pG*)) cross-link adducts.[27,50,51,54,76] Thus, the favored N-pucker observed for the 5′-G* sugar appears to be independent of the carrier ligand. The absence or weakness of the 3′-G* H8-H3′ cross-peak indicated that the 3′-G* sugar for all the four conformers of the (**R_4dt**)Pt(d(G*pG*)) adduct has the S-sugar pucker. The S-pucker is favored by the 3′-G* in free d(GpG) and also for the conformers of (**5,5′-Me_2bipy**)Pt(d(G*pG*))[23], (**Me_2ppz**)Pt(d(G*pG*))[54] and **Bip**Pt(d(G*pG*)).[43,50,53] Moreover, the shifts of the sugar proton signals of the commonly observed HH1, HH2 and ΔHT conformers of the (**R_4dt**)Pt(d(G*pG*)) adduct were very similar to those of the (**5,5′-Me_2bipy**)Pt(d(G*pG*))[23] and the (**Me_2ppz**)Pt(d(G*pG*)) adducts.[54] Such similarity in the chemical shifts indicates that the sugar-phosphodiester backbone has a similar structure in all adducts.

The similarity in the structure-sensitive ^{31}P NMR chemical shifts of the (**R$_4$dt**)Pt(d(G*pG*)) conformers and the respective conformers of the previously studied **L**Pt(d(G*pG*)) adducts (**L = 5,5′-Me$_2$bipy**,[23] **Me$_2$ppz**,[54] (*S,R,R,S*)-**Bip**,[43] and (*R,S,S,R*)-**Bip**[50]) provides further evidence that the carrier ligand has little influence on the structure of the sugar-phosphodiester backbone for all conformers of **L**Pt(d(G*pG*)) adducts.

The ^{31}P NMR shifts (for the HH conformers) and the H8 chemical shifts for the d(G*pG*) moiety of the (**R$_4$dt**)Pt(d(G*G*T)) adduct are very similar to those of the respective (**R$_4$dt**)Pt(d(G*pG*)) adduct (Figure 4.9 and 4.10) indicating that the 3′-T residue is positioned far from the 3′-G* residue and has little effect on the structure of the G*pG* sugar-phosphodiester backbone. The 3′-T flanking a crosslink normally has no effect, the ΛHT conformer becomes much less abundant in adducts with a 3′-residue. These results are in agreement with those for HH and ΔHT conformers of the (**Me$_2$ppz**)Pt(d(G*G*T)) adduct[68] as well as for the HH conformers of the dynamic **L**Pt(d(GGTT)) adducts (**L** = ethylenediamine and $(MeNH_2)_2$).[25]

For **L**Pt(oligo) adducts (**L** = sp^3 N-donor ligands) having a 5′-T residue, a downfield ^{31}P NMR signal ~-2.5 to -3.2 ppm was observed, a characteristic shift of the HH1 conformation of the G*pG* cross-link.[25] The structure sensitive ^{31}P NMR signal for the exclusively formed HH1 conformer of both the (**R$_4$dt**)Pt(d(TG*G*)) and the (**R$_4$dt**)Pt(d(TG*G*T) adducts is ~1 ppm upfield from the ^{31}P NMR shift of the HH1 conformer of the respective (**R$_4$dt**)Pt(d(G*pG*)) adduct. The ^{31}P NMR signal shifts for the HH1 conformer of these (**R$_4$dt**)Pt(oligo) adducts were very similar to the shifts for unstrained phosphodiester groups in oligos (~-4 ppm).[25] This may be attributed to the overall low steric effects of the **R$_4$dt** ligand, with two N + N lone pair groupings which allow more space for the HH conformer to exist[65] resulting in a less distorted backbone

structure. Thus, it can be said that a 5′-T residue in a (**R$_4$dt**)Pt(oligo) may slightly affect the conformation of the sugar-phosphodiester backbone.

4.4.3 Base Canting

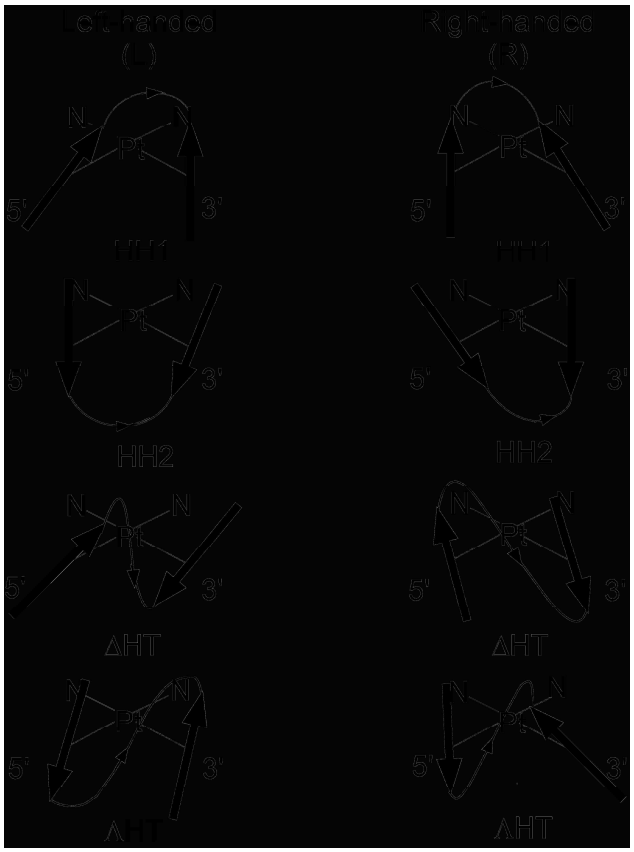

Figure 4.12. HH1, HH2, ΔHT and ΛHT conformers, showing variants with left-handed and right-handed canting.

Besides the HH or HT orientation and backbone propagation direction, the other significant structural feature is base canting. The bases are not exactly perpendicular to the coordination plane, and the degree and the direction (left- or right-handed, Figure 4.12) of canting differ depending on a number of factors and particularly the carrier ligand, the presence or absence of a link between the bases, the sugar (ribo or deoxyribo), and the single-stranded or duplex character of the DNA. Fortunately, the G* H8 signals are a good probe for assessing the degree of base canting.[43] Typically, H8 signals of the HH conformers of **L**Pt(d(G*pG*)) adducts

have chemical shifts of ~7.8-8.1 ppm (canted base) and ~8.8-9.2 ppm (less canted base), respectively.[43] For the HH orientation, often only one base is significantly canted, such that the H8 atom is positioned toward the other cis base, which is less canted.[55,61,63] The H8 atom of the canted base is within the shielding region of the less canted base and has a relatively upfield H8 signal. The H8 signal of the less canted base is relatively downfield because this H8 is far from the cis base shielding region.[61,62] The HH H8 signals can be dispersed by as much as ~1 ppm.[43]

4.4.3.1 (R_4dt)Pt(d(G*pG*)). According to the H8 shift method[43] for assessing base canting in the HH conformers of d(G*pG*) adducts with sp^3 N-donor ligands, an H8 signal shift of ~9.0 (3′-G*) and ~8.7 (5′-G*) ppm is associated with less canted bases.[43] The (**Me_2ppz**)Pt(d(G*pG*)) G* H8 shifts reported for the HH1 conformer at 8.93 (3′-G*) and 8.51 (5′-G*) ppm and for the HH2 conformer at 8.78 (3′-G*) and 8.71 (5′-G*) ppm indicate low base canting.[54] Also, the G* bases in the HH conformers of the (**5,5′-Me_2bipy**)Pt(d(G*pG*)) adduct were relatively less canted, with H8 signals at 9.14 and 8.76 ppm for the HH1 L conformer and at 9.07 and 8.83 ppm for the HH2 R conformer.[23] The relatively downfield H8 signals of the (**5,5′-Me_2bipy**)Pt(d(G*pG*)) adduct were attributed to the greater inductive effect of Pt because of the relatively poor electron-donating ability of the aromatic **5,5′-Me_2bipy** ligand compared to that of the **Me_2ppz** ligand.[23] The even more downfield H8 signals for the (**R_4dt**)Pt(d(G*pG*)) adduct can be attributed to the presence of six nitrogen atoms in the aromatic rings, making this ligand a poorer electron donor than the **5,5′-Me_2bipy** ligand. We have experimental evidence that the presence of DMSO in the solvent mixture also causes the signals to have a more downfield shift than in water. The H8 signals for the (**R_4dt**)Pt(d(G*pG*)) solutions containing ~36% DMSO were ~0.15 ppm more downfield than when the solution contained ~10% DMSO.

For the HH1 and the HH2 conformers of the (**R_4dt**)Pt(d(G*pG*)) adducts, only HH2 gives sufficient dispersion to assess the canting direction. The 5′-G* is slightly canted toward the cis 3′-G*, hence a more upfield 5′-G* H8 signal compared to the 3′-G* H8 signal. The bases in the HH2 conformer of (**Me_4dt**)Pt(d(G*pG*)) and (**Et_4dt**)Pt(d(G*pG*)) adducts are right-hand canted (Figure 4.12). The H8 chemical shifts and the small dispersion between the H8 signals of the HH conformers of the (**Me_4dt**)Pt(d(G*pG*)) and (**Et_4dt**)Pt(d(G*pG*)) adducts (Table 4.2) suggest relatively less canted bases in all cases.

Shift relationships to canting are not so easily interpreted for the ΔHT conformer.[23,54] For the (**R_4dt**)Pt(d(G*pG*)) adduct, both 3′- and 5′-G* H8 signals are upfield (Table 4.2) but are comparatively more downfield than the H8 signals of 3′-G* (8.01 ppm) and the 5′-G* bases (8.18 ppm) of the ΔHT conformer of the **5,5′-Me_2bipy**Pt(d(G*pG*)) adduct. However, allowing for the poor electron-donating effect of the **R_4dt** ligand and the solvent effect (discussed above), the bases in the ΔHT conformer for (**R_4dt**)Pt(d(G*pG*)) and (**5,5′-Me_2bipy**)Pt(d(G*pG*)) will most likely cant in almost identical manner.[23]

For the ΛHT conformer of the (**R_4dt**)Pt(d(G*pG*)) adduct, the small separations of H8 shifts, 0.38 ppm for the (**Me_4dt**)Pt(d(G*pG*)) adduct and 0.33 ppm for the (**Et_4dt**)Pt(d(G*pG*)) adduct, suggest the conformer has relatively small base canting.

4.4.3.2 Influence of Flanking T Residues on Base Canting. In order to use chemical shifts to assess the influence of the flanking residue (T) on the base canting, it is important to allow for the possible through-space and inductive effects of the T residue on the chemical shifts. These effects can alter the shifts of the G* H8 and sugar proton signals of the respective parent (**R_4dt**)Pt(d(G*pG*)) adduct. First, the anisotropic effect of the phosphate group can deshield the nearest H8 atom. The presence of a 5′-p group was found to cause a downfield shift of the 5′-G

H8 signal.[25,46,78] When this group is on the 3′-carbon, it is too far from the G* H8 to have much direct influence on the H8 shift. Second, the anisotropy of the T base might also influence the H8 signals.

- **Influence of the 3′-T on G* Base Canting.** The conformers of the (**R_4dt**)Pt(d(G*G*T)) adduct with a 3′-flanking T residue have 5′- and 3′-G* H8 signal shifts very similar to the respective signals of the (**R_4dt**)Pt(d(G*pG*)) adduct (Table 4.2). The 3′-residue has no significant influence on the H8 chemical shifts or the degree of canting for the d(G*pG*) moiety.[68] These results are consistent with those reported for the (**Me_2ppz**)Pt(d(G*G*T)) adduct.[68] Because the 3′-T residue is far from the 3′-G* residue, it has little or no effect on the direction or degree of canting.

- **Influence of the 5′-T on G* Base Canting**. For the (**R_4dt**)Pt(d(TG*G*)) HH1 conformer, the 5′-G* H8 signals are slightly upfield from the 5′-G* H8 signals of the respective (**R_4dt**)Pt(d(G*pG*)) adduct; however, the 3′-G* H8 signals were considerably downfield [0.38 ppm for (**Me_4dt**)Pt(d(TG*G*)) and 0.62 ppm for (**Et_4dt**)Pt(d(TG*G*))] from the 3′-G* H8 signal of the respective (**R_4dt**)Pt(d(G*pG*)) adduct (Table 4.2). A very downfield 3′-G* H8 signal compared to the 5′-G* H8 signal indicates L canting in the HH1 conformer.[44,47,68] The doublet of doublets coupling pattern of the 5′-T H1′ signal indicates an S-sugar for the HH **L** conformer of (**R_4dt**)Pt(d(TG*G*)) adducts. From X-ray structural data of *cis*-$Pt(NH_3)_2$(d(pG*pG*) and *cis*-$Pt(NH_3)_2$(d(CG*G*), the ammine cis to the canted 5′-G* in L-canted, single-stranded (ss) cross-links always has an H-bond to the oligo,[24,49] and the 5′-flanking residue has an S-sugar.[24] Because **R_4dt** ligands cannot form H-bonds, we conclude that the degree of L canting is a consequence of the steric effects of the 5′ residue, and the H-bonding

interactions are inconsequential. Our results are in agreement with the findings for (**Me$_2$ppz**)Pt(d(TG*G*)) and (**Me$_2$ppz**)Pt(d(TG*G*T)) showing that any 5′-substituent, including the 5′-p group, favors the HH1 L conformer.[68]

4.5 Conclusions

We report here the first evidence of formation of a substantial amount of a fourth form of an **L**Pt(d(G*pG*)) adduct. HPLC data suggest that this is the elusive ΛHT conformer of the N7–Pt–N7 d(G*pG*) cross-link adduct. The putative ΛHT conformer of (**R$_4$dt**)Pt(d(G*pG*)) is kinetically less favored when compared to the HH1, HH2 and ΔHT conformers and becomes abundant slowly (~8 weeks) by conformer isomerization. It is possible that this ΛHT conformer was not detected in the previously reported less dynamic adducts, even after long time periods, because of its slow rate of formation. However, for the (**R$_4$dt**)Pt(d(G*pG*)) adduct all four expected conformers could be identified and characterized by ^{1}H NMR spectroscopy. Our results with (**R$_4$dt**)Pt(5′-GMP)$_2$ revealed that the **R$_4$dt** carrier ligand is sterically less demanding and allows a less restricted rotation of **G** about the Pt–N7 bond. The detection of all four conformers and absence of any EXSY cross-peaks for the (**R$_4$dt**)Pt(d(G*pG*)) adduct provides the first clear evidence that the sugar-phosphodiester backbone between two adjacent G's slows the exchange between the conformers.

From the distribution of conformers for (**R$_4$dt**)Pt(d(G*pG*)), (**5,5′-Me$_2$bipy**)Pt(d(G*pG*)),[23] **Bip**Pt-(d(G*pG*))[43,50] and **Me$_2$ppz**Pt(d(G*pG*))[54] adducts, regardless of the carrier ligand the HH1 conformer is most abundant. However, the thermodynamically favored putative ΛHT conformer for (**Me$_4$dt**)Pt(d(G*pG*)) was almost as abundant as the HH1 conformer at equilibrium. NMR results in this study also show that the structure of the sugar-phosphodiester backbone differ from conformer to conformer, but the ^{31}P

NMR data for the (**R$_4$dt**)Pt(d(TG*G*)) adduct, for the first time indicated that for a given conformer, the backbone structure may depend on the carrier ligand. The low steric effects of the N lone pairs of the **R$_4$dt** ligand allow more space for the HH conformer to exist resulting in a less distorted backbone for the HH1 conformer.

For all the (**Et$_4$dt**)Pt(d(G*pG*)) conformers (except for ΔHT conformer present in 9% abundance only), weak NOE cross-peaks (comparable in size) between the 3′-G* H8 and the methyl peaks of the carrier ligand indicated that the substituents at the 6/6′ position in a bis-3,3′-(1,2,4-triaizine) are close to the cis G*. The (**Et$_4$dt**)Pt(d(G*pG*)) conformers isolated by HPLC, upon re-injection, redistributed slowly (~2 days) compared to the (**Me$_4$dt**)Pt(d(G*pG*)) conformers, which interconverted significantly after ~1day. Also, in contrast to the (**Me$_4$dt**)Pt(d(G*G*T)) adduct, the ΛHT conformer does not form for the (**Et$_4$dt**)Pt(d(G*G*T)) adduct. These evidences in addition to the results from the (**R$_4$dt**)Pt(5′-GMP)$_2$ studies[65] suggest that placing greater bulk at the 6,6′ positions by changing **R** in **R$_4$dt** from Me to Et has a clear effect on the **G*** base rotation rate about Pt–N7 bond.

Because of the symmetrical nature of the carrier ligand in (**R$_4$dt**)Pt(d(G*pG*)), the two bases of the HH and HT conformers may ‘wag’ between R and L canting, causing the H8 signals of the conformers to have relatively similar shifts. However, the H8 shifts also indicate that the base canting in (**R$_4$dt**)Pt(d(G*pG*)) conformers is small. These results agree with the low base canting observed for the (**5,5′-Me$_2$bipy**)Pt(d(G*pG*)) conformers. However, the presence of a 5′-flanking T residue on the d(GpG) sequence introduces L canting of the bases in the HH1 conformer. Unless a carrier ligand such as (*R,S,S,R*)-**Bip** (which favors right-handed canting) is present,[44,79] all single-stranded N7–Pt–N7 cross-links regardless of oligonucleotide length are left-handed.[20,54,68] The highly L nature of the ss adducts with a 5′-T residue is chiefly a

consequence of the bulk of the 5′ substituents; factors such as H-bonding are inconsequential. Also, the 5′-T residue maintains an S-sugar pucker in the ss adducts even in the absence of H-bonding, providing further support to the finding that the N-pucker of this residue in the Lippard bp step of duplexes is related to stacking and Watson-Crick H-bonding and not to the insignificance of ammine H-bonding.[68]

Several important points have emerged from a comparison of the (**R_4dt**)Pt(oligo) adducts with (**R_4dt**)Pt(d(G*pG*)). For (**R_4dt**)Pt adducts at equilibrium, d(G*pG*) and d(G*G*T) uniquely have all the four conformers (except for the (**Et_4dt**)Pt(d(G*G*T)) ΛHT conformer which does not form), but, in contrast, d(TG*G*) has only the HH1 conformer. The ΛHT conformer becomes much less abundant in adducts with a 3′-residue. The structure sensitive ^{31}P NMR shifts were similar for the HH conformers of (**R_4dt**)Pt(d(G*G*T)) and (**R_4dt**)Pt(d(G*pG*)), however, for the HH1 conformer of (**R_4dt**)Pt(d(TG*G*)) the signals were ~1 ppm upfield to that for the respective (**R_4dt**)Pt(d(G*pG*)). Evidently, the 3′-flanking T residue has little or no effect, but the 5′-flanking T residue has a dramatic effect on the conformer distribution and the d(G*pG*) cross-link structure.

4.6 References

1. Rosenberg, B. In *Cisplatin. Chemistry and Biochemistry of a Leading Anticancer Drug*; Lippert, B., Ed.; Wiley-VCH: Weinheim, 1999, pp 3-27.

2. Hambley, T. W. *Coord. Chem. Rev.* **1997**, *166*, 181-223.

3. Decatris, M. P.; Sundar, S.; O'Byrne, K. J. *Cancer Treat. Rev.* **2004**, *4*, 53-81.

4. Ho, Y. P.; Au-Yeung, S. C.; To, K. K. *Med. Res. Rev.* **2003**, *23*, 633-655.

5. Bloemink, M. J.; Reedijk, J. In *Metal Ions in Biological Systems*; Sigel, H., Ed.; Marcel Dekker, Inc.: New York, 1996; Vol. 32, pp 641-685.

6. Lebwohl, D.; Canetta, R. *Eur. J. Cancer* **1998**, *34*, 1522-1534.

7. Jamieson, E. R.; Lippard, S. J. *Chem. Rev.* **1999**, *99*, 2467-2498.

8. Barnes, K. R.; Lippard, S. J. In *Metal Ions in Biological Systems*; Sigel, H., Ed.; Marcel Dekker: New York, 2004, pp 143-177.

9. Bloemink, M. J.; Engelking, H.; Karentzopoulos, S.; Krebs, B.; Reedijk, J. *Inorg. Chem.* **1996**, *35*, 619-627.

10. Sundquist, W.; Lippard, S. J. *Coord. Chem. Rev.* **1990**, *100*, 293-322.

11. Reedijk, J. *J. Chem. Soc. Chem. Commun.* **1996**, 801-806.

12. Zamble, D. B.; Lippard, S. J. In *Cisplatin: Chemistry and Biochemistry of a Leading Anticancer Drug*; Lippert, B., Ed.; Wiley-VCH: Weinheim, 1999, pp 73-110.

13. Kelland, L. *Nature (London)* **2007**, *7*, 573-584.

14. Kasparkova, J.; Vojtiskova, M.; Natile, G.; Brabec, V. *Chem. Eur. J.* **2008**, *14*, 1330-1341.

15. Spingler, B.; Whittington, D. A.; Lippard, S. J. *Inorg. Chem.* **2001**, *40*, 5596-5602.

16. Silverman, A. P.; Bu, W.; Cohen, S. M.; Lippard, S. J. *J. Biol. Chem.* **2002**, *277*, 49743-49749.

17. Raymond, E.; Faivre, S.; Chaney, S.; Woynarowski, J.; Cvitkovic, E. *Mol. Cancer Ther.* **2002**, *1*, 227-235.

18. Blommaert, F. A.; Van Dijk-Knijnenburg, H. C. M.; Dijt, F. J.; Den Engelse, L.; Baan, R. A.; Berends, F.; Fichtinger-Schepman, A. M. J. *Biochemistry* **1995**, *34*, 8474-8480.

19. Sherman, S. E.; Lippard, S. J. *Chem. Rev.* **1987**, *87*, 1153-1181.

20. Beljanski, V.; Villanueva, J. M.; Doetsch, P. W.; Natile, G.; Marzilli, L. G. *J. Am. Chem. Soc.* **2005**, *127*, 15833-15842.

21. Marzilli, L. G.; Saad, J. S.; Kuklenyik, Z.; Keating, K. A.; Xu, Y. *J. Am. Chem. Soc.* **2001**, *123*, 2764-2770.

22. Cohen, S. M.; Lippard, S. J. *Prog. Nucleic Acid Res. Mol. Biol.* **2001**, *67*, 93-130.

23. Bhattacharyya, D.; Marzilli, P. A.; Marzilli, L. G. *Inorg. Chem.* **2005**, *44*, 7644-7651.

24. Admiraal, G.; Van der Veer, J. L.; de Graaff, R. A. G.; den Hartog, J. H.; Reedijk, J. *J. Am. Chem. Soc.* **1987**, *109*, 592-594.

25. Fouts, C.; Marzilli, L. G.; Byrd, R.; Summers, M. F.; Zon, G.; Shinozuka, K. *Inorg. Chem.* **1988**, *27*, 366-376.

26. Sherman, S. E.; Gibson, D.; Wang, A. H.-J.; Lippard, S. J. *Science (Washington, D. C.)* **1985**, *230*, 412-417.

27. Mukundan, S., Jr.; Xu, Y.; Zon, G.; Marzilli, L. G. *J. Am. Chem. Soc.* **1991**, *113*, 3021-3027.

28. Berners-Price, S. J.; Frenkiel, T. A.; Ranford, J. D.; Sadler, P. J. *J. Chem. Soc., Dalton Trans.* **1992**, 2137-2139.

29. den Hartog, J. H. J.; Altona, C.; van der Marel, G. A.; Reedijk, J. *Eur. J. Biochem.* **1985**, *147*, 371-379.

30. Kline, T. P.; Marzilli, L. G.; Live, D.; Zon, G. *J. Am. Chem. Soc.* **1989**, *111*, 7057-7068.

31. Caradonna, J. P.; Lippard, S. J. *Inorg. Chem.* **1988**, *27*, 1454-1466.

32. Neumann, J.-M.; Tran-Dinh, S.; Girault, J.-P.; Chottard, J.-C.; Huynh-Dinh, T. *Eur. J. Biochem.* **1984**, *141*, 465-472.

33. den Hartog, J. H. J.; Altona, C.; Chottard, J.-C.; Girault, J.-P.; Lallemand, J.-Y.; de Leeuw, F. A.; Marcelis, A. T. M.; Reedijk, J. *Nucleic Acids Res* **1982**, *21*, 1352-1356.

34. van Boom, S. S. G. E.; Yang, D.; Reedijk, J.; Van der Marel, G. A.; Wang, A. H.-J. *Biomol. Struct. Dyn.* **1996**, *13*, 989-998.

35. Berners-Price, S. J.; Barnham, K. J.; Frey, U.; Sadler, P. J. *Chem. Eur.J.* **1996**, *2*, 1283-1291.

36. Sullivan, S. T.; Ciccarese, A.; Fanizzi, F. P.; Marzilli, L. G. *Inorg. Chem.* **2000**, *39*, 836-842.

37. Ohndorf, U.-M.; Rould, M. A.; He, Q.; Pabo, C. O.; Lippard, S. J. *Nature (London)* **1999**, *399*, 708-712.

38. Crul, M.; Schellens, J. H. M.; Beijnen, J. H.; Maliepaard, M. *Cancer Treat. Rev.* **1997**, *23*, 341-366.

39. Naegeli, H. *FASEB J.* **1995**, *9*, 1043-1050.

40. Ohndorf, U.-M.; Whitehead, J. P.; Raju, N.; Lippard, S. J. *Biochemistry* **1997**, *36*, 14807-14815.

41. Dunham, S. U.; Lippard, S. J. *Biochemistry* **1997**, *36*, 11428-11436.

42. Partrick, S. M.; Turchi, J. J. *Biochemistry* **1998**, *37*, 8808-8815.

43. Marzilli, L. G.; Ano, S. O.; Intini, F. P.; Natile, G. *J. Am. Chem. Soc.* **1999**, *121*, 9133-9142.

44. Ano, S. O.; Kuklenyik, Z.; Marzilli, L. G. In *Cisplatin. Chemistry and Biochemistry of a Leading Anticancer Drug*; Lippert, B., Ed.; Wiley-VCH: Weinheim, 1999, pp 247-291.

45. Ano, S. O.; Intini, F. P.; Natile, G.; Marzilli, L. G. *J. Am. Chem. Soc.* **1997**, *119*, 8570-8571.

46. Girault, J.-P.; Chottard, G.; Lallemand, J.-Y.; Chottard, J.-C. *Biochemistry* **1982**, *21*, 1352-1356.

47. Kozelka, J.; Fouchet, M. H.; Chottard, J.-C. *Eur. J. Biochem.* **1992**, *205*, 895-906.

48. Berners-Price, S. J.; Ranford, J. D.; Sadler, P. J. *Inorg. Chem.* **1994**, *33*, 584-5846.

49. Sherman, S. E.; Gibson, D.; Wang, A.; Lippard, S. J. *J. Am. Chem. Soc.* **1988**, *110*, 7368-7381.

50. Ano, S. O.; Intini, F. P.; Natile, G.; Marzilli, L. G. *J. Am. Chem. Soc.* **1998**, *120*, 12017-12022.

51. Yang, D.; van Boom, S.; Reedijk, J.; van Boom, J.; Wang, A. *Biochemistry* **1995**, *34*, 12912-12920.

52. Chottard, J.-C.; Girault, J.-P.; Chottard, G.; Lallemand, J.-Y.; Mansuy, D. *J. Am. Chem. Soc.* **1980**, *102*, 5565-5572.

53. Williams, K. M.; Cerasino, L.; Natile, G.; Marzilli, L. G. *J. Am. Chem. Soc.* **2000**, *122*, 8021-8030.

54. Sullivan, S. T.; Ciccarese, A.; Fanizzi, F. P.; Marzilli, L. G. *J. Am. Chem. Soc.* **2001**, *123*, 9345-9355.

55. Ano, S. O.; Intini, F. P.; Natile, G.; Marzilli, L. G. *Inorg. Chem.* **1999**, *38*, 2989-2999.

56. Saad, J. S.; Scarcia, T.; Natile, G.; Marzilli, L. G. *Inorg. Chem.* **2002**, *41*, 4923-4935.

57. Williams, K. M.; Cerasino, L.; Intini, F. P.; Natile, G.; Marzilli, L. G. *Inorg. Chem.* **1998**, *37*, 5260-5268.

58. Sullivan, S. T.; Ciccarese, A.; Fanizzi, F. P.; Marzilli, L. G. *Inorg. Chem.* **2001**, *40*, 455-462.

59. Cramer, R. E.; Dahlstrom, P. L. *J. Am. Chem. Soc.* **1979**, *101*, 3679-3681.

60. Benedetti, M.; Gabriella, T.; Cini, R.; Marzilli, L. G.; Natile, G. *Chem. Eur. J.* **2007**, *13*, 3131-3142.

61. Marzilli, L. G.; Intini, F. P.; Kiser, D.; Wong, H. C.; Ano, S. O.; Marzilli, P. A.; Natile, G. *Inorg. Chem.* **1998**, *37*, 6898-6905.

62. Saad, J. S.; Scarcia, T.; Shinozuka, K.; Natile, G.; Marzilli, L. G. *Inorg. Chem.* **2002**, *41*, 546-557.

63. Xu, Y.; Natile, G.; Intini, F. P.; Marzilli, L. G. *J. Am. Chem. Soc.* **1990**, *112*, 8177-8179.

64. Wong, H. C.; Shinozuka, K.; Natile, G.; Marzilli, L. G. *Inorg. Chim. Acta* **2000**, *297*, 36-46.

65. Maheshwari, V.; Marzilli, P. A.; Marzilli, L. G. *Inorg. Chem.* **2008**, Submitted.

66. Ishibashi, T.; Lippard, S. J. *Proc. Natl. Acad. Sci. U.S.A.* **1998**, *95*, 4219-4223.

67. Villanueva, J. M.; Jia, X.; Yohannes, P. G.; Doetsch, P. W.; Marzilli, L. G. *Inorg. Chem.* **1999**, *38*, 6069-6080.

68. Sullivan, S. T.; Saad, J. S.; Fanizzi, F. P.; Marzilli, L. G. *J. Am. Chem. Soc.* **2002**, *124*, 1558-1559.

69. Jensen, R. E.; Pflaum, R. T. *Anal. Chim. Acta* **1965**, *32*, 235-244.

70. Fasman, G. D. *CRC Handbook of Biochemistry and Molecular Biology*; 3rd ed.; CRC Press Inc.: Cleveland, 1975; Vol. 1, Nucleic Acids, p 589.

71. Saenger, W. *Principles of Nucleic Acid Structure*; Springer-Verlag: New York, 1984, pp 1-556.

72. Wuthrich, K. *NMR of Proteins and Nucleic Acids*; John Wiley & Sons: New York, 1986

73. Kaspárková, J.; Mellish, K. J.; Qu, Y.; Brabec, V.; Farrell, N. *Biochemistry* **1996**, *35*, 16705-16713.

74. Patel, D. J.; Kozlowski, S. A.; Nordheim, A.; Rich, A. *Proc. Natl. Acad. Sci. U.S.A.* **1982**, *79*, 1413-1417.

75. Dijt, F. J.; Canters, G. W.; den Hartog, J. H.; Marcelis, A. T. M.; Reedijk, J. *J. Am. Chem. Soc.* **1984**, *106*, 3644-3647.

76. van der Veer, J. L.; van der Marel, G. A.; van den Elst, H.; Reedijk, J. *Inorg. Chem.* **1987**, *26*, 2272-2275.

77. Wong, H. C.; Coogan, R.; Intini, F. P.; Natile, G.; Marzilli, L. G. *Inorg. Chem.* **1999**, *38*, 777-787.

78. van Garderen, C. J.; Bloemink, M. J.; Richardson, E.; Reedijk, J. *J. Inorg. Biochem.* **1991**, *42*, 199-205.

79. van der Veer, J. L.; Reedijk, J. *Chem. Br,* **1988**, *24*, 775-780.

CHAPTER 5. LIGAND AND COORDINATION-PLANE DISTORTIONS IN Pt(II) COMPLEXES OF ISOMERS OF DIMETHYL-2,2′-BIPYRIDINE*

5.1 Introduction

Rosenberg's serendipitous discovery of the anticancer activity of cisplatin, *cis*-$Pt(NH_3)_2Cl_2$,[1] has stimulated extensive interest in the interaction of Pt complexes with nucleic acids. Pt compounds can bind to DNA by either covalent or non-covalent interactions. Cisplatin and several other Pt anticancer drugs interact with nucleic acids by forming 1,2-intrastrand cross-links having covalent Pt–N7 bonds with two adjacent guanines.[2,3] Dichloro Pt(II) complexes of aromatic sp^2 N-donor ligands such as 5,5′-dimethyl-2,2′-bipyridine (**5,5′-Me$_2$bipy**),[4] 2,9-dimethyl-1,10-phenanthroline (**2,9-Me$_2$phen**)[5] and 3-(4-methylpyridin-2′-yl)-5,6-dimethyl-1,2,4-triazine (**MepyMe$_2$t**)[6] (Figure 5.1) also form adducts with Pt–N7 bonds to two guanine ligands. From these adducts it is possible to gain insight into structure by using NMR methods, because the dynamic motion around the Pt–N7 bonds is decreased compared to adducts of active drugs. A Pt(II) complex having aromatic ligands can not only bind to nucleobases but can also intercalate into DNA.[7-14] Aromatic ring stacking between nucleobases and the intercalating molecule is considered to be one of the driving forces leading to binding; the extent of binding is expected to depend on the planarity of the complex.[11,15]

Because of the planar nature of bipyridine ligands, intercalation of Pt bipyridine complexes has been the focus of considerable interest.[9,11,16,17] The cation, $[(\mathbf{bipy})_2Pt]^{2+}$ (**bipy** = 2,2′-bipyridine), was reported to intercalate into DNA through only one of the **bipy** ligands.[9]

---

* Reproduced with permission from International Union of Crystallography: Maheshwari, V.; Carlone, M.; Fronczek, F. R.; Marzilli, L. G., "Ligand and Coordination-Plane Distortions in Pt(II) Complexes of Isomers of Dimethyl-2,2′-bipyridine," Acta Crystallographica, Section B: Structural Science, **2007**, *B63*, 603-611.

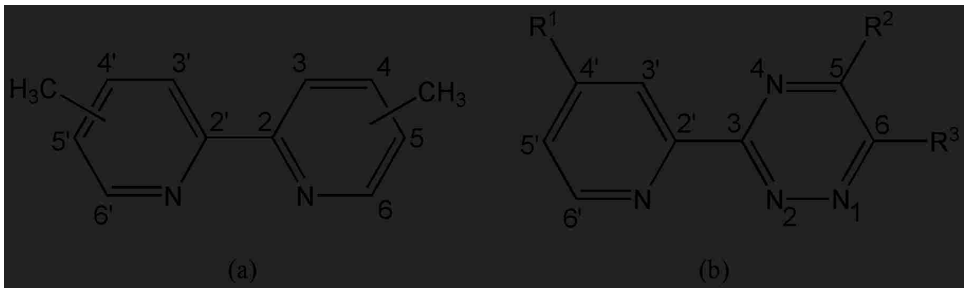

Figure 5.1 Stick representations and numbering schemes for coordinated (a) dimethyl-2,2′-bipyridine (**Me$_2$bipy**) and (b) 3-(4′-substituted pyridin-2′-yl)-5,6-disubstituted-1,2,4-triazine (**R^{1}pyR^{2}R^{3}t**) ligands.

For [(**R$_2$bipy**)M(**en**)](ClO$_4$)$_2$ (M = Pt or Pd, R = H or CH$_3$ and **en** = ethylenediamine) complexes, the binding constant value was found to be higher for R = CH$_3$ when M = Pd.[11] Previously we speculated that the antiviral activity of the [(**pyPh$_2$t**)$_2$Pt](BF$_4$)$_2$ (**pyPh$_2$t =** 3-(pyridin-2-yl)-5,6-diphenyl-1,2,4-triazine) complex[18] could arise from intercalation of the highly planar [*trans*-(**pyPh$_2$t**)$_2$Pt](BF$_4$)$_2$ complex into nucleic acids.[6]

Because the uncoordinated 2,2′-bipyridine ligand is essentially planar with an anti conformation,[19,20] the H3 to H3′ repulsion is avoided. However, except in rare, unusual cases, coordinated bipyridines have a syn conformation (Figure 5.1) leading to the possibility that the H3 to H3′ repulsion will explain distortions from planarity found in the coordinated ligand.[21] In this study we have synthesized and crystallized such dimethyl-2,2′-bipyridine platinum complexes as (**Me$_2$bipy**)PtCl$_2$ and [(**Me$_2$bipy**)$_2$Pt]X$_2$. Structural analysis of these **Me$_2$bipy** complexes has allowed us to evaluate the effect of having methyl groups at the 4,4′, 5,5′, and 6,6′ positions on distortions from planarity of these complexes. The extent of distortion of coordinated bipyridine ligands is characterized by parameters in Figure 5.2, defined by Hazell (2004). We also discuss the extent of distortions by using the following dihedral angles: θ_{di}, between the best planes through the two pyridyl rings in a bipyridine ligand; and θ_S, between the coordination plane (defined by the best plane through the four donor atoms surrounding the

metal) and the plane of the aromatic portion of the bipyridine ligand (defined by NCC′N′ atoms) (Figure 5.3).[22] The structural features and coordination parameters of **I**-**IV** are compared with those of published Pt/Pd complexes with bipyridine or 3-(pyridin-2′-yl)-5,6-disubstitued-1,2,4-triazine (**R^{1}pyR^{2}R^{3}t**) ligands (Figure 5.1). The latter have no H3 to H3′ repulsive interactions.[6]

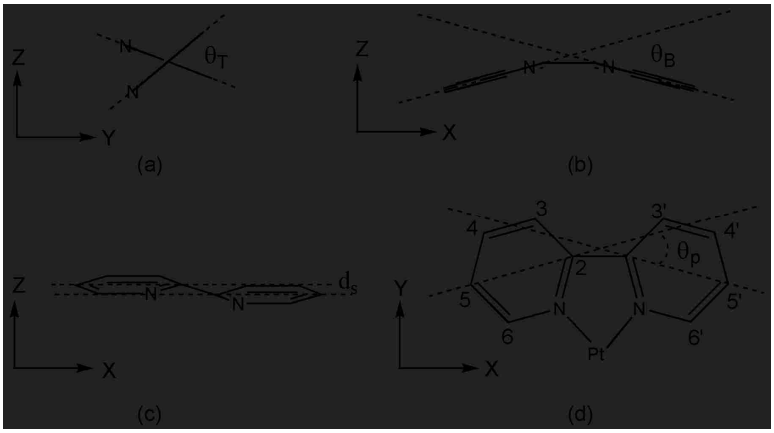

Figure 5.2 Distortions in bipyridine ligands: (a) twist angle (θ_T), (b) bowing (θ_B), (c) S-shaped distortion (d_s), (d) in-plane bending (θ_P). θ_T, θ_B and θ_P are the angles between the best straight lines ($ax + c = z$) through each pyridyl ring of the bipyridine ligand in the *yz*, *xz* and *xy* projections, respectively. d_s is the perpendicular distance between the best straight lines through each pyridyl ring in the *xz* projection.[21]

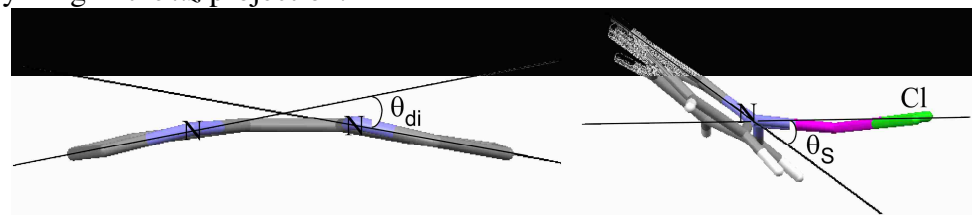

Figure 5.3 The dihedral angles: θ_{di} between the best planes through the two pyridyl rings in a bipyridine ligand; and θ_S, between the metal coordination plane and the plane containing the NCC′N′ atoms of the bipyridine ligand.

5.2 Experimental

5.2.1 Starting Materials

4,4′-Dimethyl-2,2′-bipyridine (**4,4′-Me$_2$bipy**), 5,5′-dimethyl-2,2′-bipyridine (**5,5′-Me$_2$bipy**), and 6,6′-dimethyl-2,2′-bipyridine (**6,6′-Me$_2$bipy**) were used as received (Aldrich). *cis*-Pt(Me$_2$SO)$_2$Cl$_2$ was prepared as described in the literature.[23]

5.2.2 NMR Measurements

^{1}H NMR spectra were recorded on a Bruker spectrometer operating at 400 MHz. TMS was used to reference the signals.

5.2.3 General Synthesis of Dichloro Bipyridine Platinum Complexes

Two methods were employed to obtain (**Me$_2$bipy**)PtCl$_2$ complexes. Method A involved heating a methanol solution (30 mL) of *cis*-Pt(Me$_2$SO)$_2$Cl$_2$ (0.101 g, 0.24 mmol) and the desired **Me$_2$bipy** ligand (0.044 g, 0.24 mmol) at 60 °C for 12 h. The yellow solid that precipitated was collected, washed with diethyl ether followed by chloroform, and dried in vacuo. This method produced high yields of powdered (**Me$_2$bipy**)PtCl$_2$ complexes that required no further purification. Method B, employed to obtain X-ray-quality crystals, involved mixing equal volumes of 10 mM solutions of *cis*-Pt(Me$_2$SO)$_2$Cl$_2$ and the ligand in acetonitrile (total volume ~2 mL) and allowing this mixture to stand at 25 °C. Yellow to orange colored crystals of the (**Me$_2$bipy**)PtCl$_2$ complex were collected after 24 h.

5.2.3.1 Dichloro(4,4′-dimethyl-2,2′-bipyridyl)platinum(II) ((4,4′-Me$_2$bipy)PtCl$_2$, I). Method A gave a yellow precipitate: yield, 73.5 mg (68%). Method B afforded thin yellow needles. $C_{12}H_{12}Cl_2N_2Pt$: yield, 1.7 mg (38%).^{1}H NMR (ppm) in DMSO-d_6: 9.27 (d, H6/6'), 8.44 (s, H3/3'), 7.66 (d, H5/5'), 2.48 (s, 4/4'-CH_3).

5.2.3.2 Dichloro(5,5′-dimethyl-2,2′-bipyridyl)platinum(II) ((5,5′-Me$_2$bipy)PtCl$_2$, II). Method A resulted in a yellow powder: yield, 75.8 mg (70%). Yellow plates were obtained by method B. $C_{12}H_{12}Cl_2N_2Pt$: yield, 1.9 mg (42%).^{1}H NMR (ppm) in DMSO-d_6: 9.28 (s, H6/6'), 8.42 (d, H3/3'), 8.23 (d, H4/4'), 2.49 (s, 5/5'-CH_3).

5.2.3.3 Dichloro(6,6′-dimethyl-2,2′-bipyridyl)platinum(II) ((6,6′-Me$_2$bipy)PtCl$_2$, III). The complex was obtained as a yellow solid by method A: yield, 48.6 mg (45%). Slow

evaporation of an acetonitrile solution of (**6,6'-Me$_2$bipy**)PtCl$_2$ (~10.0 mg in 1 mL) produced X-ray quality orange needle-shaped crystals. The Pt(**6,6′-Me$_2$bipy**)Cl$_2$ complex co-crystallized with a molecule of acetonitrile. $C_{12}H_{12}N_2Cl_2Pt{\bullet}C_2H_3N$: yield, 1.1 mg (25%).^{1}H NMR (ppm) in $(CD_3)_2CO$: 7.55 (d, H(5/5'), 8.15 (t, H4/4'), 8.22 (d, H3/3'), 2.99 (s, 6/6'-CH_3).

5.2.3.4 Bis(4,4'-dimethyl-2,2'-bipyridyl)platinum(II) Tetra-fluoroborate ([(4,4'-Me$_2$bipy)$_2$Pt](BF$_4$)$_2$, IV). *cis*-Pt(Me$_2$SO)$_2$Cl$_2$ (42.22 mg, 0.1 mmol) was added to a methanol solution of **4,4'-Me$_2$bipy** (73.69 mg, 0.4 mmol, 10 mL), and the resulting suspension became a solution when stirred at 60 °C for 24 h. The mixture was allowed to cool to room temperature. Any precipitate that formed was removed by filtration. Crystals were obtained from the clear filtrate by dropwise addition of a methanol solution of $NaBF_4$ (10 mM, ~500 μL) to 10 mL of filtrate. Thin, colorless, needle-shaped crystals of [(**4,4'-Me$_2$bipy**)$_2$Pt](BF$_4$)$_2$ co-crystallized with uncomplexed ligand on allowing the solution to stand undisturbed for 24 h. A set of upfield signals in the NMR spectrum of the crystals provided evidence of the free **4,4'-Me$_2$bipy** ligand. $C_{24}H_{24}N_4B_2F_8Pt{\bullet}C_{12}H_{12}N_2$: yield, 15 mg (21%). ^{1}H NMR (ppm) in DMSO-d_6: for [(**4,4'-Me$_2$bipy**)$_2$Pt](BF$_4$)$_2$: 8.85 (d, H6/6'), 8.66 (s, H3/3'), 7.82 (d, H5/5'), 2.63 (s, 4/4'-CH_3) and for **4,4'-Me$_2$bipy**: 8.49 (d, H6/6'), 8.19 (s, H3/3'), 7.24 (d, H5/5'), 2.38 (s, 4/4'-CH_3).

5.2.4 X-ray Data Collection and Structure Determination

Single crystals were placed in a cooled nitrogen gas stream at 105 or 110 K on a Nonius Kappa CCD diffractometer fitted with an Oxford Cryostream cooler with graphite-monochromated Mo Kα (0.71073 Å) radiation. Data reduction included absorption corrections by the multi-scan method, using HKL Denzo and Scalepack.[24] All X-ray structures were determined by direct methods and difference Fourier techniques. SIR97[25] and SHELXL97[26] programs were used to solve and refine the crystal structures.

All H atoms were visible in difference maps, but were placed in idealized positions, with C–H = 0.95-1.00 Å, depending on atom type. A torsional parameter was refined for each methyl group. Displacement parameters for H were assigned as $U_{iso} = 1.2U_{eq}$ of the attached atom (1.5 for methyl groups). All non-hydrogen atoms were refined anisotropically. For all structures, maximum residual densities were located near the Pt positions.

5.3 Results and Discussion

Structures of **I**-**IV** are reported here (Figure 5.4). Crystal data and structure refinement parameters are listed in Table 5.1.

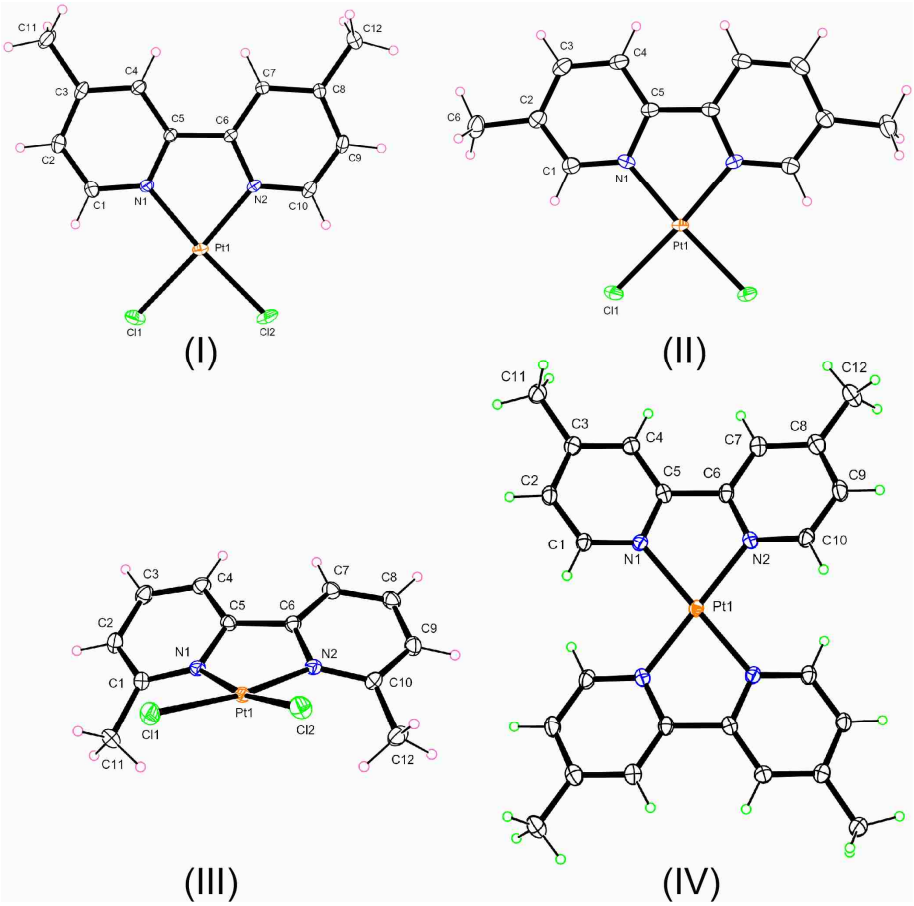

Figure 5.4 ORTEP plots of (**4,4′-Me$_2$bipy**)PtCl$_2$ (**I**); (**5,5′-Me$_2$bipy**)PtCl$_2$ (**II**); (**6,6′-Me$_2$bipy**)PtCl$_2$ (**III**); and [(**4,4′-Me$_2$bipy**)$_2$Pt](BF$_4$)$_2$ (**IV**). The solvent molecule in **III** and the uncomplexed **4,4′-Me$_2$bipy** ligand and the counter ion (BF$_4$) in **IV** are not shown for clarity. Thermal ellipsoids are drawn with 50% probability.

Table 5.1 Crystal Data and Experimental Details for (**4,4′-Me$_2$bipy**)PtCl$_2$ (**I**), (**5,5′-Me$_2$bipy**)PtCl$_2$ (**II**), (**6,6′-Me$_2$bipy**)PtCl$_2$ (**III**), and [(**4,4′-Me$_2$bipy**)$_2$Pt](BF$_4$)$_2$ (**IV**).

	I	**II**	**III**	**IV**
Crystal data				
Chemical formula	$C_{12}H_{12}Cl_2N_2Pt$	$C_{12}H_{12}Cl_2N_2Pt$	$C_{12}H_{12}Cl_2N_2Pt$• C_2H_3N	$[Pt(C_{12}H_{12}N_2)_2](BF_4)_2$• $C_{12}H_{12}N_2$
M_r	450.23	450.23	491.28	921.42
Cell setting, space group	Monoclinic, $P2_1/n$	Monoclinic, $C2/c$	Triclinic, $P\bar{1}$	Triclinic, $P\bar{1}$
Temperature (K)	110	105	105	110
a, b, c (Å)	6.7739 (10), 10.755 (2), 17.312 (3)	13.162 (3), 9.088 (2), 12.125 (3)	8.1049 (10), 8.7028 (10), 12.005 (2)	7.3395 (10), 10.580 (2), 12.093 (2)
α, β, γ (°)	90, 93.80 (2), 90	90, 121.110 (11), 90	73.863 (5), 73.919 (5), 77.132 (6)	70.602 (9), 87.384 (12), 79.978 (12)
V (Å^3)	1258.5 (4)	1241.8 (5)	771.78 (18)	872.1 (2)
Z	4	4	2	1
D_x (Mg m^{-3})	2.376	2.408	2.114	1.754
Radiation type	Mo $K\alpha$	Mo $K\alpha$	Mo $K\alpha$	Mo $K\alpha$
μ (mm^{-1})	11.55	11.71	9.43	4.10
Crystal form, colour	Needle, yellow	Plate, yellow	Needle, orange	Needle, colorless
Crystal size (mm)	0.22 × 0.10 × 0.10	0.11 × 0.10 × 0.04	0.15 × 0.05 × 0.05	0.15 × 0.05 × 0.03
Data collection				
Diffractometer	KappaCCD (with Oxford Cryostream)	KappaCCD (with Oxford Cryostream)	KappaCCD (with Oxford Cryostream)	KappaCCD (with Oxford Cryostream)
Data collection method	ω scans with κ offsets	ω scans with κ offsets	ω scans with κ offsets	ω scans with κ offsets
Absorption correction	Multi-scan (based on symmetry-related measurements)	Multi-scan (based on symmetry-related measurements)	Multi-scan (based on symmetry-related measurements)	Multi-scan (based on symmetry-related measurements)
T_{min}	0.150	0.341	0.380	0.578
T_{max}	0.315	0.626	0.624	0.887
No. of measured, independent and observed reflections	16686, 7208, 5830	15159, 2482, 2283	34009, 6114, 5654	19893, 6773, 6435
Criterion for observed reflections	$I > 2\sigma(I)$	$I > 2\sigma(I)$	$I > 2\sigma(I)$	$I > 2\sigma(I)$

(table 5.1 continued)

R_{int}	0.039	0.025	0.022	0.045
θ_{max} (°)	40.7	33.7	33.7	33.7
Refinement				
Refinement on	F^2	F^2	F^2	F^2
$R[F^2 > 2\sigma(F^2)]$, $wR(F^2)$, S	0.037, 0.085, 1.04	0.026, 0.056, 1.06	0.023, 0.045, 1.06	0.043, 0.082, 1.06
No. of relections	7208	2482	6114	6773
No. of parameters	157	80	193	245
H-atom treatment	Constrained to parent site	Constrained to parent site	Constrained to parent site	Constrained to parent site
Weighting scheme	$w = 1/[\sigma^2(F_o^2) + (0.0235P)^2 + 6.6393P]$ where $P = (F_o^2 + 2F_c^2)/3$	$w = 1/[\sigma^2(F_o^2) + (0.0176P)^2 + 3.5799P]$ where $P = (F_o^2 + 2F_c^2)/3$	$w = 1/[\sigma^2(F_o^2) + (0.0062P)^2 + 1.4431P]$ where $P = (F_o^2 + 2F_c^2)/3$	$w = 1/[\sigma^2(F_o^2) + (0.0253P)^2 + 1.6231P]$ where $P = (F_o^2 + 2F_c^2)/3$
$(\Delta/\sigma)_{max}$	0.001	0.001	0.002	<0.0001
$\Delta\rho_{max}$, $\Delta\rho_{min}$ (e Å^{-3})	2.84, –3.50	1.59, –2.48	1.23, –2.26	1.42, –1.87
Extinction method	SHELXL	SHELXL	SHELXL	SHELXL
Extinction coefficient	0.00231 (17)	0.00066 (8)	0.0073 (2)	0.0013 (4)

Computer programs: *COLLECT* ;[30] *HKL Scalepack;*[24] *HKL Denzo and Scalepack*;[24] *SIR97*;[25] *SIR97;*[25] *SHELXL-97*;[26] *ORTEP-3 for Windows.*[31]

The X-ray structures of (**6,6′-Me$_2$bipy**)$PdCl_2$ and (**6-Mebipy**)$PdCl_2$ complexes were reported at room temperature by Newkome *et al.* (1982). The deformation calculations were done using X-ray data at T = 100 K.[27] The structure of **II** at room temperature was first reported by Miskowski (1993) with Z′ = 1 in space group *Cc*. Marsh (1997), revisiting the perils of *Cc*, pointed out that the structure can be better described with the molecule lying on a twofold axis in *C*2/*c*.[29] Our refinement using low-temperature data confirms Marsh's assessment. In the structure of **IV,** both the Pt complex and uncomplexed ligand lie on inversion centers. The acetonitrile molecule in **III** is disordered into two orientations with populations 0.720(5):0.280(5), with a common methyl site.

5.3.1 Out-of-Plane Distortions

5.3.1.1 Dichloro Pt(II)/Pd(II) Complexes. Hazell noted that bipyridines are not planar in metal complexes that have M–N distances within the typical range of ~2.0 to 2.2 Å.[32] The out-of-plane distortions that these complexes display can be described in terms of bowing, twisting, and S-shaped deformation (Figure 5.2).[21] Hazell examined distortions for 551 metal complexes containing 2,2′-bipyridine (**bipy**) or substituted 2,2′-bipyridines from the Cambridge Structural Database[33] and calculated that the twist angle (θ_T) ranges from 0.0 to 26.1° and the bow angle (θ_B) ranges from 0.0 to 19.8°.[21]

Table 5.2 Ligand deformation in platinum and palladium complexes.[a]

Compound	Twist angle (θ_T)	Bow angle (θ_B)	S-shaped distortion (d_s)	In-plane distortion (θ_P)	M–N distance (Å)	Dihedral angles (θ_{di})	Cl–M–Cl
(**4,4′-Me$_2$bipy**)PtCl$_2$ (**I**)[b]	2.4	0.1	0.002	5.9	2.023(3) 2.027(3)	2.8(6)	89.49(4)
(**5,5′-Me$_2$bipy**)PtCl$_2$ (**II**)[b]	5.5	0.0	0.075	8.9	2.017(3)	5.56(6)	89.76(5)
(**6,6′-Me$_2$bipy**)PtCl$_2$ (**III**)[b]	6.1	19.2	0.000	10.9	2.028(2) 2.030(2)	20.18(14)	86.25(2)
(**bipy**)PtCl$_2$[34]	0.0	0.0	0.000	8.8	2.009(6)	0.0	89.1(1)
(**bipy**)PdCl$_2$[35]	2.3	1.9	0.009	8.9	2.03(1)	3.0	89.9(1)
(**6,6′-Me$_2$bipy**)PdCl$_2$[c]	1.2	15.7	0.039	10.0	2.059(1) 2.043(1)	15.7(2)	86.42(2)
(**6-Mebipy**)PdCl$_2$[c]	5.6	13.3	0.006	9.3	2.055(1) 2.021(1)	14.5(1)	88.74(1)
(**pyMe$_2$t**)PtCl$_2$[6]	2.4	1.9	0.003	8.9	2.020(3) 2.001(3)	2.9	89.13(3)
(**pyPht**)PtCl$_2$[6]	2.1	9.3	0.008	8.1	2.011(11) 1.996(11)	9.4	90.12(13)
(**pyPh$_2$t**)PtCl$_2$[6]	6.2	2.2	0.032	8.4	2.027(3) 1.996(3)	6.6	89.16(3)
[(**4,4′-Me$_2$bipy**)$_2$Pt](BF$_4$)$_2$ (**IV**)[b]	4.6	24.2	0.005	8.7	2.032(3)	24.8(2)	
[(**pyPh$_2$t**)$_2$Pt](BF$_4$)$_2$[6]	4.1	0.2	0.031	8.5	2.050(3)	4.1	

(table 5.2 continued)

					2.019(3)	
[(**bipy**)$_2$Pt](NO$_3$)$_2$[32]	2.1	1.2	0.073	7.5	2.025(4)	2.3
	10.4	0.4	0.006	7.4	2.028(5)	11.9
[(**bipy**)$_2$Pd](NO$_3$)$_2$[39]	1.8	0.2	0.098	7.9	2.030(1)	1.8
					2.030(1)	
	7.7	0.3	0.089	8.3	2.028(1)	7.7
					2.050(1)	
[(**bipy**)$_2$Pd](BF$_4$)$_2$[40]	8.8	0.2	0.089	8.9	2.031(4)	8.7
					2.029(3)	
	7.9	2.1	0.104	8.5	2.031(4)	8.1
					2.030(3)	
[(**bipy**)$_2$Pd](PF$_6$)$_2$[22]	0.1	19.0	0.006	8.8	2.039(2)	19.1
					2.032(2)	

[a] Angles are in degrees; d_s and the M–N distances are in Å. θ_T, θ_B, θ_P, θ_{di} and d_s values were calculated by using a program in FORTRAN provided by Dr. Alan Hazell. θ_{di} for structures reported in this work were calculated using SHELXL. [b] This work. [c] Newkome *et al.* (1982). Based on new refinements using 100 K data.[27]

No substantial twisting or bowing distortions were observed for the unsubstituted **bipy** ligand in the (**bipy**)PtCl$_2$[34] and (**bipy**)PdCl$_2$[35] complexes (Table 5.2), although the small distortions that do occur may be the result of packing forces.[36-38] These complexes do show typical θ_P (see below) values, but θ_{di} values are small or zero (Table 5.2).

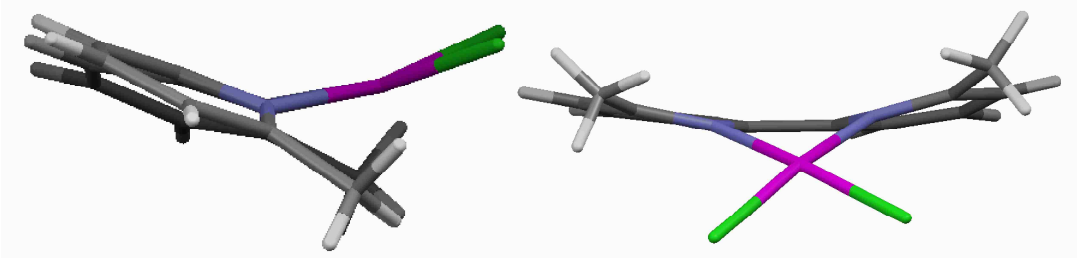

Figure 5.5 Side (left) and front (right) view of (**6,6′-Me$_2$bipy**)PtCl$_2$ (**III**).

Among the dichloro Pt complexes in Table 5.2, (**6,6′-Me$_2$bipy**)PtCl$_2$ (**III**) is the most distorted, with an exceptionally large bowing angle (θ_B = 19.2°) and a comparatively large twist angle (θ_T = 6.1°). These distortions can be attributed to steric repulsion resulting from the close

proximity of the 6,6′ methyl groups and the cis chlorides. The θ_S value shows that the aromatic portion of **6,6′-Me$_2$bipy** in **III** is out of the Pt coordination plane by 36.73(11)° (Figure 5.5). Similar out-of-plane distortions characterized by θ_S of 38.84(9)° for (**6,6′-Me$_2$bipy**)$PdCl_2$ and 27.44(7)° for (**6-Mebipy**)$PdCl_2$ (**6-Mebipy** = 6-methyl-2,2′-bipyridine) were observed. For all the other dichloro complexes in Table 5.2, the θ_S values are small, ranging from 0 to 8°. No S-shaped distortion (Figure 5.2) is observed for **III** (Table 5.2). The S-shaped distortions characterized by the d_s values and calculated for all the dichloro metal complexes listed in Table 5.2, are within the 0-0.127 Å range reported by Hazell (2004).

In contrast to the Pt/Pd dichloro complexes of **6,6′-Me$_2$bipy** and **6-Mebipy**, for all the other Pt/Pd dichloro bipyridine complexes studied here and for those in Table 5.2, the distortion is characterized more by twisting than bowing (Table 5.2). The two pyridyl rings of the ligand in (**4,4′-Me$_2$bipy**)$PtCl_2$ (**I**) and (**5,5′-Me$_2$bipy**)$PtCl_2$ (**II**) were only slightly twisted with respect to each other. The θ_S values for **I** (3.9(5)°) and **II** (0.6(2)°) suggest that the aromatic portion of the ligands is only slightly out of the Pt coordination plane. The weakness of the interactions between the H6,6′ hydrogens and the cis chlorides may explain the relatively undistorted structures of **I**, **II**, (**bipy**)$PtCl_2$ and (**bipy**)$PdCl_2$. A comparison of these dichloro bipyridine complexes with (**R^{1}pyR^{2}R^{3}t**)$PtCl_2$ complexes is revealing. The twisting and bowing are smaller in (**pyMe$_2$t**)$PtCl_2$ (**pyMe$_2$t** = 3-(pyridin-2′-yl)-5,6-dimethyl-1,2,4-triazine) and generally similar for those in the dichloro bipyridine Pt/Pd complexes. In (**pyPh$_2$t**)$PtCl_2$ (**pyPh$_2$t** = 3-(pyridin-2′-yl)-5,6-diphenyl-1,2,4-triazine), the pyridyl and the triazine rings are more twisted (θ_T = 6.2°), whereas in (**pyPht**)$PtCl_2$ (**pyPht** = 3-(pyridin-2′-yl)-5-phenyl-1,2,4-triazine), the pyridyl and the triazine rings are more bowed (θ_B = 9.3°). However, the interactions which can occur in the (**R^{1}pyR^{2}R^{3}t**)$PtCl_2$ complexes should be similar. Thus, the larger distortions in the complexes

with phenyl substituents are undoubtedly due to solid state effects. These effects are apparently less important for ligands with the smaller methyl substituents.

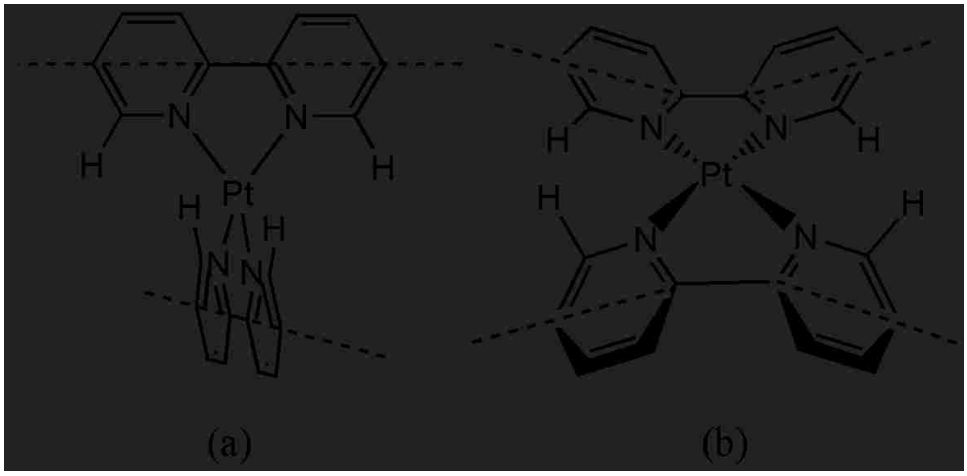

Figure 5.6 (a) Canting, and (b) bow-incline deformations in [(**bipy**)$_2$Pt]X_2 complexes.

5.3.1.2 Bis Chelate Pt/Pd Complexes. For bis bipyridine metal complexes, the hydrogen atoms on the 6,6′ carbons of opposite ligands are expected to have a non-bonded internuclear separation less than the sum of the van der Waals radii (2.4 Å).[41] Consequently, to relieve this steric strain, the molecule undergoes either a tetrahedral deformation at the metal, resulting in canting of the ligands relative to each other, or bowing of the two pyridyl rings of the bipyridine ligand (Figure 5.6).[6,42] The bis bipyridine Pt/Pd complexes are more distorted than the dichloro bipyridine complexes (Table 5.2). However, the d_s values for the S-shaped distortion (Figure 5.2) calculated for all the bis chelate metal complexes in Table 5.2 were comparable to those for the dichloro metal complexes. The θ_T and θ_B values calculated for all the metal complexes in Table 5.2, except θ_B in [(**4,4′-Me$_2$bipy**)$_2$Pt](BF$_4$)$_2$ (**IV**), lie within the range calculated by Hazell (2004). The strain induced by the close approach of the H6 hydrogens on the opposing ligands in **IV** is relieved partly by adopting an incline conformation and partly by bowing of the two pyridyl rings of the **4,4′-Me$_2$bipy** ligand. The incline conformation in bis chelate complexes is

characterized by the dihedral angle (θ_S), between the metal coordination plane and the NCC′N′ ligand plane (18.80(13)°). Figure 5.7 shows that the two pyridyl rings of **4,4′-Me$_2$bipy** ligands in **IV** are bowed (θ_B = 24.2°) away from each other. This type of bow-incline distortion has been described previously as a bow-step distortion.[22] A slight twisting (θ_T = 4.6°) of the two pyridyl rings in **4,4′-Me$_2$bipy** in **IV** is also seen.

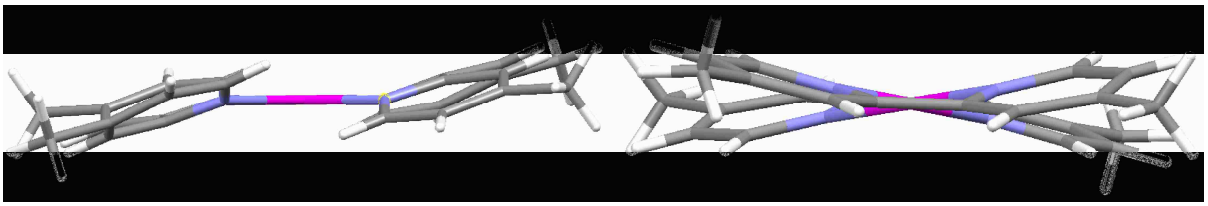

Figure 5.7 Side (left) and front (right) view of [(**4,4′-Me$_2$bipy**)$_2$Pt](BF$_4$)$_2$ (**IV**).

An alternative distortion to relieve steric stress is canting (Figure 5.6). The canting angle (θ_C) is defined by the dihedral angle between the best planes through the two bipyridine ligands. In contrast to the bow-incline distortion in **IV**, Pt and Pd complexes of the unsubstituted bipyridine distort more frequently by canting. In [(**bipy**)$_2$Pt](NO$_3$)$_2$,[32] the two **bipy** ligands are canted relative to one another (θ_C = 34.47°). In order to further relieve the repulsion due to the interligand 6,6′-hydrogens, each **bipy** ligand is also twisted, with one **bipy** twisted (θ_T = 10.4°) more than the other (θ_T = 2.1°). A very similar structure was reported for [(**bipy**)$_2$Pd](NO$_3$)$_2$[39] (Table 5.2). In [(**bipy**)$_2$Pd](BF$_4$)$_2$[40] the two **bipy** ligands are canted (θ_C = 36.45°) and also twisted (θ_T = 8.8° and 7.9°). In contrast, a bow-incline distortion (θ_B = 19.0°, θ_S = 21.6°) similar to that in **IV** was found for the PF$_6$ salt, [(**bipy**)$_2$Pd](PF$_6$)$_2$.[40] However, unlike **IV**, the **bipy** ligands in [(**bipy**)$_2$Pd](PF$_6$)$_2$ are not twisted.

In contrast to [(**4,4′-Me$_2$bipy**)$_2$Pt](BF$_4$)$_2$, the geometry of [*trans*-(**pyPh$_2$t**)$_2$Pt](BF$_4$)$_2$ is planar and symmetrical because of the trans relationship of the coordinated **pyPh$_2$t** ligands.[6] The complex, [*trans*-(**pyPh$_2$t**)$_2$Pt](BF$_4$)$_2$, has no apparent bowing or canting. The attractive

interaction between the lone pairs on the non-bonded triazine N of one ligand and the pyridyl H6′ of the opposing ligand is probably responsible for the planarity of [*trans*-(**pyPh$_2$t**)$_2$Pt](BF$_4$)$_2$. The interactions between the juxtaposed groups on the two rings ortho to the bridging carbons and on the periphery of the bidentate ligand are favorable for **R^{1}pyR^{2}R^{3}t** ligands but unfavorable for 2,2′-bipyridine-type ligands. For all the bis bipyridine metal complexes discussed above, the interligand hydrogen-hydrogen separations are less than the sum of the van der Waals radii, indicating that unfavorable repulsions lead to the canting and bow-incline distortions. These distortions must be similar in energy with solid-state effects determining which distortion occurs for a particular cation/anion combination.

5.3.2 In-Plane Bending and Coordination-Plane Distortion of Dichloro Pt(II)/Pd(II) Complexes

5.3.2.1 In-Plane Bending. The in-plane bending for all the metal complexes studied here is well within the range (θ_P = 2.9-12.5°) reported by Hazell (2004). As mentioned, the repulsive interaction of the H3 to H3′ in the metal complexes bearing bipyridine ligands was postulated to cause an in-plane bending.[32] However, for all the dichloro bipyridine Pt/Pd complexes and (**R^{1}pyR^{2}R^{3}t**)PtCl$_2$ complexes in Table 5.2, the M–N distances are comparable. It is noteworthy that in-plane bending in Pt complexes of **R^{1}pyR^{2}R^{3}t** ligands, unlike bipyridines, cannot be increased by H3-H3′ repulsions because the pyridyl H3 is near the lone-pair-bearing triazine N; this juxtaposition should create a slight favorable attractive interaction. Therefore, any stress resulting from H3 to H3′ repulsion in bipyridine metal complexes does not produce any substantial effect on the in-plane bending. Rather, coordination of these bidentate ligands to the metal may require in-plane bending of the ligands in order to allow optimal overlap of the N and

metal orbitals. This interpretation is consistent with the report that the θ_P values decrease with increasing M–N distances.[21]

The Cl–Pt–Cl bond angle is significantly smaller in **III** and (**6,6′-Me$_2$bipy**)$PdCl_2$ than in all other dichloro bipyridine metal complexes in Table 5.2. The Cl–M–Cl bond angle increases in the order: **III** ≈ (**6,6′-Me$_2$bipy**)$PdCl_2$ < (**6-Mebipy**)$PdCl_2$ < (**pyMe$_2$t**)$PtCl_2$ ≈ (**pyPh$_2$t**)$PtCl_2$ < **I** ≈ **II** ≈ (**bipy**)$PtCl_2$ ≈ (**bipy**)$PdCl_2$ (Table 5.2). Complexes with larger θ_P values are observed to have generally smaller Cl–Pt–Cl bond angles (Table 5.2).

For **III** and (**6,6′-Me$_2$bipy**)$PdCl_2$, the θ_P values are comparatively larger and the Cl–M–Cl bond angles are smaller than those for all other dichloro metal complexes in Table 5.2. A large in-plane bending will cause the 6,6′ methyl groups to be closer to the Cl's. The internuclear distances between the C's of the methyl groups and the cis chlorides ($C_{Me}\cdots Cl$) are 3.138 and 3.186 Å for **III** and 3.151 and 3.178 Å for (**6,6′-Me$_2$bipy**)$PdCl_2$. These values are even smaller than the sum of the minimum value calculated for the van der Waals radii of the methyl group[43] and the Cl atom (3.461 Å), as well as for the C and the Cl atoms (3.45 Å).[41] Thus, the repulsions between the 6,6′ methyl groups and the cis chlorides push the Cl atoms toward one another, causing the Cl–Pt–Cl bond angle to be smaller than that for the other dichloro metal complexes in Table 5.2. The Cl to Cl internuclear distance (3.148 Å) in **III** and (**6,6′-Me$_2$bipy**)$PdCl_2$ is smaller than the sum of the van der Waals radii (3.5 Å), resulting in repulsive interactions.

5.3.2.2 Coordination-Plane Distortion. Cl-to-Cl and Cl-to-methyl group repulsions can distort the coordination plane (Figure 5.8). This distortion is best analyzed using the dihedral angle (α) between the N,M,N′ plane and Cl,M,Cl plane. The α values for **III** and (**6,6′-Me$_2$bipy**)$PdCl_2$ are 11.5(3)° and 14.3(1)°, whereas for the less distorted dichloro metal complexes listed in Table 5.1, the α values range from 0° to 4.3°.

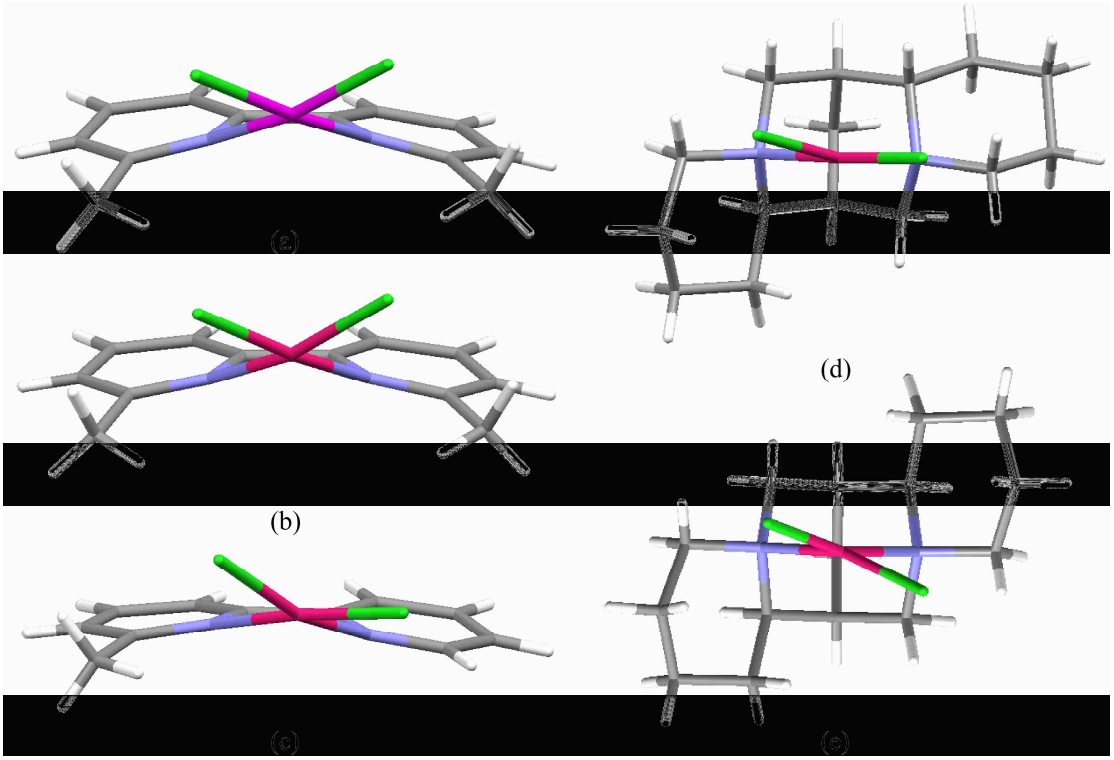

Figure 5.8 Stick representation of (a) (**6,6′-Me$_2$bipy**)PtCl$_2$, (b) (**6,6′-Me$_2$bipy**)PdCl$_2$, (c) (**6-Mebipy**)PdCl$_2$, (d) ((**–**)**-sparteine**)PdCl$_2$ and (e) ((**–**)**-α-isosparteine**)PdCl$_2$.

In order to understand better the steric effect of the group on the carbon adjacent to the coordinated N on the Cl–M–Cl grouping, we compared the complexes studied here with ((**–**)**-α-isosparteine**)PdCl$_2$ and ((**–**)**-sparteine**)PdCl$_2$.[44] For the symmetrical ((**–**)**-α-isosparteine**)PdCl$_2$, the Cl–M–Cl angle (86.205(15)°) and the internuclear separations found between the C's adjacent to the coordinated N's and the cis Cl's (3.130 and 3.168 Å) are comparable to those in **III** and in (**6,6′-Me$_2$bipy**)PdCl$_2$. Because of the bulk near the coordinated N's of ((**–**)**-α-isosparteine**)PdCl$_2$, the Cl atoms are largely pushed out of the N,Pd,N′ plane (α = 22.1°) and are 3.172 Å apart. Because of the less accommodating geometry of the **(–)-sparteine** than the **(–)-α-isosparteine** or bipyridine-type ligands, ((**–**)**-sparteine**)PdCl$_2$ has an even smaller Cl–Pd–Cl angle (83.09(3)°) and shorter C···Cl (3.034 and 3.072 Å) and Cl···Cl (3.071 Å) distances. One of the Cl atoms in the unsymmetrical ((**–**)**-sparteine**)PdCl$_2$ complex is displaced from the N,Pd,N′

plane, while the other Cl is located close to this plane (α = 9.9°) (Figure 5.8). For the unsymmetrical (**6-Mebipy**)$PdCl_2$ complex, the Cl cis to the 6-methyl group is displaced from the N,Pd,N′ plane, but the Cl cis to the H6' is closer to the plane (Figure 5.8). Both the Cl–Pd–Cl angle and α (14.30(7)°) are larger than those for ((**–**)**-sparteine**)$PdCl_2$. Thus, dichloro complexes with ligands accommodating distortions characterized by larger values of α tend to have a less distorted Cl–M–Cl grouping.

5.4 Conclusions

The platinum complexes characterized here have typical M–N distances of ~2.0 Å, and thus can be viewed as being representative of pseudo square-planar complexes of bipyridine-type ligands. When combined with literature data, the new results allow conclusions to be reached about the relative influence on structural distortions of intramolecular interactions vs. solid-state effects.

The distortions in (**6,6'-Me_2bipy**)$PtCl_2$ (**III**) are best appreciated by comparison to its relatively undistorted isomers, **I** and **II**, which have 6,6′ hydrogens. The Cl–M–Cl grouping in the latter is normal, indicating good overlap of the metal and chloride bonding orbitals, a situation allowed by the weakness of the repulsive 6,6′-C to Cl interactions for the distances of ~3.1 Å. Also, attractive interactions between the 6,6′ hydrogens and the cis chlorides may exist. However, the presence of 6,6′ methyl groups in the **6,6'-Me_2bipy** ligand of **III** and its Pd analogue gives rise to a highly distorted structure, characterized by large bowing and an incline of the aromatic ring relative to the coordination plane. This bow-incline distortion creates ~3.1 Å C to Cl distances and allows the chlorides to remain close to the coordination plane in these Pt and Pd complexes. When the bulky ligand is not aromatic, the complex must either distort the coordination plane (e.g. ((**–**)**-α-isosparteine**)$PdCl_2$) or adopt an acute Cl-Pd-Cl angle (e.g. ((**–**)**-**

sparteine)$PdCl_2$) to maintain the ~3.1 Å C to Cl distances. The coordination plane of ((**–**)-**sparteine**)$PdCl_2$ is less distorted and has an α value similar to those in **III** and also in the structurally similar **2,9-Me$_2$phen**[45] and Pd analogues of **III**. Thus, distortions found in dichloro complexes are quite diverse but are not dependent on whether the metal is Pt or Pd. In contrast, as discussed next, we can conclude that the highly distorted dichloro compounds have some features that can be related to those found for bis bipyridine-type complexes.

In bis bipyridine complexes, the strain induced by the close proximity of the H's on the C6 carbons of the opposing ligands is relieved either by a bow-incline distortion or by canting of the two bipyridine ligands. Of the five relevant structures in Table 5.2, three have canting and two have bow-incline distortion. The structure of **IV** adds a new bipyridine ligand to the existing bis bipyridine structures and also demonstrates that the bow-incline distortion can occur in a Pt complex. Consequently, there are now examples of both types of distortions for both Pt and Pd. It is reasonable to conclude that these two types of distortions are similar in energy and that minor solid-state effects determine which distortion type is observed. In contrast to **IV,** [*trans*-(**pyPh$_2$t**)$_2$Pt]$(BF_4)_2$ has a relatively planar structure, which can be attributed to the favorable juxtaposition of the pyridyl H6′ proton and the triazine lone pair of electrons, adding support to the conclusion that the distortions in bis bipyridine complexes arise from interligand repulsions involving 6,6' hydrogens.

Average values of θ_P for bipyridine complexes **I** to **IV** and for the four pyridyl triazine complexes in Table 5.2 are very similar. Thus, while the present study indicates that interligand repulsions involving H6 and H6' influence structure, sometimes dramatically, H3 to H3' intraligand repulsions have no evident effect on structure.

5.5 References

1. Rosenberg, B.; Van Camp, L.; Krigas, T. *Nature (London)* **1965**, *205*, 698.

2. Blommaert, F. A.; Van Dijk-Knijnenburg, H. C. M.; Dijt, F. J.; Den Engelse, L.; Baan, R. A.; Berends, F.; Fichtinger-Schepman, A. M. J. *Biochemistry* **1995**, *34*, 8474-8480.

3. Beljanski, V.; Villanueva, J. M.; Doetsch, P. W.; Natile, G.; Marzilli, L. G. *J. Am. Chem. Soc.* **2005**, *127*, 15833-15842.

4. Bhattacharyya, D.; Marzilli, P. A.; Marzilli, L. G. *Inorg. Chem.* **2005**, *44*, 7644-7651.

5. Margiotta, N.; Papadia, P.; Fanizzi, F. P.; Natile, G. *Eur. J. Inorg. Chem.* **2003**, 1136-1144.

6. Maheshwari, V.; Bhattacharyya, B.; Fronczek, F. R.; Marzilli, P. A.; Marzilli, L. G. *Inorg. Chem.* **2006**, *45*, 7182-7190.

7. Sundquist, W. I.; Lippard, S. J. *Coord. Chem. Rev.* **1990**, *100*, 293-322.

8. Lippard, S. J.; Bond, P. J.; Wu, K. C.; Bauer, W. R. *Science (Washington, D. C.)* **1976**, *194*, 726-728.

9. Cusumano, M.; Di Pietro, M. L.; Giannetto, A. *Inorg. Chem.* **1999**, *38*, 1754-1758.

10. Wang, A. H. J.; Nathans, J.; Van der Marel, G.; Van Boom, J. H.; Rich, A. *Nature (London)* **1978**, *276*, 471-474.

11. Cusumano, M.; Giannetto, A. *J. Inorg. Biochem.* **1997**, *65*, 137-144.

12. Brodie, C. R.; Collins, J. G.; Aldrich-Wright, J. R. *Dalton Trans.* **2004**, *8*, 1145-1152.

13. Collins, J. G.; Rixon, R. M.; Aldrich-Wright, J. R. *Inorg. Chem.* **2000**, *39*, 4377-4379.

14. Jaramillo, D.; Buck, D. P.; Collins, J. G.; Fenton, R. R.; Stootman, F. H.; Wheate, N. J.; Aldrich-Wright, J. R. *Eur. J. Inorg. Chem.* **2006**, 839-849.

15. Wilson, W. D.; Jones, R. L. In *Intercalation Chemistry*; Wittingham, N. S., Jacobson, A. J., Eds.; Academic Press: New York, 1982, pp 445-501.

16. Cusumano, M.; Di Pietro, M. L.; Giannetto, A.; Vainiglia, P. A. *J. Inorg. Biochem.* **2005**, *99*, 560-565.

17. Heng-Qian, L.; Shei-Ming, P.; Chi Ming, C. *J. Chem. Soc., Chem. Commun.* **1995**, *5*, 509-510.

18. Vzorov, A. N.; Bhattacharyya, D.; Marzilli, L. G.; Compans, R. W. *Antiviral Research* **2005**, *65*, 57-67.

19. Merritt, L. L.; Schroeder, E. D. *Acta Cryst.* **1956**, *9*, 801-804.

20. Kuhn, F. E.; Groarke, M.; Bencze, E.; Herdtweck, E.; Prazares, A.; Santos, A. M.; Calhorda, M. J.; Ramao, C. C.; Goncalves, I. S.; Lopes, A. D.; Pillinger, M. *Chem. Eur. J.* **2002**, *8*, 2370-2383.

21. Hazell, A. *Polyhedron* **2004**, *23*, 2081-2083.

22. Geremia, S.; Randaccio, L.; Mestroni, G.; Milani, B. *J. Chem. Soc., Dalton Trans.* **1992**, 2117-2118.

23. Price, J. H.; Williamson, A. N.; Schramm, R. F.; Wayland, B. B. *Inorg. Chem.* **1972**, *11*, 1280-1284.

24. Otwinowski, Z.; Minor, W. *Macromolecular Crystallography, part A*; New York Academic Press: New York, 1997; Vol. 276, pp 307-326.

25. Altomare, A.; Burla, M. C.; Camalli, M. C.; Cascarano, G. L.; Giacovazzo, G. L.; Guagliardi, A.; Moliterni, A. G. G.; Polidori, G.; Spagna, R. *J. Appl. Cryst.* **1999**, *32*, 115-119.

26. Sheldrick, G. M. *SHELXL-97, SHELXL97*; University of Gottingen: Germany, **1997**

27. Fronczek, F. R. *Private Communications to Cambridge Structural Database* **2007**, CCDC 643925 & CCDC 643926.

28. Miskowski, V. M.; Houliding, V. H.; Che, C., -M.; Wang, Y. *Inorg. Chem.* **1993**, *32*, 2518-2524.

29. Marsh, R. E. *Acta Cryst.* **1997**, *B53*, 317-322.

30. Nonius *Nonius 2000. COLLECT,* The Netherlands, **2000**

31. Farrugia, L. J. *J. Appl. Crystallogr.* **1997**, *30*, 565.

32. Hazell, A.; Simenson, O.; Wernberg, O. *Acta Cryst.* **1986**, *C42*, 1707-1711.

33. Allen, F. H. *Acta Crystallogr., Sect. B: Struct. Sci.* **2002**, *58*, 380-388.

34. Connick, W. B.; Henling, L. M.; Marsh, R. E.; Gray, H. B. *Inorg. Chem.* **1996**, *35*, 6261-6265.

35. Canty, A. J.; Skelton, B. W.; Traill, P. R.; White, A. H. *Aust. J. Chem.* **1992**, *45*, 417-422.

36. Camus, A.; Marsich, M.; Nardin, G. *Acta Cryst.* **1977**, *33*, 1669-1673.

37. Arora, S. K.; Carter, D. E.; Fernando, Q.; Seff, K. *Acta Cryst.* **1977**, *33*, 3230-3234.

38. Newkome, G. R.; Fronczek, F. R.; Gupta, V. K.; Puckett, W. E.; Pantaleo, D. C.; Kiefer, G. E. *J. Am. Chem. Soc.* **1982**, *104*, 1782-1783.

39. Chieh, P. C. *J. Chem. Soc., Dalton Trans.* **1972**, 1643-1646.

40. Milani, B.; Anzilutti, A.; Vicentini, L.; Sassanta o Santi, A.; Zangrando, E.; Geremia, S.; Mestroni, G. *Organometallics* **1997**, *16*, 5064-5075.

41. Bondi, A. *J. Phys. Chem.* **1964**, *68*, 441-451.

42. McKenzie, E. D. *Coord. Chem. Rev.* **1971**, *6*, 187-216.

43. Charton, M. *J. Am. Chem. Soc.* **1969**, *91*, 615-618.

44. Trend, R. M.; Stoltz, B. M. *J. Am. Chem. Soc.* **2004**, *126*, 4482-4483.

45. Fanizzi, F. P.; Intini, F. P.; Maresca, L.; Natile, G.; Lanfranchi, M.; Tiripicchio, A. *Dalton Trans.* **1991**, 1007-1015.

CHAPTER 6. SUMMARY AND CONCLUSIONS

The platinum complexes of the type **L**$PtCl_2$ and $[\mathbf{L}_2Pt]^{2+}$ (**L** = bidentate sp^2 N-donor ligands) were successfully synthesized and crystallized. The platinum complexes characterized here have typical M–N distances of ~2.0 Å, and thus can be viewed as being representative of pseudo square-planar complexes of bipyridine-type ligands. The X-ray crystallographic data allowed conclusions to be reached about the relative influence of intramolecular interactions on the structural distortions.

The **L**$PtCl_2$ complexes with **L** = dimethyl-2,2′-bipyridine (**Me_2bipy**) have a more planar structure when compared to complexes having 3-(2′-pyridyl)-1,2,4-triazine (**pyt**) ligands. For the **4,4′-** and the **5,5′- Me_2bipy,** the attractive interactions between the H6 protons and the cis Cl results in a highly planar structure. However, presence of 6,6′ methyl groups in the **6,6'-Me_2bipy** ligand gives rise to a highly distorted structure, characterized by large bowing and an incline of the aromatic ring relative to the coordination plane. On the contrary the $\mathbf{L}_2Pt^{2+}$ complexes with **L** = **Me_2bipy** are more distorted than when **L** = **pyt**. The juxtaposition of the pyridyl H6 proton and the triazine lone pair of electrons in $[\mathbf{L}_2Pt]X_2$ allows formation of a planar structure. Also, this juxtaposition favors the trans arrangement of the bidentate ligands in $[(\mathbf{pyt})_2Pt]X_2$. For a given bidentate ligand, the interactions between the juxtaposed groups on the two rings ortho to the bridging carbons and on the periphery of the bidentate ligand are favorable for **pyt** ligands but unfavorable for **Me_2bipy**.

The reaction of **L**$PtCl_2$ complexes (**L** = **5,5′-Me_2bipy, MepyMe$_2$t** and bis-3,3′-(5,6-disubstituted-1,2,4-triazine) (**R_4dt**)) with guanine derivatives (**G**) were informative. The bulk of the bidentate sp^2 N-donor ligands is sufficient to impede the rotation of the **G**

bases about the Pt–N7 bonds of the **L**Pt**G**$_2$ adducts; thus, H8 signals for conformers could be resolved and assigned. From NMR data (including EXSY results), for **L**Pt(GMP)$_2$, the qualitative rates of conformer interconversion follow the order, **Me$_4$dt** > **Et$_4$dt** > **MepyMe$_2$t** > **5,5′-Me$_2$bipy**. Thus, we conclude that the pyridyl H6′ atom strongly impedes the rotation of the cis **G** base about the Pt–N7 bond by clashing with **G** O6, whereas the equivalently placed lone pair of the relevant non-bonded N of the triazine does not so strongly impede **G** rotation. Thus, the triazine ring has a lower overall steric effect than the pyridyl ring. Our conclusion that the lone pair on the non-bonded nitrogen, N1, of the triazine ring is not sterically demanding is also supported by results from the reaction of (**MepyMe$_2$t**)PtCl$_2$ with Guo to form a [(**MepyMe$_2$t**)Pt(Guo)$_2$]$^{2+}$ adduct. The intermediate properties of **MepyMe$_2$t**, with one triazine and one pyridyl ring led to EXSY data for the (**MepyMe$_2$t**)Pt(5′-GMP)$_2$ adduct that allowed us to unambiguously determine and assign the conformation of the two HH conformers, HHa and HHb.

The nature of the carrier ligand in **L**Pt**G**$_2$ adducts influences the distribution of conformers and their characteristics. Typically, one HT conformer dominates over the other HT and the HH conformer at low pH (~4), especially at neutral pH. We have discovered that carrier ligands of the type, **R$_4$dt**, lead to the HH having almost comparable abundance to the total of the two HT conformers for the (**R$_4$dt**)Pt(5′-GMP)$_2$ adduct at equilibrium at pH 4. We conclude that the sterically less demanding nature of the **R$_4$dt** ligand allows ample space for the HH conformer to exist with less significant clashes between the O6 atoms of the 5′-GMP's. Normally, second-sphere communication raises the abundance of one HT conformer as the pH is raised to near neutrality. This trend was found for the (**R$_4$dt**)Pt(5′-GMP)$_2$ adducts. However, the abundance of the HH

isomer remains high. Given the finding that carrier ligands favoring the HH conformer in the cross-link are associated with anticancer activity,[1] Pt complexes of **R_4dt** ligand should be tested for activity.

The interesting results with (**R_4dt**)Pt$(GMP)_2$ adducts led us to expand our study to single-stranded (ss) DNA adducts. Studies with the (**R_4dt**)Pt(d(G*pG*)) adduct provided the first evidence of formation of a substantial amount of a fourth form of an **L**Pt(d(G*pG*)) adduct. HPLC data suggest that this is the elusive ΛHT conformer of the N7–Pt–N7 d(G*pG*) cross-link adduct. The putative ΛHT conformer of (**R_4dt**)Pt(d(G*pG*)) is kinetically less favored when compared to the HH1, HH2 and ΔHT conformers and becomes abundant slowly (~8 weeks) by conformer isomerization. It is possible that this ΛHT conformer was not detected in the previously reported less dynamic adducts, even after long time periods, because of its slow rate of formation. However, for the (**R_4dt**)Pt(d(G*pG*)) adduct all four expected conformers could be identified and characterized by ^{1}H NMR spectroscopy. Our results with (**R_4dt**)Pt(5′-$GMP)_2$ revealed that the **R_4dt** carrier ligand is sterically less demanding and allows a less restricted rotation of **G** about the Pt–N7 bond. The detection of all four conformers and absence of any EXSY cross-peaks for the (**R_4dt**)Pt(d(G*pG*)) adduct provides the first clear evidence that the sugar-phosphodiester backbone between two adjacent G's slows the exchange between the conformers.

From the distribution of conformers for (**R_4dt**)Pt(d(G*pG*)), (**5,5′-Me_2bipy**)Pt(d(G*pG*)),[2] **Bip**Pt-(d(G*pG*))[3,4] and **Me_2ppz**Pt(d(G*pG*))[5] adducts, regardless of the carrier ligand the HH1 conformer is most abundant. However, the

thermodynamically favored putative ΛHT conformer for (**Me$_4$dt**)Pt(d(G*pG*)) was almost as abundant as the HH1 conformer at equilibrium.

NMR results in this study also show that the structure of the sugar-phosphodiester backbone differ from conformer to conformer, but the ^{31}P NMR data for the (**R$_4$dt**)Pt(d(TG*G*)) adduct, for the first time indicated that for a given conformer, the backbone structure may depend on the carrier ligand. The low steric effects of the N lone pairs of the **R$_4$dt** ligand allow more space for the HH conformer to exist resulting in a less distorted backbone for the HH1 conformer.

The effect of flanking residues in **L**Pt(d(oligo)) adducts is presented here for the first time for **L** = planar sp^2 N-donor ligand. Several important points have emerged from a comparison of the (**R$_4$dt**)Pt(oligo) adducts with (**R$_4$dt**)Pt(d(G*pG*)). For (**R$_4$dt**)Pt adducts at equilibrium, d(G*pG*) and d(G*G*T) uniquely have all the four conformers (except for the (**Et$_4$dt**)Pt(d(G*G*T)) ΛHT conformer which does not form). The ΛHT conformer becomes much less abundant in adducts with a 3′-residue. However, the 5′-flanking T residue exclusively favors the HH1 L conformer. The highly L nature of the single-strand DNA adducts with a 5′-T residue is chiefly a consequence of the bulk of the 5′ substituents; factors like H-bonding are inconsequential. Evidently, the 3′-flanking T residue has little or no effect, but the 5′-flanking T residue has a dramatic effect on the the d(G*pG*) cross-link structure, conformer distribution and canting.

6.1 References

1. Ano, S. O.; Kuklenyik, Z.; Marzilli, L. G. In *Cisplatin. Chemistry and Biochemistry of a Leading Anticancer Drug*; Lippert, B., Ed.; Wiley-VCH: Weinheim, 1999, pp 247-291.

2. Bhattacharyya, D.; Marzilli, P. A.; Marzilli, L. G. *Inorg. Chem.* **2005**, *44*, 7644-7651.

3. Marzilli, L. G.; Ano, S. O.; Intini, F. P.; Natile, G. *J. Am. Chem. Soc.* **1999**, *121*, 9133-9142.

4. Ano, S. O.; Intini, F. P.; Natile, G.; Marzilli, L. G. *J. Am. Chem. Soc.* **1998**, *120*, 12017-12022.

5. Sullivan, S. T.; Ciccarese, A.; Fanizzi, F. P.; Marzilli, L. G. *J. Am. Chem. Soc.* **2001**, *123*, 9345-9355.

APPENDIX A. SUPPLEMENTARY MATERIAL FOR CHAPTER 2

A.1 ^{1}H NMR Spectra of $[L_2Pt]^{2+}$ Complexes.

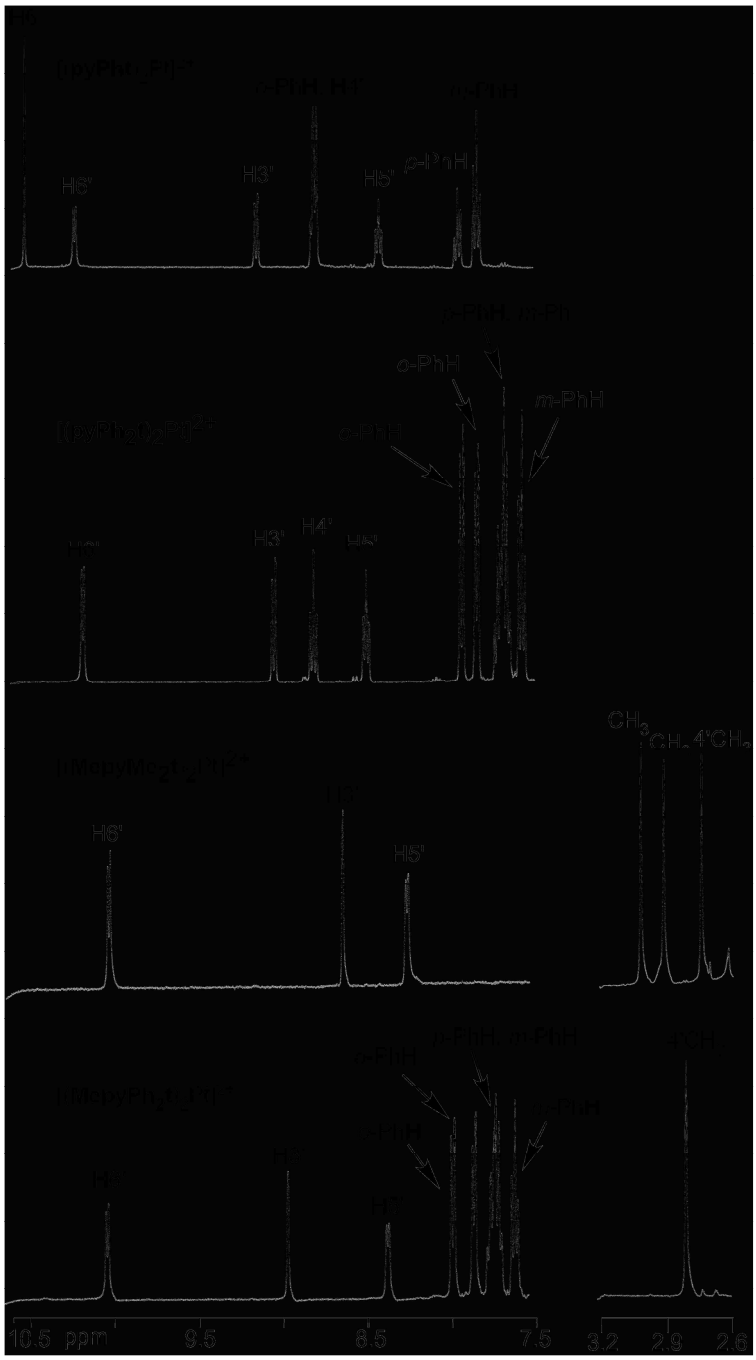

Figure A.1 ^{1}H NMR spectra of $[(\mathbf{pyPht})_2Pt]^{2+}$, $[(\mathbf{pyPh_2t})_2Pt]^{2+}$, $[(\mathbf{MepyMe_2t})_2Pt]^{2+}$, and $[(\mathbf{MepyPh_2t})_2Pt]^{2+}$ in DMSO-d_6 solution at 25 °C. The signals for the substituents on C5 and C6 are assigned by type only, except for $[(\mathbf{pyPht})_2Pt]^{2+}$, which is completely assigned.

A.2 ^{1}H NMR Chemical Shifts for $[L_2Pt]^{2+}$ Complexes

Table A.1 ^{1}H NMR Chemical Shifts (ppm) in DMSO-d_6 for $[\mathbf{L}_2Pt]X_2$ Complexes

$[\mathbf{L}_2Pt]^{2+}$	H6′	H5′	C4′ substituent	H3′	C5, C6 substituents[a]
$[(\mathbf{MepyMe_2t})_2Pt]^{2+}$	9.99(d)	8.23(d)	2.74(s, CH_3)	8.60(s)	2.91(s, CH_3), 3.01(s, CH_3)
$[(\mathbf{pyPht})_2Pt]^{2+}$	10.23(d)	8.80(t)	8.42(t, H)	9.15(d)	10.51(s, H), 8.78(d, *o*-PhH), 7.96(t, *p*-PhH), 7.83(t, *m*-PhH)
$[(\mathbf{pyPh_2t})_2Pt]^{2+}$	10.18(d)	8.81(t)	8.50(t, H)	9.06(d)	7.86(d, *o*-PhH), 7.95(d, *o*-PhH), 7.71(t, *m*-PhH), 7.59(t, *p*-PhH)
$[(\mathbf{MepyPh_2t})_2Pt]^{2+}$	9.99(d)	8.34(d)	2.58(s, CH_3)	8.92(s)	7.83(d, *o*-PhH), 7.96(d, *o*-PhH), 7.70(*m*-PhH), 7.58(t, *p*-PhH)

[a]The C5 and C6 substituents were not specifically assigned, except for $[(\mathbf{pyPht})_2Pt]^{2+}$.

A.3 Reactions of $\mathbf{pyMe_2t}$ and *cis*-$Pt(Me_2SO)_2Cl_2$ Studied by ^{1}H NMR Spectroscopy.

A.3.1 Formation and Properties of $(\mathbf{pyMe_2t})PtCl_2$.

Cis-$Pt(Me_2SO)_2Cl_2$ (1.16 mg, 5 mM) was added to a DMSO-d_6 solution (550 μL) of **pyMe$_2$t** (0.51 mg, 5 mM) to obtain a 1:1 molar ratio of Pt:**pyMe$_2$t**. Within 1 h of mixing, two new sets of bound **pyMe$_2$t** signals in a ratio of ~4:1 were observed (Figure A.2). The intensity of the new sets of signals increased with time. Two experiments were performed to assign the products and to determine if either product had the triazine ring bound to the Pt through N4 instead of N2.

Two separate solutions of $(\mathbf{pyMe_2t})PtCl_2$ (1.25 mg, 5 mM) in DMSO-d_6 (550 μL) were prepared. Within 5 min of dissolving $(\mathbf{pyMe_2t})PtCl_2$ in DMSO-d_6, two sets of signals were observed in a ratio of ~4:1, which remained constant, even after three days. These were the same signals observed in the 1:1 reaction. To the first solution $[NEt_4]Cl$ (2 mM) was added; the H6′ signal corresponding to the minor complex (at 9.44 ppm) disappeared, while the intensity of the H6′ signal (at 9.61 ppm) of the major complex increased. We attribute this result to conversion

of a minor solvolysis product to the dichloro complex by the high concentration of chloride. Thus, the H6′ doublet at 9.61 ppm was assigned to (**pyMe$_2$t**)PtCl$_2$, and the doublet at ~9.44 ppm was assigned to [(**pyMe$_2$t**)Pt(Me$_2$SO-d_6)Cl]$^+$. To the second solution, 10% D$_2$O was added, and within 30 min the intensity of the H6 signal at 9.44 ppm increased, while that of the signal at 9.61 ppm decreased, confirming that the 9.44 and 9.61 signals are due to a solvolysis product and to the dichloro complex, respectively. No isomer of the pyridyl triazine with **L** bound via N4 was detected.

A.3.2 Formation of [(pyMe$_2$t)$_2$Pt]$^{2+}$.

Cis-Pt(Me$_2$SO)$_2$Cl$_2$ (1.16 mg, 5 mM) was added to a DMSO-d_6 solution (550 μL) of **pyMe$_2$t** (2.05 mg, 20 mM) to obtain a 1:4 molar ratio of Pt:**pyMe$_2$t**. After 1 h of mixin, one set of new signals appeared in addition to the signals of the uncomplexed **pyMe$_2$t** ligand (Figure A.2). In this 4:1 experiment, the same doublet found in the 1:1 experiment at 9.61 ppm was present as the most downfield of the four new signals and was assigned to (**pyMe$_2$t**)PtCl$_2$. Within ~2 h, the neutral (**pyMe$_2$t**)PtCl$_2$ complex started precipitating. After ~1 day, four additional, but very weak signals for bound **L** were observed, the most downfield signal appearing at 10.2 ppm. This second reaction did not go to completion even in the presence of a threefold excess of **pyMe$_2$t** ligand. However, on addition of 10% D$_2$O to the sample, the signal at 10.2 ppm grew almost immediately. After ~1 h, signals assigned to (**pyMe$_2$t**)PtCl$_2$ disappeared, while the more downfield set of signals for bound **L** remained (Figure A.2). Again, no evidence for platinum binding at N4 of the triazine ring was observed in any spectra. The doublet at 10.2 ppm was thus assigned to the pyridyl H6′ of the [(**pyMe$_2$t**)$_2$Pt]$^{2+}$ cation having a trans relationship of the bound **pyMe$_2$t** ligands as found crystallographically for **8**. These findings indicate that the bound dichloro complex is favored thermodynamically in DMSO-d_6 and does not lose the chloro ligand

unless enough water is present to solvate the released chloride. Therefore, in studying the reaction of (**pyMe$_2$t**)PtCl$_2$ with Guo we used a D$_2$O/DMSO-d_6 solution as the solvent.

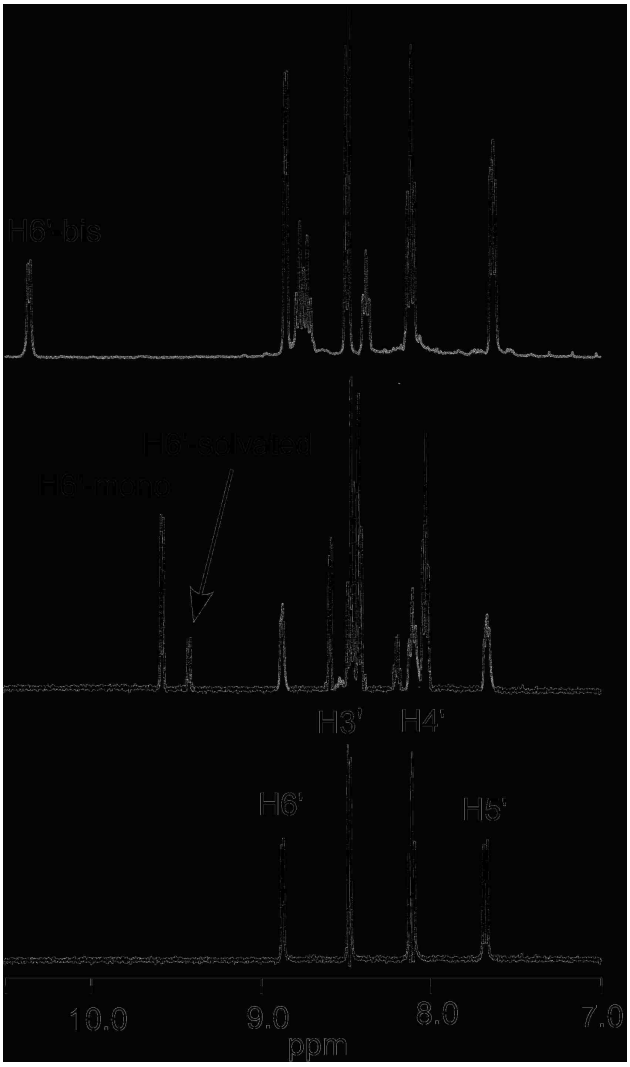

Figure A.2 ^{1}H NMR spectra, using numbering system in Scheme 2.1, of DMSO-d_6 solutions at 25 °C: **pyMe$_2$t** (bottom); 1:1 reaction mixture of **pyMe$_2$t** and *cis*-Pt(Me$_2$SO)$_2$Cl$_2$, 1 h after mixing (middle); and 4:1 reaction mixture of **pyMe$_2$t** and *cis*-Pt(Me$_2$SO)$_2$Cl$_2$, 1 h after addition of 10% D$_2$O (top).

APPENDIX B. SUPPLEMENTARY MATERIAL FOR CHAPTER 3

B.1 Conformer Assignment And Their Characteristics

B.1.1 (Me$_4$dt)Pt(5′-GMP)$_2$.

Within 24 h of mixing 1 equiv of (**Me$_4$dt**)PtCl$_2$ with 2 equiv of 5′-GMP at pH 4.0, six new broad and poorly resolved downfield H8 NMR signals (at ~25 °C) were observed, suggesting relatively fast 5′-GMP rotation. Most spectra were collected at 5 °C, where the reduced rate of **G** base rotation led to resolved sharp signals. Of the six new 5′-GMP H8 signals of (**Me$_4$dt**)Pt(5′-GMP)$_2$, the two comparably intense H8 signals at 8.87 and 8.82 ppm diminished with time, and after 4 days these were very small compared to the other four H8 signals (Figure B.1). These two H8 signals were the major signals when (**Me$_4$dt**)PtCl$_2$ and 5′-GMP were mixed in a 1:1 ratio and were absent when the two were mixed in a 1:3 ratio; thus, the two signals were assigned to the two rotamers of the mono 5′-GMP Pt adduct. The 5′-GMP in the mono 5′-GMP Pt adduct can have the H8 atom pointing either upward or downward out of the Pt coordination plane.

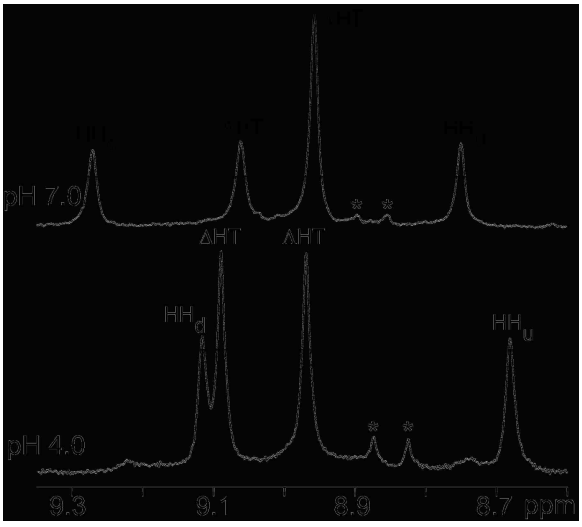

Figure B.1 H8 region of ^{1}H NMR spectra of (**Me$_4$dt**)Pt(5′-GMP)$_2$ at 5 °C. The H8 signals of the 1:1 adduct are labeled with asterisks.

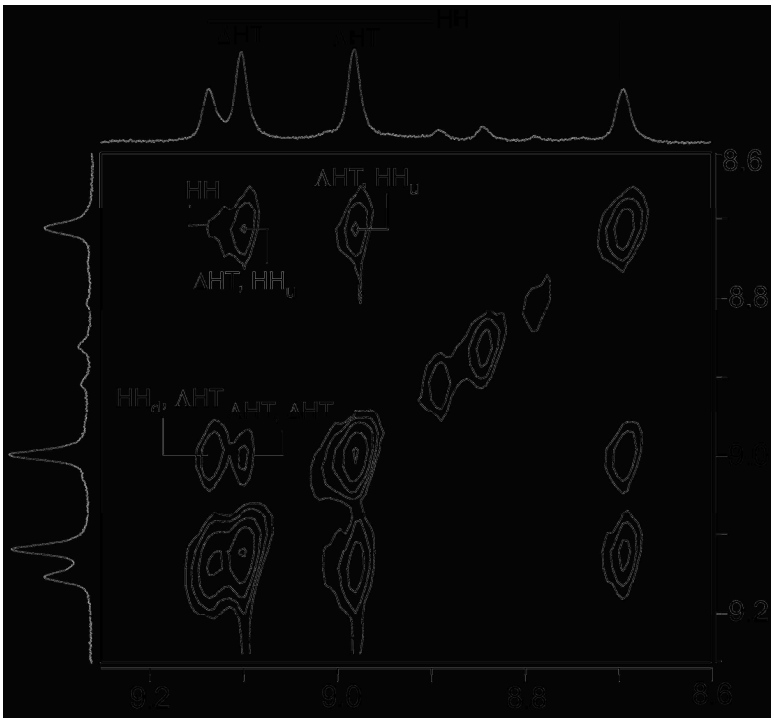

Figure B.2 ROESY spectrum of the (**Me$_4$dt**)Pt(5′-GMP)$_2$ adduct in the H8 region at pH 4.0 and 5 °C. The cross-peak labeled as HH is an NOE between the H8 signals of the HH conformer. The other labeled cross-peaks are EXSY cross-peaks between the H8 signals of two different conformers.

Solution studies of the (**Me$_4$dt**)Pt(GMP)$_2$ adducts were conducted in the pH range of ~4 to ~7 because decomposition produced free GMP at high pH. For the (**Me$_4$dt**)Pt(5′-GMP)$_2$ adduct, from pH 4.0-7.0 the two H8 signals at 9.10 and 8.66 ppm shifted downfield to 9.27 and 8.74 ppm, respectively. These signals were assigned to the HH conformer because they remained nearly equal throughout the pH titration, and they were connected by an NOE cross-peak in a ROESY spectrum (Figure B.2). Upon aising the pH from 4.0 to 7.0, the H8 signals at 9.08 and 8.96 ppm belonging to the HT rotamers shifted slightly upfield to 9.06 and 8.95 ppm, respectively (Table 3.1 and Figure B.1). At pH ~4, the HT H8 signals are nearly equal in intensity, the weak CD signal is consistent with nearly equal abundance of the ΔHT and ΛHT conformers. At pH 7.0 the H8 signal at 8.95 ppm became the dominant H8 signal. The CD signal shape at pH ~7 (Figure B.3) is characteristic of the ΛHT conformer[1-5] favored by SSC on

phosphate deprotonation.[5-8] Thus, the H8 signal at 8.95 ppm was assigned to the ΛHT conformer. The remaining H8 signal at 9.06 ppm (pH 7.0) was assigned to the ΔHT conformer.

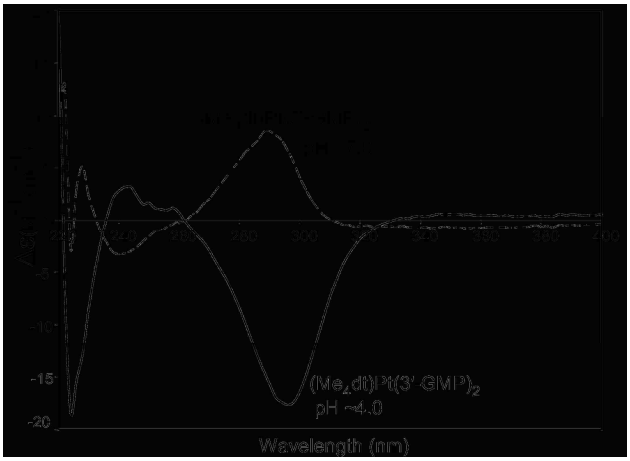

Figure B.3 CD spectra of (**Me$_4$dt**)Pt(5′-GMP)$_2$ and (**Me$_4$dt**)Pt(3′-GMP)$_2$ at 25 °C.

For the (**Me$_4$dt**)Pt(5′-GMP)$_2$ adduct at pH 7.0, the H8 signal of the major ΛHT conformer is upfield to that of the minor ΔHT conformer, as also observed for the (**Et$_4$dt**)Pt(5′-GMP)$_2$ adduct. In both cases, if the major ΛHT conformer is the '6-out' form and the minor ΔHT conformer is the '6-in' form, the canting is R-handed.

A ROESY spectrum of (**Me$_4$dt**)Pt(5′-GMP)$_2$ at pH 4.0 shows four EXSY cross-peaks even at 5 °C (Figure B.2). Both the HH$_d$ signal (9.10 ppm) and the HH$_u$ signal (8.66 ppm) have an EXSY cross-peak with the H8 signal (8.96 ppm) of the ΛHT rotamer. A ΔHT H8 - HH$_u$ H8 EXSY cross-peak is seen, but no ΔHT H8 - HH$_d$ H8 cross-peak could be detected because the two H8 signals have very similar shifts. Also, the presence of a weak EXSY cross-peak between the H8 signals of the ΔHT and the ΛHT rotamers indicates that this interconversion is rapid, even though it proceeds via the intermediacy of the HH rotamer. Thus, relatively faster interchange occurs between the rotamers for the (**Me$_4$dt**)Pt(5′-GMP)$_2$ adduct than for adducts with ligands containing a pyridyl moiety.

Increasing the pH from 4.0 to 7.0 changed the abundance of the HH, ΛHT, and ΔHT atropisomers of (**Me$_4$dt**)Pt(5′-GMP)$_2$ adduct from 40%, 30%, and 30% to 35%, 46%, and 19%, respectively (Figure B.1). At pH 4.0, the two HT conformers are equally abundant, and the HH conformer has a relatively high abundance. With increasing pH, SSC effects favor the ΛHT conformer; however, the abundance of the HH conformer is still relatively high, as compared to previously studied **L**Pt(5′-GMP)$_2$ adducts.

B.1.2 (Me$_4$dt)Pt(3′-GMP)$_2$.

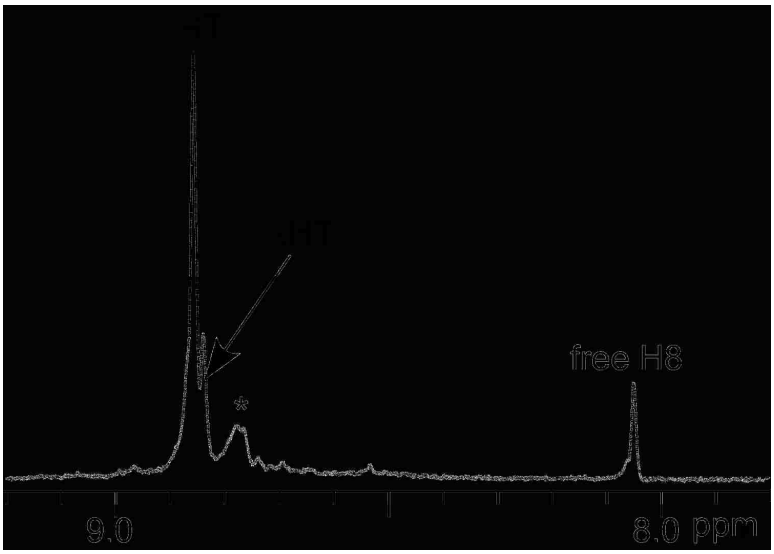

Figure B.4. H8 region of the ^{1}H NMR spectrum of (**Me$_4$dt**)Pt(3′-GMP)$_2$ at pH 4.0 and 5 °C. The H8 signal of the 1:1 adduct is indicated by an asterisk.

Three new H8 signals were observed downfield to the free 3′-GMP H8 signal at 5 °C and pH 4.0 (Figure B.4). The most upfield H8 signal (at 8.78 ppm, Figure B.4), which disappeared with time, was assigned to the two rapidly interconverting rotamers of the 1:1 3′-GMP adduct. After 2 days, only the two downfield H8 signals at 8.85 and 8.83 ppm were present in a 3:1 ratio. The CD signal shape observed at pH ~4 (Figure B.3) is characteristic of the ΔHT conformation,[1,3,4,8] which is the usually favored conformer by SSC at pH ~7 and below.[5-8] Therefore, at pH 4.0, the dominant H8 signal at 8.85 ppm was assigned to the ΔHT conformer

(major) and that at 8.83 ppm was assigned to the ΛHT conformer (minor). The '6-in' major form is the ΔHT R conformer and the '6-out' minor form is the ΛHT R. No evidence for the HH rotamer of the (**Me$_4$dt**)Pt(3′-GMP)$_2$ adduct was detected, even at 5 °C. At pH 7.0 the H8 signals are highly overlapped, but we estimate that the percent abundance of the ΔHT H8 signal increases from 75% to over 80%.

B.2 Chemical Shifts of the H1′ and H6/H6′ Signals of LPt(GMP)$_2$ Adducts

Table B.1 Chemical Shifts of the H1′ Signals of **L**Pt(GMP)$_2$ Adducts (**L = 5,5′-Me$_2$bipy**, **Et$_4$dt**, **Me$_4$dt**) and the H6/H6′ Signals of (**5,5′-Me$_2$bipy**)Pt(GMP)$_2$ Adducts at 5 °C [a]

complex	pH		ΔHT	ΛHT	HH_d	HH_u
(**5,5′-Me$_2$bipy**)Pt(5′-GMP)$_2$ [b]	4.0	H1′	6.03	6.00	6.10	6.08
	4.0	H6/H6′	7.78	7.90	7.72	7.82
	7.5	H1′	6.00	5.97	6.09	6.04
	7.5	H6/H6′	7.84	8.03	7.70	7.84
(**5,5′-Me$_2$bipy**)Pt(3′-GMP)$_2$ [b]	4.0	H1′	6.12	6.03	*c*	*c*
	4.0	H6/H6′	8.06	7.79	*c*	*c*
	7.5	H1′	6.12	6.01	*c*	*c*
	7.5	H6/H6′	8.24	7.82	*c*	*c*
(**Et$_4$dt**)Pt(5′-GMP)$_2$	4.0	H1′	6.07	6.03	6.08	6.03
(**Et$_4$dt**)Pt(3′-GMP)$_2$	4.0	H1′	6.10	6.07	*c*	*c*
	7.5	H1′	6.07	6.07	*c*	*c*
(**Me$_4$dt**)Pt(5′-GMP)$_2$	4.0	H1′	6.11	6.06	6.11	6.02
	7.0	H1′	6.10	6.03	6.09	6.03
(**Me$_4$dt**)Pt(3′-GMP)$_2$	4.0	H1′	6.11	6.09	*c*	*c*
	7.0	H1′	6.10	6.10	*c*	*c*

[a] Signal assignments are based on the 2D NMR studies. [b] NMR spectrum recorded at 25 °C. [c] Signal not detected.

Table B.2 Chemical Shifts of the H1′and the H6′ Signals of (**MepyMe$_2$t**)Pt(GMP)$_2$ Adducts at 25 °C [a]

complex	pH		ΔHT		ΛHT		HHa		HHb	
			ΔHT_d (py)	ΔHT_u (t)	ΛHT_d (py)	ΛHT_u (t)	HHa_d (t)	HHa_u (py)	HHb_d (t)	HHb_u (py)
(**MepyMe$_2$t**)Pt(5′-GMP)$_2$	2.5	H1′	6.05	6.09	6.05	6.05	6.05	6.05	6.07	6.07
	2.5	H6′	8.09		8.09			8.09		8.02
	7.5	H6′	8.10		8.25			8.10		7.99
(**MepyMe$_2$t**)Pt(3′-GMP)$_2$	4.5	H1′	6.12	6.09	6.07	6.06	*b*		*b*	
	4.5	H6′	8.25		8.02					
	7.5	H1′	6.29	6.29	6.25	6.25	*b*		*b*	
	7.5	H6′	8.44		8.02					

[a] The py and t notations designate **G**'s cis to the pyridyl and triazine rings, respectively. Signal assignments are based on the 2D NMR and pH titration studies. [b] Signal not detected.

B.3 References

1. Marzilli, L. G.; Intini, F. P.; Kiser, D.; Wong, H. C.; Ano, S. O.; Marzilli, P. A.; Natile, G. *Inorg. Chem.* **1998**, *37*, 6898-6905.

2. Wong, H. C.; Coogan, R.; Intini, F. P.; Natile, G.; Marzilli, L. G. *Inorg. Chem.* **1999**, *38*, 777-787.

3. Wong, H. C.; Intini, F. P.; Natile, G.; Marzilli, L. G. *Inorg. Chem.* **1999**, *38*, 1006-1014.

4. Williams, K. M.; Cerasino, L.; Intini, F. P.; Natile, G.; Marzilli, L. G. *Inorg. Chem.* **1998**, *37*, 5260-5268.

5. Sullivan, S. T.; Ciccarese, A.; Fanizzi, F. P.; Marzilli, L. G. *Inorg. Chem.* **2001**, *40*, 455-462.

6. Ano, S. O.; Kuklenyik, Z.; Marzilli, L. G. In *Cisplatin. Chemistry and Biochemistry of a Leading Anticancer Drug*; Lippert, B., Ed.; Wiley-VCH: Weinheim, 1999, pp 247-291.

7. Saad, J. S.; Scarcia, T.; Shinozuka, K.; Natile, G.; Marzilli, L. G. *Inorg. Chem.* **2002**, *41*, 546-557.

8. Wong, H. C.; Shinozuka, K.; Natile, G.; Marzilli, L. G. *Inorg. Chim. Acta* **2000**, *297*, 36-46.

APPENDIX C. SUPPLEMENTARY MATERIAL FOR CHAPTER 4

C.1 Conformational Features of (Et$_4$dt)Pt(d(G*pG*)) Conformers.

The H8 peaks of (**Et$_4$dt**)Pt(d(G*pG*)) at 8.97 and 9.04 ppm are connected by H8-H8 NOE cross-peaks. The H8-H2′ cross-peaks are stronger than the H8-H1′ cross-peaks (Figure C1), indicating a predominantly anti conformation for both 3′-G* and 5′-G* nucleotides. A 5′-G* H8-H3′ NOE cross-peak and a doublet for the H1′ signal (6.39 ppm) is characteristic of an N-sugar of a 5′-G (Figure C1).[1-6] The H8 signal at 8.97 ppm, which must be the 3′-G* H8 signal, has no H8-H3′ cross-peak, the H1′ signal at 6.43 ppm is doublet of a doublet, thus indicating an S-sugar pucker. Therefore, the dominant (**Et$_4$dt**)Pt(d(G*pG*)) conformer is an anti,anti-HH1 conformer, as observed for the (**Me$_4$dt**)Pt(d(G*pG*)).

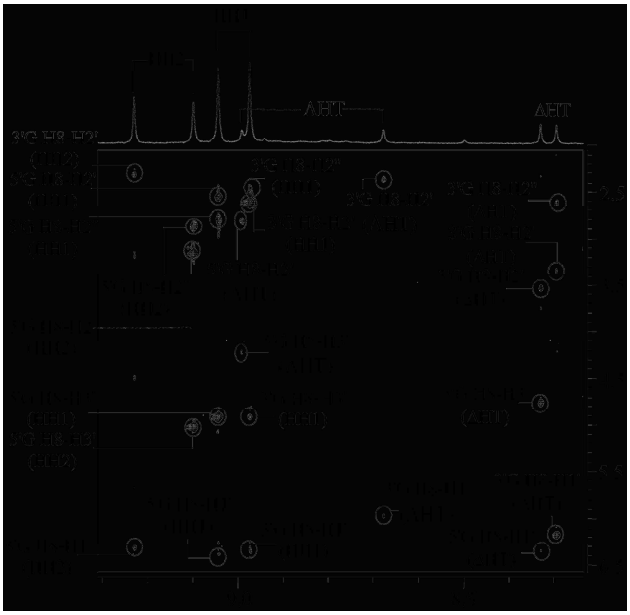

Figure C1. ^{1}H-^{1}H ROESY spectrum (700 MHz, 600 ms mixing time) of a 1-week-old (**Et$_4$dt**)Pt(d(G*pG*)) sample at pH 4.0 and 25 °C, showing G* H8 to sugar NOE cross-peaks for the HH1, HH2, and ΔHT and ΛHT conformers.

The two most downfield H8 signals at 9.23 and 9.10 ppm connected by an H8-H8 NOE cross-peak belong to the HH2 conformer (minor). The G* H8 signal at 9.10 ppm has a strong

H8-H3′ cross-peak, indicating an N-sugar pucker for the 5′-G* nucleotide (Figure C1). For the 5′-G* residue, a strong H8-H2′ cross-peak and the absence of an H8-H1′ NOE cross-peak indicate an anti G* conformation (Figure C1). The 9.23 ppm H8 signal belongs to the 3′-G* because of the S-sugar pucker indicated by the absence of an H8-H3′ NOE cross-peak. This H8 signal has a weak NOE cross-peak to the H1′ signal and a strong NOE to the H2′ signal. Therefore, this HH2 conformer has an anti,anti conformation.

The upfield pair of H8 signals at 8.29 and 8.32 ppm for the (**Et$_4$dt**)Pt(d(G*pG*)) adduct has no H8-H8 NOE cross-peak, indicating that the bases of this form adopt the HT arrangement.[2,3,7] These upfield H8 signal positions are characteristic of the ΔHT conformer. The chemical shifts of these HT H8 signals were similar to those of the (**Me$_4$dt**)Pt(d(G*pG*)) ΔHT conformer. The H8 peak at 8.32 ppm exhibits an intraresidue H8-H3′ NOE cross-peak (Figure C1) consistent with an N-sugar pucker. Because the H1′ signal of this conformer at 6.35 ppm overlaps with H1′ signals of the other (**Et$_4$dt**)Pt(d(G*pG*)) conformers, the coupling pattern could not be determined. However, because all the d(G*pG*) adducts typically adopt a 5′-G* N-sugar pucker, we can assign the downfield signal of this conformer to the 5′-G* sugar residue. The presence of a strong H8-H2′ cross-peak (Figure C2) and a weak H8-H1′ cross-peak indicates an anti 5′-G* conformation. The presence of an intraresidue H8-H1′ NOE cross-peak for the upfield ΔHT H8 signal at 8.29 ppm (which must be the 3′-G* H8) suggests that the conformation of 3′-G* is syn. Both the H8-H2′/H2″ and the H8-H3′ cross-peaks were absent. The doublet of doublets coupling of the 3′-G* H1′ signal (6.19 ppm) is typical of an S-sugar. Thus, this (**Et$_4$dt**)Pt(d(G*pG*)) conformer has an *anti,syn*-ΔHT conformation. In contrast to the H8 shifts

of the (**Me$_4$dt**)Pt(d(G*pG*)) ΔHT conformer, the 5′-G* H8 signal for the (**Et$_4$dt**)Pt(d(G*pG*)) ΔHT conformer is downfield to the 3′-G* H8 signal.

For the (**Et$_4$dt**)Pt(d(G*pG*)) adduct, no H8-H8 NOE cross-peak was observed for the fourth pair of G* H8 signals at 8.66 and 8.99 ppm, indicating that the bases adopt an HT arrangement that could possibly be the elusive ΛHT conformer. The G* H8 signals have strong H8-H2′ cross-peaks and weak H8-H1′ cross-peaks (Figure C1), indicating an anti conformation for both G* nucleotides. A strong H8-H3′ NOE cross-peak for the H8 signal at 8.99 ppm and a doublet for the H1′ signal indicate an N-sugar pucker. Thus, the 8.99 ppm H8 signal was assigned to the 5′-G* residue. For the H8 signal at 8.68 ppm, an H8-H3′ cross-peak was absent and the doublet of doublets coupling pattern indicated an S-sugar pucker. Thus, this upfield signal was assigned to the 3′-G*. This HT conformer has an anti,anti conformation. For the putative ΛHT conformer of the (**Et$_4$dt**)Pt(d(G*pG*)) adduct, the 5-G* H8 signal is downfield of the 3-G* H8 signal, as observed for the putative ΛHT conformer of the (**Me$_4$dt**)Pt(d(G*pG*)) adduct.

C.2 (Me$_4$dt)Pt(d(G*pG*)).

Within ~30 min of mixing (**Me$_4$dt**)$PtCl_2$ and d(GpG) in a 1:1 molar ratio in 64:36 D_2O:DMSO-d_6 solution at pH ~4.0 at 5 °C, the (**Me$_4$dt**)Pt(d(G*pG*)) adduct was fully formed. The eight H8 signals of the four conformers of the (**Me$_4$dt**)Pt(d(G*pG*)) adduct are fully resolved (Figure C2). The intensity of the H8 signals for the putative ΛHT conformer at 9.04 and 8.65 ppm slowly increased during a period ~3 months (Figure C2). A ROESY spectrum of this 3-months-old sample (Figure C3) helped us to confirm the sugar signal assignment for the (**Me$_4$dt**)Pt(d(G*pG*)) conformers.

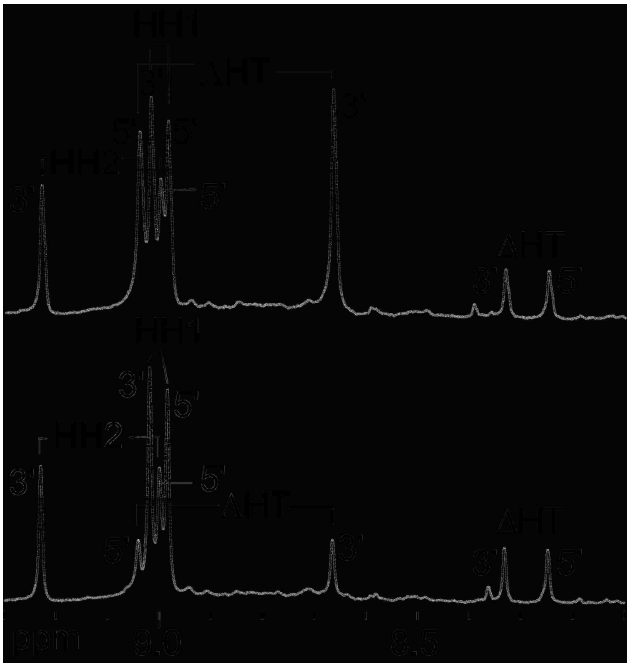

Figure C2. ^{1}H NMR spectra (400 MHz) in the H8 region for (**Me$_4$dt**)Pt(d(G*pG*)) collected at 25 °C after 1 week (bottom) and after 3 months (top) (pH 4.0, in D_2O/DMSO-d_6).

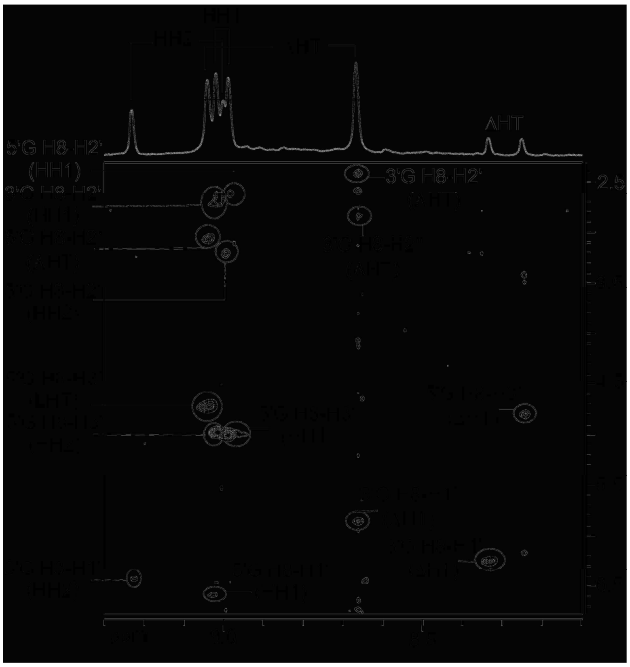

Figure C3. ^{1}H-^{1}H ROESY spectrum (400 MHz, 500 ms mixing time) of a 3-months-old (**Me$_4$dt**)Pt(d(G*pG*)) sample at pH 4.0 and 25 °C, showing G* H8 to sugar NOE cross-peaks.

C.3 References

1. Marzilli, L. G.; Saad, J. S.; Kuklenyik, Z.; Keating, K. A.; Xu, Y. *J. Am. Chem. Soc.* **2001**, *123*, 2764-2770.

2. Marzilli, L. G.; Ano, S. O.; Intini, F. P.; Natile, G. *J. Am. Chem. Soc.* **1999**, *121*, 9133-9142.

3. Ano, S. O.; Intini, F. P.; Natile, G.; Marzilli, L. G. *J. Am. Chem. Soc.* **1998**, *120*, 12017-12022.

4. Sullivan, S. T.; Ciccarese, A.; Fanizzi, F. P.; Marzilli, L. G. *J. Am. Chem. Soc.* **2001**, *123*, 9345-9355.

5. Mukundan, S., Jr.; Xu, Y.; Zon, G.; Marzilli, L. G. *J. Am. Chem. Soc.* **1991**, *113*, 3021-3027.

6. van der Veer, J. L.; van der Marel, G. A.; van den Elst, H.; Reedijk, J. *Inorg. Chem.* **1987**, *26*, 2272-2275.

7. Williams, K. M.; Cerasino, L.; Natile, G.; Marzilli, L. G. *J. Am. Chem. Soc.* **2000**, *122*, 8021-8030.

APPENDIX D. PERMISSION LETTERS

American Chemical Society's Policy on Theses and Dissertations

If your university requires a signed copy of this letter see contact information below.

Thank you for your request for permission to include **your** paper(s) or portions of text from **your** paper(s) in your thesis. Permission is now automatically granted; please pay special attention to the implications paragraph below. The Copyright Subcommittee of the Joint Board/Council Committees on Publications approved the following:

> Copyright permission for published and submitted material from theses and dissertations
> ACS extends blanket permission to students to include in their theses and dissertations their own articles, or portions thereof, that have been published in ACS journals or submitted to ACS journals for publication, provided that the ACS copyright credit line is noted on the appropriate page(s).
>
> Publishing implications of electronic publication of theses and dissertation material
> Students and their mentors should be aware that posting of theses and dissertation material on the Web prior to submission of material from that thesis or dissertation to an ACS journal may affect publication in that journal. Whether Web posting is considered prior publication may be evaluated on a case-by-case basis by the journal's editor. If an ACS journal editor considers Web posting to be "prior publication", the paper will not be accepted for publication in that journal. If you intend to submit your unpublished paper to ACS for publication, check with the appropriate editor prior to posting your manuscript electronically.

If your paper has **not** yet been published by ACS, we have no objection to your including the text or portions of the text in your thesis/dissertation in **print and microfilm formats**; please note, however, that electronic distribution or Web posting of the unpublished paper as part of your thesis in electronic formats might jeopardize publication of your paper by ACS. Please print the following credit line on the first page of your article: "Reproduced (or 'Reproduced in part') with permission from [JOURNAL NAME], in press (or 'submitted for publication'). Unpublished work copyright [CURRENT YEAR] American Chemical Society." Include appropriate information.

If your paper has already been published by ACS and you want to include the text or portions of the text in your thesis/dissertation in **print or microfilm formats**, please print the ACS copyright credit line on the first page of your article: "Reproduced (or 'Reproduced in part') with permission from [FULL REFERENCE CITATION.] Copyright [YEAR] American Chemical Society." Include appropriate information.

Submission to a Dissertation Distributor: If you plan to submit your thesis to UMI or to another dissertation distributor, you should not include the unpublished ACS paper in your thesis if the thesis will be disseminated electronically, until ACS has published your paper. After publication of the paper by ACS, you may release the entire thesis (**not the individual ACS article by itself**) for electronic dissemination through the distributor; ACS's copyright credit line should be printed on the first page of the ACS paper.

Use on an Intranet: The inclusion of your ACS unpublished or published manuscript is permitted in your thesis in print and microfilm formats. If ACS has published your paper you may include the manuscript in your thesis on an intranet that is not publicly available. Your ACS article cannot be posted electronically on a publicly available medium (i.e. one that is not password protected), such as but not

limited to, electronic archives, Internet, library server, etc. The only material from your paper that can be posted on a public electronic medium is the article abstract, figures, and tables, and you may link to the article's DOI or post the article's author-directed URL link provided by ACS. This paragraph does not pertain to the dissertation distributor paragraph above.

Questions? Call +1 202/872-4368/4367. Send e-mail to copyright@acs.org or fax to +1 202-776-8112. 10/10/03, 01/15/04, 06/07/06

IUCr journals

journals.iucr.org

18 June 2008

Vidhi Maheshwari
Chemistry Department, Room 232,
Choppin Hall, Louisiana State University,
Baton Rouge - LA 70803
USA

Copyright Permission

Dear Vidhi Maheshwari

Permission is hereby granted, on behalf of the IUCr, for the reproduction of the material specified in your email subject to the following conditions.

1. Reproduction is intended in a primary journal, secondary journal, CD ROM, book or thesis:

2. The original article in which the material appeared is cited.

3. IUCr's copyright permission is indicated in print. In electronic form, this acknowledgement must be hyperlinked to Crystallography Journals Online (http://journals.iucr.org/).

Material to be reproduced: "Ligand and coordination-plane distortions in platinum(II) complexes of isomers of dimethyl-2,2'-bipyridine" Vidhi Maheshwari, Maria Carlone, Frank R. Fronckzek and Luigi G. Marzilli, Acta Crystallogr., Sect. B: Struct. Sci. 2007, B63, 603-611.

Yours sincerely

Peter Strickland

Peter Strickland
Managing Editor
IUCr Journals

Managing Editor: Mr P. R. Strickland, 5 Abbey Square, Chester CH1 2HU, England
Telephone: 44 1244 342878 Fax: 44 1244 314888 E-mail: med@iucr.org

VITA

Vidhi Maheshwari received her Bachelor of Science degree in chemistry from Delhi University, Delhi, India, in 2000. After studying chemistry at the master's level for a year (2000-2001) at Indian Institute of Technology, Delhi, India, she moved to the United States in 2001. She received a Master of Science in Chemical Engineering degree from the University of Louisiana at Lafayette in 2003. She is enrolled in the doctoral program of chemistry at Louisiana State University, Baton Rouge, Louisiana. She is a candidate for the degree of Doctor of Philosophy during the Summer Commencement 2008.

She is a member of American Chemical Society. Her area of interest includes medicinal chemistry, material science and metallurgy.